9-2016

# Probing the Structure and Photophysics of Porphyrinoid Systems for Functional Materials

Christopher D. Farley
*The Graduate Center, City University of New York*

# PROBING THE STRUCTURE AND PHOTOPHYSICS OF PORPHYRINOID SYSTEMS FOR FUNCTIONAL MATERIALS

by

Christopher Farley

A dissertation submitted to the Graduate Faculty in Chemistry in partial fulfillment of the requirements for the degree of Doctor of Philosophy, The City University of New York

2016

Probing the Structure and Photophysics of Porphyrinoid Systems for Functional Materials

by

Christopher Farley

This manuscript has been read and accepted for the Graduate Faculty in Chemistry in satisfaction of the dissertation requirement for the degree of Doctor of Philosophy.

| | |
|---|---|
| Date | Charles Michael Drain<br>Chair of Examining Committee |
| Date | Brian Gibney<br>Executive Officer |

Supervisory Committee:

Hiroshi Matsui

Yuhang Ren

Michele Vittadello

Neepa Maitra

THE CITY UNIVERSITY OF NEW YORK

ABSTRACT

Probing the Structure and Photophysics of Porphyrinoid Systems for Functional Materials

by

Christopher Farley

Advisor: Charles Michael Drain

Porphyrins (Pors) and their many cousins, including phthalocyanines (Pcs), corroles (Cors), subphthalocyanines (SubPcs), porphyrazines (Pzs), and naphthalocyanines (NPcs), play amazingly diverse roles in biological and non-biological systems because of their unique and tunable physical and chemical properties. These compounds, collectively known as porphyrinoids, can be employed in any number of functional devices that have the potential to address the challenges of modern society. Their incorporation into such devices, however, depends on many structural factors that must be well understood and carefully controlled in order to achieve the desired behavior. Self-assembly and self-organization are key processes for developing these new technologies, as they will allow for inexpensive, efficient, and scalable designs. The overall goal of this dissertation is to elucidate and ultimately control the interplay between the hierarchical structure and the photophysical properties of these kinds of systems. This includes several case studies concerning the design and spectroscopic analysis of supramolecular systems formed through simple, scalable synthetic methods. We also present detailed experimental and computational studies on some porphyrin and phthalocyanine compounds that provide evidence for fundamental changes in their molecular structure. In addition to their impact on the

photophysics, these changes also have implications for the organization of these molecules into higher order materials and devices. It is our hope that these findings will help to drive chemists and engineers to look more closely at every level of hierarchical structure in the search for the next generation of advanced materials.

Dedicated to my wife, Valerie, who made every step possible.

Acknowledgements

It would be impossible to complete a journey like this without the help and support of countless people. Over the last several years at the Graduate Center and Hunter College I have met many incredible people that I am happy to call my friends and colleagues today. First and foremost I would like to thank my advisor and mentor, Professor Charles Michael Drain, for his constant support and inspiration. When I first reached out to Professor Drain about applying to the Graduate Center, his welcoming attitude was crucial in helping me to follow through on this long-held goal. Since that time, his advice and encouragement have consistently helped me to grow academically, professionally, and personally. I would also like to thank my gracious and attentive committee members, Professor Hiroshi Matsui, Professor Yuhang Ren, Professor Michele Vittadello, and Professor Neepa Maitra. Their valuable feedback has helped sharpen this dissertation and make it into a much better work than it would have been otherwise.

Working in Professor Drain's lab has been more fun and rewarding than I ever expected, all thanks to friends and colleagues like Dr. Sunaina Singh, Dr. Amit Aggarwal, Dr. Jacopo Samson, Dr. Matthew Jurow, Dr. Dinesh Bhupathiraju, Waqar Rizvi, Junior Gonzalez, Aaron Dolor, Cesar Pabon, Brian Hageman, David Nissenbaum, Viacheslav Manichev, Bianca John, Naxhije Berisha, Bibi Begum, Philip To, Taylor Giovan, and many more than can be reasonably listed. Many thanks also to my other friends at Hunter, especially Laura Oliveira, Jasmine Hatcher, Vanessa Sanders, Sam Groveman, and Patricia Gonzalez, who all helped me to keep things in perspective.

I would also like to express my love and gratitude to the friends and family that have been there to support me from the very beginning. To mom and dad, thank you for more than I can ever

repay, but especially for teaching me that learning is a goal in itself, and one that can be pursued in many ways. To my brothers and sisters, thank you for instilling me with an almost neurotic level of perfectionism, and then tempering it with an endless supply of glibness and sarcasm. To my mother-in-law, Beryl, thank you for welcoming me into your family and for your support as we begin to grow our own.

And finally, to my wife, Valerie, and my son, Damien, I love you both more than I can ever express. Valerie, your unwavering faith in me gave me the courage to return to school in the first place, and you have been a constant source of comfort and strength ever since. I could never have completed this work without you, nor would I ever have wanted to. But thank you most of all for giving me Damien and for being there with me to experience his warmth and light. I can already see him growing up into an amazing, brave, caring, intelligent young man thanks to you, and I look forward to a lifetime with you both.

## List of Figures

**Chapter 1.**



**Chapter 2.**



**Chapter 3.**

**Chapter 4.**



**Chapter 5.**

**Appendix A.**

**Appendix B.**

**Appendix C.**

## List of Tables

# Chapter 1. Porphyrinoid Systems as Functional Materials[§]

## 1.1. Introduction

Porphyrins (Pors) and their many cousins, including phthalocyanines (Pcs), corroles (Cors), subphthalocyanines (SubPcs), porphyrazines (Pzs), and naphthalocyanines (NPcs), play amazingly diverse roles in biological and non-biological systems because of their unique and tunable physical and chemical properties. Porphyrinoids and metalloporphyrinoids can have functions that go beyond mimicking biological processes such as the redox catalysis of cytochrome P450 or the photonic properties of photosynthetic pigments. For instance, they may be used as catalytic materials to destroy environmental pollutants for bioremediation, as robust light absorbing materials for solar energy harvesting, or as sensors, imaging agents, or therapeutics. Materials and multichromophoric arrays composed of Pors and related compounds have received considerable attention over the last few decades due to their useful spectroscopic, photophysical and redox properties.

Multichromophoric systems may be linked covalently or self-assembled *via* weak intermolecular forces, with important consequences for the relevant properties. Most studies and applications of porphyrinoid materials focus on systems containing one type of chromophore, but heterochromophoric or heteroporphyrinoid systems combining different kinds of dyes can be exploited to further enhance the photonic and functional properties beyond what can be achieved by a single dye. One advantage of making such heteroporphyrinoid systems is the potential to molecularly engineer a strong, broad absorption spectra that can range from the near UV to the

[§] This chapter is adapted from publications in *Energy & Environmental Science*,[1] and *The Handbook of Porphyrin Science*, Vol. 41. (in press)[2]

near IR. Thus, heterochromophoric systems can cover a broader swath of the solar spectrum in order to harvest the maximum amount of sunlight and convert it into electrical or chemical energy. Because of the tunable and overlapping band gaps, *de novo* design of materials with vectorial electron and energy transfer is now routine. The photonic properties of porphyrinoids can be exploited for high sensitivity chemical sensing, nonlinear optics, improved photodynamic activity for therapeutics and diagnostics, and many other functional materials.

Self-assembly and self-organization have the potential to play pivotal roles in addressing some of the great challenges in science today. They can aid in the development of cost-effective solar energy harvesting systems and devices with lower power consumption in order to meet the ever increasing energy requirements of the world in an environmentally responsible way.[3] The continued development of concepts in supramolecular chemistry will also have an impact on many other important applications, *e.g.* sensors, smart materials, nanoelectronics and theranostics. For example, the manufacturing costs for organic and hybrid devices can be quite competitive compared to silicon-based standards.[4]

One of the first reports of functional supramolecular materials, concerning multiporphyrin arrays acting as ionic photo-gated transistors, was published in 1989 by Drain and coworkers.[5] Since that time, multichromophoric porphyrinoid systems have proven to be a solid experimental and theoretical basis for understanding the photonic properties of a wide variety of functional materials. In order for functional organic materials to be commercially viable into the future, these supramolecular strategies will need be employed to ensure scalability and cost effectiveness. In this spirit, the overarching theme of this thesis is an exploration of the complex role that hierarchical structure plays in determining the properties of various functional porphyrinoid

materials. We begin here with a brief introduction to the language of supramolecular chemistry, followed by a broad overview of the landscape of potential applications.

### 1.2. Self-Assembly *vs*. Self-Organization

The organization of molecules into macro-scale devices, whether spontaneous or controlled, can be described in terms of a hierarchy of interactions. Broadly speaking, there are four levels of structure to be considered: molecular (primary), supramolecular (secondary), the organization of supramolecular systems into functional materials (tertiary), and the arrangement of materials into devices (quaternary).[6] At each level, strategies of self-assembly and self-organization can be employed to achieve the desired structure and function. In organic photovoltaics, for instance, they may be combined to aid in the formation of active layers with several spectrally complementary chromophores in pre-specified geometries to more effectively harvest and convert solar radiation. Robust but reversible intermolecular interactions, such as metal ion coordination,[7-12] can realize complex supramolecular architectures in which the chromophores are arranged in a manner that promotes electron or energy transfer in predictable directions. Conversely, self-organized nanoparticles (NP aggregates) of Por[13-15] or Pc[16,17] will have much less structural order, but can manifest significantly enhanced or modulated photonic properties because of quantum mechanical effects at this scale.[16,18]

Self-assembly generally encompasses those processes that result in discrete supramolecular systems.[6] These systems are usually topologically closed because the component molecules are carefully designed with complementary recognition groups and geometries to maximize specific intermolecular interactions. This strategy allows the predictable formation of nano-architectures, such as squares and rosettes, with a degree of predictability in their supramolecular properties. Self-organization, on the other hand, utilizes non-specific

intermolecular interactions to create non-discrete systems with a lower level of order than self-assembly. Self-organized systems generally require less complex molecular structures and can be more robust against defects than self-assembled ones, but it can also be more difficult to tune their properties with the same level of precision. Since each approach has its own benefits and drawbacks, and since there is a great deal of overlap or gray-area between them, both are expected to be important in future technologies.

### 1.3. Applications and Properties of Porphyrinoid Systems

Solar energy is the most important source of free energy on our planet Earth. The solar spectrum contains a continuum of light energy from *ca*. 350 nm to 2.5 μm, although the irradiance depends on the wavelength. In terms of capturing solar energy and driving photocatalysis, the visible region from 400-800 nm contains the most useful part of the spectrum because of its photon energy and flux. Most dye-based solar energy harvesting systems available can convert only a few percent of solar energy into chemical or electrical energy, primarily because molecular systems have narrow absorption bands in the visible region of the spectrum. Significant research focuses on the development of systems and materials that can absorb a broader range of the solar spectrum to maximize the amount of energy harvested. Organic photonic materials can be robust and are generally less toxic than many inorganic materials such as quantum dots and perovskites. Porphyrinoid dyes, for example, possess tunable chemical and photophysical properties and can be readily processed into nanometer thick active layers. Though chlorophylls and pheophytins are the primary dyes in photosynthesis responsible for most of the transduction of solar energy into biochemical energy on Earth, they are not robust in most materials applications. Similarly, the catalytic activity of cytochrome P450 enzymes is difficult to exploit in large, commercial applications. Thus, synthetic porphyrinoids are likely some of the best dyes available to develop

materials for photovoltaics, as well as for organic optoelectronic devices such as organic light emitting diodes, sensors, photocatalysts, electrocatalysts, photodynamic therapy (PDT) agents, and biomimetic models of photosynthesis.

Pors and related porphyrinoid compounds are at the forefront of organic photonics research because of their strong absorption in the visible to near IR region, tunable optical properties, and robustness. While discrete synthetic systems containing several different chromophores are possible, these are rarely commercially viable because of the synthetic complexity arising from the need to generate low symmetry porphyrinoids as building blocks. On the other hand, systems containing different porphyrinoids stitched together by high-yield polymerization reactions and click chemistry are more feasible avenues to new polymeric photonic materials. In addition, supramolecular chemistry can be used to create multichromophoric systems by self-assembly or self-organization. In all cases, the goal is to make materials that exhibit optimal photophysical properties: light absorption, luminescence, photothermal yield, photocatalytic activity, *etc*. In porphyrin-phthalocyanine (Por–Pc) systems, for instance, the strong absorption band of Pcs around 650-750 nm has some overlap with the emission spectra of Pors in the same region. Thus, Por excitation energy can be efficiently transferred to the Pc in a directed manner. Similar processes can be expected for other heteroporphyrinoid systems, and these behaviors can be independently optimized for a given application.

Typical UV-Vis absorption and fluorescence emission spectra of some representative macrocycles can be seen in **Figure 1.1**, demonstrating how they span the electromagnetic spectrum. Many multicomponent systems are reported wherein the various chromophores are either covalently linked, directly or with spacers, or else held together *via* supramolecular chemistry. Examples of these systems include Por–Pcs, porphyrin-corroles (Por–Cors), and

phthalocyanine-subphthalocyanines (Pc–SubPcs). Different porphyrinoids have been prepared and studied by numerous research groups because of their broad biological and technological applications.[20-22] Their photonic properties, such as strong absorbance in the visible region of the electromagnetic spectrum, enable applications in light harvesting systems,[23-34] photochemical sensors,[35-41] catalysis,[42-49] nonlinear optics,[50-53] and PDT.[54-60] While there is significant literature concerning the applications of multichromophoric arrangements of multiple copies of the same dye, there are fewer examples of heteroporphyrinoid systems. Combining together different chromophores can lead to emergent, system-level properties that can be further optimized to meet the requirements of all the applications mentioned above, and more.

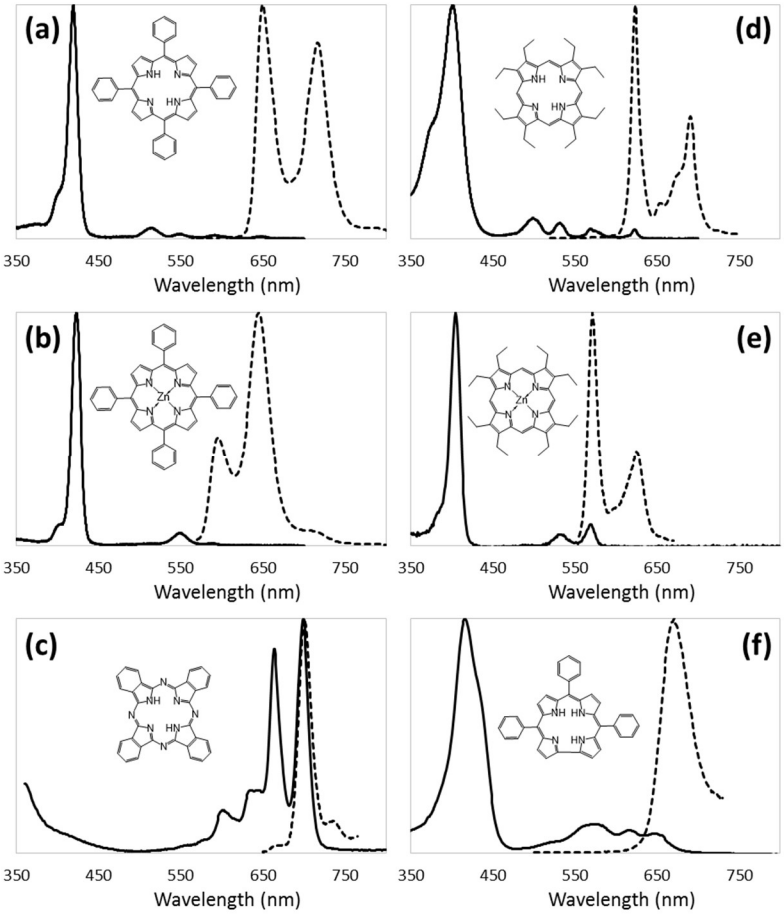


**Figure 1.1**. UV-Vis absorbance (solid lines) and fluorescence emission (dashed lines) spectra of (a) tetraphenylporphyrin, (b) zinc tetraphenylporphyrin, (c) phthalocyanine, (d) octaethylporphyrin, (e) zinc octaethylporphyrin, and (f) triphenylcorrole. All data was taken from the PhotochemCAD 2.1 software package, developed by Lindsey and coworkers.[19]

### 1.3.1. Artificial Photosynthesis and Solar Energy Harvesting

Pors are generally poor solar energy harvesting candidates because the intense but narrow Soret absorption band near 400 nm and the *ca*. 15-fold weaker Q bands between 500-650 nm capture only a small fraction of the incident light. Pcs weakly absorb 400-600 nm light, but are characterized by strong Q bands from 650-750 nm[21,22] and are gaining interest for applications such as PDT.[54-57] In contrast, Por–Pc hybrid materials[31-34,51,61-115] exhibit unique and interesting optical phenomena that neither type of dye possesses. Therefore, one obvious means to improve organic photovoltaic efficiency is to harvest a larger fraction of the solar spectrum using heteroporphyrinoid systems.

In natural photosynthetic systems, sunlight is collected by the primary pigments of the antenna complexes, *e.g.* chlorophyll and carotenoids. This captured energy is then funneled *via* excitation energy transfer (EET) to the reaction center where it initiates a series of electron transfer (ET) reactions. For over three decades, a tremendous effort has focused on construction of artificial antenna complexes in which the dyes are covalently linked. In general, however, the syntheses of covalently linked systems are tedious and have low yields of the final product. In addition, the degree of electronic communication amongst the dyes depends both on the linker chemistry and on the relative orientation of the macrocycles and their respective dipoles. While covalent systems have generated a wealth of information on the fundamental mechanisms of EET and ET, these are unsuitable for commercialization.[1]

Natural photosynthetic systems exhibit many of the hallmarks of both self-assembly and self-organization processes in achieving their remarkable quantum efficiency. The very existence of life on earth is therefore a proof-of-concept argument for the bottom-up construction of systems that can capture and convert solar energy with near unit efficiency. In pursuit of this goal, various

self-assembly strategies, such as electrostatic interaction, π-π stacking, hydrogen bonding, dispersion forces, and metal-ion coordination, have been explored to produce a wide range of supramolecular porphyrinoid systems.[35,116] These systems are employed especially as a means to create novel artificial antenna complexes and reaction centers that can mimic the primary events of natural photosynthesis. Supramolecular chemistry has been employed more recently to fabricate heteroporphyrinoid assemblies, with Por–Pc systems dominating the literature.[33,61,62,66-83]

### 1.3.2. Photodynamic Therapy (PDT)

PDT has existed in some form or another for over a century,[117] and has become a widely accepted treatment for a range of maladies from acne to cancer. In PDT, a photoactive chemical agent is introduced into the target site and activated by the application of light, usually of a specific wavelength. The activated photosensitizer then undergoes either ET reactions to produce free radicals (Type I mechanism) or EET to molecular oxygen to produce highly reactive singlet oxygen (Type II mechanism). Porphyrinoid compounds have been known to act as PDT agents since at least the early 1900s, and their development took off in the 1970s with the creation of the so-called "hematoporphyrin derivative" which ultimately led to the production of Photofrin®, the most commonly used PDT sensitizer. Further research led to the discovery of aluminum Pc sulfonates, tetra-(*meta*-hydroxyphenyl)chlorin, and many others.[117,118] Several porphyrinoids have even been approved for commercial clinical use in the United States, Europe or Russia, including Chlorin-e6®, Photosan-3®, Visudyne®, Foscan®, Photogem®, and Photofrin®. These last two are actually mixtures of covalently attached Por oligomers, further suggesting the usefulness of multichromophoric systems for this application.[56,91,118]

There are several factors that must be balanced against one another in designing a photosensitizer for PDT. Among the most important are: (1) good absorbance in the so-called

therapeutic window from 650-1350 nm, (2) high singlet oxygen quantum yield, (3) low dark-toxicity, (4) high selectivity for cancer cells or other targeted tissues or diseases, (5) water solubility for biological compatibility, and (6) short biological half-life for rapid elimination from the body. Other properties can impart additional benefits, such as good fluorescence quantum yield for concomitant *in situ* imaging, but these may come at the cost of compromising the primary factors.

Multichromophoric systems may be able to address these challenges by bringing together different dyes that separately meet the necessary requirements without having to make the same tradeoffs.[66] Many of these constructs are reported to have broad absorbance in the near-IR, good singlet oxygen quantum yield,[27,52,61,91,92,119] or increased water solubility,[66,119-122] all of which are highly desirable for PDT. It is also worth pointing out that the most common mechanism of PDT is the generation of singlet oxygen by the interaction of ground-state molecular oxygen with the excited triplet state of the sensitizer. Intersystem crossing from the excited singlet state of the PDT agent to the triplet state is promoted by the presence of heavy atoms. Thus, many supramolecular metal-ion coordination or sandwich complexes may potentially have a "built-in" mechanism for populating the triplet state and enhancing the singlet oxygen quantum yield.

### 1.3.3. Molecular Electronics

Self-assembly and self-organization of Pors with different chromophores, *e.g*. Cors, Pcs, SubPcs, NPcs, are relevant to light harvesting systems, but the multiple redox states can also be exploited in potential molecular electronics devices.[6,116,123-130] Many of these materials, especially including heteroleptic sandwich compounds and the metal-ion coordination complexes, are proposed to be viable components of hybrid organic-inorganic electronics, optoelectronics, and

other photonics because of their reversible redox states, tunable band gaps, and electronic spectra.[114,116,131-135]

While the supramolecular chemistry of Pors has been extensively reviewed,[35,116,120] there are far fewer reports on the photophysical, ET, and EET properties of self-assembled multichromophore systems. As in the covalent systems, the mode of assembly, the supramolecular architecture, and the supramolecular dynamics dictate the degree of electronic communication between the dyes. Additionally, the supramolecular dynamics, in terms of intermolecular bond formation convoluted with the complex equilibria that are exploited in self-assembly, can be a liability that diminishes interactions between the chromophores.[6,116] These considerations also complicate probing the mechanisms of both molecular electronics and light harvesting. Here again, complexes involving Pors and Pcs are the most studied,[6,35,63-66,114-116,120,121,127-142] with relatively few other porphyrinoid assemblies appearing in the molecular electronics literature.[116,143]

### 1.3.4. Catalysis and Photocatalysis

Porphyrinoids such as heme and chlorophyll are present in nearly all forms of life and are responsible for a vast array of metabolic processes. Their diverse enzymatic activity makes them an important paradigm for catalysis in synthetic chemistry. Indeed, many articles are published regarding the catalytic and photocatalytic activity of porphyrinoid based materials.[45,46,119,144-147] Most biological porphyrinoids exist in a larger protein matrix, indicating the particular importance of structure and conformation to these chemical reactions. Thus, it is reasonable to expect that the catalytic action of these macrocycles could be tuned or improved by rational incorporation into larger, multichromophoric arrays or supramolecular assemblies in which the hierarchical structure is carefully controlled. Many such systems have in fact been reported.[44-

49,144,145,148] Again, the inclusion of disparate porphyrinoid types with complementary properties presents another pathway to engineer and optimize this function.[42,43,47,48,149] Besides simply combining the different redox properties of the constituent compounds, these kinds of systems can also display molecular recognition and enhanced selectivity for certain substrates or reactions.[66,119,150]

### 1.3.5. Other Applications

There are more potential applications for porphyrinoids and porphyrinoid systems than can be comprehensively addressed in one chapter. However, most, if not all, of these rely on the same suite of photophysical and chemical properties discussed. Each of these functions has the potential to be greatly enhanced by the synergistic cooperation of heteroporphyrinoid systems. For example, such systems have shown the potential to play novel roles as chemical sensors[37,40] and non-linear optical materials.[50,65]

## 1.4. Themes and Future Directions

The importance of Pors and related macrocycles, such as chlorins, to biological systems has been recognized for well over a century, and Pcs have been known and employed for almost as long. Thus, the potential to use porphyrinoids as photonic materials has a long history. Improved higher yield synthetic methods for functionalized Pors, Cors, Pcs, SubPcs, and related dyes have opened the door for many researchers to design new porphyrinoids with different photonic or chemical properties. There are a variety of synthetic strategies that yield photonic materials based on porphyrinoids. Self-assembled and self-organized constructs have the benefits of simpler molecular components and high yield supramolecular chemistry, whereas covalent, discrete multichromophoric arrays offer more robust molecular architectures. Covalent and supramolecular systems of dyes each have advantages and disadvantages and both strategies have their place in

the design of functional materials. It may also be that some of the more demanding requirements for new functional materials will necessitate the incorporation of both covalent and supramolecular motifs.

In Chapters 2 and 3 of this thesis, we discuss two approaches that highlight this interplay between organic synthesis and supramolecular chemistry. The first method utilizes a high-yield synthesis of a Por tecton bearing a uracyl moiety at the *meso* position. In turn, these uracyls impart a specific pattern of hydrogen bond donors and acceptors that mediate the self-assembly of the dye into discrete, robust cage-like structures that persist even into the solid state. In Chapter 3, a different "click-chemistry" type reaction is utilized to covalently join two pre-fabricated asymmetric Pors into a flexible dimer. This dimer is then found to exhibit enhanced π-π interactions with unfunctionalized fullerene ($C_{60}$ and $C_{70}$) electron acceptors, allowing the two components to self-organize into donor-acceptor pairs with a reasonably high binding constant.

Chemical modification of a molecular component is almost always necessary in the design and fabrication of supramolecular systems. Thus, it is imperative to understand how these modifications will influence the properties of the individual molecules themselves. To this end, Chapters 4 and 5 will focus on the structures and photophysics of individual dye components that have been modified with typical substituents of the type that might be employed in tectons for self-organized or functional materials. In both cases we find evidence that the influence of these groups is not strictly confined to electronic effects, but also results in dramatic and unexpected changes to the molecular structure. These changes in the geometry can potentially have enormous effects that will ripple through all of the levels of hierarchical structure, and therefore must be accounted for in any attempt at rational device design. Finally, this thesis will conclude in Chapter 6 with a

description of the design and preliminary investigation into the synthesis of porphyrinoid materials that purport to take advantage of some of the supramolecular motifs discussed herein.

The yearly number of citations for published papers related to supramolecular and self-assembled Por or Pc systems (between 1985 and 2014) is shown in **Figure 1.2**. Data for the actual number of publications related to these topics (not shown) demonstrates similar trends, but speaks more towards the supply of papers within this research subject. The number of citations, on the other hand, may be more correlated to demand for research within this subject, and thus more important in considering its prospects for the future. It is clear from the chart that the field experienced a dramatic growth beginning in the 1990s and extending into the new millennium. In addition, a more recent expansion into the design of materials containing more than one type of porphyrinoid has opened new vistas to photonics that exploit the photophysical and architectural features of the components. This is reflected in the late arrival and growth of results for the composite "porphyrin AND phthalocyanine" search terms, which can be regarded as representative of the trends in the area of mixed chromophore systems. Despite this development, however, it appears

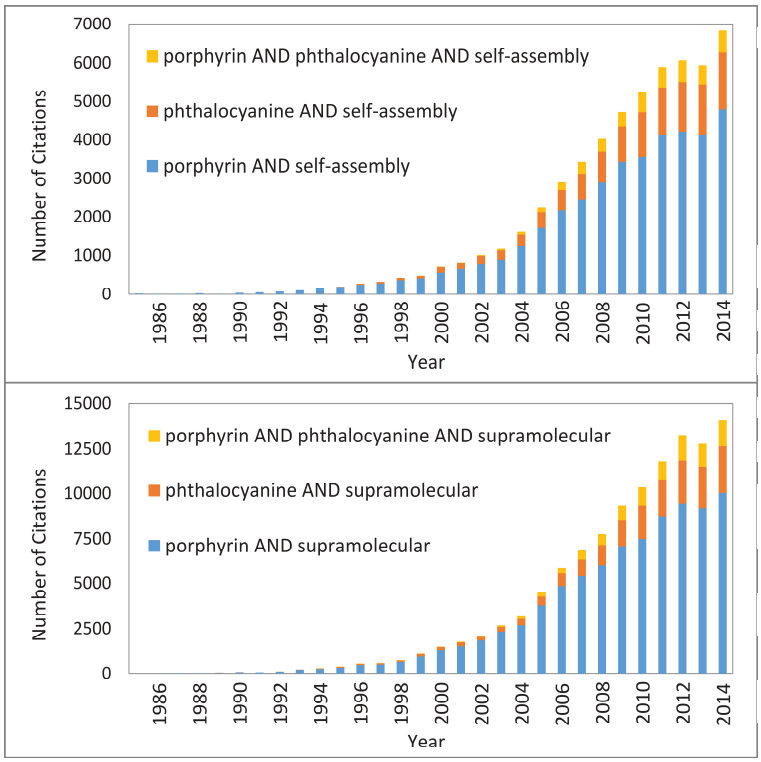


**Figure 1.2**. Stacked bar graph showing the number of citations of the papers meeting the relevant search terms given in the legends for every year from 1985 to 2014. The metadata was derived from the Thomson Reuters Web of Science™ online database.[151]

from the chart that the growth of the field as a whole has significantly slowed and ultimately leveled off in recent years.

For over 25 years, interesting covalent and supramolecular systems have been reported, along with comprehensive photophysical studies of many of these systems. Thus, both the synthesis and photophysics of multichromophoric systems are very well established. Novel materials that are chemically and visually quite appealing, but which utilize components arising from low yield syntheses, will contribute little towards the development of realistic materials unless they can exhibit new and/or unexpected photonic properties. Given the incredible versatility of porphyrinoid and heteroporphyrinoid systems, it is likely that they will continue to play important roles in every aspect of chemistry and materials science. In the end, however, commercialization of the materials will dictate the specific dyes used and the approach taken for a given application.

### 1.5. References


1. Radivojevic, I.; Varotto, A.; Farley, C.; Drain, C. M. Commercially viable porphyrinoid dyes for solar cells. *Energy Environ. Sci.* **2010**, *3*, 1897.
2. Farley, C.; Ferreira, J. T.; Aggarwal, A.; Bhupathiraju, N. V. S. D. K.; Singh, S.; Drain, C. M.; Tomé, J. P. C. In *Handbook of Porphyrin Science*; Kadish, K. M., Smith, K. M., Guilard, R., Eds.; World Scientific Publishing Co., Pte. Ltd.: Singapore, **2016**; Vol. 41 (forthcoming).
3. Service, R. F. Solar energy. Is it time to shoot for the sun? *Science* **2005**, *309*, 548.
4. Kalowekamo, J.; Baker, E. Estimating the manufacturing cost of purely organic solar cells. *Solar Energy* **2009**, *83*, 1224.
5. Drain, C. M.; Christensen, B.; Mauzerall, D. Photogating of ionic currents across a lipid bilayer. *Proc. Natl. Acad. Sci. U.S.A.* **1989**, *86*, 6959.
6. Drain, C. M. Self-organization of self-assembled photonic materials into functional devices: photo-switched conductors. *Proc. Natl. Acad. Sci. U.S.A.* **2002**, *99*, 5178.
7. Drain, C. M.; Nifiatis, F.; Vasenko, A.; Batteas, J. D. Porphyrin Tessellation by Design: Metal-Mediated Self-Assembly of Large Arrays and Tapes. *Angew. Chem. Int. Ed.* **1998**, *37*, 2344.

8. Drain, C. M.; Varotto, A.; Radivojevic, I. Self-organized porphyrinic materials. *Chem. Rev.* **2009**, *109*, 1630.

9. Drain, C. M.; Hupp, J. T.; Suslick, K. S.; Wasielewski, M. R.; Chen, X. A perspective on four new porphyrin-based functional materials and devices. *J. Porphyrins Phthalocyanines* **2002**, *06*, 243.

10. Ariga, K.; Hill, J. P.; Wakayama, Y.; Akada, M.; Barrena, E.; de Oteyza, D. G. New aspects of porphyrins and related compounds: self-assembled structures in two-dimensional molecular arrays. *J. Porphyrins Phthalocyanines* **2009**, *13*, 22.

11. Cheng, K. F.; Thai, N. A.; Teague, L. C.; Grohmann, K.; Drain, C. M. Supramolecular squares of porphyrazines. *Chem. Commun.* **2005**, 4678.

12. Lee, S. J.; Hupp, J. T. Porphyrin-containing molecular squares: Design and applications. *Coord. Chem. Rev.* **2006**, *250*, 1710.

13. Drain, C. M.; Smeureanu, G.; Patel, S.; Gong, X.; Garno, J.; Arijeloye, J. Porphyrin nanoparticles as supramolecular systems. *New J. Chem.* **2006**, *30*, 1834.

14. Gong, X.; Milic, T.; Xu, C.; Batteas, J. D.; Drain, C. M. Preparation and Characterization of Porphyrin Nanoparticles. *J. Am. Chem. Soc.* **2002**, *124*, 14290.

15. Smeureanu, G.; Aggarwal, A.; Soll, C. E.; Arijeloye, J.; Malave, E.; Drain, C. M. Enhanced catalytic activity and unexpected products from the oxidation of cyclohexene by organic nanoparticles of 5,10,15,20-tetrakis-(2,3,4,5,6-pentafluorophenyl)porphyrinatoiron(III) in water by using O2. *Chem. Eur. J.* **2009**, *15*, 12133.

16. Nitschke, C.; O'Flaherty, S. M.; Kröll, M.; Doyle, J. J.; Blau, W. J. Optical properties of zinc phthalocyanine nanoparticle dispersions. *Chem. Phys. Lett.* **2004**, *383*, 555.

17. Van Keuren, E.; Bone, A.; Ma, C. Phthalocyanine nanoparticle formation in supersaturated solutions. *Langmuir* **2008**, *24*, 6079.

18. Rangel-Rojo, R.; Matsuda, H.; Kasai, H.; Nakanishi, H. Irradiance dependence of the resonant nonlinearities in an organic material. *Journal of the Optical Society of America B* **2000**, *17*, 1376.

19. Dixon, J. M.; Taniguchi, M.; Lindsey, J. S. PhotochemCAD 2: A Refined Program with Accompanying Spectral Databases for Photochemical Calculations. *Photochem. Photobiol.* **2007**, *81*, 212.

20. Kadish, K. M.; Smith, K. M.; Guilard, R., Eds.; *Handbook of Porphyrin Science*, Academic Press: San Diego, CA, **2010-2011**; Vol. 1-15.

21. de la Torre, G.; Claessens, C. G.; Torres, T. Phthalocyanines: old dyes, new materials. Putting color in nanotechnology. *Chem. Commun.* **2007**, 2000.

22. Claessens, C. G.; Hahn, U.; Torres, T. Phthalocyanines: from outstanding electronic properties to emerging applications. *Chem. Rec.* **2008**, *8*, 75.

23. Gust, D.; Moore, T. A.; Moore, A. L. Mimicking photosynthetic solar energy transduction. *Acc. Chem. Res.* **2001**, *34*, 40.

24. Guldi, D. M. Fullerene-porphyrin architectures; photosynthetic antenna and reaction center models. *Chem. Soc. Rev.* **2002**, *31*, 22.

25. Li, X.; Sinks, L. E.; Rybtchinski, B.; Wasielewski, M. R. Ultrafast aggregate-to-aggregate energy transfer within self-assembled light-harvesting columns of zinc phthalocyanine tetrakis(perylenediimide). *J. Am. Chem. Soc.* **2004**, *126*, 10810.

26. Vail, S. A.; Krawczuk, P. J.; Guldi, D. M.; Palkar, A.; Echegoyen, L.; Tomé, J. P. C.; Fazio, M. A.; Schuster, D. I. Energy and electron transfer in polyacetylene-linked zinc-porphyrin-[60]fullerene molecular wires. *Chem. Eur. J.* **2005**, *11*, 3375.

27. Gonzalez-Rodriguez, D.; Claessens, C. G.; Torres, T.; Liu, S.; Echegoyen, L.; Vila, N.; Nonell, S. Tuning photoinduced energy- and electron-transfer events in subphthalocyanine-phthalocyanine dyads. *Chem. Eur. J.* **2005**, *11*, 3881.

28. Wasielewski, M. R. Energy, charge, and spin transport in molecules and self-assembled nanostructures inspired by photosynthesis. *J. Org. Chem.* **2006**, *71*, 5051.

29. El-Khouly, M. E.; Ju, D. K.; Kay, K. Y.; D'Souza, F.; Fukuzumi, S. Supramolecular tetrad of subphthalocyanine-triphenylamine-zinc porphyrin coordinated to fullerene as an "antenna-reaction-center" mimic: formation of a long-lived charge-separated state in nonpolar solvent. *Chem. Eur. J.* **2010**, *16*, 6193.

30. Bottari, G.; Trukhina, O.; Ince, M.; Torres, T. Towards artificial photosynthesis: Supramolecular, donor–acceptor, porphyrin- and phthalocyanine/carbon nanostructure ensembles. *Coord. Chem. Rev.* **2012**, *256*, 2453.

31. Li, J.; Diers, J. R.; Seth, J.; Yang, S. I.; Bocian, D. F.; Holten, D.; Lindsey, J. S. Synthesis and Properties of Star-Shaped Multiporphyrin−Phthalocyanine Light-Harvesting Arrays. *J. Org. Chem.* **1999**, *64*, 9090.

32. Miller, M. A.; Lammi, R. K.; Prathapan, S.; Holten, D.; Lindsey, J. S. A tightly coupled linear array of perylene, bis(porphyrin), and phthalocyanine units that functions as a photoinduced energy-transfer cascade. *J. Org. Chem.* **2000**, *65*, 6634.

33. Jacobs, R.; Stranius, K.; Maligaspe, E.; Lemmetyinen, H.; Tkachenko, N. V.; Zandler, M. E.; D'Souza, F. Syntheses and excitation transfer studies of near-orthogonal free-base porphyrin-ruthenium phthalocyanine dyads and pentad. *Inorg. Chem.* **2012**, *51*, 3656.

34. KC, C. B.; Ohkubo, K.; Karr, P. A.; Fukuzumi, S.; D'Souza, F. A 'two-point' bound zinc porphyrin-zinc phthalocyanine-fullerene supramolecular triad for sequential energy and electron transfer. *Chem. Commun.* **2013**, *49*, 7614.

35. Beletskaya, I.; Tyurin, V. S.; Tsivadze, A. Y.; Guilard, R.; Stern, C. Supramolecular chemistry of metalloporphyrins. *Chem. Rev.* **2009**, *109*, 1659.

36. Ozoemena, K. I.; Zhao, Z.; Nyokong, T. Immobilized cobalt(II) phthalocyanine–cobalt(II) porphyrin pentamer at a glassy carbon electrode: Applications to efficient amperometric sensing of hydrogen peroxide in neutral and basic media. *Electrochem. Commun.* **2005**, *7*, 679.

37. Purrello, R.; Gurrieri, S.; Lauceri, R. Porphyrin assemblies as chemical sensors. *Coord. Chem. Rev.* **1999**, *190-192*, 683.

38. Souto, J.; RodrÍGuez, M. L.; Desaja, J. A.; Aroca, R. Langmuir-Blodgett films of lanthanide bysphthalocyanines: applications as gas sensors. *Int. J. Electron.* **1994**, *76*, 763.

39. Bassoul, P.; Toupance, T.; Simon, J. Semiconductivity and gas-sensing properties of crown-ether-substituted lutetium bisphthalocyanines. *Sens. Actuators, B Chem.* **1995**, *26*, 150.

40. Álvarez, J.; Souto, J.; Rodríguez-Méndez, M. L.; de Saja, J. A. Response of a sensor based on ytterbium bisphthalocyanine Langmuir–Blodgett films to selected herbicides. *Sens. Actuators, B Chem.* **1998**, *48*, 339.

41. Amao, Y.; Asai, K.; Miyakawa, K.; Okura, I. Oxygen sensing using palladium porphyrin with long alkyl chain self-assembled film. *J. Porphyrins Phthalocyanines* **2000**, *04*, 19.

42. Kadish, K. M.; Fremond, L.; Shen, J.; Chen, P.; Ohkubo, K.; Fukuzumi, S.; El Ojaimi, M.; Gros, C. P.; Barbe, J. M.; Guilard, R. Catalytic activity of biscobalt porphyrin-corrole dyads toward the reduction of dioxygen. *Inorg. Chem.* **2009**, *48*, 2571.

43. Kadish, K. M.; Fremond, L.; Ou, Z.; Shao, J.; Shi, C.; Anson, F. C.; Burdet, F.; Gros, C. P.; Barbe, J. M.; Guilard, R. Cobalt(III) corroles as electrocatalysts for the reduction of dioxygen: reactivity of a monocorrole, biscorroles, and porphyrin-corrole dyads. *J. Am. Chem. Soc.* **2005**, *127*, 5625.

44. Oliveri, C. G.; Gianneschi, N. C.; Nguyen, S. T.; Mirkin, C. A.; Stern, C. L.; Wawrzak, Z.; Pink, M. Supramolecular allosteric cofacial porphyrin complexes. *J. Am. Chem. Soc.* **2006**, *128*, 16286.

45. Lee, S. J.; Cho, S. H.; Mulfort, K. L.; Tiede, D. M.; Hupp, J. T.; Nguyen, S. T. Cavity-tailored, self-sorting supramolecular catalytic boxes for selective oxidation. *J. Am. Chem. Soc.* **2008**, *130*, 16828.

46. Fruhbeisser, S.; Grohn, F. Catalytic activity of macroion-porphyrin nanoassemblies. *J. Am. Chem. Soc.* **2012**, *134*, 14267.

47. Jérôme, F.; Gros, C. P.; Tardieux, C.; Barbe, J.-M.; Guilard, R. Synthesis of a 'face-to-face' porphyrin-corrole. A potential precursor of a catalyst for the four-electron reduction of dioxygen. *New J. Chem.* **1998**, *22*, 1327.

48. Kadish, K. M.; Fremond, L.; Burdet, F.; Barbe, J. M.; Gros, C. P.; Guilard, R. Cobalt(IV) corroles as catalysts for the electroreduction of O2: reactions of heterobimetallic dyads containing a face-to-face linked Fe(III) or Mn(III) porphyrin. *J. Inorg. Biochem.* **2006**, *100*, 858.

49. Slagt, V. F.; van Leeuwen, P. W. N. M.; Reek, J. N. H. Multicomponent Porphyrin Assemblies as Functional Bidentate Phosphite Ligands for Regioselective Rhodium-Catalyzed Hydroformylation. *Angew. Chem.* **2003**, *115*, 5777.

50. de la Torre, G.; Vazquez, P.; Agullo-Lopez, F.; Torres, T. Role of structural factors in the nonlinear optical properties of phthalocyanines and related compounds. *Chem. Rev.* **2004**, *104*, 3723.

51. Chen, L.; Hu, R.; Xu, J.; Wang, S.; Li, X.; Li, S.; Yang, G. Third-order nonlinear optical properties of a series of porphyrin-appended europium(III) bis(phthalocyaninato) complexes. *Spectrochim. Acta A Mol. Biomol. Spec.* **2013**, *105*, 577.

52. Ke, H.; Li, W.; Zhang, T.; Zhu, X.; Tam, H. L.; Hou, A.; Kwong, D. W. J.; Wong, W. K. Acetylene bridged porphyrin-monophthalocyaninato ytterbium(III) hybrids with strong two-photon absorption and high singlet oxygen quantum yield. *Dalton Trans.* **2012**, *41*, 4536.

53. Morisue, M.; Ogawa, K.; Kamada, K.; Ohta, K.; Kobuke, Y. Strong two-photon and three-photon absorptions in the antiparallel dimer of a porphyrin-phthalocyanine tandem. *Chem. Commun.* **2010**, *46*, 2121.

54. Soares, A. R. M.; Tomé, J. P. C.; Neves, M. G. P. M. S.; Tomé, A. C.; Cavaleiro, J. A. S.; Torres, T. Synthesis of water-soluble phthalocyanines bearing four or eight D-galactose units. *Carbohydr. Res.* **2009**, *344*, 507.

55. Silva, S.; Pereira, P. M. R.; Silva, P.; Paz, F. A. A.; Faustino, M. A. F.; Cavaleiro, J. A. S.; Tomé, J. P. C. Porphyrin and phthalocyanine glycodendritic conjugates: synthesis, photophysical and photochemical properties. *Chem. Commun.* **2012**, *48*, 3608.

56. Bonnett, R. Photosensitizers of the porphyrin and phthalocyanine series for photodynamic therapy. *Chem. Soc. Rev.* **1995**, *24*, 19.

57. Pereira, J. B.; Carvalho, E. F. A.; Faustino, M. A. F.; Fernandes, R.; Neves, M. G. P. M. S.; Cavaleiro, J. A. S.; Gomes, N. C. M.; Cunha, A.; Almeida, A.; Tomé, J. P. C. Phthalocyanine thio-pyridinium derivatives as antibacterial photosensitizers. *Photochem. Photobiol.* **2012**, *88*, 537.

58. Gomes, M. C.; Woranovicz-Barreira, S. M.; Faustino, M. A. F.; Fernandes, R.; Neves, M. G. P. M. S.; Tomé, A. C.; Gomes, N. C. M.; Almeida, A.; Cavaleiro, J. A. S.; Cunha, A.; Tomé, J. P. C. Photodynamic inactivation of Penicillium chrysogenum conidia by cationic porphyrins. *Photochem. Photobiol. Sci.* **2011**, *10*, 1735.

59. Tavares, A.; Dias, S. R. S.; Carvalho, C. M. B.; Faustino, M. A. F.; Tomé, J. P. C.; Neves, M. G. P. M. S.; Tomé, A. C.; Cavaleiro, J. A. S.; Cunha, A.; Gomes, N. C. M.; Alves, E.; Almeida, A. Mechanisms of photodynamic inactivation of a gram-negative recombinant bioluminescent bacterium by cationic porphyrins. *Photochem. Photobiol. Sci.* **2011**, *10*, 1659.

60. Silva, J. N.; Bosca, F.; Tomé, J. P. C.; Silva, E. M. P.; Neves, M. G. P. M. S.; Cavaleiro, J. A. S.; Patterson, L. K.; Filipe, P.; Maziere, J. C.; Santus, R.; Morliere, P. Tricationic porphyrin conjugates: evidence for chain-structure-dependent relaxation of excited singlet and triplet States. *J. Phys. Chem. B* **2009**, *113*, 16695.

61. Agirtas, S.; Ion, R. M.; Bekaroglu, O. Spectral study of the supramolecular assemblies porphyrins-phthalocyanines. *Mater. Sci. Eng., C* **2000**, *7*, 105.

62. Bao, G.; Wang, W.; Mao, Y.; Lu, F. Raman spectroscopic characteristics of phthalocyanine in mixed [5-(4-hydroxyphenyl)-10,15,20-tris(4-octyloxyphenyl)porphyrinato]-(phthalocyaninato) rare earth triple-deckers. *Spectrochim. Acta A Mol. Biomol. Spec.* **2013**, *102*, 275.

63. Bian, Y.; Chen, X.; Wang, D.; Choi, C. F.; Zhou, Y.; Zhu, P.; Ng, D. K. P.; Jiang, J.; Weng, Y.; Li, X. Porphyrin-appended europium(III) bis(phthalocyaninato) complexes: synthesis, characterization, and photophysical properties. *Chem. Eur. J.* **2007**, *13*, 4169.

64. Zhao, Z.; Ozoemena, K. I.; Maree, D. M.; Nyokong, T. Synthesis and electrochemical studies of a covalently linked cobalt(II) phthalocyanine-cobalt(II) porphyrin conjugate. *Dalton Trans.* **2005**, 1241.

65. Zhao, Z.; Poon, C.-T.; Wong, W.-K.; Wong, W.-Y.; Tam, H.-L.; Cheah, K.-W.; Xie, T.; Wang, D. Synthesis, Photophysical Characterization, and Surface Photovoltage Spectra of

Windmill-Shaped Phthalocyanine–Porphyrin Heterodimers and Heteropentamers. *Eur. J. Inorg. Chem.* **2008**, *2008*, 119.

66. Leng, X.; Choi, C. F.; Lo, P. C.; Ng, D. K. P. Assembling a mixed phthalocyanine-porphyrin array in aqueous media through host-guest interactions. *Org. Lett.* **2007**, *9*, 231.
67. Berber, G.; Cammidge, A. N.; Chambrier, I.; Cook, M. J.; Hough, P. W. Controlled synthesis of ruthenium phthalocyanines and their use in the construction of supramolecular arrays. *Tetrahedron Lett.* **2003**, *44*, 5527.
68. Cammidge, A. N.; Berber, G.; Chambrier, I.; Hough, P. W.; Cook, M. J. Octaalkylphthalocyaninato ruthenium(II) complexes with mixed axial ligands and supramolecular porphyrin : phthalocyanine structures derived from them. *Tetrahedron* **2005**, *61*, 4067.
69. Chabach, D.; DeCian, A.; Fischer, J.; Weiss, R.; Bibout, M. E. M. induce. *Angew. Chem. Int. Ed.* **1996**, *35*, 898.
70. Chabach, D.; Tahiri, M.; DeCian, A.; Fischer, J.; Weiss, R.; Bibout, M. E. M. Tervalent-Metal Porphyrin-Phthalocyanine Heteroleptic Sandwich-Type Complexes - Synthesis, Structure, and Spectroscopic Characterization of Their Neutral, Singly-Oxidized, and Singly-Reduced States. *J. Am. Chem. Soc.* **1995**, *117*, 8548.
71. Gusev, A. V.; Danilov, E. O.; Rodgers, M. A. J. Association Complexes between Cationic Metallophthalocyanines and Anionic Metalloporphyrins II: Ultrafast Studies of Excited State Dynamics. *J. Phys. Chem. A* **2002**, *106*, 1993.
72. Gusev, A. V.; Rodgers, M. A. J. Association Complexes between Cationic Metallophthalocyanines and Anionic Metalloporphyrins I: Spectrometric Studies of Electronic Interactions. *J. Phys. Chem. A* **2002**, *106*, 1985.
73. Jiang, J. Z.; Lau, R. L. C.; Chan, T. W. D.; Mak, T. C. W.; Ng, D. K. P. Synthesis and spectroscopic properties of heteroleptic sandwich-type (phthalocyaninato)(porphyrinato)lanthanide(III) complexes. *Inorg. Chim. Acta* **1997**, *255*, 59.
74. Jiang, J. Z.; Liu, W.; Law, W. F.; Ng, D. K. P. Heteroleptic triple-decker (phthalocyaninato)(porphyrinato)europium(III) complexes: synthesis and electrochemical study. *Inorg. Chim. Acta* **1998**, *268*, 49.
75. Jiang, J.; Xie, J.; Choi, M. T. M.; Yan, Y.; Sun, S.; Ng, D. K. P. Double-decker Yttrium(III) Complexes with Phthalocyaninato and Porphyrinato Ligands. *J. Porphyrins Phthalocyanines* **1999**, *03*, 322.
76. Kandhadi, J.; Kanaparthi, R. K.; Giribabu, L. Germanium(IV) phthalocyanine-porphyrin based hetero trimers: synthesis, spectroscopy and photochemistry. *J. Porphyrins Phthalocyanines* **2012**, *16*, 282.
77. Kwag, G.; Park, E.; Kim, S. Self-assembled and alternative porphyrin-phthalocyanine array. *Bull. Korean Chem. Soc.* **2004**, *25*, 298.
78. Li, X. Y.; Ng, D. K. P. Self-assembly of meso-pyridylporphyrins and zinc phthalocyanines through axial coordination. *Eur. J. Inorg. Chem.* **2000**, *2000*, 1845.

79. Liu, J. X.; Xu, L. G.; Shen, S. Y.; Zhou, Q. F.; Li, T. K.; Xu, H. J. Novel Langmuir-Blodgett-Films, Consisting of Amphiphilic Zinc Phthalocyanine and Hydrophobic Porphyrin. *J. Photochem. Photobiol., A Chem.* **1993**, *71*, 275.

80. Maligaspe, E.; Kumpulainen, T.; Lemmetyinen, H.; Tkachenko, N. V.; Subbaiyan, N. K.; Zandler, M. E.; D'Souza, F. Ultrafast singlet-singlet energy transfer in self-assembled via metal-ligand axial coordination of free-base porphyrin-zinc phthalocyanine and free-base porphyrin-zinc naphthalocyanine dyads. *J. Phys. Chem. A* **2010**, *114*, 268.

81. Morisue, M.; Kobuke, Y. Tandem cofacial stacks of porphyrin-phthalocyanine dyads through complementary coordination. *Chem. Eur. J.* **2008**, *14*, 4993.

82. Pereira, A. M. V. M.; Hausmann, A.; Tomé, J. P. C.; Trukhina, O.; Urbani, M.; Neves, M. G. P. M. S.; Cavaleiro, J. A. S.; Guldi, D. M.; Torres, T. Porphyrin-phthalocyanine/pyridylfullerene supramolecular assemblies. *Chem. Eur. J.* **2012**, *18*, 3210.

83. Sun, Y. P.; Zhang, X.; Sun, C. Q.; Wang, Z. Q.; Shen, J. C.; Wang, D. J.; Li, T. J. Supramolecular assembly of alternating porphyrin and phthalocyanine layers based on electrostatic interactions. *Chem. Commun.* **1996**, 2379.

84. Ali, H.; van Lier, J. E. An efficient method for the synthesis of C–C connected phthalocyanine–porphyrin oligomers. *Tetrahedron Lett.* **2009**, *50*, 1113.

85. Bartelmess, J.; Soares, A. R. M.; Martinez-Diaz, M. V.; Neves, M. G. P. M. S.; Tomé, A. C.; Cavaleiro, J. A. S.; Torres, T.; Guldi, D. M. Panchromatic light harvesting in single wall carbon nanotube hybrids-immobilization of porphyrin-phthalocyanine conjugates. *Chem. Commun.* **2011**, *47*, 3490.

86. Calvete, M. J. F.; Tomé, J. P. C.; Cavaleiro, J. A. S. Synthesis and Characterization of New Cross-like Porphyrin-Naphthalocyanine and Porphyrin-Phthalocyanine Pentads. *J. Heterocycl. Chem.* **2014**, *51*, E202.

87. Enes, R. F.; Cid, J. J.; Hausmann, A.; Trukhina, O.; Gouloumis, A.; Vazquez, P.; Cavaleiro, J. A. S.; Tomé, A. C.; Guldi, D. M.; Torres, T. Synthesis and photophysical properties of fullerene-phthalocyanine-porphyrin triads and pentads. *Chem. Eur. J.* **2012**, *18*, 1727.

88. Ermilov, E. A.; Leng, X.; Roder, B.; Ng, D. K. P. Preparation and photophysical properties of a tetraethylene glycol-linked phthalocyanine-porphyrin dyad and triad. *New J. Chem.* **2013**, *37*, 1746.

89. Ermilov, E. A.; Tannert, S.; Werncke, T.; Choi, M. T. M.; Ng, D. K. P.; Röder, B. Photoinduced electron and energy transfer in a new porphyrin–phthalocyanine triad. *Chem. Phys.* **2006**, *328*, 428.

90. Fortage, J.; Goransson, E.; Blart, E.; Becker, H. C.; Hammarstrom, L.; Odobel, F. Strongly coupled zinc phthalocyanine-tin porphyrin dyad performing ultra-fast single step charge separation over a 34 A distance. *Chem. Commun.* **2007**, 4629.

91. Fournier, T.; Liu, Z.; Tran-Thi, T. H.; Houde, D.; Brasseur, N.; La Madeleine, C.; Langlois, R.; van Lier, J. E.; Lexa, D. Influence of molecular oxygen on the charge transfer properties of a Co(II)porphyrin-Al(III)phthalocyanine aggregate. Excited states dynamics and photobiological activities. *J. Phys. Chem. A* **1999**, *103*, 1179.

92. Gaspard, S.; Giannotti, C.; Maillard, P.; Schaeffer, C.; Tran-Thi, T.-H. The first synthesis of covalently linked mixed dimer complexes containing phthalocyanine and porphyrin. *J. Chem. Soc., Chem. Commun.* **1986**, 1239.

93. Hausmann, A.; Soares, A. R. M.; Martinez-Diaz, M. V.; Neves, M. G. P. M. S.; Tomé, A. C.; Cavaleiro, J. A. S.; Torres, T.; Guldi, D. M. Transduction of excited state energy between covalently linked porphyrins and phthalocyanines. *Photochem. Photobiol. Sci.* **2010**, *9*, 1027.

94. Yang, S. I.; Li, J.; Cho, H. S.; Kim, D.; Bocian, D. F.; Holten, D.; Lindsey, J. S. Synthesis and excited-state photodynamics of phenylethyne-linked porphyrin–phthalocyanine dyads. *J. Mater. Chem.* **2000**, *10*, 283.

95. Kameyama, K.; Satake, A.; Kobuke, Y. Light-harvesting composites of directly connected porphyrin–phthalocyanine dyads and their coordination dimers. *Tetrahedron Lett.* **2004**, *45*, 7617.

96. Ito, F.; Ishibashi, Y.; Khan, S. R.; Miyasaka, H.; Kameyama, K.; Morisue, M.; Satake, A.; Ogawa, K.; Kobuke, Y. Photoinduced electron transfer and excitation energy transfer in directly linked zinc porphyrin/zinc phthalocyanine composite. *J. Phys. Chem. A* **2006**, *110*, 12734.

97. KC, C. B.; Stranius, K.; D'Souza, P.; Subbaiyan, N. K.; Lemmetyinen, H.; Tkachenko, N. V.; D'Souza, F. Sequential Photoinduced Energy and Electron Transfer Directed Improved Performance of the Supramolecular Solar Cell of a Zinc Porphyrin-Zinc Phthalocyanine Conjugate Modified TiO2 Surface. *J. Phys. Chem. C* **2013**, *117*, 763.

98. Li, J. Z.; Lindsey, J. S. Efficient synthesis of light-harvesting arrays composed of eight porphyrins and one phthalocyanine. *J. Org. Chem.* **1999**, *64*, 9101.

99. Li, L.; Shen, S. Y.; Yu, Q.; Zhou, Q. F.; Xu, H. J. Photoinduced Electron-Transfer and Charge Separation in Anthraquinone-Substituted Porphyrin Phthalocyanine Heterodimer. *J. Chem. Soc., Chem. Commun.* **1991**, 619.

100. Li, X. Y.; Zhou, Q. F.; Tian, H. J.; Xu, H. J. Synthesis and photophysical properties of porphyrin-phthalocyanine heterodimer linked by piperazine. *Chin. J. Chem* . **1998**, *16*, 97.

101. Liu, M. O.; Hu, A. T. Microwave-assisted synthesis of phthalocyanine–porphyrin complex and its photoelectric conversion properties. *J. Organomet. Chem.* **2004**, *689*, 2450.

102. Osati, S.; Safari, N.; Jamaat, P. R. Synthesis and characterization of three covalently linked porphyrin-phthalocyanine pentamers with nucleophilic substitution. *Inorg. Chim. Acta* **2010**, *363*, 2180.

103. Pereira, A. M. V. M.; Soares, A. R. M.; Hausmann, A.; Neves, M. G. P. M. S.; Tomé, A. C.; Silva, A. M. S.; Cavaleiro, J. A. S.; Guldi, D. M.; Torres, T. Distorted fused porphyrin-phthalocyanine conjugates: synthesis and photophysics of supramolecular assembled systems with a pyridylfullerene. *Phys. Chem. Chem. Phys.* **2011**, *13*, 11858.

104. Soares, A. R. M.; Martinez-Diaz, M. V.; Bruckner, A.; Pereira, A. M. V. M.; Tomé, J. P. C.; Alonso, C. M. A.; Faustino, M. A. F.; Neves, M. G. P. M. S.; Tomé, A. C.; Silva, A. M. S.; Cavaleiro, J. A. S.; Torres, T.; Guldi, D. M. Synthesis of novel N-linked porphyrin-phthalocyanine dyads. *Org. Lett.* **2007**, *9*, 1557.

105. Sutton, J. M.; Boyle, R. W. First synthesis of porphyrin-phthalocyanine heterodimers with a direct ethynyl linkage. *Chem. Commun.* **2001**, 2014.

106. Tannert, S.; Ermilov, E. A.; Vogel, J. O.; Choi, M. T. M.; Ng, D. K. P.; Roder, B. The influence of solvent polarity and metalation on energy and electron transfer in porphyrin-phthalocyanine heterotrimers. *J. Phys. Chem. B* **2007**, *111*, 8053.

107. Tasso, T. T.; Moreira, W. C. Heteroarray of cobalt(II) tetrasulfophthalocyanine and cobalt(II) tetrakis(N-methyl-4-pyridyl)porphyrin: synthesis, isolation and electronic properties. *J. Porphyrins Phthalocyanines* **2012**, *16*, 244.

108. Tomé, J. P. C.; Pereira, A. M. V. M.; Alonso, C. M. A.; Neves, M. G. P. M. S.; Tomé, A. C.; Silva, A. M. S.; Cavaleiro, J. A. S.; Martínez-Díaz, M. V.; Torres, T.; Rahman, G. M. A.; Ramey, J.; Guldi, D. M. Synthesis and Photophysical Studies of New Porphyrin-Phthalocyanine Dyads with Hindered Rotation. *Eur. J. Org. Chem.* **2006**, *2006*, 257.

109. Tran-Thi, T. H.; Lipskier, J. F.; Simoes, M.; Palacin, S. Photoinduced charge transfer in semi-amphiphilic porphyrin-phthalocyanine mixed dimers. *Thin Solid Films* **1992**, *210-211*, 150.

110. Zhao, Z.; Cammidge, A. N.; Cook, M. J. Towards black chromophores: mu-oxo linked phthalocyanine-porphyrin dyads and phthalocyanine-subphthalocyanine dyad and triad arrays. *Chem. Commun.* **2009**, 7530.

111. Zhao, Z.; Cammidge, A. N.; Hughes, D. L.; Cook, M. J. Modular face-to-face assembly of multichromophore arrays that absorb across the complete UV-visible spectrum and into the near-IR. *Org. Lett.* **2010**, *12*, 5138.

112. Zhao, Z.; Nyokong, T.; Maree, M. D. Synthesis and photochemical characterization of a zinc phthalocyanine-zinc porphyrin heterotrimer and heterononamer. *Dalton Trans.* **2005**, 3732.

113. Zhao, Z. X.; Ogunsipe, A. O.; Maree, M. D.; Nyokong, T. Synthesis and photophysical properties of a covalently linked porphyrin-phthalocyanine conjugate. *J. Porphyrins Phthalocyanines* **2005**, *9*, 186.

114. Wei, L.; Padmaja, K.; Youngblood, W. J.; Lysenko, A. B.; Lindsey, J. S.; Bocian, D. F. Diverse redox-active molecules bearing identical thiol-terminated tripodal tethers for studies of molecular information storage. *J. Org. Chem.* **2004**, *69*, 1461.

115. Yamada, Y.; Okamoto, M.; Furukawa, K.; Kato, T.; Tanaka, K. Switchable intermolecular communication in a four-fold rotaxane. *Angew. Chem. Int. Ed.* **2012**, *51*, 709.

116. Drain, C. M.; Varotto, A.; Radivojevic, I. Self-organized porphyrinic materials. *Chem. Rev.* **2009**, *109*, 1630.

117. Moan, J.; Peng, Q. An Outline of the History of PDT. *Photodynamic Therapy* **2006**, *2*, 1.

118. Ormond, A. B.; Freeman, H. Dye Sensitizers for Photodynamic Therapy. *Materials* **2013**, *6*, 817.

119. Vinodh, M.; Alipour, F. H.; Mohamod, A. A.; Al-Azemi, T. F. Molecular assemblies of porphyrins and macrocyclic receptors: recent developments in their synthesis and applications. *Molecules* **2012**, *17*, 11763.

120. Lo, P. C.; Leng, X. B.; Ng, D. K. P. Hetero-arrays of porphyrins and phthalocyanines. *Coord. Chem. Rev.* **2007**, *251*, 2334.

121. Lu, G. F.; Ou, Z. P.; Jiang, J. Z.; Bian, Y. Z. Nanoscale Hollow Spheres of an Amphiphilic Mixed (Phthalocyaninato)(porphyrinato)europium Double-Decker Complex. *Eur. J. Inorg. Chem.* **2010**, *2010*, 753.

122. Lipskier, J. F.; Tran-Thi, T. H. Supramolecular assemblies of porphyrins and phthalocyanines bearing oppositely charged substituents. First evidence of heterotrimer formation. *Inorg. Chem.* **1993**, *32*, 722.

123. Radivojevic, I.; Bazzan, G.; Burton-Pye, B. P.; Ithisuphalap, K.; Saleh, R.; Durstock, M. F.; Francesconi, L. C.; Drain, C. M. Zirconium((IV)) and Hafnium((IV)) Porphyrin and Phthalocyanine Complexes as New Dyes for Solar Cell Devices. *J. Phys. Chem. C* **2012**, *116*, 15867.

124. Milic, T.; Garno, J. C.; Batteas, J. D.; Smeureanu, G.; Drain, C. M. Self-organization of self-assembled tetrameric porphyrin arrays on surfaces. *Langmuir* **2004**, *20*, 3974.

125. Jurow, M.; Varotto, A.; Manichev, V.; Travlou, N. A.; Giannakoudakis, D. A.; Drain, C. M. Self-organized nanostructured materials of alkylated phthalocyanines and underivatized C60 on ITO. *RSC Advances* **2013**, *3*, 21360.

126. Singh, S.; Aggarwal, A.; Farley, C.; Hageman, B. A.; Batteas, J. D.; Drain, C. M. Hierarchical organization of a robust porphyrin cage self-assembled by hydrogen bonds. *Chem. Commun.* **2011**, *47*, 7134.

127. Chan, Y. H.; Schuckman, A. E.; Perez, L. M.; Vinodu, M.; Drain, C. M.; Batteas, J. D. Synthesis and characterization of a thiol-tethered tripyridyl porphyrin on Au(111). *J. Phys. Chem. C* **2008**, *112*, 6110.

128. Jurow, M.; Schuckman, A. E.; Batteas, J. D.; Drain, C. M. Porphyrins as Molecular Electronic Components of Functional Devices. *Coord. Chem. Rev.* **2010**, *254*, 2297.

129. Garno, J. C.; Xu, C.; Bazzan, G.; Batteas, J. D.; Drain, C. M. In *Metal-Containing and Metallosupramolecular Polymers and Materials*; American Chemical Society: **2006**; Vol. 928, p 168.

130. Schuckman, A. E.; Ewers, B. W.; Yu, L. H.; Tomé, J. P. C.; Pérez, L. M.; Drain, C. M.; Kushmerick, J. G.; Batteas, J. D. Utilizing Nearest-Neighbor Interactions To Alter Charge Transport Mechanisms in Molecular Assemblies of Porphyrins on Surfaces. *J. Phys. Chem. C* **2015**, *119*, 13569.

131. Gryko, D.; Li, J. Z.; Diers, J. R.; Roth, K. M.; Bocian, D. F.; Kuhr, W. G.; Lindsey, J. S. Studies related to the design and synthesis of a molecular octal counter. *J. Mater. Chem.* **2001**, *11*, 1162.

132. Lysenko, A. B.; Malinovskii, V. L.; Padmaja, K.; Wei, L. Y.; Diers, J. R.; Bocian, D. F.; Lindsey, J. S. Multistate molecular information storage using S-acetylthio-derivatized dyads of triple-decker sandwich coordination compounds. *J. Porphyrins Phthalocyanines* **2005**, *9*, 491.

133. Padmaja, K.; Youngblood, W. J.; Wei, L.; Bocian, D. F.; Lindsey, J. S. Triple-decker sandwich compounds bearing compact triallyl tripods for molecular information storage applications. *Inorg. Chem.* **2006**, *45*, 5479.

134. Schweikart, K. H.; Malinovskii, V. L.; Diers, J. R.; Yasseri, A. A.; Bocian, D. F.; Kuhr, W. G.; Lindsey, J. S. Design, synthesis, and characterization of prototypical multistate counters in three distinct architectures. *J. Mater. Chem.* **2002**, *12*, 808.

135. Schweikart, K. H.; Malinovskii, V. L.; Yasseri, A. A.; Li, J.; Lysenko, A. B.; Bocian, D. F.; Lindsey, J. S. Synthesis and characterization of bis(S-acetylthio)-derivatized europium triple-decker monomers and oligomers. *Inorg. Chem.* **2003**, *42*, 7431.

136. Ambroise, A.; Wagner, R. W.; Rao, P. D.; Riggs, J. A.; Hascoat, P.; Diers, J. R.; Seth, J.; Lammi, R. K.; Bocian, D. F.; Holten, D.; Lindsey, J. S. Design and synthesis of porphyrin-based optoelectronic gates. *Chem. Mater.* **2001**, *13*, 1023.

137. Engelkamp, H.; Middelbeek, S.; Nolte, R. J. Self-assembly of disk-shaped molecules to coiled-coil aggregates with tunable helicity. *Science* **1999**, *284*, 785.

138. Gao, J.; Li, D.; Chen, Y. Controllable Self-assembly of Sandwich-type Mixed (phthalocyaninato)(porphyrinato) Rare Earth Triple-Decker Complexes. *J. Inorg. Organomet. P.* **2011**, *21*, 876.

139. Lu, G.; Chen, Y.; Zhang, Y.; Bao, M.; Bian, Y.; Li, X.; Jiang, J. Morphology controlled self-assembled nanostructures of sandwich mixed (phthalocyaninato)(porphyrinato) europium triple-deckers. Effect of hydrogen bonding on tuning the intermolecular interaction. *J. Am. Chem. Soc.* **2008**, *130*, 11623.

140. Balakumar, A.; Lysenko, A. B.; Carcel, C.; Malinovskii, V. L.; Gryko, D. T.; Schweikart, K. H.; Loewe, R. S.; Yasseri, A. A.; Liu, Z.; Bocian, D. F.; Lindsey, J. S. Diverse redox-active molecules bearing O-, S-, or Se-terminated tethers for attachment to silicon in studies of molecular information storage. *J. Org. Chem.* **2004**, *69*, 1435.

141. Goransson, E.; Boixel, J.; Fortage, J.; Jacquemin, D.; Becker, H. C.; Blart, E.; Hammarstrom, L.; Odobel, F. Long-range electron transfer in zinc-phthalocyanine-oligo(phenylene-ethynylene)-based donor-bridge-acceptor dyads. *Inorg. Chem.* **2012**, *51*, 11500.

142. Zhu, P.; Zhang, X.; Wang, H.; Zhang, Y.; Bian, Y.; Jiang, J. Ferrocene-decorated (phthalocyaninato)(porphyrinato) double- and triple-decker rare earth complexes: synthesis, structure, and electrochemical properties. *Inorg. Chem.* **2012**, *51*, 5651.

143. Cheng, K. F.; Thai, N. A.; Grohmann, K.; Teague, L. C.; Drain, C. M. Tessellation of porphyrazines with porphyrins by design. *Inorg. Chem.* **2006**, *45*, 6928.

144. Smeureanu, G.; Aggarwal, A.; Soll, C. E.; Arijeloye, J.; Malave, E.; Drain, C. M. Enhanced catalytic activity and unexpected products from the oxidation of cyclohexene by organic nanoparticles of 5,10,15,20-tetrakis-(2,3,4,5,6-pentafluorophenyl)porphyrinatoiron(III) in water by using O2. *Chem. Eur. J.* **2009**, *15*, 12133.

145. Meunier, B. Metalloporphyrins as versatile catalysts for oxidation reactions and oxidative DNA cleavage. *Chem. Rev.* **1992**, *92*, 1411.

146. Nam, W.; Lim, M. H.; Oh, S.-Y.; Lee, J. H.; Lee, H. J.; Woo, S. K.; Kim, C.; Shin, W. Remarkable Anionic Axial Ligand Effects of Iron(III) Porphyrin Complexes on the Catalytic Oxygenations of Hydrocarbons by H2O2 and the Formation of Oxoiron(IV) Porphyrin Intermediates bym-Chloroperoxybenzoic Acid. *Angew. Chem. Int. Ed.* **2000**, *39*, 3646.

147. Sheldon, R. A., Ed.; *Metalloporphyrins in Catalytic Oxidations*, Marcel Dekker: New York, NY, **1994**.

148. Collman, J. P.; Wagenknecht, P. S.; Hutchison, J. E. Molecular Catalysts for Multielectron Redox Reactions of Small Molecules: The"Cofacial Metallodiporphyrin" Approach. *Angew. Chem. Int. Ed.* **1994**, *33*, 1537.

149. Kadish, K. M.; Shao, J.; Ou, Z.; Fremond, L.; Zhan, R.; Burdet, F.; Barbe, J. M.; Gros, C. P.; Guilard, R. Electrochemistry, spectroelectrochemistry, chloride binding, and O2 catalytic reactions of free-base porphyrin-cobalt corrole dyads. *Inorg. Chem.* **2005**, *44*, 6744.

150. Menting, R.; Lau, J. T. F.; Xu, H.; Ng, D. K. P.; Roder, B.; Ermilov, E. A. Formation and photoinduced processes of a self-assembled subphthalocyanine-porphyrin-phthalocyanine supramolecular complex. *Chem. Commun.* **2012**, *48*, 4597.

151. *Web of Science*; Thomson Reuters: New York, NY, **2015**; http://www.webofknowledge.com.

## Chapter 2. Synthesis and Characterization of a Self-Assembled Porphyrin Cage[§]

### 2.1. Introduction.

Given that the spontaneous assembly of molecular units into higher order systems is so crucial to the development of advanced materials and devices, it is important to explore compounds that can satisfy the relevant design criteria at every level of hierarchical structure. Specific interactions between molecules can offer the ability to fine-tune processes such as electron and energy transport, but may have little influence over longer-range order. Other motifs must then be incorporated which will govern the tertiary structure in predictable ways. The study described here represents one attempt at simultaneously addressing these competing design challenges.

Porphyrinoids appended with H-bond motifs have been designed to assemble into diverse arrangements such as rosettes, squares, tapes, and nanoparticles, yielding materials for solar energy harvesting, photonic devices, sensors, catalysts, and biomimetic electron transport models.[2-8] In addition to directing supramolecular architectures, the functional groups on the macrocycle and the mode of assembly can modulate the photophysical and chemical properties of the arrays. It is also possible to construct responsive H-bond materials, in which environmental conditions such as temperature and solvent can modulate the supramolecular structure, the catalytic host-guest chemistry, or the electronic communication between subunits.[9-12] While functional materials of H-bond assembled porphyrins have demonstrated utility,[2] dyes bearing rigidly attached hydrogen bonding motifs can be difficult to synthesize.[6-8]

---

[§] This chapter is adapted from an article published in *Chemical Communications*.[1]

In this chapter we describe the synthesis of porphyrins appended with four rigid hydrogen bonding motifs on the *meso* positions and their subsequent self-assembly into cofacial cages *via* bis(decyl)melamine mediators. The cages assembled in this manner are then drop cast onto a mica surface, where the hydrocarbon chains on the melamine regulate the formation of thin films. These steps thus span the first three levels of hierarchical structure, from porphyrin design and synthesis (primary), to cage formation through hydrogen bonding (secondary), and finally to thin film deposition and organization (tertiary).

## 2.2. Materials and Methods

All reagents were obtained from commercial sources and used without purification. 5-Formyl-6-methyluracil and 1-ethoxymethyl-5-formyl-6-methyluracil were synthesized according to previous literature procedures.[3,4,13] NMR ($^{1}$H and $^{13}$C) Spectra were recorded on a Brüker Avance 500 MHz spectrometer. Variable temperature NMR measurements were performed from the range 279 K to 323 K. Mass spectrometry analyses were performed at the CUNY Mass Spectrometry Facility at Hunter College by electrospray ionization on an Agilent Technologies G6520 Q-TOF instrument and Agilent 1200 HPLC system. The electrospray ionization was done in methanol, with 0.1% formic acid.

UV-visible spectra were recorded on a Varian Bio3 spectrophotometer. Steady-state fluorescence spectra and fluorescence lifetimes were measured with a Fluorolog τ3 TCSPC (time correlated single photon counting) from Jobin-SPEX Instrument S. A., (Horiba Scientific. Inc.) TCSPC fluorescence lifetime measurements used a 405 nm NanoLED laser for excitation, with a 2nm bandpass, an average power of 13.6 pJ/pulse, and a pulse width <200 ps to excite the molecules. The data was fit to a multiexponential decay equation using the Decay Analysis Software package (v. 6.4) bundled with the instrument. The fluorescence signal was recorded at

651 nm. Dynamic light scattering (DLS) used a Precision Detector PD2000DLS Cool-Batch instrument in batch mode at 25 $^{o}$C to determine size of the aggregates and the cages.

Samples for AFM were prepared in the following manner: freshly cleaved sheets of mica, approximately 2.5×2.5 cm, were placed in a clean Petri dish on a flat surface. For each sample, the given solution was drawn up into a pipette, and then a single drop was drop cast onto a mica square. In the voids between the samples, dry THF was deposited via pipette, taking care that the THF did not contact any of the samples. A watch glass was then placed over the Petri dish, sealing the environment so the evaporating THF could not escape. The samples were allowed to sit for 24 hrs, and then examined using an Asylum Research MFP-3D™ Stand Alone AFM in contact mode under ambient conditions. Images collected from the AFM were analyzed using a program called "WSxM 4.0 Develop 11.4", developed by Nanotec Electronica S.L. All samples were imaged with a Park 0.1 silicon nitride tip (nominal k = 0.1 N $m^{-1}$) in contact mode.

### 2.2.1. Porphyrin Synthesis

Uracylporphyrin **1b** and *N*-alkyluracyl porphyrin **2b** were synthesized from 5-formyl-6-methyluracil[14] and 1-ethoxymethyl-5-formyl-6-methyluracil[3-5,9-12,15] under Adler conditions with $Zn(OAc)_2$ (**Scheme 2.1**). *N*-alkylation of the uracil inhibits tautomerization at this position, diminishes unproductive H-bond formation, and improves solubility. The free bases, **1a** and **2a**, were obtained by demetallation of the zinc complex. The bis(decyl)melamine (IUPAC name: 2,4-di(*n*-decylamino)-6-amino-1,3,5-triazine) was prepared similarly to previous reports.[16,17]

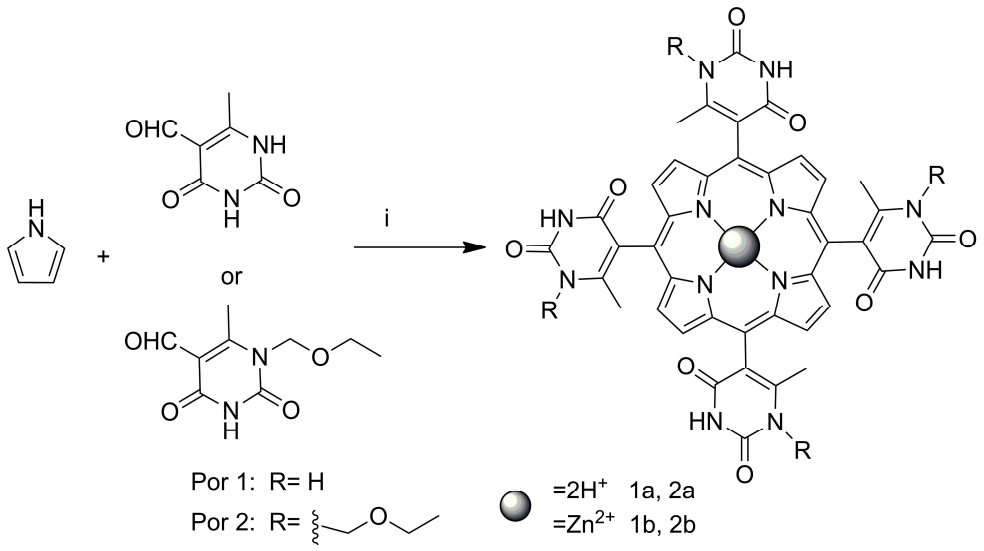


**Scheme 2.1**. Synthesis of uracylporphyrin. (i) reflux 10 h in 10% nitrobenzene in acetic acid with 0.05 M $Zn(OAc)_2$. The porphyrin is prepared as a mixture of the four atropisomers (αααα, ααaβ, ααββ, αβαβ) since the uracyl moieties are nominally orthogonal to the macrocycle plane.

### 2.2.2. Cage Assembly

Solutions of each of the porphyrins (**1a**, **1b**, **2a**, and **2b**) with bis(decyl)melamine in dry THF were made at concentrations around 38-42 μM. The alkoxy-substituted compounds (**2a** and **2b**) exhibited much greater solubility in this solvent, and we primarily focus on those systems here. To accelerate the dissolution and H-bond formation with bis(decyl)melamine, the solutions were sonicated for *ca*. five minutes and then transferred to 3.5 mL quartz cuvettes. Nitrogen gas was then purged through the solution for *ca*. 10 minutes to ensure the complete removal of oxygen. The 1.0 cm pathlength cuvette was then sealed with a Teflon cap and wrapped with Parafilm to make sure the system remained closed. The solutions were kept and monitored spectroscopically for several days, first being held at room temperature to ensure equilibrium, and then being heated continuously at 45-50 °C to overcome the barrier to atropisomer interconversion (*vide infra*) and aid in the formation of the thermodynamically stable cage structures (**Scheme 2.2**). Solutions without any bis(decyl)melamine were also observed under nearly identical conditions as a control.

## 2.3. Results and Discussion

There are two notable features of this methodology: (1) the porphyrins are made in one step, and (2) the supramolecular dynamics are significantly reduced because all four *meso*-uracyls participate cooperatively in the assembly process.[2-8] Each cage is formed from the co-facial arrangement of two porphyrins held together by four bis(decyl)melamine units as intermediates (**Scheme 2.2**). NMR, DLS, and photophysical spectroscopy in solution all point to the formation of the cages, and AFM studies elucidate the self-organization of the materials cast onto mica.

### 2.3.1. Atropisomers

Both porphyrins **1** and **2** show atropisomerism due to steric hindrance to rotation of the uracyl group created by interactions between the uracyl 2-carbonyl and 6-methyl groups and the pyrrole βH. The most stable self-assembled cage structure requires both porphyrins to be in the αααα arrangement. The thermodynamics of atropisomerization were determined for **2b** in deuterated methanol. The $^{1}$H NMR spectra of porphyrin **2** has distinct resonances for the uracyl 6-

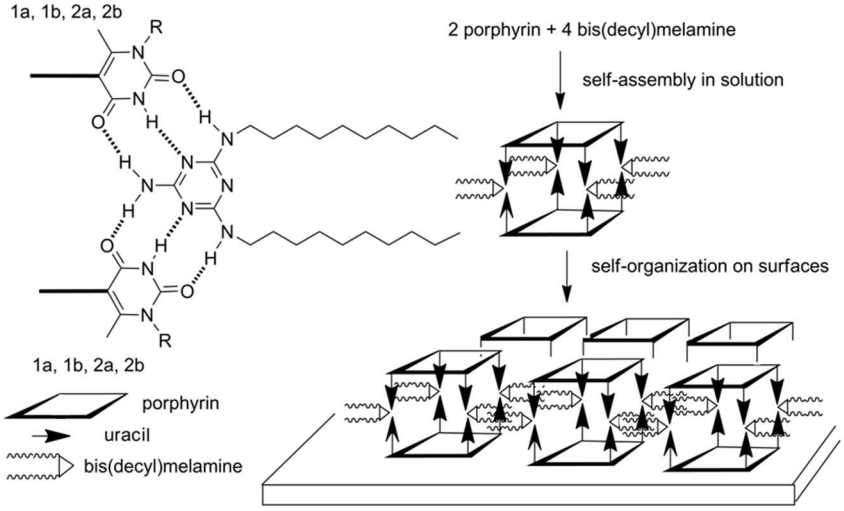


**Scheme 2.2**. Prolonged heating of two equivalents of a uracylporphyrin with four equivalents of the complementary bis(decyl)melamine (left) results in formation of the αααα atropisomer and its self-assembly into the cage in solution. The decyl groups on the melamine derivative mediate formation of monolayer films of the cage on mica (right).

methyl due to ring current effects and the 1-N methylene groups. There should be six resonances for both the 6-methyl near 2 ppm, and the 1-N methylene group, observed as complex multiplets near 5 ppm. The ratio of the resonances for the 6-methyl group was used to determine the ratio of the four atropisomers, which in the initially prepared porphyrin was approximately the expected 1:4:2:1 for αααα:αααβ:ααββ:αβαβ. The rotational barrier was determined for porphyrin **2b** by performing variable temperature NMR from 5 °C to 50 °C in MeOD-$d_4$.[18] The value of K was determined by shift in the (N-$CH_2$-O) protons of the alkoxy group. The equilibrium constant was determined by a Van 't Hoff plot (ln K *vs*. 1/T) and the $\Delta G^{\ddagger}$ was found to be about 123 kJ/mol for **2b**.[19,20] The $\Delta G^{\ddagger}$ for the free base is typically less by about 20 kJ/mol because the metalloporphyrin is more rigid.[21-23] The poor solubility of porphyrins **1a** and **1b** made similar analysis difficult, but the barriers should be about the same.

The porphyrins are poorly soluble in dry THF but slowly become more soluble upon addition of the melamine and heating between 40-50 °C for more than four days for **1a** and **1b**, and for two days for **2a** and **2b**. The formation of the cage effectively removes the αααα atropisomer from the solution, shifting the equilibrium and driving the continued self-assembly.[24] The self-assembled cage is characterized by the NMR chemical shifts of both the uracil and melamine NH protons within the H-bonds. Once the cages are formed, only one resonance, instead of six, for the uracyl methyl group is observed, confirming the presence of only one atropisoner (αααα).

### 2.3.2. Photophysical Analysis

The UV-visible absorption spectra, fluorescence emission spectra, and lifetime measurements were first recorded at room temperature for a few days until an equilibrium was observed. To drive the equilibrium towards the cages, the solutions were then heated and stirred

continuously for several days with continued monitoring. Heating at 45-47 °C for 2 days caused an increase in the UV-visible band intensities, indicating increased solubility and a shift in the equilibrium towards formation of the αααα atropisomer and assembly of the cages (**Figure 2.1**). The emission spectra of the **2a:2a** and **2b:2b** cage solutions, excited in either the Soret or Q bands, are in agreement with the UV-visible results. An initial small decrease in the fluorescence intensity due to porphyrin aggregation is followed by an increase upon formation of the more soluble cages (**Figure 2.1**). For the **1a:1a** and **1b:1b** porphyrins, the Soret band near 420 nm redshifts by about 4 nm with a small decrease in intensity, indicating the formation of amorphous aggregates. The UV-visible and emission spectra of all the control solutions (without melamine) exhibit aggregation but do not change after one day.

Time correlated single photon counting experiments on these self-assembled cages were carried out in dry THF under $N_2$ at the same concentration used for the UV-visible studies (**Table 2.1**). Incomplete demetallation of the $Zn^{2+}$ complexes to form the free bases results in some contamination by residual metalloporphyrin present in samples of **1a** and **2a**. The lifetimes for **1a**,

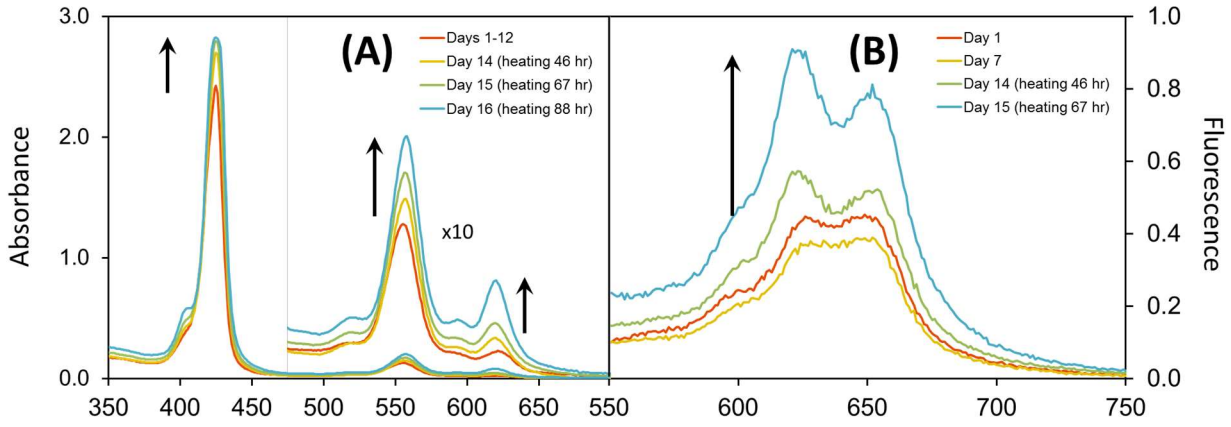


**Figure 2.1** . Absorbance (A) and fluorescence emission (B) spectra of the 2b:2b cage formation over time. The absorbance in the Q band region from 475-700 nm has been scaled up ten times. The solution concentrations are 39 μM. The excitation wavelength for the emission was $\lambda_{ex}$ = 516 nm.

**2a**, **1b**, **2b** are somewhat shorter than standard tetraphenylporphyrin (TPP, 11 ns) and ZnTPP (2.7 ns) under similar conditions[25,26] because of some aggregation. However, the solutions of cages, in which aggregation is reduced by the assembly process, generally display lifetimes closer to those for other *meso*-aryl porphyrins. This is also consistent with a static binding mechanism for cage formation, as dynamic association processes would tend to decrease the lifetimes.

**Table 2.1**. Fluorescence lifetimes of porphyrins and cages.

| Compound | $\tau_1$ (ns) | $\tau_2$ (ns) |
|---|---|---|
| **1a** | 2.20 (19%)[a] | 8.80 (81%) |
| **1b** | 2.50 | – |
| **2a** | 1.80 (5%)[a] | 8.60 (95%) |
| **2b** | 3.76 | – |
| **1a:1a cage** | 2.80 (20%)[a] | 10.2 (80%) |
| **1b:1b cage** | 2.90 | – |
| **1a:1b mixed cage** | 3.10 (58%)[a] | 8.60 (42%) |
| **2a:2a cage** | 3.64 (11%)[a] | 9.60 (89%) |
| **2b:2b cage** | 2.40 | – |
| **2a:2b mixed cage** | 3.50 (60%)[a] | 9.70 (40%) |

[a] some residual metalloporphyrins present

A one-to-one mixture of free base and $Zn^{2+}$ macrocycles, cage **2a:2b** (and **1a:1b**), was also examined. At equilibrium, if the intermolecular forces that mediate the assembly are equivalent, there should be a 1:2:1 mixture of cages **2a**:**2a**, **2a**:**2b**, and **2b**:**2b**, respectively. The UV-visible spectra for this mixture shows similar trends as the above cages; the initial formation of amorphous aggregates and the more soluble cage after heating at 45-47 °C for a few days. The fluorescence spectra of cage **2a:2b** evolve in a complex manner. Initially, in the aggregation stage of the self-assembly process, some energy transfer from the metalloporphyrins to the free bases is observed. The solution may contain more aggregates of the $Zn^{2+}$ complexes because they are less soluble. After heating the solution, only a small amount of energy transfer is observed, which is consistent with separation of the porphyrins in the cage structure. Thus, after about three days UV-visible, fluorescence, and NMR all indicate that the system has reached equilibrium.

### 2.3.3. NMR Diffusion Ordered Spectroscopy

Diffusion ordered spectroscopy (DOSY) allows the molecular weights of the assemblies to be determined.[3-5,9-12,27-30] For DOSY experiments on a Bruker 500 MHz instrument, the normalized diffusion coefficient ($D_{norm}$) was measured as the ratio of the observed value ($D_{obs}$) to $D_{\beta\text{-CD}}$, where $D_{\beta\text{-CD}}$ is the diffusion coefficient for the internal standard, heptakis(2,3,6-tri-O-methyl)-β-cyclodextrin (β-CD). A calibration curve of $D_{norm}$ *vs*. molecular weight could then be constructed using a series of polystyrene standards. The value of $D_{norm}$ for Por **1b** + melamine was found to be 0.64, which indicates a **1b:1b** cage with a molecular weight of 3360 amu (calculated 3295 amu), while $D_{norm}$ for Por **2b** + melamine was 0.60, correlating to a molecular weight of 3820 amu (calculated 3717 amu).

### 2.3.4. Dynamic Light Scattering

Dynamic light scattering (DLS) data reveals the hydrodynamic radius of the initially formed aggregates of **2a:2a, 2b:2b**, and **2a:2b** cages is about 42 nm. After heating, the average particle size is between 7-9 nm. There is a broad distribution of sizes for the aggregates of **1a:1a, 1b:1b,** and **1a:1b** centered at about 420 nm, while the cages are found to be about 9-13 nm. Assuming extended decyl groups, the cage dimensions estimated using ChemBio3D© are about 5.2 nm from terminal methyl to terminal methyl on opposite sides of the cage, and about 2 nm perpendicular to the porphyrin planes.

### 2.3.5. Atomic Force Microscopy

Since self-assembled materials must interact with surfaces when incorporated into devices, we also examined the self-organization of the cages into films. The supramolecular cage was drop cast from the above 30-40 μM THF solutions onto freshly cleaved mica and imaged with AFM. When the **2a**:**2a** was cast onto the mica, a film corresponding to a single layer of the cage

structures, approximately 2.8 nm thick, was observed (**Figure 2.2**).[3-5] In the film, the self-assembled cage is hierarchically organized by interactions between the protruding hydrocarbon chains on the four bis(decyl)melamine units.[31] Friction images show no indication of separation of the porphyrin and the melamine components. When the **2b**:**2b** cage is cast onto mica, somewhat thicker 12 nm films are observed, with root-mean-square roughness of about 4 nm. The three different cages resulting from the mixture of **2a** and **2b** apparently yield more complex patterns on the surface. This hierarchical self-organization into films is analogous to those observed for squares of porphyrins self-assembled by coordination chemistry.[32]

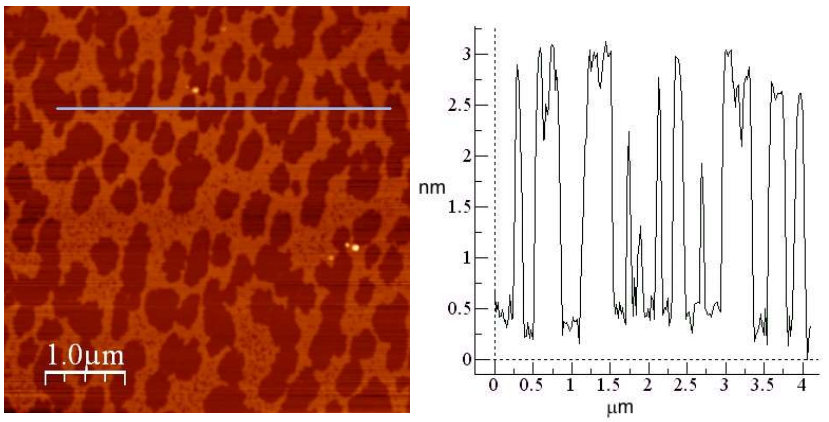


**Figure 2.2**. Contact mode AFM topography image of the **2a**:**2a** cage on mica (left) and height profile (right).

## 2.4. Conclusion

The synthesis of the porphyrins and aldehydes described here is straightforward. The cooperative self-assembly of the porphyrin cages mediated by four rigid *meso*-uracyl groups and the bis(decyl)melamine forms a stiff cage robust enough to allow organization on surfaces driven by the long hydrocarbon chains into nm thick films on mica. All of the spectroscopic and photophysical evidence supports this explanation. In addition, we attempted to probe the dynamics of energy exchange between the free base and metallated porphyrins in the **2a:2b** mixed cages. Exciting the cages into an absorption band of either the free base or zinc component resulted in some observed fluorescence from the other component, suggesting a weak excitation energy

transfer mechanism. Unfortunately, due to both aggregation effects and the presence of residual metallated porphyrin in the free base samples, these results were not fully conclusive. It may also be the case that the assembly process holds the porphyrin units far enough apart to effectively turn off electronic communication between the chromophores.

### 2.5. References


1. Singh, S.; Aggarwal, A.; Farley, C.; Hageman, B. A.; Batteas, J. D.; Drain, C. M. Hierarchical organization of a robust porphyrin cage self-assembled by hydrogen bonds. *Chem. Commun.* **2011**, *47*, 7134-7136.
2. Balaban, T. S.; Berova, N.; Drain, C. M.; Hauschild, R.; Huang, X.; Kalt, H.; Lebedkin, S.; Lehn, J. M.; Nifaitis, F.; Pescitelli, G.; Prokhorenko, V. I.; Riedel, G.; Smeureanu, G.; Zeller, J. Syntheses and energy transfer in multiporphyrinic arrays self-assembled with hydrogen-bonding recognition groups and comparison with covalent steroidal models. *Chem. Eur. J.* **2007**, *13*, 8411-8427.
3. Arai, S.; Niwa, D.; Nishide, H.; Takeoka, S. Atropisomers of meso-Conjugated Uracyl Porphyrin Derivatives and Their Assembling Structures. *Org. Lett.* **2007**, *9*, 17-20.
4. Arai, S.; Okamura, T.; Takeoka, S. Synthesis and self-assembling behavior of a porphyrin bearing multiple meso-conjugated barbiturates. *Tetrahedron Lett.* **2010**, *51*, 5177-5180.
5. Drain, C. M.; Russell, K. C.; Lehn, J.-M. Self-assembly of a multi-porphyrin supramolecular macrocycle by hydrogen bond molecular recognition. *Chem. Commun.* **1996**, 337.
6. Drain, C. M.; Fischer, R. d.; Nolen, E. G.; Lehn, J.-M. Self-assembly of a bisporphyrin supramolecular cage induced by molecular recognition between complementary hydrogen bonding sites. *J. Chem. Soc., Chem. Commun.* **1993**, 243.
7. Drain, C. M.; Shi, X.; Milic, T.; Nifiatis, F. Self-assembled multiporphyrin arrays mediated by self-complementary quadruple hydrogen bond motifs. *Chem. Commun.* **2001**, 287-288.
8. Shi, X.; Barkigia, K. M.; Fajer, J.; Drain, C. M. Design and Synthesis of Porphyrins Bearing Rigid Hydrogen Bonding Motifs: Highly Versatile Building Blocks for Self-Assembly of Polymers and Discrete Arrays. *J. Org. Chem.* **2001**, *66*, 6513-6522.
9. González-Rodríguez, D.; Schenning, A. P. H. J. Hydrogen-bonded Supramolecular π-Functional Materials. *Chem. Mater.* **2011**, *23*, 310-325.
10. Ligthart, G. B.; Ohkawa, H.; Sijbesma, R. P.; Meijer, E. W. Complementary quadruple hydrogen bonding in supramolecular copolymers. *J. Am. Chem. Soc.* **2005**, *127*, 810-811.
11. Steed, J. W. Supramolecular gel chemistry: developments over the last decade. *Chem. Commun.* **2011**, *47*, 1379-1383.
12. Wessendorf, F.; Hirsch, A. Self-assembly of supramolecular oligo-phenylene-ethynylene wires consisting of double Hamilton receptor modified OPE rods and a tetraphenylporphyrin cyanurate. *Tetrahedron* **2008**, *64*, 11480-11489.

13. Arai, S.; Ohshiro, H.; Nishide, H.; Takeoka, S. Synthesis of porphyrins bearing uracyl groups and their assembly induced by melamine derivatives. *Polym. Adv. Technol.* **2007**, *18*, 497-501.

14. Hwang, D. R.; Helquist, P.; Shekhani, M. S. Total synthesis of (+)-sparsomycin. Approaches using cysteine and serine inversion. *J. Org. Chem.* **1985**, *50*, 1264-1271.

15. Petersen, L.; Pedersen, E. B.; Nielsen, C. Three Routes for the Synthesis of 6-Benzyl-1-ethoxymethyl-2,4-dioxo-1,2,3,4-tetrahydropyrimidine-5-carbaldehyde. *Synthesis* **2001**, *2001*, 0559-0564.

16. Kimizuka, N.; Kawasaki, T.; Hirata, K.; Kunitake, T. Supramolecular Membranes. Spontaneous Assembly of Aqueous Bilayer Membrane via Formation of Hydrogen Bonded Pairs of Melamine and Cyanuric Acid Derivatives. *J. Am. Chem. Soc.* **1998**, *120*, 4094-4104.

17. Vollhardt, D.; Fainerman, V. B.; Liu, F. Thermodynamic and structural characterization of amphiphilic melamine-type monolayers. *J. Phys. Chem. B* **2005**, *109*, 11706-11711.

18. Gellman, S. H.; Dado, G. P.; Liang, G. B.; Adams, B. R. Conformation-directing effects of a single intramolecular amide-amide hydrogen bond: variable-temperature NMR and IR studies on a homologous diamide series. *J. Am. Chem. Soc.* **1991**, *113*, 1164-1173.

19. Plieger, P. G.; Burrell, A. K.; Jameson, G. B.; Officer, D. L. Metallation effects on the thermal interconversion of atropisomers of di(orthomethylarene)-substituted porphyrins. *Dalton Trans.* **2004**, 319-326.

20. Freitag, R. A.; Whitten, D. G. Thermal and photo-induced atropisomerization of picket-fence porphyrins, metalloporphyrins, and diacids: a means for examining porphyrin solution properties. *J. Phys. Chem.* **1983**, *87*, 3918-3925.

21. Freitag, R. A.; Whitten, D. G. Thermal and photo-induced atropisomerization of picket-fence porphyrins, metalloporphyrins, and diacids: a means for examining porphyrin solution properties. *J. Phys. Chem.* **1983**, *87*, 3918-3925.

22. Kottas, G. S.; Clarke, L. I.; Horinek, D.; Michl, J. Artificial molecular rotors. *Chem. Rev.* **2005**, *105*, 1281-1376.

23. Plieger, P. G.; Burrell, A. K.; Jameson, G. B.; Officer, D. L. Metallation effects on the thermal interconversion of atropisomers of di(orthomethylarene)-substituted porphyrins. *Dalton Trans.* **2004**, 319-326.

24. Lindsey, J. Increased yield of a desired isomer by equilibriums displacement on binding to silica gel, applied to meso-tetrakis(o-aminophenyl)porphyrin. *J. Org. Chem.* **1980**, *45*, 5215-5215.

25. Gouterman, M. In *The Porphyrins*; Dolphin, D., Ed.; Academic Press: New York, **1979**; Vol. III.

26. Tran Thi, T. H.; Desforge, C.; Thiec, C.; Gaspard, S. Singlet-singlet and triplet-triplet intramolecular transfer processes in a covalently linked porphyrin-phthalocyanine heterodimer. *J. Phys. Chem.* **1989**, *93*, 1226-1233.

27. Cohen, Y.; Avram, L.; Frish, L. Diffusion NMR spectroscopy in supramolecular and combinatorial chemistry: an old parameter--new insights. *Angew. Chem. Int. Ed.* **2005**, *44*, 520-554.

28. Ohkawa, H.; Arai, S.; Takeoka, S.; Shibue, T.; Nishide, H. A Duplex of Tetra(2-pyridyl)porphyrin and Tetrahydroxylcalix[4]arene. *Chem. Lett.* **2003**, *32*, 1052-1053.

29. Ohkawa, H.; Takayama, A.; Nakajima, S.; Nishide, H. Cyclic tetramer of a metalloporphyrin based on a quadruple hydrogen bond. *Org. Lett.* **2006**, *8*, 2225-2228.

30. Zhao, T.; Beckham, H. W.; Gibson, H. W. Quantitative Determination of Threading in Rotaxanated Polymers by Diffusion-Ordered NMR Spectroscopy. *Macromolecules* **2003**, *36*, 4833-4837.

31. Yang, Y.; Wang, C. Hierarchical construction of self-assembled low-dimensional molecular architectures observed by using scanning tunneling microscopy. *Chem. Soc. Rev.* **2009**, *38*, 2576-2589.

32. Milic, T.; Garno, J. C.; Batteas, J. D.; Smeureanu, G.; Drain, C. M. Self-Organization of Self-Assembled Tetrameric Porphyrin Arrays on Surfaces. *Langmuir* **2004**, *20*, 3974-3983.

## Chapter 3. Synthesis of a Flexible Porphyrin Dimer for Fullerene Complexation[§]

### 3.1. Introduction

Energy and electron transfer are fundamental processes critical to virtually every aspect of both nature and technology. Achieving reliable control over these mechanisms at the molecular level is a prerequisite to making advancements in any number of areas, from biomedical therapeutics to nanoelectronics to emerging energy technologies. To this end, the donor-acceptor paradigm of material and molecular design has proven fruitful in many areas of basic research and applied science for decades.[2-10] Porphyrins, phthalocyanines, and other related macrocycles all possess excellent photophysical characteristics that make them suitable as donors. On the other hand, fullerenes are known to be remarkably efficient electron acceptors,[12] and thus are also a natural fit in these kinds of systems. Thus, the chemical stability and tuneable photonic properties of the p-type porphyrins couple well with the electronic properties of the n-type fullerenes to form ideal donor acceptor systems.[11,13-23] Interestingly, it has also been found that there are enhanced π-π interactions between the aromatic ring of a porphyrinoid and the fullerene surface.[11,15]

Many porphyrin dimer systems have been devised to take advantage of these favorable interactions,[14,17-30] but the synthetic methods employed have been limited by factors of ease, yield, and scalability.[24,27] Keeping in mind the principles of supramolecular design that we have been advocating, we sought to design a more synthetically facile alternative. Using a simple, high yield, two-step procedure we have fabricated a thiol tethered porphyrin dimer which

[§] This chapter is adapted from an article published in *Chemical Communications*.[1]

preferentially binds $C_{70}$ over $C_{60}$, both in toluene solution and when deposited on glass. The same synthetic platform will also allow for easy incorporation of a wide variety of alkyl linkers to accommodate different fullerenes and fullerene-like structures.

### 3.2. Materials and Methods

NMR ($^{1}H$ and $^{13}C$) spectra were recorded on a Bruker 500 MHz spectrometer. Electrospray ionization mass spectrometric analyses were performed at the CUNY Mass Spectrometry Facility at Hunter College using an Agilent Technologies HP-1100 LCMSD instrument. MALDI-MS spectra were recorded as a service by the University of Illinois with a Bruker UltrafleXtreme MALDI-TOF mass spectrometer purchased in part with a grant from the National Center for Research Resources, National Institutes of Health (S10 RR027109 A). All reagents were obtained from commercial sources and used without further purification. Atomic force microscopy (AFM) measurements were conducted with an Asylum AFM (MFP-3D, Asylum Research Corp.) on organic thin films drop cast onto ozone cleaned glass.

#### 3.2.1 Synthesis

The synthesis is outlined in **Scheme 3.1**. First, a mixed aldehyde condensation in propionic acid, using one equivalent of pentafluorobenzaldehyde, three equivalents of benzaldehyde, and four equivalents of pyrrole, yielded a statistical mixture of compounds which were separated by flash chromatography. The target isomer (5,10,15-triphenyl-20-pentafluorophenylporphyrin, **$TPPF_5$**) was isolated and metallated with zinc acetate, and the metallated product was allowed to react with 1,5-dithiopentane in DMF. This crude mixture was purified by column to give the dimer **1Zn** in 79% yield, and could be subsequently demetallated with HCl to give **$1H_2$**.

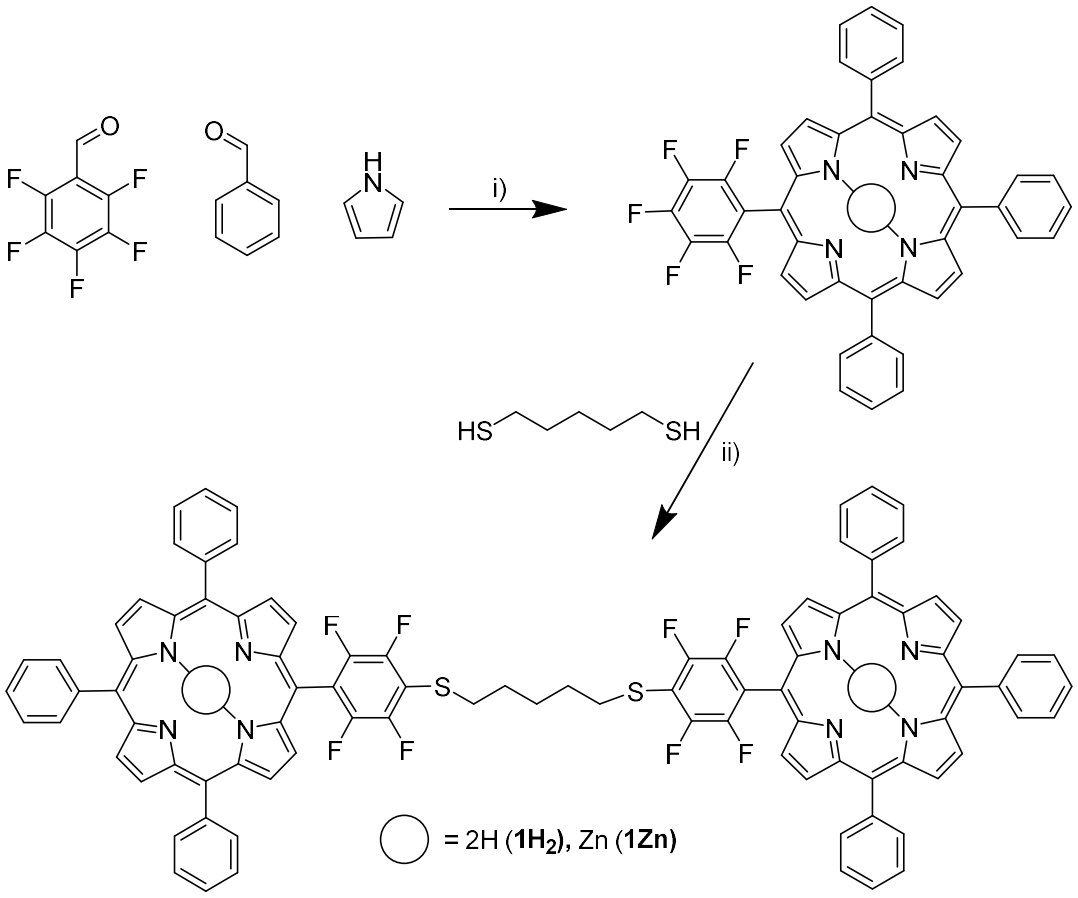


**Scheme 3.1**. (i) Reflux in propionic acid, separate isomers; (ii) metallation with $Zn(OAc)_2$ in $CHCl_3/CH_3OH$ followed by addition of pentane-1,5-dithiol in DMF.

Metallation/demetallation can be carried out at any step, but the presence of the zinc ion helps to activate the *para*-fluorine of **TPPF$_5$** for substitution. Detailed procedures are as follows.

### 3.2.1.1. 5,10,15-triphenyl-20-pentafluorophenylporphyrin (TPPF$_5$)

To a mixture of propionic acid (0.6 L) and nitrobenzene (6 ml) was added benzaldehyde (21.34 mmol, 2.17 mL) and pentafluorobenzaldehyde (7.0 mmol, 0.875 mL) with stirring. The mixture was heated to 100 ºC and pyrrole (28.3 mmol, 1.94 mL) was added slowly. The reaction was refluxed for three hours in the dark and allowed to cool. Silica gel (300 mL) was added to the reaction flask and the propionic acid was evaporated. The silica gel was washed with

dichloromethane and acetone until no more color eluted. The solution was evaporated to 100 mL and washed with sodium bicarbonate and water, dried over anhydrous sodium sulfate, and evaporated to dryness. This organic product was then recrystallized from hexanes to yield a purple powder. The porphyrin mixture was filtered, dissolved in dichloromethane, loaded onto a 600 mL silica gel column and separated with an eluent of 30:70 toluene:petroleum ether (v/v). The fifth of the six bands was collected, evaporated and recrystallized from hexanes to yield 360 mg (0.511 mmol, 7.22% yield) of product **$TPPF_5$**.

#### 3.2.1.2. Zinc (II) 5,10,15-triphenyl-20-pentafluorophenylporphyrin ($ZnTPPF_5$)

To stirring chloroform (20 mL) was added **$TPPF_5$** (0.511 mmol, 0.360 g). To stirring methanol (8 mL) was added zinc acetate dihydrate (4.09 mmol, 0.897 g). The zinc acetate solution was added to the chloroform solution of $TPPF_5$ and the mixture was refluxed for three hours. The mixture was then washed with water, extracted into dichloromethane, dried over sodium sulfate, and evaporated to dryness, yielding 276 mg of **$ZnTPPF_5$** (70.4% yield).

#### 3.2.1.3. Bis-[zinc (II) 5,10,15-triphenyl-20-pentafluorophenylporphyrin] (1Zn)

To stirring dry DMF (16.6 mL) was added **$ZnTPPF_5$** (116 mg, 0.151 mmol) under nitrogen atmosphere. To this solution 1,5-pentane-dithiol (0.23 ml, 1.7 mmol) was added, followed by diisopropylethylamine (DIPEA, 2.914 ml, 16.73 mmol). The reaction mixture was stirred at 80 ºC for 12 hours and then cooled to room temperature, washed with water, extracted into dichloromethane, dried over sodium sulfate, and evaporated to dryness under reduced pressure. The crude product was purified by column chromatography to remove starting materials and recrystallized from hexanes to give 95.37 mg of product **1Zn** (82.19% yield)

### 3.2.1.4. Bis-[5,10,15-triphenyl-20-pentafluorophenylporphyrin] ($1H_2$)

To stirring dry chloroform (5 mL) was added **1Zn** (80 mg, 0.091 mmol) under nitrogen atmosphere. To this solution concentrated HCl (0.5 ml, 20.43 mmol) was added dropwise. The mixture was stirred at room temperature for 3 hours. The reaction mixture was then washed with water, extracted into dichloromethane, dried over sodium sulfate, and evaporated to dryness under reduced pressure. The crude product was recrystallized from hexanes to give 75 mg of product **$1H_2$** (93.8% yield). MALDI: calculated 1505.6423; found 1505.4. NMR (500 MHz, $CDCl_3$): 9.02(d), 4H, β pyrrole; 9.96(m), 12H, β pyrrole; 8.20(m), 12H, ortho-phenyl; 7.77(m), 18H, meta/para-phenyl; 3.39(t), 2H, S-tether; 3.15(m), 2H, tether; 2.05(m), 2H, tether; 1.86(m), 4H, tether.

### 3.2.2 Photophysics

UV-Visible absorption spectroscopy was performed on a Cary 1-Bio UV-Visible spectrometer. Steady state fluorescence spectra were obtained on a HORIBA Jobin-Yvon FluoroLog-3 spectrometer, and singlet state lifetimes were taken using the FluoroHub Tau-3 TCSPC add-on component to the same system, with a pulsed NanoLED laser as the excitation source. In order to minimize secondary absorption and re-emission, 1.0 mm pathlength quartz or optical glass cuvettes were used for all spectroscopic studies. The emission spectra and lifetimes were taken using a front-face configuration, which also helped to minimize these inner-filter effects. All photophysical studies were carried out in spectrophotometric grade 99.99% toluene, used as purchased. Solutions of the porphyrin dimer species were prepared at one half the molar concentrations of the monomer controls in order to yield the equivalent macrocycle concentration for comparison.

For each of the porphyrins investigated, including the monomeric control **TPPF$_5$**, solutions of the desired concentration were prepared first and split into two portions. Fullerene (either $C_{60}$ or $C_{70}$) was then added to one of the portions to create a stock solution. This ensured that aliquots of the fullerene stock could be titrated into the dimer solutions under study without changing the porphyrin concentration. Absorbance, fluorescence, and fluorescence lifetime measurements were performed on each porphyrin solution as the fullerenes were titrated into the cuvettes in this way.

### 3.3. Results

**Figure 3.1** shows the UV-visible absorption spectra for the titration of $C_{60}$ and $C_{70}$ into the zinc dimer **1Zn**. There is a small ground state interaction with $C_{70}$ evident from the UV-visible absorption, demonstrated by the difference between the expected and observed Soret peaks of the porphyrin + fullerene solutions (**Figure 3.1**, inset). No such trend is observed for the titration with $C_{60}$. Similar spectra for the other compounds are shown in Appendix B (Figures B1-B4).

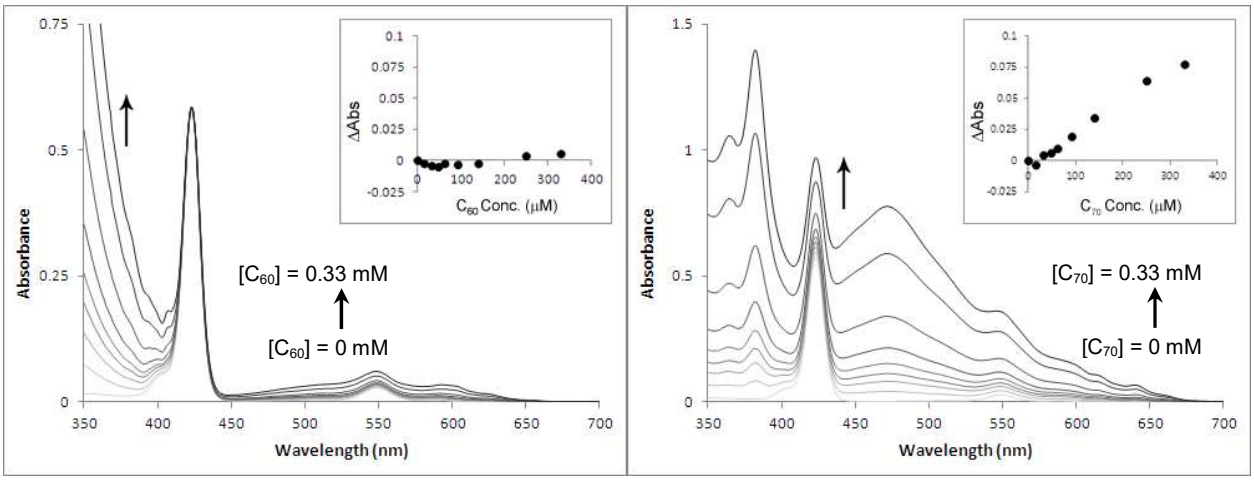


**Figure 3.1**. UV-Visible absorbances of a titration of $C_{60}$ (left) or $C_{70}$ (right) into 10.0 μM solutions of **1Zn**. The inset shows the difference between the calculated sum of the absorbance of the two components (at 419 nm) and the experimentally observed absorbance for the mixed solutions, as function of the quencher concentration.

Steady-state fluorescence spectra of these same titration experiments are shown in **Figure 3.2**. Both fullerenes quench the porphyrin fluorescence, although the effect is much larger for $C_{70}$ than for $C_{60}$, indicating an enhanced excited state interaction with the former. Stern-Volmer plots of this quenching process are shown in **Figure 3.3**. The slopes of the best fit lines to these plots are the binding constants collected in **Table 3.1**. Similar binding constants were obtained from fluorescence data corresponding to two different excitation wavelengths. No change was observed in the fluorescence lifetimes of any of the porphyrins with the addition of the fullerenes.

### 3.4. Discussion

Steady-state fluorescence measurements demonstrated quenching of the porphyrin excited state, as is clearly shown in **Figure 3.2** and in Appendix B (Figures B3 and B4). The Stern-Volmer plots (**Figure 3.3**) show greater quenching by $C_{70}$ than by $C_{60}$ for all species studied. At the same time, the porphyrin fluorescence lifetimes show virtually no change, indicating a static quenching mechanism. Assuming there is no significant difference in the nature of energy or electron transfer from the various fluorophore species, and expecting that the complexation behavior is driven by

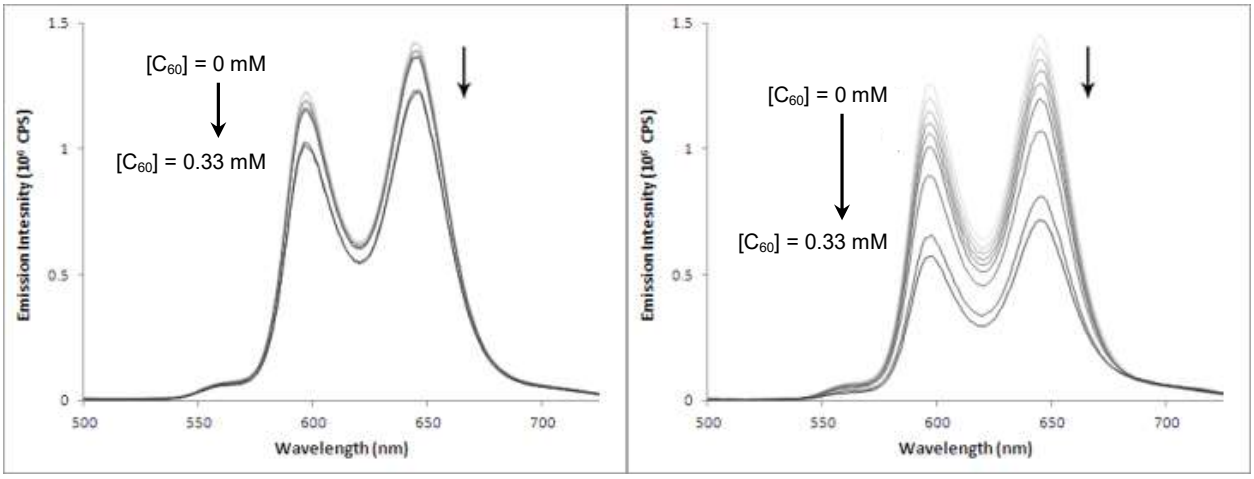


**Figure 3.2**. Fluorescence emission spectra of a titration of (left) $C_{60}$ and (right) $C_{70}$ into 10.0 μM solutions of **1Zn**. Both graphs show quenching of the porphyrin excited state, but the effect due to $C_{70}$ is much more significant. The solutions were excited at 417 nm.

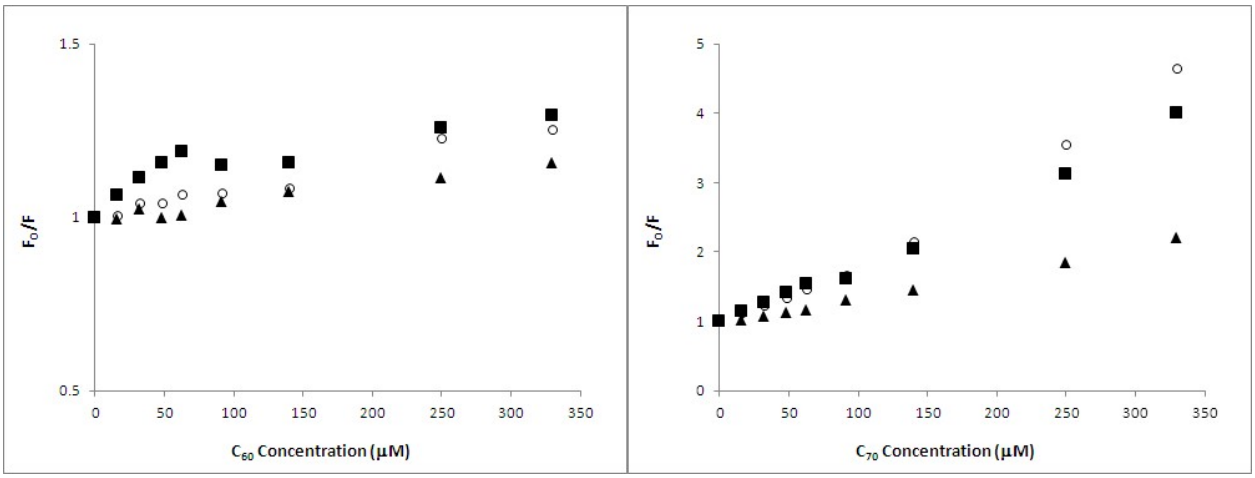


**Figure 3.3**. Stern-Volmer plots for each species discussed. The ratio of unquenched to quenched fluorescence ($F_0/F$) is plotted as a function of quencher concentration as $C_{60}$ (left) or $C_{70}$ (right) are titrated into solutions of **1Zn** (○), **$1H_2$** (■) and **$TPPF_5$** (▲). Note the difference in scale between the left and right graphs.

van der Waals forces with small contributions from electrostatics and coordinate bonding, we conclude that the greater quenching observed in the case of the $C_{70}$ can be attributed to a stronger interaction due to the larger, flatter surface in the equatorial region of the prolate molecule.[31]

All of the solution phase experiments were done in toluene in order to compare to literature results, but the extreme affinity of both molecules for this solvent likely competes with the chromophore/fullerene association. While this offers a suitable environment for examining the attractions between the donor and acceptor, a more polar solvent could be chosen for solution processing in order to drive the equilibrium towards complexation.[15] Porphyrins **$1H_2$** and **1Zn** was designed with a flexible thiol terminated linker to allow for a sandwich type binding of fullerene $C_{60}$ or $C_{70}$. The length of the linker can be easily modulated by substituting pentane-dithiol with any of the numerous commercially available dithioalkanes, thus broadening the range of potential guests for the inclusion complex.

The inclusion of the pentafluorophenyl moiety into the porphyrin allows for easy dimerization by simple click-chemistry type substitution with thioalkanes or other nucleophiles, but it may help promote interaction with the conjugated π-system of the chosen fullerene molecule as well.[32] Metallation and demetallation are simple and proceed in excellent yield, but the subtle effects of the metal ion on the complexation have yet to be fully revealed. **Table 3.1** shows the binding constants calculated from Stern-Volmer plots and compares them with values from the literature. Bis-porphyrin **1Zn** demonstrated a binding constant of $1.1\times10^4$ $M^{-1}$ which is competitive with the much more synthetically demanding molecules. Structures for the jaws, and calixarene porphyrin dimers are given in Appendix B (Figure B12).

**Table 3.1**. Binding constants for species discussed as well as literature compounds. Values calculated from slope of Stern-Volmer plots.

| Host | $K_{C60}$ ($M^{-1}$) | $K_{C70}$ ($M^{-1}$) | $K_{C70}/K_{C60}$ | Ref. |
|---|---|---|---|---|
| $TPPF_5$ (control) | $5.0\times10^2$ | $3.7\times10^3$ | 7.4 | this work |
| $1H_2$ | $7.1\times10^2$ | $8.9\times10^3$ | 12.5 | this work |
| cyclic $H_2$Por | $7.94\times10^5$ | $1.58\times10^7$ | 19.9 | [11][a] |
| jaws $H_2$Por | $5.20\times10^3$ | - | - | [11][a] |
| calix. $H_2$Por | $4.92\times10^3$ | $2.11\times10^4$ | 4.29 | [24] |
| 1Zn | $8.0\times10^2$ | $1.1\times10^4$ | 13.8 | this work |
| cyclic ZnPor | $6.31\times10^5$ | $2.00\times10^7$ | 31.7 | [11][a] |
| jaws ZnPor | $1.95\times10^3$ | - | - | [11][a] |
| calix. ZnPor | $8.6\times10^3$ | $2.80\times10^4$ | 3.26 | [24] |

[a] And references therein.

To study this system in the solid state, films were prepared on ozone cleaned glass by drop casting from toluene solutions of either fullerene, fullerene and porphyrin (**1H₂** or **1Zn**), or pure porphyrin, and were examined by atomic force microscopy (AFM). Height and friction images of the films are available in Appendix B, Figures B7-B11. Monomeric porphyrins form simple aggregates on the glass surface. Pure $C_{70}$ solutions form large nanoaggregates as compared to the long narrow rods which form from solutions of pure $C_{60}$. When combined with either porphyrin

dimer**,** the dimensions of the $C_{60}$ aggregates remain constant but are more uniformly dispersed. When mixed with $C_{70}$ however, dimers form similarly sized nanoaggregates which exhibit smoother shells and are surrounded by a region of porphyrin film, as depicted in Figure B11. These self-assembled aggregation patterns further demonstrate the increased affinity of **1H$_2$** and **1Zn** for $C_{70}$.

Carbon nanotubes share many of the interesting properties of fullerenes and have also been extensively used in porphyrin based D/A systems.[17,25,29,33-36] When DMF solutions of **1Zn** were incubated with a large excess of single walled carbon nanotubes (SWCNT), and then sonicated (20 min.) and centrifuged (8,000 RPM for 10 min.), the supernatant demonstrated fluorescence quenching and UV spectral changes similar to the experiments with the fullerene $C_{70}$. This indicates that the dimer interacts favorably with the larger aspect ratio of the SWCNT. The precipitate, which is likely a complex of the SWCNT and the dimer species, has not yet been characterized. Future studies will include synthesis of differently linked dimers, full characterization of the molecular interaction with SWCNT, and experiments employing the system as a technique for purifying crude fullerene mixtures.

### 3.5. Conclusions

We have demonstrated the synthesis of a porphyrin dimer by high yield click chemistry, using a fluorous linker and a commercially available thioalkane. The resulting species was observed to preferentially bind fullerene $C_{70}$ in solution, forming a ground state complex with significantly quenched fluorescence. While we have not conclusively determined the mechanism of quenching, the nature of the components suggests that there is an electron transfer from the local singlet state of the porphyrin dimer to the fullerene. The supramolecular structure also persists into the solid state when the nanoaggregates are cast onto glass.

### 3.6. References


1. Jurow, M.; Farley, C.; Pabon, C.; Hageman, B.; Dolor, A.; Drain, C. M. Facile synthesis of a flexible tethered porphyrin dimer that preferentially complexes fullerene C70. *Chem. Commun.* **2012**, *48*, 4731-4733.
2. Mulliken, R. S.; Person, W. B. Donor-Acceptor Complexes. *Annu. Rev. Phys. Chem.* **1962**, *13*, 107-126.
3. Williams, F. Donor-acceptor pairs in semiconductors. *Physica Status Solidi B.* **1968**, *25*, 493-512.
4. Foster, R. Electron donor-acceptor complexes. *J. Phys. Chem.* **1980**, *84*, 2135-2141.
5. Sapsford, K. E.; Berti, L.; Medintz, I. L. Materials for fluorescence resonance energy transfer analysis: beyond traditional donor-acceptor combinations. *Angew. Chem. Int. Ed.* **2006**, *45*, 4562-4589.
6. Emmett, L.; Prentice, G. M.; Pantoş, G. D. Donor–acceptor interactions in chemistry. *Annu. Rep. Prog. Chem., Sect. B: Org. Chem.* **2013**, *109*, 217.
7. Kularatne, R. S.; Magurudeniya, H. D.; Sista, P.; Biewer, M. C.; Stefan, M. C. Donor-acceptor semiconducting polymers for organic solar cells. *J. Polym. Sci.* **2013**, *51*, 743-768.
8. Mullen, K.; Pisula, W. Donor-Acceptor Polymers. *J. Am. Chem. Soc.* **2015**, *137*, 9503-9505.
9. Kc, C. B.; D'Souza, F. Design and photochemical study of supramolecular donor–acceptor systems assembled via metal–ligand axial coordination. *Coord. Chem. Rev.* **2016**, *322*, 104-141.
10. Rudolf, M.; Kirner, S. V.; Guldi, D. M. A multicomponent molecular approach to artificial photosynthesis - the role of fullerenes and endohedral metallofullerenes. *Chem. Soc. Rev.* **2016**, *45*, 612-630.
11. Boyd, P. D. W.; Reed, C. A. Fullerene−Porphyrin Constructs. *Acc. Chem. Res.* **2004**, *38*, 235-242.
12. Echegoyen, L.; Echegoyen, L. E. Electrochemistry of Fullerenes and Their Derivatives. *Acc. Chem. Res.* **1998**, *31*, 593-601.
13. Baran, P. S.; Monaco, R. R.; Khan, A. U.; Schuster, D. I.; Wilson, S. R. Synthesis and Cation-Mediated Electronic Interactions of Two Novel Classes of Porphyrin−Fullerene Hybrids. *J. Am. Chem. Soc.* **1997**, *119*, 8363-8364.
14. Bhattacharya, S.; Tominaga, K.; Kimura, T.; Uno, H.; Komatsu, N. A new metalloporphyrin dimer: Effective and selective molecular tweezers for fullerenes. *Chem. Phys. Lett.* **2007**, *433*, 395-402.
15. Boyd, P. D. W.; Hodgson, M. C.; Rickard, C. E. F.; Oliver, A. G.; Chaker, L.; Brothers, P. J.; Bolskar, R. D.; Tham, F. S.; Reed, C. A. Selective Supramolecular Porphyrin/Fullerene Interactions. *J. Am. Chem. Soc.* **1999**, *121*, 10487-10495.
16. D'Souza, F.; Chitta, R.; Gadde, S.; Zandler, M. E.; Sandanayaka, A. S.; Araki, Y.; Ito, O. Supramolecular porphyrin-fullerene via 'two-point' binding strategy: axial-coordination and cation-crown ether complexation. *Chem. Commun.* **2005**, 1279-1281.

17. D'Souza, F.; Ito, O. Supramolecular donor-acceptor hybrids of porphyrins/phthalocyanines with fullerenes/carbon nanotubes: electron transfer, sensing, switching, and catalytic applications. *Chem. Commun.* **2009**, 4913-4928.

18. Liddell, P. A.; Kodis, G.; Kuciauskas, D.; Andreasson, J.; Moore, A. L.; Moore, T. A.; Gust, D. Photoinduced electron transfer in a symmetrical diporphyrin-fullerene triad. *Phys. Chem. Chem. Phys.* **2004**, *6*, 5509-5515.

19. Mulholland, A. R.; Woodward, C. P.; Langford, S. J. Fullerene-templated synthesis of a cyclic porphyrin trimer using olefin metathesis. *Chem. Commun.* **2011**, *47*, 1494-1496.

20. Sessler, J. L.; Jayawickramarajah, J.; Gouloumis, A.; Torres, T.; Guldi, D. M.; Maldonado, S.; Stevenson, K. J. Synthesis and photophysics of a porphyrin-fullerene dyad assembled through Watson-Crick hydrogen bonding. *Chem. Commun.* **2005**, 1892-1894.

21. Sun, D.; Tham, F. S.; Reed, C. A.; Chaker, L.; Burgess, M.; Boyd, P. D. W. Porphyrin−Fullerene Host−Guest Chemistry. *J. Am. Chem. Soc.* **2000**, *122*, 10704-10705.

22. Wilson, S. R.; MacMahon, S.; Tat, F. T.; Jarowski, P. D.; Schuster, D. I. Synthesis and photophysics of a linear non-covalently linked porphyrin–fullerene dyad. *Chem. Commun.* **2003**, 226-227.

23. Zhang, Y.; Yu, Y.; Jiang, Z.; Xu, H.; Wang, Z.; Zhang, X.; Oda, M.; Ishizuka, T.; Jiang, D.; Chi, L.; Fuchs, H. Single-Molecule Study on Intermolecular Interaction between C60 and Porphyrin Derivatives: Toward Understanding the Strength of the Multivalency. *Langmuir* **2009**, *25*, 6627-6632.

24. Dudic, M.; Lhotak, P.; Stibor, I.; Petrickova, H.; Lang, K. (Thia)calix[4]arene-porphyrin conjugates: novel receptors for fullerene complexation with C70 over C60 selectivity. *New J. Chem.* **2004**, *28*.

25. He, L.; Zhu, Y.-Z.; Zheng, J.-Y.; Ma, Y.-F.; Chen, Y.-S. Meso-meso linked diporphyrin functionalized single-walled carbon nanotubes. *J. Photochem. Photobiol.* **2010**, *216*, 15-23.

26. Mukherjee, S.; Bauri, A. K.; Bhattacharya, S. Photophysical investigations and binding strength in supramolecular interaction of a newly designed diporphyrin tweezer with fullerenes C60 and C70 in solution. *Chem. Phys. Lett.* **2010**, *500*, 128-139.

27. Shoji, Y.; Tashiro, K.; Aida, T. Selective Extraction of Higher Fullerenes Using Cyclic Dimers of Zinc Porphyrins. *J. Am. Chem. Soc.* **2004**, *126*, 6570-6571.

28. Tamaki, K.; Imahori, H.; Sakata, Y.; Nishimura, Y.; Yamazaki, I. Synthesis and photophysical properties of a diporphyrin-fullerene triad. *Chem. Commun.* **1999**, 625-626.

29. Umeyama, T.; Tezuka, N.; Kawashima, F.; Seki, S.; Matano, Y.; Nakao, Y.; Shishido, T.; Nishi, M.; Hirao, K.; Lehtivuori, H.; Tkachenko, N. V.; Lemmetyinen, H.; Imahori, H. Carbon Nanotube Wiring of Donor–Acceptor Nanograins by Self-Assembly and Efficient Charge Transport. *Angew. Chem. Int. Ed.* **2011**, *50*, 4615-4619.

30. Wu, Z.-Q.; Shao, X.-B.; Li, C.; Hou, J.-L.; Wang, K.; Jiang, X.-K.; Li, Z.-T. Hydrogen-Bonding-Driven Preorganized Zinc Porphyrin Receptors for Efficient Complexation of C60, C70, and C60 Derivatives. *J. Am. Chem. Soc.* **2005**, *127*, 17460-17468.

31. Vilmercati, P.; Cudia, C. C.; Larciprete, R.; Cepek, C.; Zampieri, G.; Sangaletti, L.; Pagliara, S.; Verdini, A.; Cossaro, A.; Floreano, L.; Morgante, A.; Petaccia, L.; Lizzit, S.; Battocchio, C.; Polzonetti, G.; Goldoni, A. Molecular orientations, electronic properties and charge transfer timescale in a Zn-porphyrin/C70 donor–acceptor complex for solar cells. *Surf. Sci.* **2006**, *600*, 4018-4023.

32. Coates, G. W.; Dunn, A. R.; Henling, L. M.; Ziller, J. W.; Lobkovsky, E. B.; Grubbs, R. H. Phenyl−Perfluorophenyl Stacking Interactions: Topochemical [2+2] Photodimerization and Photopolymerization of Olefinic Compounds. *J. Am. Chem. Soc.* **1998**, *120*, 3641-3649.

33. Li, H.; Zhou, B.; Lin, Y.; Gu, L.; Wang, W.; Fernando, K. A. S.; Kumar, S.; Allard, L. F.; Sun, Y.-P. Selective Interactions of Porphyrins with Semiconducting Single-Walled Carbon Nanotubes. *J. Am. Chem. Soc.* **2004**, *126*, 1014-1015.

34. Sgobba, V.; Rahman, G. M. A.; Guldi, D. M.; Jux, N.; Campidelli, S.; Prato, M. Supramolecular Assemblies of Different Carbon Nanotubes for Photoconversion Processes. *Adv. Mater.* **2006**, *18*, 2264-2269.

35. Tasis, D.; Tagmatarchis, N.; Bianco, A.; Prato, M. Chemistry of Carbon Nanotubes. *Chem. Rev.* **2006**, *106*, 1105-1136.

36. Cheng, F.; Zhu, J.; Adronov, A. Supramolecular Functionalization of Single-Walled Carbon Nanotubes with Triply Fused Porphyrin Dimers: A Study of Structure–Property Relationships. *Chem. Mater.* **2011**, *23*, 3188-3194.

## Chapter 4. Tuning the Structure and Photophysics of a Fluorous Phthalocyanine Platform[§]

### 4.1. Introduction

Phthalocyanines (Pc) have been an important class of industrial dyes since their serendipitous discovery in the early 20$^{th}$ century.[3,4] In addition to accounting for a large percentage of organic dyes currently in production,[6] Pcs are also routinely investigated for applications ranging from solar energy conversion[7-12] to thin film electronics[13-18] to photodynamic therapy.[19-24] The chemical and thermal stability of these compounds are augmented by diverse photonic properties, including remarkably high molar extinction coefficients and fluorescence efficiencies. It has been known since their inception that functionalizing the Pc core allows for increased solubility and ease of processing, while simultaneously allowing the aforementioned photonic properties to be systematically tuned because the substituents are directly appended to the macrocycle.

Many research groups are interested in 1,2,3,4,8,9,10,11,15,16,17,18,22,23,24,25-hexadecafluorophthalocyanine ($F_{16}Pc$), and its metal-complexes ($MF_{16}Pc$).[7,9,13-16,21-28] The electron-withdrawing fluorine substituents slightly perturb the molecular orbitals causing a small bathochromic shift in the absorbance and fluorescence peaks, as well as an enhanced tendency towards aggregation.[29] Moreover, the increased dipole moment of the carbon-fluorine bond and the electron-deficient nature of the fused benzenes make this molecule an ideal substrate for attack *via* nucleophilic aromatic substitution ($S_NAr$).[7,9,25,27,28,30,31] This synthetic strategy has proven extremely versatile, allowing the creation of a large variety of substituted Pcs that might

[§] This chapter is adapted from a forthcoming article in the *Journal of Physical Chemistry, Part A.*[1]

not be otherwise accessible *via* traditional synthetic methods.[32] Thiol, amine, and alcohol nucleophiles bearing a range of functional groups can be employed, and the extent of substitution can be carefully controlled by adjusting the reaction conditions.

We previously demonstrated[7] an improved photovoltaic efficiency in bulk heterojunction solar cells fabricated from blends of ZnPcs appended with varying numbers of thioalkane chains. It was shown that successive substitution of the F atoms with these –SR groups on the $ZnF_{16}Pc$ platform causes a red-shift in the absorbance Q band, allowing a mixture of different dyes to cover a much broader range of the solar spectrum. Solar cells utilizing Pc dye-blends were compared with cells made from only one dye component, and were found to have a power conversion efficiency (PCE) greater than that predicted from summing the corresponding single-component device efficiencies. Surprisingly, this synergistic enhancement was achieved without the need to engineer the dyes into an energetically stepwise hierarchical structure at the molecular level. Using grazing incidence small angle x-ray scattering, Jurow *et al*.[9] found that the presence of the exocyclic thioalkane chains on the ZnPcs induced liquid crystal like behavior, resulting in an undesirable homogenous alignment of aggregates parallel to the electrode surface. Further, they showed that incorporating zinc tetra-*tert*-butylphthalocyanine ($Zn(tBu)_4Pc$) into the active layer increased the cell efficiencies by frustrating this unfavorable packing. It is possible that dye-blends with widely varying numbers of thioalkyl substituents could produce the same effect without the need for $Zn(tBu)_4Pc$.

While molecular structure and packing order are clearly important in determining the PCE, there are many other factors such as photophysical properties to consider in engineering Pcs for solar energy conversion and other photonic applications. Herein we assess the photophysical properties through a rigorous spectroscopic study of the $ZnF_{16-x}(SR)_xPc$ series of dyes (where x =

0–16). The photophysical properties of the molecules, including absorbance, fluorescence emission, and excited state lifetime, are measured as a function of the number of thioalkyl substituents, wherein the specific substitution pattern is discussed below. We use density functional theory (DFT) and time-dependent density functional theory (TD-DFT) calculations to help support and explain the conclusions regarding the excited state and structural dynamics. A single chain length was used since the number of substituents is the relevant variable for these studies, but the trends observed will map onto other derivatives based on the $ZnF_{16}Pc$ platform under the same conditions. Using *n*-octylthio groups imparts the desired degree of solubility and processability without resulting in undesirable liquid crystalline behavior. For the theoretical calculations we have modeled the compounds with shorter *n*-butylthio chains to significantly reduce the computational time required, while still obtaining useful information regarding the electronic and molecular structure. Neither previous reports[9,33] nor our own investigations show any difference in the inductive effects of substituents with different carbon chain lengths.

There are diverse applications for materials that harness the excited state energy of efficient light absorbers such as Pcs, so a detailed understanding of the excited state dynamics will be beneficial for areas such as solar energy conversion, photocatalysis, biomedical imaging, photoacoustic spectroscopy, and photodynamic and photothermal therapies.[24] The results presented are thus broadly applicable to the development of Pc systems wherein the substituent is appended to the conjugated macrocycle. For $ZnF_{16}Pc$, the absorbance, fluorescence quantum yields, and excited state lifetimes can all be systematically tuned by serial substitution of the F atoms on the macrocycle.[7] We demonstrate for the first time that the molecular structure of a pre-formed Pc core can be significantly distorted by simple substitution chemistry. Disrupting the normally planar aromatic system induces drastic changes in the photophysics, with important

consequences for potential applications. To date, syntheses of structurally distorted Pcs have only been accomplished through the cyclotetramerization of phthalonitriles or similar precursors already bearing bulky groups in the α position,[34-40] thereby limiting the scope of this approach. In this context, exploiting the synthetic versatility of the $ZnF_{16}Pc$ platform is an important part of the rapid design and testing of Pc compounds for commercially viable applications.

## 4.2. Experimental

### 4.2.1. Materials, Instruments, and Methods

1,2,3,4,8,9,10,11,15,16,17,18,22,23,24,25-hexadecafluorophthalocyaninato zinc (II) ($ZnF_{16}Pc$), 2,9,16,23-tetra-(*tert*-butyl)phthalocyaninato zinc (II) ($Zn(tBu)_4Pc$), tetrahydrofuran (THF), dichloromethane (DCM), acetone, ethyl acetate, petroleum ether, 1-octanethiol, potassium carbonate ($K_2CO_3$), sodium hydride (NaH) and anhydrous sodium sulfate ($Na_2SO_4$) were purchased from Sigma-Aldrich, Fisher Scientific or Acros Organics. Most reagents were used without further purification. 1-octanethiol was dried over basic alumina immediately prior to use. THF was freshly distilled over sodium and benzophenone before use to eliminate water, peroxides and butylated hydroxytoluene (BHT), a commercial stabilizer that has a pronounced fluorescence in the ultraviolet. Analytical thin-layer chromatography (TLC) was performed on polyester-backed TLC plates 254 (precoated, 200 μm, Sorbent Technologies). Preparative scale TLC was performed on glass-backed silica gel TLC plates (precoated, 1000 μm, Analtech). Silica gel 60 (70−230 mesh, Merck) was used for column chromatography.

$^1H$ NMR and $^{19}F$ NMR spectra were recorded at the Hunter College NMR facility on a 500 MHz Bruker Avance and 400 MHz Bruker Avance III spectrometers, respectively. The $^{19}F$ nucleus resonates at 376.5 MHz on the latter instrument. Proton chemical shifts are expressed in ppm

relative to the residual peak of the solvent used – either $CDCl_3$ (7.26 ppm, $^1H$) or $(CD_3)_2CO$ (2.05 ppm, $^1H$). Fluorine chemical shifts are reported relative to trichlorofluoromethane ($CCl_3F$, 0.00 ppm, $^{19}F$). Matrix-assisted laser desorption/ionization time-of-flight (MALDI-TOF) mass spectrometry was performed at the Shared Instrument Facility at New York University using a Bruker UltrafleXtreme MALDI-TOF acquired through the support of the National Science Foundation under Award Number CHE-0958457. The matrix used was a 20 $mg \cdot mL^{-1}$ solution of 2,5-dihydroxy benzoic acid (DHB, Sigma) in a 30:70 v/v ratio mixture of THF to 0.1% trifluoroacetic acid (TFA) in water. For each sample, this matrix solution was used to make a sub-millimolar Pc solution, and subsequently spotted onto a ground steel target plate and allowed to air dry. The instrument was operated in reflectance mode with positive ion detection. For the starting material of our compounds, $ZnF_{16}Pc$, the intact molecular ion was observed and used as an external single-point calibration reference for all subsequent samples.

UV-visible absorbance spectra were obtained with a Lambda 35 UV-Vis spectrophotometer from Perkin-Elmer. Calibration curves were generated from dilute solutions with absorbance less than approximately 0.1 at the $\lambda_{maz}$, as detailed in Appendix C. Steady-state fluorescence spectra were acquired on a HORIBA Scientific FluoroLog-3 fluorescence spectrometer. Quantum yields were also calculated from series of dilute solutions using the relative gradient method described in Appendix C, with $Zn(t\text{Bu})_4Pc$ in deaerated toluene as a standard. Fluorescence lifetimes were recorded using the FluoroHub Tau-3 time-correlated single photon counting (TCSPC) module for the same instrument. Excitation for TCSPC was provided by a pulsed diode laser source with a peak wavelength of either 653 nm (NanoLED-650L, HORIBA) or 667 nm (NanoLED-670L, HORIBA), each with a pulse duration of less than 200 ps. The data

collected in this manner were subjected to standard multi-exponential fitting using the Decay Analysis Software package (v. 6.4) bundled with the instrument.

DFT and TD-DFT calculations were performed with the Gaussian 09 software package using the resources of the City University of New York High Performance Computing Center based at the College of Staten Island and supported under National Science Foundation Grants CNS-0958379, CNS-0855217, ACI-1126113. Avogadro 1.1.1 was used to construct the models, generate the input files, and process and visualize the orbital surfaces. All DFT and TD-DFT calculations were performed using the B3LYP hybrid exchange-correlation functional and the 6-31G(d,p) basis set. The THF solvent contribution was simulated using the Polarizable Continuum Model (PCM). Ground state optimizations were performed with equilibrium PCM solvation and accompanied by frequency calculations to ensure the absence of imaginary frequency modes which would indicate a transition state. Vertical excitation (*i.e.* absorption) energies were obtained by performing single-point TD-DFT calculations of the excited electronic states at the ground state optimized nuclear geometry under non-equilibrium, state-specific PCM solvation conditions.

### 4.2.2. Synthesis

The synthesis for most of the compounds in the series largely follows the procedure previously reported.[7] In short, solid $ZnF_{16}Pc$ was added to dry THF under $N_2$ along with either $K_2CO_3$ or NaH as a base. Then, 1-octanethiol was injected into the reaction vessel and brought to temperature for the specified time. The extent of substitution was controlled through a combination of stoichiometry, heat, and reaction duration, with higher thiol:Pc ratios, higher temperatures, and longer times producing more substituted products. For the most highly substituted products, sodium metal was used instead of base to generate the thiolate nucleophile *in situ*, as described below.

After the reaction was stopped, the THF was evaporated and the crude mixture was washed with deionized water and extracted into ethyl acetate. The organic layer was dried over $Na_2SO_4$ and filtered, and the ethyl acetate removed under reduced pressure at low temperature to prevent oxidation of the sulfides to sulfoxides or sulfones. This was then passed through a silica column, first with hexanes to remove the unreacted thiol, followed by ethyl acetate to obtain a mixture of substituted phthalocyanines. The individual products were separated from this mixture by silica gel preparative scale TLC using a combination of ethyl acetate and hexanes as the eluent. The separated TLC bands were then scraped off and filtered through hydrophobic 0.20 μm PTFE syringe filter tips (Millipore) using ethyl acetate. See Appendix C for spectroscopic and mass spectrometry characterization.

## 4.3. Results & Discussion

### 4.3.1. Synthesis & Characterization

This series of Pcs was synthesized *via* nucleophilic substitution on the $ZnF_{16}Pc$ platform, as shown in **Scheme 4.1**. Considering only the number of substituents on the macrocycle, there are 16 possible products from the reaction described. For brevity, we refer to these as $ZnF_{16-x}(SR)_xPc$ where x = 0 to 16, indicating the number of appended thioalkyl chains. This synthetic route is remarkably robust to variations in the reaction conditions, with virtually any base and any polar aprotic solvent being suitable. NaH greatly accelerated the reaction, reducing both the time and heat required for extensive substitution. The reaction is easily monitored by UV-Vis absorbance spectroscopy, since there is a red-shift in the absorbance peak of about 6 nm as each F atom is exchanged for a thioalkane group.

The starting $ZnF_{16}Pc$ material is a turquoise blue powder which becomes a brilliant green, sticky solid upon substitution. Eventually, after about 10 thiols have been added, the green color fades to a yellowish brown and the products become a thick, viscous oil. The addition of the long chain hydrocarbons at random positions frustrates the crystal packing of the material, which also prevents aggregation in solution and greatly enhances the solubility. The most highly substituted products are fully soluble even in nonpolar hexanes. However, extensive substitution is accompanied by its own set of issues, including more difficult separation and a decreased stability towards oxidation.[41]

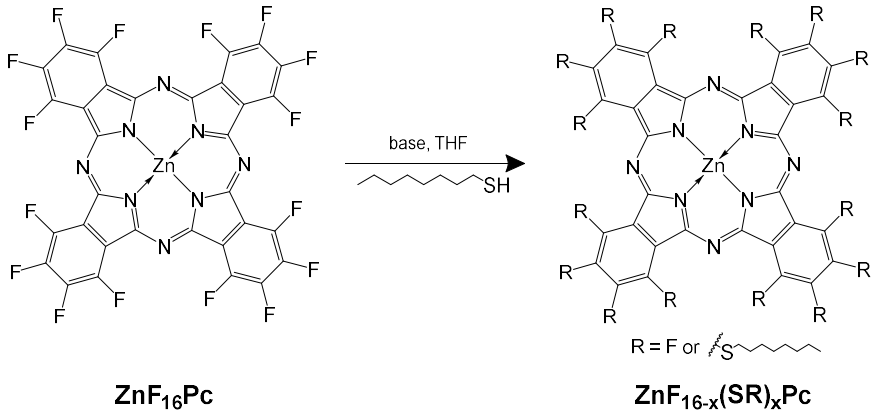


**Scheme 4.1**. Control of reaction conditions and stoichiometry of the nucleophilic aromatic substitution of the fluorine groups on $ZnF_{16}Pc$ by thiols results in a number of different substituted products and isomers.

### 4.3.2. Statistical Analysis

Given the nature of the reaction, discussion of the combinatorial statistics is warranted. The problem of analyzing the isomeric products of porphyrin and phthalocyanine condensation or substitution has been addressed.[42-51] One approach to drug development is to generate large libraries of porphyrinoid products which are then tested and optimized for some desired application. For materials, however, mixtures of these dyes may have superior properties. Lindsey *et al*. presented a detailed discussion of this problem accompanied by a custom program (PorphyrinViLiGe©) designed to generate a list of the potential products based on a statistical analysis.[42-45] Although capable of handling complex reactions involving multiple substituents

or precursors, Lindsey's program has some limitations that prevent a direct analysis of the situation discussed here. Specifically, the simulated reaction types only allow for the derivatization of at most eight equivalent positions of the macrocycle, corresponding to either all $\beta$ or all $\alpha$ substitution in the case of a Pc. The $ZnF_{16}Pc$ platform utilized may be substituted at any of the 16 fluorine positions, and in order to fully characterize the series of products, it is important to understand the distribution of isomers among them.

It is trivial to calculate the number of permutations of a given number of substituents around the 16 possible positions of the $ZnF_{16}Pc$ macrocycle. Given $n$ substituents, there are ${}_{16}C_n = 16!/[n!\,(16-n)!]$ such combinations. However, not all of these arrangements correspond to physically distinct molecules. Many of them are merely rotations of one another under the proper symmetry subgroup of the $D_{4h}$ point group of the parent molecule. While Pólya's enumeration theorem[52-54] may be used to count the true number of unique isomers under this symmetry group, it does not provide a detailed listing of the individual microstructures. To that end, we have written a program that takes the number of substitutions as an input and steps through every possible permutation according to a previously published algorithm.[55] After this enumeration, the rotational transformations of the proper symmetry subgroup are applied to each permutation to compare it to the others, eliminate the duplicates, and count the remaining isomers.

The program code is given in Appendix C along with a more detailed description and plots (Figure C1) of the number of permutations and distinct isomers as a function of the number of substituents. The two plots shown in Figure C1 correspond to two different assumptions regarding the nature of the reaction. For the unrestricted plot (A), we assume that all sixteen positions have an equal probability of being substituted during the reaction, and we therefore see a maximum number of isomers for $ZnF_8(SR)_8Pc$. In the restricted plot (B), we assume that the more kinetically

available $\beta$ positions must all react first, with equal probability, before any $\alpha$ position is substituted. This condition, which is more representative of the actual reaction products, means that $ZnF_8(SR)_8Pc$ will be nearly isomerically pure, while $ZnF_{12}(SR)_4Pc$ and $ZnF_4(SR)_{12}Pc$ have the largest number of possible isomers. It is impractical to separate all of the positional isomers, and for materials this is not *a priori* necessary. Thus, the macroscopic materials properties and spectroscopic data of any given Pc in this family actually represent a weighted statistical average of the ensemble of isomers.

### 4.3.3. UV-Vis Spectroscopy

The photophysical data is given in **Table 4.1**, and the UV-Vis absorbance spectra are shown in **Figure 4.1**. Calibration curves of absorbance vs. molar concentration (see Appendix C, Figures C3 and C4) demonstrate excellent linearity within the observed concentration range for all samples, confirming the applicability of the Beer-Lambert law and the absence of significant aggregation effects.

The intense color of Pcs is due mainly to the strong absorbance peak in the red region, the Q band, and its higher energy vibronic satellite. As seen in **Table 4.1** and **Figure 4.1**, these bands shift approximately 6 nm to the red for each appended thioalkane chain. Pcs also have a higher energy B band, which can be seen in the expanded UV-visible plots given in Appendix C (Figure C2). The B band falls mainly in the ultraviolet for the unsubstituted starting material, but grows slightly in the visible as more thioalkane groups are added to the macrocycle. In addition to the approximately linear increase in the absorbance $\lambda_{max}$, there is also an increase in the full width at half-max (FWHM, **Figure 4.1-C**). The FWHM increases slightly at first, and then discontinuously jumps by about 15 nm after eight thioalkyl substituents have been added to the core, followed by only slight increases thereafter.

**Table 4.1**. Photophysical parameters for all standards and compounds studied, in dilute THF solution.

| Compound | Abs. $\lambda_{max}$ (nm) | log ε | Fluor. $\lambda_{max}$ (nm) | $\phi_f$ | Stokes Shift (nm) | $\tau$ (ns) | $k_f$ ($ns^{-1}$) | $k_{nr}$ ($ns^{-1}$) |
|---|---|---|---|---|---|---|---|---|
| ZnPc | 666 | 5.48[a] | 671 | 0.100[b] | 5 | 3.38 | 0.030 | 0.266 |
| Zn(*t*Bu)$_4$Pc | 672 | 5.43[c] | 676 | 0.081[d] | 4 | 3.28 | 0.025 | 0.280 |
| $ZnF_{16}Pc$ | 672 | 5.24[e] | 678 | 0.057 | 6 | 2.75 | 0.021 | 0.343 |
| $ZnF_{15}(SR)Pc$ | 679 | 5.32 | 685 | 0.061 | 6 | 2.64 | 0.023 | 0.356 |
| $ZnF_{14}(SR)_2Pc$ | 686 | -- | 693 | 0.046 | 7 | 2.73 | 0.017 | 0.349 |
| $ZnF_{13}(SR)_3Pc$ | 692 | 5.08 | 701 | 0.037 | 9 | 2.52 | 0.015 | 0.382 |
| $ZnF_{12}(SR)_4Pc$ | 698 | 5.44 | 707 | 0.042 | 9 | 2.53 | 0.017 | 0.379 |
| $ZnF_{11}(SR)_5Pc$ | 704 | 5.36 | 713 | 0.033 | 9 | 2.27 | 0.015 | 0.426 |
| $ZnF_{10}(SR)_6Pc$ | 708 | 5.29 | 718 | 0.034 | 10 | 2.20 | 0.015 | 0.439 |
| $ZnF_9(SR)_7Pc$ | 716 | 5.46 | 724 | 0.030 | 8 | 2.15 | 0.014 | 0.451 |
| $ZnF_8(SR)_8Pc$ | 720 | 5.47 | 729 | 0.025 | 9 | 2.08 | 0.012 | 0.469 |
| $ZnF_7(SR)_9Pc$ | 727 | -- | 743 | -- | 16 | -- | -- | -- |
| $ZnF_6(SR)_{10}Pc$ | 731 | -- | 748 | 0.006 | 17 | 1.67[f] | 0.004 | 0.595 |
| $ZnF_5(SR)_{11}Pc$ | 733 | 4.97 | 753 | 0.009 | 20 | 1.59 | 0.006 | 0.623 |
| $ZnF_4(SR)_{12}Pc$ | 740 | 4.89 | 761 | 0.005 | 21 | 1.33 | 0.004 | 0.748 |
| $ZnF_3(SR)_{13}Pc$ | 749 | 5.12 | 771 | 0.005 | 22 | 1.29 | 0.004 | 0.771 |
| $ZnF_2(SR)_{14}Pc$ | 755 | -- | 778 | 0.004 | 23 | 1.30[f] | 0.003 | 0.766 |
| $ZnF(SR)_{15}Pc$ | 768 | -- | 796 | -- | 28 | -- | -- | -- |
| $Zn(SR)_{16}Pc$ | 777 | 5.16 | 802 | 0.003 | 25 | 1.38 | 0.002 | 0.722 |

[a] The extinction coefficient (log ε) of ZnPc in THF taken from reference [2]. [b] Quantum yield of ZnPc in toluene calculated as the average of the values in references [5] and [2]. [c] The extinction coefficient (log ε) obtained for Zn(*t*Bu)$_4$Pc in THF matches reference [2] to within less than 0.2%. [d] Quantum yield of Zn(*t*Bu)$_4$Pc standard in toluene, taken directly from reference [2]. [e] The extinction coefficient (log ε) obtained for $ZnF_{16}Pc$ in THF matches reference [19] to within less than 1.3%. [f] The decay required fitting with a second lifetime, close to the IRF width (<300 ps), as a minor component (<20%).

There are a few possible explanations for this broadening. First, the chromatographic separation becomes more difficult with increased substitution. As more thioalkanes are added, the preparative TLC bands become very close with even the most nonpolar eluents. While this does lead to traces of other compounds with x ± 1 for the more substituted compounds, this does not

cause the observed broadening and cannot account for the discontinuity. The broadening could also be the result of contributions from different positional isomers with slightly different absorption properties arising from small differences in the HOMO-LUMO gaps. However, if isomers were the primary cause of the Q band broadening, the trends in the FWHW would be expected to generally correlate with the calculated distributions of isomers (Figure C1). For the case in which the β positions react first, $ZnF_{12}(SR)_4Pc$ and $ZnF_4(SR)_{12}Pc$ would have the broadest peaks, while $ZnF_8(SR)_8Pc$ would have the broadest spectrum if the reaction were completely random. Since the observed changes in the peak widths do not correlate to either of these cases, the mixture of isomers is unlikely to be a dominant cause of the broadening.

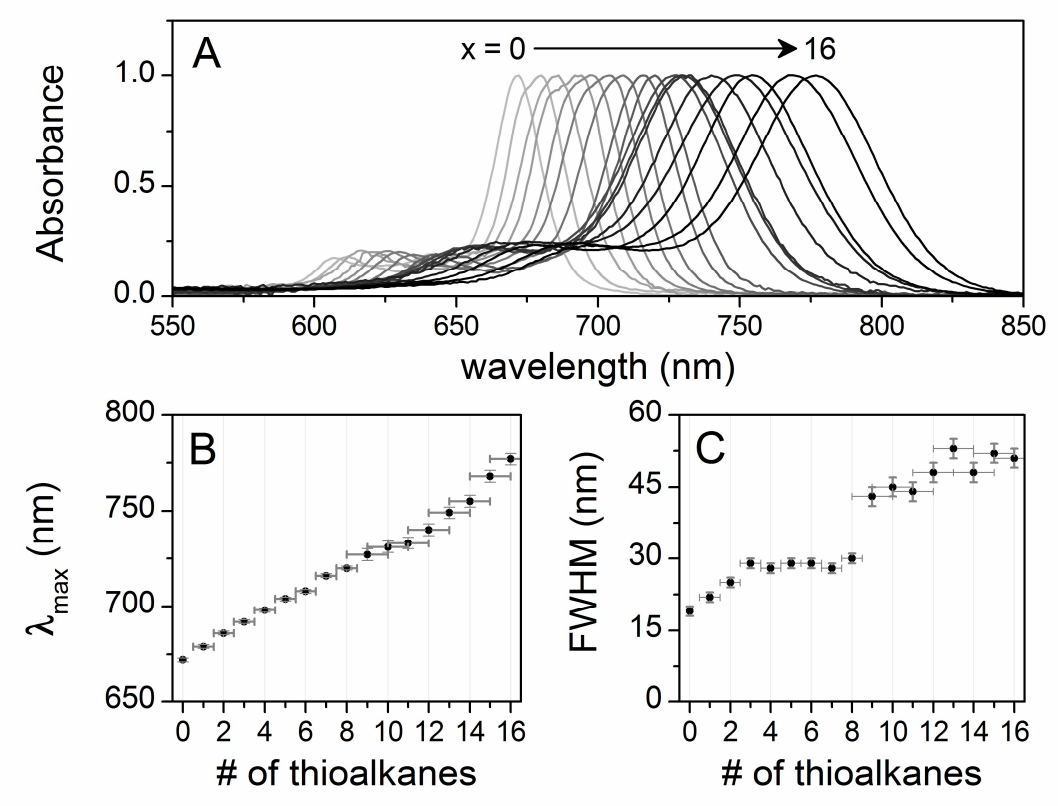


**Figure 4.1**. (A) Normalized absorbance spectra of compounds $ZnF_{16-x}(SR)_xPc$ (x = 0 to 16). (B) Wavelength of maximum absorbance ($\lambda_{max}$) as a function of the number of thioalkane substituents. (C) Peak widths as a function of the number of thioalkane substituents, as measured by the full-width at half maximum (FWHM).

A third potential explanation is that the broadening is due to fundamental changes in the electronic structure of the molecules as substituents are added. Breaking the symmetry of the degenerate LUMO orbitals, for instance, could cause the Q band transitions to become non-degenerate.[56] An extreme case of this is seen in free-base Pcs, in which the $D_{4h}$ symmetry has been completely broken to $D_{2h}$, resulting in the Q band splitting into two distinct peaks. An intermediate case might produce some of the broadening observed, as well as the asymmetry seen in some of the absorbance bands. It was reported that the asymmetry found in absorbance bands due to splitting is not mirrored in the emission band shape.[56] This is an example of Kasha's rule, which states that the initially formed excited state internally converts to the lower excited state before fluorescing. Several of the less substituted Pcs exhibit an asymmetry in their absorbance bands while all of the emission bands are nearly symmetrical. However, the emission does retain the broadness of the absorption bands (*vide infra*), indicating that Kasha's rule is not relevant. Orbital splitting is therefore unlikely to cause all of the observed band broadening.

Since the width of the absorbance spectra is related to the vibrational structure of the ground and excited electronic states, the sharp increase in the FWHMs after eight substitutions is best explained by a change in the conformational dynamics of the molecule. Substitution of the β positions is kinetically favored, and thus the first eight substitutions do not greatly alter the structure of the planar macrocycle. Upon substitution of the remaining α positions, however, steric interactions begin to either lower the energy barrier to non-planar vibrations or force non-planar distortions (*vide infra*).[33-40,57-61]

### 4.3.4. Steady-State Fluorescence Spectroscopy

Fluorescence emission spectra of all of the compounds, including $ZnF_{16}Pc$, are shown in **Figure 4.2**. The peaks of the spectra are scaled to the experimental quantum yield values to

highlight the quenching that occurs upon substitution. Like the absorbance spectra, the fluorescence bands also broaden as they shift towards the red. The quantum yields and Stokes shifts are plotted *vs.* the number of substituents in **Figure 4.2**.

Accurate values for fluorescence quantum yields can be difficult to obtain experimentally, so there is a large range of literature values for any ostensible standard. It is often impossible to ascertain from the detail given whether these discrepancies arise from aggregation effects, the presence of molecular oxygen, inner filter effects, or other unknown causes. Pcs are especially vexing in this regard due to their well-documented tendency to aggregate. For instance, addition

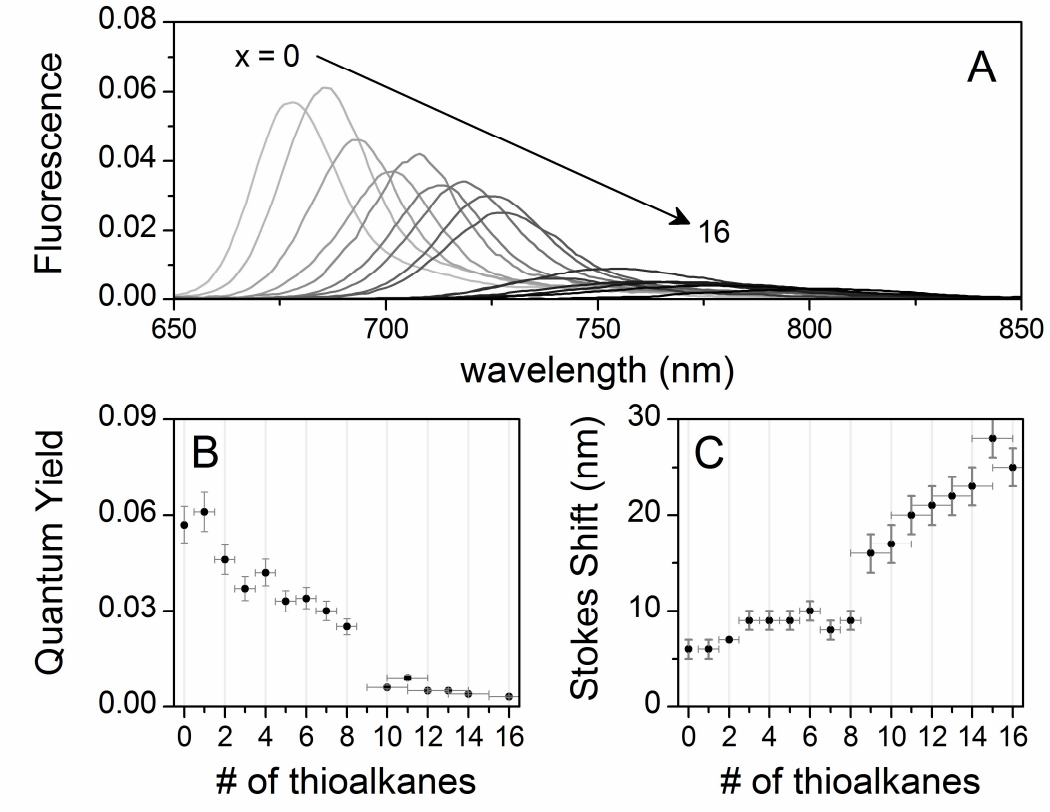


**Figure 4.2**. (A) Fluorescence emission spectra labelled by the number of thioalkane substituents, $ZnF_{16-x}(SR)_xPc$ (x = 0 to 16). The peak heights are scaled to match the quantum yield of the compound. (B) Quantum yields as a function of the number of thioalkane substituents. (C) Stokes shifts as a function of the number of thioalkane substituents.

of 1% pyridine to coordinate the zinc and frustrate π-stacking apparently increases the solubility and quantum yields.[62] However, we have preferred pure solvents for comparative purposes. As one example of the spread of literature values, Nyokong gives a $\phi_f$ value of 0.07 for ZnPc in deaerated toluene,[5] but then reports a value of 0.13 for the same compound relative to the same standard (chlorophyll *a* in ether) in a subsequent paper.[2] Therefore, Zn(*t*Bu)$_4$Pc in toluene, with $\phi_f$ = 0.081,[2] was chosen as a more reliable standard to generate an internally consistent set of quantum yields for this series.

Although the quantum yield of ZnF$_{16}$Pc in THF can also be found in the literature ($\phi_f$ = 0.15),[29] the value was calculated from a solution with relatively high absorbance near 630 nm, indicating significant formation of dimers and aggregates that do not contribute to fluorescence. We calculated $\phi_f$ = 0.057 for ZnF$_{16}$Pc (**Table 4.1**), which is almost three times less than theirs (see Appendix C). The decrease in fluorescence emission between ZnPc and ZnF$_{16}$Pc is best explained by the heavy atom effect[63-67] and the electron withdrawing effects caused by replacing hydrogens with fluorines.

The steady-state fluorescence data mirrors the absorbance data, showing a systematic red-shift in the emission $\lambda_{max}$ with increasing number of thioalkane substituents (**Figure 4.2-A**). The FWHM of the fluorescence peaks slightly increases for the first eight substitutions, followed by a discontinuous jump of about 20 nm. While there is no obvious relationship between the extent of substitution and the extinction coefficients or oscillator strengths, there is a clear correlation with the fluorescence quantum yield. **Figure 4.2-B** shows how $\phi_f$ decreases with each additional octylthio group until it is almost completely quenched by about the eighth or ninth substitution. This is consistent with the work of Kobayashi *et al*.,[68] who showed that the fluorescence is

quenched for compounds with an emission $\lambda_{max}$ greater than about 740 nm. The authors explain this relationship in terms of the Energy Gap Law,[69] which predicts an exponential increase in the rate of radiationless transitions between two electronic states as the energetic separation between them decreases.

The Stokes shift also correlates to the number of thioalkanes (**Figure 4.2-C**), with a slight increase observed over the first 8 substitutions, followed by a jump around the $11^{th}$ substitution and a steeper increase thereafter. The Stokes shift is a measure of the difference between the excitation and emission energies, which arises from differences in the nuclear configurations of the ground and excited states. The range of values for Pcs is generally around 5–10 nm.[40] Increased Stokes shifts and broadened, asymmetric peak shapes are characteristic of non-planar porphyrins and Pcs.[40,70] The Stokes shifts for the most substituted compounds in this study are almost 30 nm. These are among some of the highest reported for Pc compounds in the literature, indicating that substantial conformational changes are induced upon substitution at the α position.

### 4.3.5. Lifetimes and Rate Constants

The fluorescence lifetimes are also given in **Table 4.1** and plotted *vs*. the number of appended thioalkyl chains in **Figure 4.3**. A general decrease in the lifetime with substitution is observed, tracking the decrease in quantum yield. The lifetime and the quantum yield allow determination of the fluorescent radiative rate constant using **Eq. 4.1**.

$$\phi_f = \frac{k_f}{k_f + k_{nr}} = k_f \tau \qquad (4.1)$$

Here, $k_f$ is the natural fluorescence rate constant, and $\tau$ is the observed fluorescence lifetime. In the absence of other non-radiative deactivation pathways, the observed lifetime would

approach the natural fluorescent lifetime, $1/k_f$, and the quantum yield would approach unity. The $k_{nr}$ term accounts for all of the non-radiative excited state energy, and can be calculated through the complement to the fluorescence quantum yield using **Eq. 4.2**.

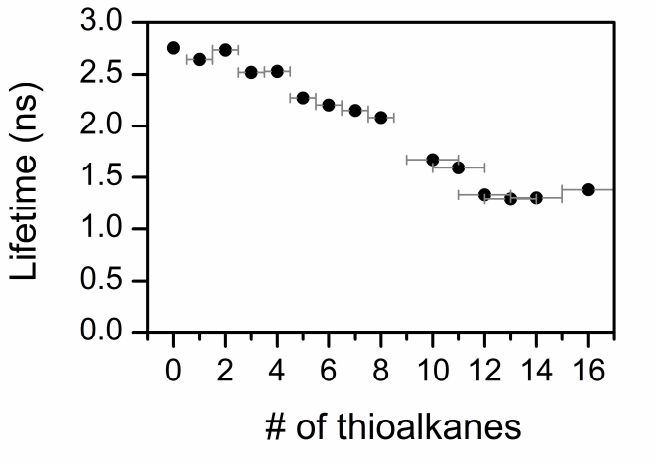


**Figure 4.3**. Fluorescence lifetimes as a function of the number of thioalkane substituents.

$$1 - \phi_f = \frac{k_{nr}}{k_f + k_{nr}} = k_{nr}\tau \tag{4.2}$$

These photophysical parameters are plotted as a function of substitution number in Figure C6. In the absence of quenching, excited state reactions, or other competing pathways, $k_{nr}$ only includes contributions from intersystem crossing to the triplet state and internal conversion. The fluorescence rate constant $k_f$ decreases with the quantum yield and lifetime, reaching an apparent minimum by the 10$^{th}$ substitution. The non-radiative rate constant $k_{nr}$ steadily increases and then jumps up at the 10$^{th}$ substitution. Both trends are consistent with the observations regarding the FWHM and the Stokes shift.

Intersystem crossing to the triplet state generally takes place through spin-orbit coupling, and is enhanced by the presence of atoms with greater atomic numbers. This heavy atom effect is known to be promoted by sulfur atoms.[71-74] At the same time, thermal relaxation can be enhanced through the addition of thioalkyl groups. First, the addition of long chain alkanes will introduce new vibrational modes that help to dissipate heat.[75] The contribution of this "loose-bolt effect"[76] depends on the coupling between the substituents and the core macrocycle.

Another mechanism is the aforementioned Energy Gap Law.[69] When there is a small energy difference between the ground and excited states, and correspondingly similar molecular geometries, there will be a large overlap in the Franck-Condon factors determining vibronic coupling between them. This leads to an approximately exponential increase in the strength of radiationless transitions from $S_1$ to $S_0$ as the energy gap decreases upon substitution. In addition to these internal conversion processes, there are also external conversion mechanisms that transfer excess energy as heat to another particle, such as a solvent molecule. Attaching thioalkyl chains to the Pc core changes the size, weight, aggregation, and polarity of the molecule, all of which will affect how it interacts with solvent molecules to dissipate energy.

In addition to these factors, there are also literature reports that describe an enhancement of non-radiative relaxation due to the distortion of the macrocycle. The photophysical consequences of non-planar distortions are reported for porphyrins,[77-85] but are much less well understood in Pcs.[58,61,70] Distorted or non-planar Pcs have been reported, but the accompanying photophysical studies focus on the electronic and emission spectra.[33-39,59,60] Conversely, detailed photophysical studies of Pcs often neglect considering the possibility of structural distortions.[68] In porphyrins, distortion is known to cause broadened, red-shifted absorption and emission bands, increased Stokes shifts, lower fluorescence quantum yields and lifetimes, and even higher rates of intersystem crossing.[86-88] All of these characteristics were unexpectedly observed in our series of Pcs, lending credibility to the hypothesis that the more highly substituted members adopt non-planar conformations. Our assumption that the β position reacts first is also consistent with the trends in the photophysical data, since the distortion is induced by steric crowding of the α substituents after the $8^{th}$ addition, with this effect being further exacerbated after the $11^{th}$ substitution.

It is important to note that the nuclear potential energy surfaces will be more complex for a distorted Pc than a planar one. The former will have multiple local minima separated by barriers to interconversion, and these barriers may be lower in the excited states. Upon light absorption, the initially formed excited state will internally convert to the lowest excited state $S_1$, imparting a significant amount of energy into the macrocycle. This energy can be enough to overcome the barriers in the potential energy surface and open up new conformational dynamics.[89]

### 4.3.6. DFT and TD-DFT

Many authors explain the photophysical properties in terms of the electronic effects of electron withdrawing and releasing groups, with mixed success. It is generally agreed[68,90-93] that the HOMO is more sensitive to substituent effects than the LUMO, and that α substitution has a larger effect on the size of the HOMO-LUMO gap than β substitution. In turn, these observations are justified by noting the relative size of the orbital coefficients at the α and β positions of the HOMO. However, octa-α substituted Pcs can be as much as three times more red-shifted than their tetra-α substituted counterparts, and the red-shift induced by octa-α substitution is nearly 20 times larger than that caused by octa-β substitution, despite there being only small differences in the α and β orbital coefficients.[68] Thus, inductive electronic effects cannot account for all of the photophysics. To further clarify these electronic and structural factors, we performed quantum chemical calculations on a series of model compounds.

Representative compounds from this series were analyzed using Density Functional Theory (DFT) and Time-Dependent DFT (TD-DFT). Given computational limitations, it was necessary to choose a handful of compounds spanning the series of products. To fully elucidate both structural and electronic inductive effects, this analysis was undertaken in three parts. First, a series of compounds in which the $\beta$ positions have been substituted first were studied. The

particular isomers are depicted in the first row of **Figure 4.4**. These structures were optimized to find the minimum energy conformations, ground state energy levels, and molecular orbital surfaces by DFT. Subsequent to this, TD-DFT was used to find all of the excited states with energies below about 3.5 eV, including the transition energies, oscillator strengths, and the Configuration Interaction (CI) expansions of the excited state wavefunctions.

A second series of compounds was also generated in which the α positions were substituted first. This series is seen in the second row of **Figure 4.4**. While these α isomers are probably only a very minor component of the overall ensembles to which they belong, they are nevertheless physically realistic. They can be taken to provide a rough estimate of the range of HOMO and LUMO energies expected within the isomeric ensembles, and provide some insight into how substitution can distort the Pc core. As with the first series, the structures were optimized by DFT, and the orbital energies and surfaces were calculated.

For the final series, seen in the last row of **Figure 4.4**, we wished to investigate the effects of structural distortions on the core macrocycle. Several compounds were constructed and analyzed with fixed, non-equilibrium geometries in order to compare them to their optimized counterparts. For $ZnF_{16}Pc$-d, $ZnF_{12}(SR)_4Pc$-β-d, $ZnF_{12}(SR)_4Pc$-α-d, and $ZnF_8(SR)_8Pc$-β-d, the molecules were constructed with a distorted conformation by taking the optimized $Zn(SR)_{16}Pc$ result from the first series and modifying the substituents appropriately. On the other hand, the core macrocycles for $ZnF_8(SR)_8Pc$-α-p and $Zn(SR)_{16}Pc$-p were frozen into a planar structure taken from the optimized $ZnF_{16}Pc$ result from the first series. The structures for this series were not optimized, so as to preserve the artificially imposed conformations chosen. Instead, single-point energy calculations were performed by DFT to find the MO levels and surfaces.

For the compounds in the first series, isosurfaces of the two $e_g$ LUMOs and the $a_{1u}$ HOMO are depicted in **Figure 4.5** along with an edge-on perspective of the molecular structure to help visualize deviations from planarity. It should be noted that while $ZnF_4(SR)_{12}Pc$-β is designated as nominally planar in **Figure 4.5**, there is some distortion despite it being the least sterically hindered 12-substituted isomer possible. It is clear from the figure that the overall shapes of the relevant frontier orbitals are not dramatically changed by the addition of the thioalkyls. Interestingly, this is even true for the most highly substituted compounds, despite significantly distorted geometries. The underlying symmetry of the parent molecule is largely preserved, with only small perturbations depending on the substitution pattern.

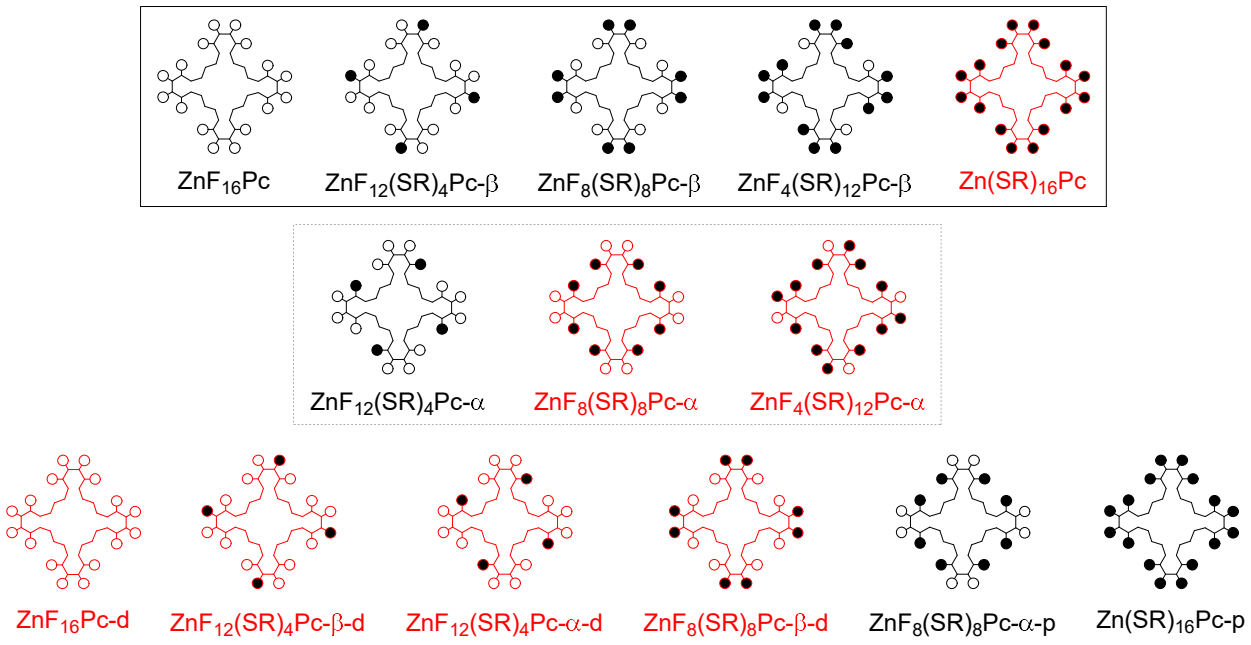


**Figure 4.4**. Schematic diagram of the specific compounds studied by DFT. Open circles (○) represent fluorine atoms and closed circles (●) represent *n*-butylthio substituents. Structures drawn in black are nominally planar, while those drawn in red are distorted. The first row, enclosed in a solid rectangle, includes isomers in which the β positions have been substituted first. The second row, enclosed in a dashed rectangle, includes isomers in which the α positions have been substituted first. The last row includes some of the same positional isomers, but with the core macrocycle artificially "frozen" into either a distorted or planar geometry, indicated by the suffix "-d" or "-p", respectively. For this row, geometry optimization was only performed on the substituent chains, and then a single-point energy calculation was done to find the orbital energies.

In Gouterman's four-orbital model for metalloporphyrins,[94,95] the two LUMOs are a set of degenerate $e_g$ orbitals, while the two HOMOs are "accidentally" degenerate, with $a_{1u}$ and $a_{2u}$ symmetry designations. Configuration interaction between these four states results in a pair of pseudo-parity forbidden, low energy transitions (the Q bands) and a pair of fully allowed, high energy transitions (the B or Soret bands). In Pcs, the near-degeneracy of the HOMO levels is broken by the presence of the aza-bridge nitrogens and the fused benzene rings.[90,91,96] The $a_{2u}$ orbital, having significant electron density on the more electronegative aza bridges, is lowered in energy by several electron volts relative to the $a_{1u}$ orbital. This electronic structure is essentially the same in $ZnF_{16}Pc$, despite the overall energies being slightly lowered by the presence of the fluorine atoms.[97] From the DFT results we have obtained for $ZnF_{16}Pc$, it is actually the HOMO-9 level (*i.e.* the 10$^{th}$ highest MO, see **Figure 4.6**) which corresponds to the $a_{2u}$ HOMO found in metalloporphyrins. With the $a_{1u}/a_{2u}$ degeneracy removed, the low energy transition no longer cancels, and the Q band becomes fully allowed. The $e_g$ LUMOs retain their degeneracy but are slightly stabilized, red-shifting the Pc peak relative to porphyrin.

The energies of these frontier orbitals are shown in **Figure 4.6**, along with some other lower lying occupied MOs that are involved in transitions in the UV-visible region. From the diagram it is clear that the orbitals are generally destabilized as electron releasing thioalkane groups are introduced. This effect is greater for the HOMO, which has significant probability density around all sixteen reactive positions, than for the LUMOs, which have density on only eight of these positions each. This leads to the red-shift observed in the Q band, and is also consistent with cyclic voltammetry studies carried out by Varotto *et al*., which show the HOMO is raised relative to the LUMO.[7] Furthermore, the addition of various thioalkyl chains introduces many new orbitals at energies between the original Gouterman $a_{1u}$ and $a_{2u}$ HOMOs. These new

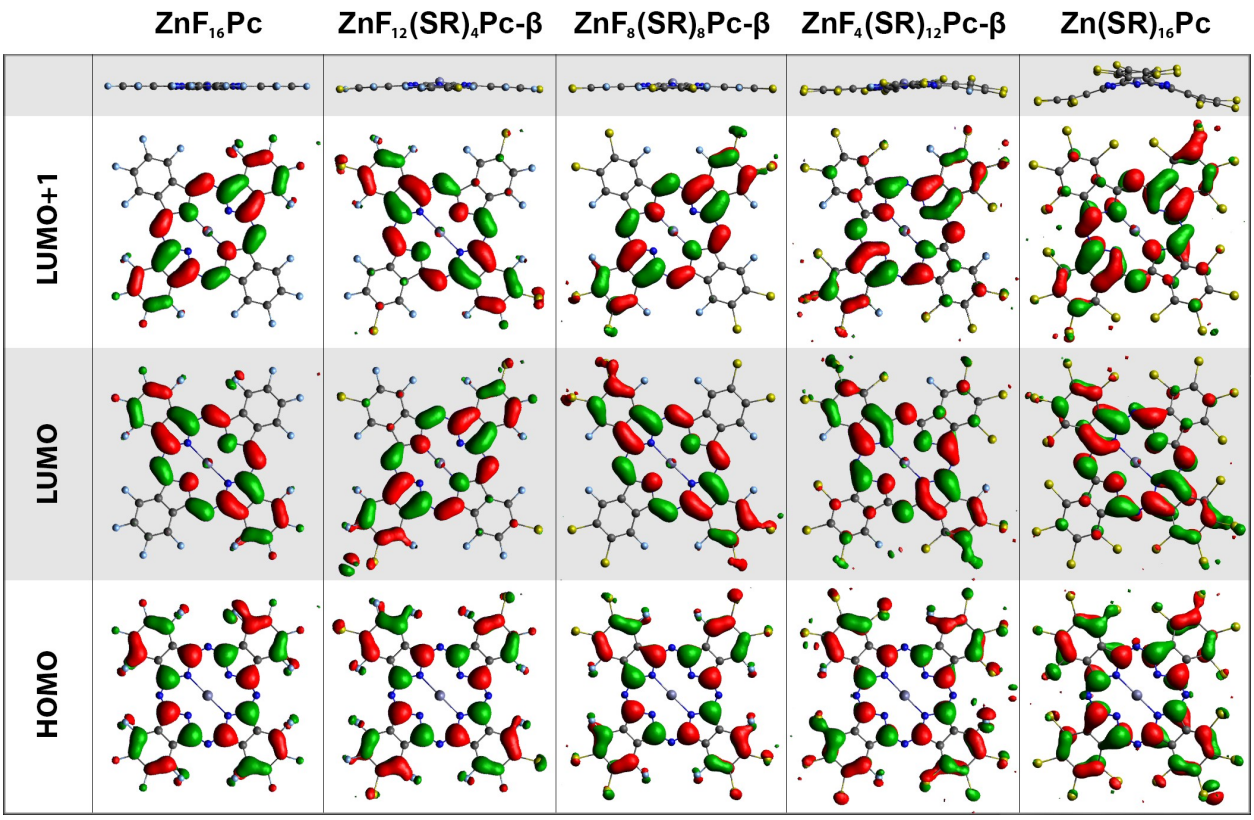


**Figure 4.5**. Frontier molecular orbitals (bottom rows) and edge-on views (top row) of the optimized molecular structures for representative (alkylthio)-Zn(II)Pcs. Gray atoms are carbon, dark blue are nitrogen, light blue are fluorine, and yellow are sulfur. Structures were optimized with *n*-butylthio groups in place to reduce computation time. For visual clarity, the hydrocarbon chains have been deleted from the images, along with some small regions of electron density associated with them.

orbitals are likely to play some part in the band broadening, and could also have an effect on the peak position as they begin to mix with the HOMO-LUMO transition.

The DFT results shown in **Figure 4.6** predict that the additive electronic effect of the substituents will only be approximately linear through the first eight substitutions, after which it becomes smaller and even reverses by the time all sixteen fluorines have been replaced. It appears that at some point after the first eight thioalkanes have been added, further destabilization of the HOMO is offset by a corresponding destabilization of the LUMOs. In fact, this data suggests that

the fully substituted $Zn(SR)_{16}Pc$ should actually be blue-shifted relative to $ZnF_8(SR)_8Pc$, a prediction that is reinforced by the TD-DFT transitions calculated for these compounds.

The TD-DFT calculated oscillator strengths of these transitions are plotted *vs*. wavelength in **Figure 4.7**. This data is also presented in **Table 4.2**, along with the weights and characters of the singly-excited configurations contributing to each transition. The decomposition of the excited-state wavefunctions shows that, in all cases, the observed Q bands arise almost exclusively from HOMO→LUMO transitions. This also yields a double-band structure due to the LUMO and

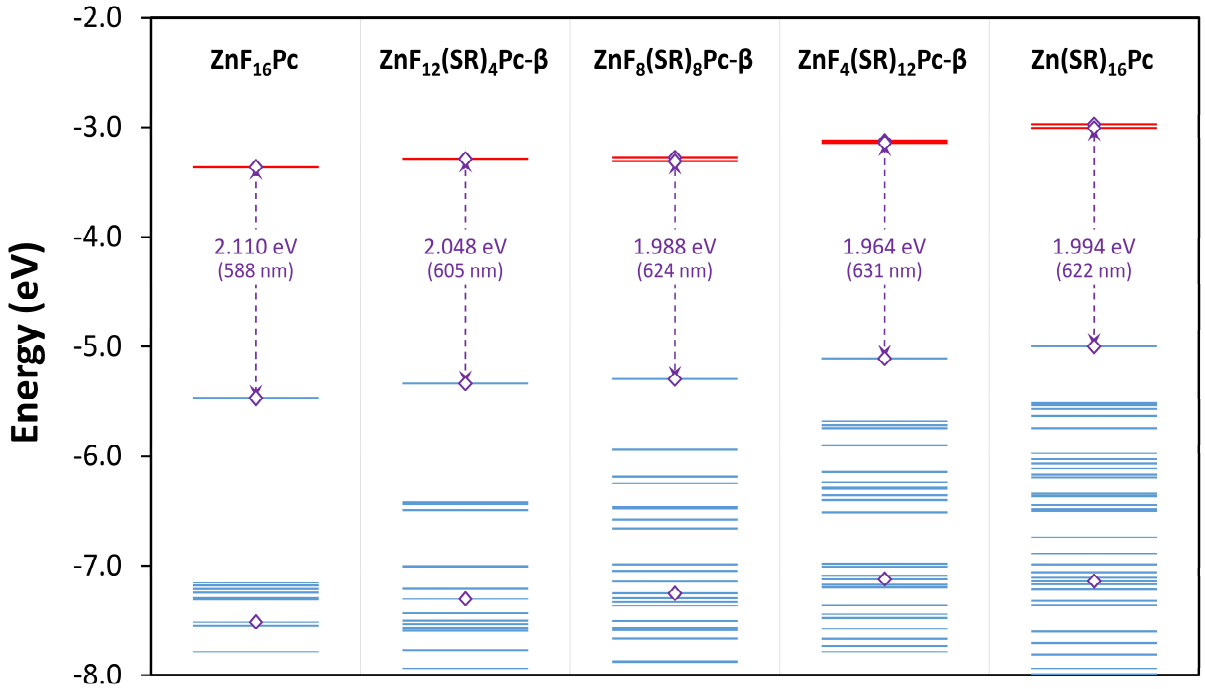


**Figure 4.6**. Energies for the frontier molecular orbitals of $ZnF_{16}Pc$, $ZnF_{12}(SR)_4Pc$-β, $ZnF_8(SR)_8Pc$-β, $ZnF_4(SR)_{12}Pc$-β, and $Zn(SR)_{16}Pc$ between -2.0 and -8.0 eV, as calculated by DFT using the B3LYP hybrid functional and the 6-31G(d,p) basis set. The highest occupied orbitals are shown as blue lines, and the lowest unoccupied virtual orbitals are shown as red lines. There are two LUMOs shown for every compound, though they appear as a single line when the energies are degenerate or nearly so. Purple diamonds (◊) mark the orbitals associated with Gouterman's original model. The HOMO-LUMO energy gaps are also shown in both electron volts and nanometers.

LUMO+1 levels, which are degenerate or nearly degenerate. The degeneracy is broken by the addition of the thioalkyl chains, which leads to a splitting of the transitions associated with the Q bands. Again, the splitting is not resolved in the experimental UV-visible spectra, but it is likely to be at least partially responsible for the broadening of the bands observed in more substituted compounds.

The simulated TD-DFT spectra also predicts the appearance of a very broad, shallow absorbance in the region between the Q and B bands as the Pc is progressively substituted. This feature is, in fact, observed in the experimentally observed UV-visible spectra shown in Figure C2. The decomposition of the wavefunctions for these transitions show that they arise due to the

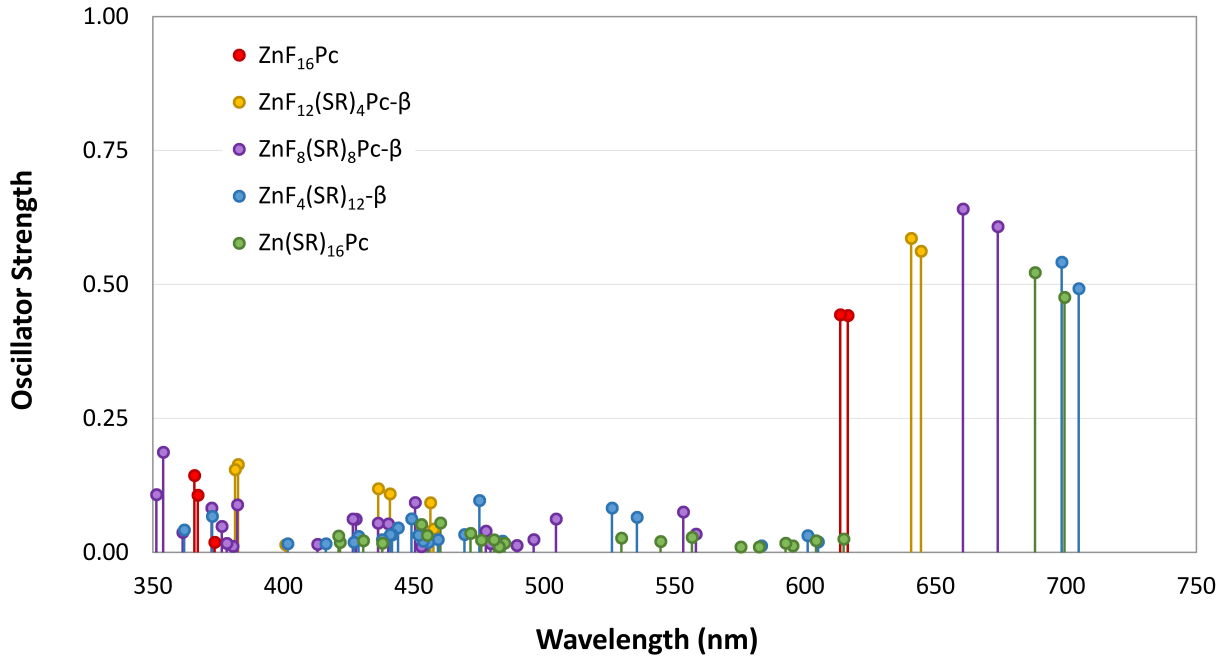


**Figure 4.7**. Electronic transitions between 350 and 750 nm for compounds $ZnF_{16}Pc$, $ZnF_{12}(SR)_4Pc$-β, $ZnF_8(SR)_8Pc$-β, $ZnF_4(SR)_{12}Pc$-β, and $Zn(SR)_{16}Pc$. Only transitions with oscillator strengths above 0.01 are included.

manifold of new energy levels introduced between the two original Gouterman HOMOs, marked with purple diamonds in the chart. Inspection of the orbital surfaces for these new levels shows that they are primarily associated with the sulfur atoms introduced around the periphery. Many of them also appear to be hybridized with the core macrocycle orbitals, breaking the symmetry enough to relax the Laporte selection rules.

**Table 4.2**. Electronic transitions for $ZnF_{16}Pc$, $ZnF_{12}(SR)_4Pc$-β, $ZnF_8(SR)_8Pc$-β, $ZnF_4(SR)_{12}Pc$-β, and $Zn(SR)_{16}Pc$, calculated by TD-DFT using the B3LYP hybrid exchange-correlation functional and the 6-31G(d,p) basis set.

| λ (nm)[a] | $f$[b] | Wavefunction[c] |
|---|---|---|
| | | ***$ZnF_{16}Pc$*** |
| 616 | 0.442 | 95% (H→L) + … |
| 613 | 0.444 | 95% (H→L+1) + … |
| 374 | 0.019 | 61% (H–5→L+1) + 34% (H–3→L) + … |
| 367 | 0.107 | 5% (H–9→L+1) + 30% (H–5→L+1) + 63% (H–3→L) + … |
| 366 | 0.144 | 6% (H–9→L) + 21% (H–5→L) + 67% (H–3→L+1) + … |
| | | ***$ZnF_{12}(SR)_4Pc$–β*** |
| 644 | 0.562 | 96% (H→L) + … |
| 641 | 0.586 | 96% (H→L+1) + … |
| 458 | 0.044 | 10% (H–2→L) + 84% (H–2→L+1) + … |
| 456 | 0.093 | 7% (H–4→L) + 72% (H–2→L) + 9% (H–2→L+1) + 10% (H–1→L) + … |
| 441 | 0.110 | 88% (H–4→L) + 7% (H–2→L) + … |
| 436 | 0.119 | 94% (H–4→L+1) + … |
| 401 | 0.014 | 93% (H–8→L+1) + … |
| 383 | 0.164 | 93% (H–6→L) + … |
| 382 | 0.155 | 93% (H–6→L+1) + … |
| | | ***$ZnF_8(SR)_8Pc$–β*** |
| 674 | 0.608 | 96% (H→L) + … |
| 661 | 0.641 | 95% (H→L+1) + … |
| 558 | 0.034 | 6% (H–1→L) + 92% (H–1→L+1) + … |
| 553 | 0.076 | 92% (H–1→L) + 6% (H–1→L+1) + … |
| 505 | 0.063 | 8% (H–4→L) + 87% (H–2→L) + … |

| | | |
|---|---|---|
| 496 | 0.024 | 5% (H–2→L) + 87% (H–2→L+1) + … |
| 490 | 0.013 | 84% (H–4→L) + 6% (H–2→L) + 5% (H–2→L+1) + … |
| 479 | 0.017 | 97% (H–3→L+1) + … |
| 478 | 0.040 | 94% (H–4→L+1) + … |
| 454 | 0.014 | 21% (H–5→L) + 72% (H–5→L+1) + … |
| 453 | 0.011 | 44% (H–6→L) + 30% (H–5→L) + 21% (H–5→L+1) + … |
| 451 | 0.093 | 44% (H–6→L) + 46% (H–5→L) + … |
| 440 | 0.053 | 6% (H–8→L) + 85% (H–7→L) + … |
| 436 | 0.055 | 92% (H–6→L+1) + … |
| 428 | 0.062 | 6% (H–11→L+1) + 7% (H–8→L) + 80% (H–7→L+1) + … |
| 427 | 0.063 | 81% (H–8→L) + 7% (H–7→L) + 5% (H–7→L+1) + … |
| 413 | 0.015 | 6% (H–11→L) + 77% (H–8→L+1) + … |
| 382 | 0.089 | 12% (H-15→L) + 22% (H-10→L) + 51% (H-9→L) + 10% (H-9→L+1) + … |
| 381 | 0.012 | 83% (H-15→L) + 6% (H-9→L) + … |
| 378 | 0.017 | 22% (H-10→L) + 64% (H-9→L+1) + … |
| 376 | 0.049 | 30% (H-10→L) + 29% (H-10→L+1) + 25% (H-9→L) + … |
| 373 | 0.083 | 14% (H-10→L) + 62% (H-10→L+1) + 5% (H-9→L) + 10% (H-9→L+1) + … |
| 361 | 0.037 | 36% (H-14→L) + 14% (H-13→L) + 37% (H-12→L) + … |
| 354 | 0.187 | 6% (H-18→L) + 36% (H-14→L) + 25% (H-13→L) + 14% (H-13→L+1) + 6% (H-12→L+1) + … |
| 351 | 0.108 | 10% (H-13→L) + 31% (H-13→L+1) + 13% (H-12→L) + 29% (H-12→L+1) + … |
| | | ***$ZnF_4(SR)_{12}Pc$–β*** |
| 705 | 0.492 | 95% (H→L) + … |
| 698 | 0.542 | 95% (H→L+1) + … |
| 605 | 0.020 | 8% (H–2→L) + 79% (H–1→L) + 10% (H–1→L+1) + … |
| 601 | 0.032 | 11% (H–2→L) + 79% (H–1→L+1) + … |
| 583 | 0.013 | 29% (H–3→L+1) + 13% (H–2→L) + 50% (H–2→L+1) + … |
| 536 | 0.066 | 94% (H–4→L) + … |
| 526 | 0.083 | 92% (H–4→L+1) + …` |
| 484 | 0.021 | 94% (H–5→L) + … |
| 475 | 0.097 | 89% (H–5→L+1) + … |
| 469 | 0.034 | 12% (H–8→L) + 75% (H–6→L) + … |
| 459 | 0.024 | 28% (H–7→L) + 32% (H–7→L+1) + 26% (H–6→L+1) + … |
| 456 | 0.019 | 7% (H–9→L+1) + 33% (H–8→L) + 14% (H–8→L+1) + 28% (H–7→L) + 6% (H–6→L) + … |

| | | |
|---|---|---|
| 454 | 0.021 | 13% (H–9→L) + 61% (H–8→L+1) + 6% (H–7→L+1) + 8% (H–6→L) + … |
| 452 | 0.032 | 12% (H–9→L) + 19% (H–9→L+1) + 18% (H–8→L) + 7% (H–8→L+1) + 9% (H–7→L) + 27% (H–7→L+1) + … |
| 449 | 0.063 | 6% (H–11→L) + 47% (H–9→L) + 9% (H–8→L) + 5% (H–8→L+1) + 16% (H–7→L) + 6% (H–7→L+1) + … |
| 444 | 0.046 | 6% (H–10→L+1) + 17% (H–9→L) + 49% (H–9→L+1) + 13% (H–8→L) + … |
| 442 | 0.033 | 33% (H-11→L) + 58% (H-10→L) + … |
| 441 | 0.033 | 19% (H-11→L) + 59% (H-10→L+1) + 9% (H-9→L+1) + … |
| 438 | 0.024 | 32% (H-11→L) + 25% (H-10→L) + 24% (H-10→L+1) + … |
| 429 | 0.030 | 88% (H-11→L+1) + … |
| 427 | 0.019 | 78% (H-12→L) + … |
| 416 | 0.016 | 18% (H-13→L+1) + 71% (H-12→L+1) + … |
| 402 | 0.016 | 8% (H-14→L+1) + 63% (H-13→L+1) + 23% (H-12→L+1) + … |
| 373 | 0.067 | 17% (H-19→L) + 9% (H-17→L) + 8% (H-16→L) + 11% (H-15→L) + 41% (H-14→L) + … |
| 362 | 0.042 | 8% (H-14→L) + 55% (H→L+5) + … |
| | | ***Zn (SR)$_{16}$Pc*** |
| 700 | 0.476 | 93% (H→L) + … |
| 688 | 0.522 | 92% (H→L+1) + … |
| 615 | 0.025 | 48% (H–2→L) + 44% (H–1→L) + … |
| 604 | 0.022 | 9% (H–3→L) + 21% (H–2→L) + 16% (H–2→L+1) + 23% (H–1→L) + 26% (H–1→L+1) + … |
| 595 | 0.013 | 6% (H–3→L) + 69% (H–2→L+1) + 15% (H–1→L+1) + … |
| 593 | 0.017 | 77% (H–3→L) + 5% (H–2→L) + 11% (H–1→L+1) + … |
| 582 | 0.010 | 86% (H–3→L+1) + … |
| 575 | 0.010 | 85% (H–4→L) + 6% (H–3→L+1) + … |
| 557 | 0.028 | 5% (H–5→L) + 13% (H–5→L+1) + 80% (H–4→L+1) + … |
| 545 | 0.021 | 87% (H–5→L) + 6% (H–4→L+1) + … |
| 530 | 0.027 | 82% (H–5→L+1) + 11% (H–4→L+1) + … |
| 485 | 0.017 | 7% (H–9→L) + 5% (H–9→L+1) + 40% (H–7→L) + 36% (H–7→L+1) + … |
| 483 | 0.011 | 12% (H–10→L) + 17% (H–9→L+1) + 7% (H–8→L) + 7% (H–8→L+1) + 22% (H–7→L) + 6% (H–7→L+1) + 21% (H–6→L+1) + … |
| 481 | 0.024 | 24% (H–9→L) + 11% (H–8→L+1) + 40% (H–7→L+1) + 7% (H–6→L+1) + … |
| 476 | 0.023 | 19% (H–8→L) + 10% (H–8→L+1) + 51% (H–6→L+1) + … |
| 472 | 0.036 | 12% (H–10→L) + 28% (H–9→L) + 6% (H–9→L+1) + 21% (H–8→L) + 21% (H–7→L) + … |

| | | |
|---|---|---|
| 460 | 0.055 | 6% (H-11→L+1) + 39% (H-10→L) + 7% (H-10→L+1) + 10% (H-9→L) + 6% (H-9→L+1) + 14% (H-8→L) + 7% (H-8→L+1) + … |
| 455 | 0.032 | 50% (H-11→L) + 37% (H-10→L+1) + … |
| 453 | 0.052 | 17% (H-11→L) + 38% (H-11→L+1) + 33% (H-10→L+1) + … |
| 438 | 0.017 | 8% (H-17→L) + 11% (H-14→L) + 8% (H-13→L) + 57% (H-12→L) + … |
| 431 | 0.022 | 12% (H-14→L+1) + 24% (H-13→L) + 42% (H-12→L+1) + … |
| 422 | 0.019 | 9% (H-14→L+1) + 41% (H-13→L+1) + 14% (H-12→L+1) + 23% (H→L+2) + … |
| 421 | 0.031 | 14% (H-13→L+1) + 7% (H-12→L) + 62% (H→L+2) + … |

[a] Transition wavelengths in nanometers. Only transitions with energies below ~3.5 eV (>350 nm) are given. [b] Calculated oscillator strengths. Only transitions with oscillator strengths greater than 0.01 are given. [c] Excited state wavefunction, in terms of the contributions of single-excitations of the ground state Slater determinant. Only single-excitations with contributions greater than 5% are given. The HOMO is designated "H", the second HOMO is "H-1", *etc*. The LUMO is designated "L", the second LUMO is "L+1", *etc*.

It is perhaps more interesting to note the predictive failures of these calculations. In particular, the reversal of the peak wavelength on going from $ZnF_8(SR)_8$Pc-β to $ZnF_4(SR)_{12}$Pc-β to $Zn(SR)_{16}$Pc is not observed in the UV-visible data for the series. While the absolute energies of DFT calculations for porphyrinoids are known to be overestimated by several tenths of an electron volt,[98-100] we would expect the relative energies to be more consistent with observations.

Considering the possibility that this deviation is an artifact of using single isomers to represent large ensembles, we next calculated energy levels for the α substituted compounds shown in the second row of **Figure 4.4**. While the α and β isomers may not strictly bound the range of energies of all possible isomers for a given Pc, they will give a general idea of the magnitude of that range. The difference in the effects of α and β substitution can be seen in **Figure 4.8-A**. It is clear from the trends in the energy gaps that the β series more accurately predicts the red-shift up until at least $ZnF_8(SR)_8$Pc-β, after which both the α and β models begin to deviate significantly from observation.

Since conformational dynamics are likely the next most important factors in determining the energy levels, we went on to study the artificially manipulated structures shown in the last line of **Figure 4.4**. The HOMO-LUMO gaps for planar and non-planar geometries of the α and β Pcs are depicted in **Figure 4.8-B** and **C**. The experimental gaps are gaps calculated by converting the peak absorbance wavelengths to eV and adding a constant factor of 0.260 eV. This factor is an *ad hoc* correction which represents the difference between the calculated and observed energy gaps for $ZnF_{16}Pc$. It is again clear from these two panels that the β series is in better agreement with the experimental values. It is also interesting to note that, for both α and β Pcs, the planar geometries display a much steeper slope and more variation than the distorted geometries, indicating a greater red-shift over the series. This is expected since the distorted geometry will tend to disrupt the

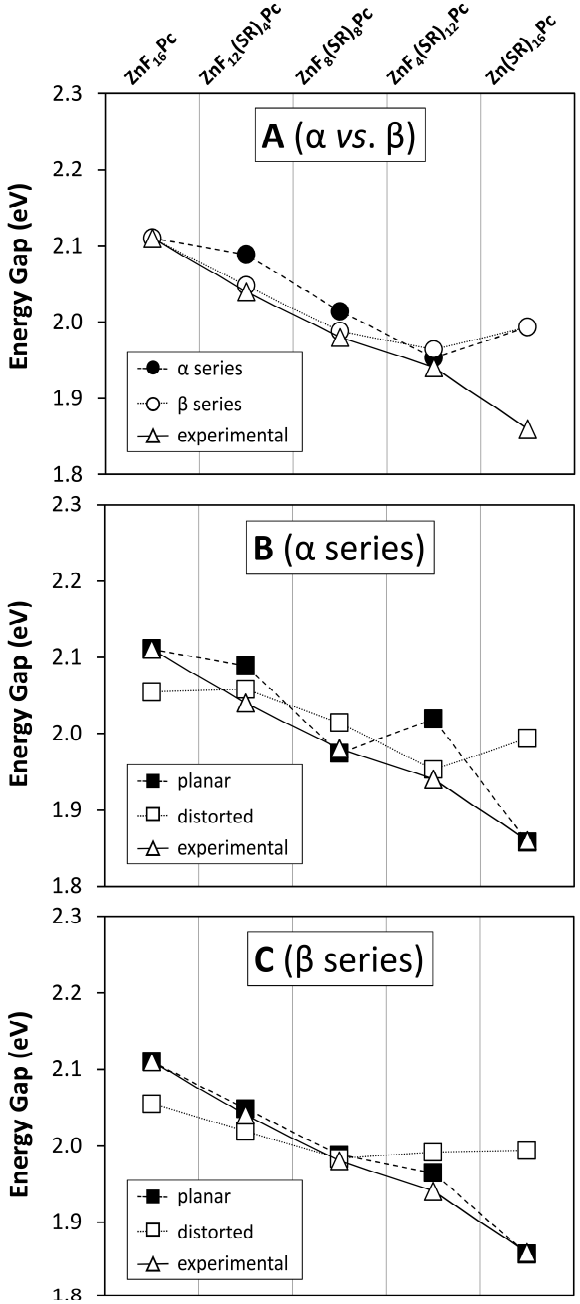


**Figure 4.8**. Calculated and experimental HOMO-LUMO energy gaps of various model Pc compounds. In all three panels, the open triangles (△) indicate the experimentally observed energy gaps. The top panel (A) shows a comparison of gap energies for α (filled circles: ●) and β (open circles: ○) substituted Pcs. The middle and bottom panels show comparisons of gap energies for planar (filled squares: ■) and distorted (open squares: □) geometries for α (middle panel, B) and β (bottom panel, C) substituted compounds.

conjugation of the macrocycle and thus reduce the electronic influence of the substituents. However, it is surprising for two reasons. First, it predicts that distorted Pcs will sometimes be *blue-shifted* relative to their planar counterparts, by as much as 40 nm or more. In fact, these calculations predict that a distorted $Zn(SR)_{16}Pc$ should have approximately the same energy gap as a $ZnF_8(SR)_8Pc$ in any conformation, with any substitution pattern. This is, of course, in sharp contrast to the observed UV-Vis spectra, and therefore requires some explanation. Second, it is the series of Pcs with planar geometries that most accurately matches the observed red-shifts, even for the most highly substituted compounds, which we expect to be severely distorted.

There are a few possible reasons for the above discrepancies between calculated and observed spectra. First, it may be that the DFT calculations are simply inaccurate, most likely due to limitations in the 6-31G(d,p) basis set used. This basis in particular gives acceptable accuracy for planar chromophores, but is known to break down for more polarizable, non-planar systems that require better descriptions of the diffuse states. Similar issues can arise from our choice of the B3LYP exchange-correlation functional, which may fail to accurately capture long-range electron correlations as the macrocyclic distortion becomes more significant. A second possible issue with the calculations themselves could be that the energy levels are accurate for the structures found, but that the optimization procedure has generated incorrect structures. For instance, the planar structures could be the true minimum conformations, despite the distortion ostensibly found by DFT optimization. However, this would contradict a great deal of the literature, especially concerning α-thioalkyl substituted Pcs. Unfortunately we were unable to obtain crystals of these more substituted compounds in order to conclusively determine their structure by X-ray diffraction.

It may also be that there is no significant deficiency in the computation at all, but rather that the model compounds we have chosen do not faithfully represent the compounds actually present in solution. Non-planar porphyrinoids are known to twist or "flap" from one conformation to another,[61] most likely through a planar or nearly planar transition state. It is unclear how the transient appearance of these planar states would affect the observed spectra, if at all, but it may serve to shift the absorbance of a molecule with a distorted minimum closer to that expected for a planar structure. Lastly, there has been some debate[101-107] in the literature over the nature of distorted porphyrins and the photophysical implications thereof. While the controversy has not explicitly involved Pcs, there is no reason that the arguments presented on either side would not apply equally well to them. In short, some groups have attributed the observed red-shift in distorted porphyrins to the accompanying in-plane nuclear reorganizations (IPNRs) rather than to the out-of-plane distortion *per se*. These IPNRs consist of changes in the nuclear coordinates, bond lengths, bond angles, *etc*. Our method, which freezes the nuclear positions of the artificially flattened or distorted Pcs during the calculations, would not be able to account for these changes and thus could be introducing substantial error. Detailed photophysical and dynamic NMR studies versus temperature and solvent may shed light on these issues for Pcs.

### 4.4. Conclusion

We have presented a comprehensive study of a family of substituted Pcs, including their photophysical and structural characteristics. As electron releasing thioalkanes are appended to the core macrocycle, the absorbance band is red-shifted due to the inductive effect. However, while the literature reports typically show a larger red-shift for α substituents than for β, our experimental spectroscopy indicates that the change remains mostly linear. This may be a consequence of the fluorine atoms around the periphery strongly counterbalancing the electron donating thioalkanes.

We have also shown that the red-shift is accompanied by some strongly non-linear effects, including broadening of the absorbance and emission bands, increase in the Stokes shift, and decreases in the fluorescence quantum yields and lifetimes. All of these results point towards distortion of the planar macrocycle caused by extensive substitution. DFT calculations further support this interpretation, although there still remain some unresolved discrepancies between the theory and experiment.

One of the most important outcomes of this study is the development of a facile, flexible method for rapidly generating Pcs with tunable properties, using only inexpensive, commodity reagents. Investigating the structure-function relationships in Pcs and other photoactive macrocycles is an active area of research,[24] and our results offer a new perspective on the competing mechanisms at play. In particular, we have highlighted a distinct approach to easily manipulating these properties through distortion of the planar Pc structure. These kinds of non-planar chromophores have found use in a variety of applications such as organic photovoltaics, photodynamic therapy, non-linear optics, and photoacoustic spectroscopy, all of which underscores the importance of further exploring this pathway. For instance, correlating molecular properties (*e.g.* solubility, cell permeability, tumor uptake, phototoxicity, singlet oxygen yield, *etc*.) to spectroscopic signatures for aromatic distortion (*e.g.* FWHM or Stokes shift) could lead to new insights for the development of the next generation of phototherapeutics.

### 4.5. References


1. Farley, C.; Bhupathiraju, N. V.; John, B. K.; Drain, C. M. Tuning the Structure and Photophysics of a Fluorous Phthalocyanine Platform. *J. Phys. Chem. A.* **2016**, *(in press)*.
2. Chidawanyika, W.; Nyokong, T. The synthesis and photophysicochemical properties of low-symmetry zinc phthalocyanine analogues. *J. Photochem. Photobiol., A Chem.* **2009**, *206*, 169-176.

3. Braun, A.; Tcherniac, J. Über die Produkte der Einwirkung von Acetanhydrid auf Phthalamid. *Ber. Dtsch. Chem. Ges.* **1907**, *40*, 2709-2714.

4. de Diesbach, H.; von der Weid, E. Quelques sels complexes des o-dinitriles avec le cuivre et la pyridine. *Helv. Chim. Acta.* **1927**, *10*, 886-888.

5. Ogunsipe, A.; Maree, D.; Nyokong, T. Solvent effects on the photochemical and fluorescence properties of zinc phthalocyanine derivatives. *J. Mol. Struct.* **2003**, *650*, 131-140.

6. Löbbert, G. In *Ullmann's Encyclopedia of Industrial Chemistry, Electronic Release*; Wiley-VCH: Weinheim, **2000**; Vol. 27.

7. Varotto, A.; Nam, C. Y.; Radivojevic, I.; Tome, J. P.; Cavaleiro, J. A.; Black, C. T.; Drain, C. M. Phthalocyanine blends improve bulk heterojunction solar cells. *J. Am. Chem. Soc.* **2010**, *132*, 2552-2554.

8. Walter, M. G.; Rudine, A. B.; Wamser, C. C. Porphyrins and phthalocyanines in solar photovoltaic cells. *J. Porphyrins Phthalocyanines.* **2010**, *14*, 759-792.

9. Jurow, M. J.; Hageman, B. A.; Dimasi, E.; Nam, C. Y.; Pabon, C.; Black, C. T.; Drain, C. M. Controlling Morphology and Molecular Packing of Alkane Substituted Phthalocyanine Blend Bulk Heterojunction Solar Cells. *J. Mater. Chem. A.* **2013**, *1*, 1557-1565.

10. Ragoussi, M.-E.; Ince, M.; Torres, T. Recent Advances in Phthalocyanine-Based Sensitizers for Dye-Sensitized Solar Cells. *Eur. J. Org. Chem.* **2013**, *2013*, 6475-6489.

11. Ince, M.; Yum, J.-H.; Kim, Y.; Mathew, S.; Grätzel, M.; Torres, T.; Nazeeruddin, M. K. Molecular Engineering of Phthalocyanine Sensitizers for Dye-Sensitized Solar Cells. *J. Phys. Chem. C.* **2014**, *118*, 17166-17170.

12. Martín-Gomis, L.; Fernández-Lázaro, F.; Sastre-Santos, Á. Advances in phthalocyanine-sensitized solar cells (PcSSCs). *J. Mater. Chem. A.* **2014**, *2*, 15672-15682.

13. Debnath, A. K.; Kumar, A.; Samanta, S.; Prasad, R.; Singh, A.; Chauhan, A. K.; Veerender, P.; Singh, S.; Basu, S.; Aswal, D. K.; Gupta, S. K. Fluorinated copper-phthalocyanine/cobalt-phthalocyaine organic heterojunctions: Charge transport and Kelvin probe studies. *Appl. Phys. Lett.* **2012**, *100*, 142104.

14. Wang, H.; Liu, Z.; Fai Lo, M.; Wai Ng, T.; Yan, D.; Lee, C.-S. Electron depletion and accumulation regions in n-type copper-hexadecafluoro-phthalocyanine and their effects on electronic properties. *Appl. Phys. Lett.* **2012**, *100*, 103302.

15. Komolov, A. S.; Lazneva, E. F.; Komolov, S. A.; Repin, P. S.; Gavrikov, A. A. Potential barrier and photovoltage at interfaces of hexadecafluoro-copper-phthalocyanine and copper phthalocyanine films on the surface of tin dioxide. *Semiconductors.* **2012**, *46*, 988-992.

16. Gao, Y. L.; Ding, H. J.; Wang, H. B.; Yan, D. H. Electronic structure of interfaces between copper-hexadecafluoro-phthalocyanine and 2,5-bis(4-biphenylyl) bithiophene. *Appl. Phys. Lett.* **2007**, *91*, 142112.

17. Jiang, H.; Ye, J.; Hu, P.; Wei, F.; Du, K.; Wang, N.; Ba, T.; Feng, S.; Kloc, C. Fluorination of metal phthalocyanines: single-crystal growth, efficient N-channel organic field-effect transistors, and structure-property relationships. *Sci. Rep.* **2014**, *4*, 7573.

18. Jurow, M. J.; Schuckman, A. E.; Batteas, J. D.; Drain, C. M. Porphyrins as Molecular Electronic Components of Functional Devices. *Coord. Chem. Rev.* **2010**, *254*, 2297-2310.

19. Decreau, R.; Richard, M.-J.; Julliard, M. Photodynamic therapy against achromic M6 melanocytes: phototoxicity of lipophilic axially substituted aluminum phthalocyanines and hexadecahalogenated zinc phthalocyanines. *J. Porphyrins Phthalocyanines.* **2001**, *05*, 390-396.

20. Stanley, C. F., Durham University, 1997.

21. Boyle, R. W.; Rousseau, J.; Kudrevich, S. V.; Obochi, M. O. K.; van Lier, J. E. Hexadecafluorinated zinc phthalocyanine: photodynamic properties against the EMT-6 tumour in mice and pharmacokinetics using 65Zn as a radiotracer. *Br. J. Cancer.* **1996**, *73*, 49-53.

22. Allémann, E.; Rousseau, J.; Brasseur, N.; Kudrevich, S. V.; Lewis, K.; van Lier, J. E. Photodynamic therapy of tumours with hexadecafluoro zinc phthalocyanine formulated in PEG-coated poly(lactic acid) nanoparticles. *Int. J. Cancer.* **1996**, *66*, 821-824.

23. Allémann, E.; Brasseur, N.; Kudrevich, S. V.; La Madeleine, C.; van Lier, J. E. Photodynamic activities and biodistribution of fluorinated zinc phthalocyanine derivatives in the murine EMT-6 tumour model. *Int. J. Cancer.* **1997**, *72*, 289-294.

24. Sekkat, N.; van den Bergh, H.; Nyokong, T.; Lange, N. Like a bolt from the blue: phthalocyanines in biomedical optics. *Molecules.* **2012**, *17*, 98-144.

25. Leznoff, C. C.; Hiebert, A.; Ok, S. Titration syntheses of polyaminosubstituted phthalocyanines via nucleophilic aromatic substitutions on zinc(II) 1,2,3,4,8,9,10,11,15,16,17,18,22,23,24,25-hexadecafluorophthalocyanine. *J. Porphyrins Phthalocyanines.* **2007**, *11*, 537-546.

26. Alonso, M. I.; Garriga, M.; Ossó, J. O.; Schreiber, F.; Barrena, E.; Dosch, H. Strong optical anisotropies of F[sub 16]CuPc thin films studied by spectroscopic ellipsometry. *J. Chem. Phys.* **2003**, *119*, 6335.

27. Leznoff, C. C.; Sosa-Sanchez, J. L. Polysubstituted phthalocyanines by nucleophilic substitution reactions on hexadecafluorophthalocyanines. *Chem. Commun.* **2004**, 338-339.

28. Jurow, M. J.; Varotto, A.; Manichev, V.; Travlou, N. A.; Giannakoudakis, D. A.; Drain, C. M. Self-organized nanostructured materials of alkylated phthalocyanines and underivatized C60 on ITO. *RSC Adv.* **2013**, *3*, 21360.

29. Garcia, A. M.; Alarcon, E.; Munoz, M.; Scaiano, J. C.; Edwards, A. M.; Lissi, E. Photophysical behaviour and photodynamic activity of zinc phthalocyanines associated to liposomes. *Photochem. Photobiol. Sci.* **2011**, *10*, 507-514.

30. Bartoli, G.; Ciminale, F.; Todesco, P. E. Electronic and steric effects in nucleophilic aromatic substitution. Reaction by phenoxides as nucleophiles in dimethyl sulfoxide. *J. Org. Chem.* **1975**, *40*, 872-874.

31. Wang, J.; Khanamiryan, A. K.; Leznoff, C. C. Multisubstituted phthalonitriles for phthalocyanine synthesis. *J. Porphyrins Phthalocyanines.* **2004**, *08*, 1293-1299.

32. Bhupathiraju, N. V.; Rizvi, W.; Batteas, J. D.; Drain, C. M. Fluorinated porphyrinoids as efficient platforms for new photonic materials, sensors, and therapeutics. *Org. Biomol. Chem.* **2016**, *14*, 389-408.

33. Chambrier, I.; J. Cook, M.; T. Wood, P. Conformationally stressed phthalocyanines: the non-planarity of the 1,4,8,11,15,18,22,25-octaisopentyl derivative. *Chem. Commun.* **2000**, 2133-2134.

34. Zorlu, Y.; Kumru, U.; Isci, U.; Divrik, B.; Jeanneau, E.; Albrieux, F.; Dede, Y.; Ahsen, V.; Dumoulin, F. 1,4,8,11,15,18,22,25-Alkylsulfanyl phthalocyanines: effect of macrocycle distortion on spectroscopic and packing properties. *Chem. Commun.* **2015**, *51*, 6580-6583.

35. Honda, T.; Kojima, T.; Kobayashi, N.; Fukuzumi, S. Crystal structures and electronic properties of saddle-distorted and protonated phthalocyanines. *Angew. Chem. Int. Ed.* **2011**, *50*, 2725-2728.

36. Furuyama, T.; Satoh, K.; Kushiya, T.; Kobayashi, N. Design, synthesis, and properties of phthalocyanine complexes with main-group elements showing main absorption and fluorescence beyond 1000 nm. *J. Am. Chem. Soc.* **2014**, *136*, 765-776.

37. Kobayashi, N.; Fukuda, T.; Ueno, K.; Ogino, H. Extremely Non-Planar Phthalocyanines with Saddle or Helical Conformation: Synthesis and Structural Characterizations. *J. Am. Chem. Soc.* **2001**, *123*, 10740-10741.

38. Cammidge, A. N.; Tseng, C.-H.; Chambrier, I.; Hughes, D. L.; Cook, M. J. Phthalocyanines bearing bulky cycloalkylmethyl substituents on non-peripheral sites. *Tetrahedron Lett.* **2009**, *50*, 5254-5256.

39. Kobayashi, N.; Furuyama, T.; Satoh, K. Rationally designed phthalocyanines having their main absorption band beyond 1000 nm. *J. Am. Chem. Soc.* **2011**, *133*, 19642-19645.

40. Isago, H. In *Optical Spectra of Phthalocyanines and Related Compounds*; Springer: New York, **2015**, p 107-131.

41. Golchoubian, H.; Hosseinpoor, F. Effective Oxidation of Sulfides to Sulfoxides with Hydrogen Peroxide under Transition-Metal-Free Conditions. *Molecules.* **2007**, *12*, 304-311.

42. Taniguchi, M.; Du, H.; Lindsey, J. S. Virtual libraries of tetrapyrrole macrocycles. Combinatorics, isomers, product distributions, and data mining. *J. Chem. Inf. Model.* **2011**, *51*, 2233-2247.

43. Taniguchi, M.; Soares, A. R. M.; Chandrashaker, V.; Lindsey, J. S. A tandem combinatorial model for the prebiogenesis of diverse tetrapyrrole macrocycles. *New J. Chem.* **2012**, *36*, 1057.

44. Taniguchi, M.; Lindsey, J. S. Diversity, isomer composition, and design of combinatorial libraries of tetrapyrrole macrocycles. *J. Porphyrins Phthalocyanines.* **2012**, *16*, 1-13.

45. Taniguchi, M.; Lindsey, J. S. In *Handbook of Porphyrin Science*; World Scientific: Singapore, **2012**; Vol. 23, p 1-80.

46. Drain, C. M.; Singh, S. In *Handbook of Porphyrin Science*; Kadish, K. M., Smith, K. M., Guilard, R., Eds.; World Scientific: Singapore, **2011**; Vol. 3, p 485-530.

47. Berlin, K.; Jain, R. K.; Tetzlaff, C.; Steinbeck, C.; Richert, C. Spectrometrically monitored selection experiments: quantitative laser desorption mass spectrometry of small chemical libraries. *Chem. Biol.* **1997**, *4*, 63-77.

48. Stulz, E.; Scott, S. M.; Bond, A. D.; Teat, S. J.; Sanders, J. K. Selection and amplification of mixed-metal porphyrin cages from dynamic combinatorial libraries. *Chem. Eur. J.* **2003**, *9*, 6039-6048.

49. Ding, S.; Gray, N. S.; Wu, X.; Ding, Q.; Schultz, P. G. A Combinatorial Scaffold Approach toward Kinase-Directed Heterocycle Libraries. *J. Am. Chem. Soc.* **2002**, *124*, 1594-1596.

50. Drain, C. M.; Gong, X.; Ruta, V.; Soll, C. E.; Chicoineau, P. F. Combinatorial Synthesis and Modification of Functional Porphyrin Libraries: Identification of New, Amphipathic Motifs for Biomolecule Binding. *J. Comb. Chem.* **1999**, *1*, 286-290.

51. Samaroo, D.; Vinodu, M.; Chen, X.; Drain, C. M. meso-Tetra(pentafluorophenyl)porphyrin as an efficient platform for combinatorial synthesis and the selection of new photodynamic therapeutics using a cancer cell line. *J. Comb. Chem.* **2007**, *9*, 998-1011.

52. Read, R. C. Pólya's Theorem and Its Progeny. *Math. Mag.* **1987**, *60*, 275.

53. Pólya, G. Kombinatorische Anzahlbestimmungen für Gruppen, Graphen und chemische Verbindungen. *Acta Math.* **1937**, *68*, 145-254.

54. Redfield, J. H. The Theory of Group-Reduced Distributions. *Am. J. Math.* **1927**, *49*, 433.

55. Williams, A. Loopless Generation of Multiset Permutations using a Constant Number of Variables by Prefix Shifts. *Proceedings of the Twentieth Annual ACM-SIAM Symposium on Discrete Algorithms.* **2009**, 987-996.

56. Iagatti, A.; Doria, S.; Marcelli, A.; Angelini, N.; Notarantonio, S.; Paoletti, A. M.; Pennesi, G.; Rossi, G.; Zanotti, G.; Calogero, G.; Foggi, P. Photophysical Processes Occurring in a Zn-phthalocyanine in Ethanol Solution and on TiO2 Nanostructures. *J. Phys. Chem. C.* **2015**, *119*, 20256-20264.

57. Dick, S.; Peisert, H.; Dini, D.; Hanack, M.; Cook, M. J.; Chambrier, I.; Chassé, T. Influence of the alkyl-chains length on the electronic structure and interface properties of 1,4-octasubstituted zinc phthalocyanines on gold. *J. Appl. Phys.* **2005**, *97*, 073715.

58. Mack, J.; Kobayashi, N.; Stillman, M. J. Re-examination of the emission properties of alkoxy- and thioalkyl-substituted phthalocyanines. *J. Inorg. Biochem.* **2010**, *104*, 310-317.

59. Gorun, S. M.; Rathke, J. W.; Chen, M. J. Long-range solid-state ordering and high geometric distortions induced in phthalocyanines by small fluoroalkyl groups. *Dalton Trans.* **2009**, 1095-1097.

60. Gao, Y.; Chen, Y.; Li, R.; Bian, Y.; Li, X.; Jiang, J. Nonperipherally octa(butyloxy)-substituted phthalocyanine derivatives with good crystallinity: effects of metal-ligand coordination on the molecular structure, internal structure, and dimensions of self-assembled nanostructures. *Chem. Eur. J.* **2009**, *15*, 13241-13252.

61. Gunaratne, T. C.; Gusev, A. V.; Peng, X.; Rosa, A.; Ricciardi, G.; Baerends, E. J.; Rizzoli, C.; Kenney, M. E.; Rodgers, M. A. Photophysics of octabutoxy phthalocyaninato-Ni(II) in

toluene: ultrafast experiments and DFT/TDDFT studies. *J. Phys. Chem. A.* **2005**, *109*, 2078-2089.

62. Bishop, S. M.; Beeby, A.; Parker, A. W.; Foley, M. S. C.; Phillips, D. The preparation and photophysical measurements of perdeutero zinc phthalocyanine. *J. Photochem. Photobiol., A Chem.* **1995**, *90*, 39-44.
63. Alberto, M. E.; De Simone, B. C.; Mazzone, G.; Sicilia, E.; Russo, N. The heavy atom effect on Zn(II) phthalocyanine derivatives: a theoretical exploration of the photophysical properties. *Phys. Chem. Chem. Phys.* **2015**, *17*, 23595-23601.
64. Azenha, E. l. G.; Serra, A. C.; Pineiro, M.; Pereira, M. M.; Seixas de Melo, J.; Arnaut, L. G.; Formosinho, S. J.; Rocha Gonsalves, A. M. d. A. Heavy-atom effects on metalloporphyrins and polyhalogenated porphyrins. *Chem. Phys.* **2002**, *280*, 177-190.
65. Bonnett, R.; Harriman, A.; Kozyrev, A. N. Photophysics of halogenated porphyrins. *J. Chem. Soc., Faraday Trans.* **1992**, *88*, 763.
66. Makhseed, S.; Ghazal, B.; Abdelmoniem, A. M.; Novakova, V.; Zimcik, P. Photophysical and theoretical studies of peripherally halogenated octaphenoxyphthalocyanines. *RSC Adv.* **2015**, *5*, 58854-58864.
67. Lo, P.-C.; Wang, S.; Zeug, A.; Meyer, M.; Röder, B.; Ng, D. K. P. Preparation and photophysical properties of halogenated silicon(IV) phthalocyanines substituted axially with poly(ethylene glycol) chains. *Tetrahedron Lett.* **2003**, *44*, 1967-1970.
68. Kobayashi, N.; Ogata, H.; Nonaka, N.; Luk'yanets, E. A. Effect of peripheral substitution on the electronic absorption and fluorescence spectra of metal-free and zinc phthalocyanines. *Chem. Eur. J.* **2003**, *9*, 5123-5134.
69. Bixon, M.; Jortner, J.; Cortes, J.; Heitele, H.; Michel-Beyerle, M. E. Energy Gap Law for Nonradiative and Radiative Charge Transfer in Isolated and in Solvated Supermolecules. *J. Phys. Chem.* **1994**, *98*, 7289-7299.
70. Gutierrez-Meza, E.; Noria, R.; Granados, G.; Gomez-Vidales, V.; Ramirez, J. Z.; Beltran, H. I.; Peon, J. Photophysics of a cis axially disubstituted macrocycle: rapid intersystem crossing in a tin(IV) phthalocyanine with a half-domed geometry. *J. Phys. Chem. B.* **2012**, *116*, 14107-14114.
71. Peceli, D.; Hu, H.; Fishman, D. A.; Webster, S.; Przhonska, O. V.; Kurdyukov, V. V.; Slominsky, Y. L.; Tolmachev, A. I.; Kachkovski, A. D.; Gerasov, A. O.; Masunov, A. E.; Hagan, D. J.; Van Stryland, E. W. Enhanced intersystem crossing rate in polymethine-like molecules: sulfur-containing squaraines versus oxygen-containing analogues. *J. Phys. Chem. A.* **2013**, *117*, 2333-2346.
72. Orchin, M.; Macomber, R. S.; Pinhas, A. R.; Wilson, R. M. *The Vocabulary and Concepts of Organic Chemistry*; Second ed.; John Wiley & Sons, Inc.: Hoboken, NJ, **2005**.
73. Zander, M. The Intra-annular Internal Heavy-atom Effect on the Fluorescence and Phosphorescence Properties of Oxygen, Sulphur or Selenium Containing Heterocyclic Systems Related to Dibenzo [b,n] perylene. *Zeitschrift für Naturforschung A.* **1989**, *44*.

74. Goldacker, W.; Schweitzer, D.; Zimmermann, H. Electronic properties of the triplet state of fluorene, carbazole, dibenzofuran and dibenzothiophene (X-traps). *Chem. Phys.* **1979**, *36*, 15-26.

75. Wróbel, D.; Graja, A. Photoinduced electron transfer processes in fullerene–organic chromophore systems. *Coord. Chem. Rev.* **2011**, *255*, 2555-2577.

76. Turro, N. J.; Ramamurthy, V.; Scaiano, J. C. *Principles of Molecular Photochemistry: An Introduction*; University Science Books: Sausalito, CA, **2009**.

77. Ravikanth, M.; Reddy, D.; Chandrashekar, T. K. Fluorescence properties of distorted short-chain basket handle porphyrins. *J. Photochem. Photobiol., A Chem.* **1993**, *72*, 61-67.

78. Maiti, N. C.; Ravikanth, M. Photophysical properties of structurally deformed basket-handle prophyrins. *J. Chem. Soc., Faraday Trans.* **1995**, *91*, 4369.

79. Senge, M. O. In *The Porphyrin Handbook*; Kadish, K. M., Smith, K. M., Guilard, R., Eds.; Academic Press: New York, **2000**; Vol. 1, p 239-348.

80. Ivashin, N. V.; Shchupak, E. E.; Panarin, A. Y.; Sagun, E. I. Photophysical properties of porphyrins with sterically distorted and partially screened macrocycles. *Opt. Spectrosc.* **2015**, *118*, 882-892.

81. Sazanovich, I. V.; Galievsky, V. A.; van Hoek, A.; Schaafsma, T. J.; Malinovskii, V. L.; Holten, D.; Chirvony, V. S. Photophysical and Structural Properties of Saddle-Shaped Free Base Porphyrins: Evidence for an "Orthogonal" Dipole Moment. *J. Phys. Chem. B.* **2001**, *105*, 7818-7829.

82. Nifiatis, F.; Su, W.; Haley, J. E.; Slagle, J. E.; Cooper, T. M. Comparison of the photophysical properties of a planar, PtOEP, and a nonplanar, PtOETPP, porphyrin in solution and doped films. *J. Phys. Chem. A.* **2011**, *115*, 13764-13772.

83. Gentemann, S.; Medforth, C. J.; Forsyth, T. P.; Nurco, D. J.; Smith, K. M.; Fajer, J.; Holten, D. Photophysical Properties of Conformationally Distorted Metal-Free Porphyrins. Investigation into the Deactivation Mechanisms of the Lowest Excited Singlet State. *J. Am. Chem. Soc.* **1994**, *116*, 7363-7368.

84. Röder, B.; Büchner, M.; Rückmann, I.; Senge, M. O. Correlation of photophysical parameters with macrocycle distortion in porphyrins with graded degree of saddle distortion. *Photochem. Photobiol. Sci.* **2010**, *9*, 1152-1158.

85. Lebedev, A. Y.; Filatov, M. A.; Cheprakov, A. V.; Vinogradov, S. A. Effects of structural deformations on optical properties of tetrabenzoporphyrins: free-bases and Pd complexes. *J. Phys. Chem. A.* **2008**, *112*, 7723-7733.

86. Drain, C. M.; Kirmaier, C.; Medforth, C. J.; Nurco, D. J.; Smith, K. M.; Holten, D. Dynamic Photophysical Properties of Conformationally Distorted Nickel Porphyrins. 1. Nickel(II) Dodecaphenylporphyrin. *J. Phys. Chem.* **1996**, *100*, 11984-11993.

87. Drain, C. M.; Gentemann, S.; Roberts, J. A.; Nelson, N. Y.; Medforth, C. J.; Jia, S.; Simpson, M. C.; Smith, K. M.; Fajer, J.; Shelnutt, J. A.; Holten, D. Picosecond to Microsecond Photodynamics of a Nonplanar Nickel Porphyrin: Solvent Dielectric and Temperature Effects. *J. Am. Chem. Soc.* **1998**, *120*, 3781-3791.

88. Retsek, J. L.; Drain, C. M.; Kirmaier, C.; Nurco, D. J.; Medforth, C. J.; Smith, K. M.; Sazanovich, I. V.; Chirvony, V. S.; Fajer, J.; Holten, D. Photoinduced Axial Ligation and Deligation Dynamics of Nonplanar Nickel Dodecaarylporphyrins. *J. Am. Chem. Soc.* **2003**, *125*, 9787-9800.

89. Rodriguez, J.; Kirmaier, C.; Holten, D. Time-resolved and static optical properties of vibrationally excited porphyrins. *J. Chem. Phys.* **1991**, *94*, 6020.

90. Mack, J.; Kobayashi, N. Low symmetry phthalocyanines and their analogues. *Chem. Rev.* **2011**, *111*, 281-321.

91. Rio, Y.; Salome Rodriguez-Morgade, M.; Torres, T. Modulating the electronic properties of porphyrinoids: a voyage from the violet to the infrared regions of the electromagnetic spectrum. *Org. Biomol. Chem.* **2008**, *6*, 1877-1894.

92. Li, R.; Zhang, X.; Zhu, P.; Ng, D. K.; Kobayashi, N.; Jiang, J. Electron-donating or -withdrawing nature of substituents revealed by the electrochemistry of metal-free phthalocyanines. *Inorg. Chem.* **2006**, *45*, 2327-2334.

93. Shinohara, H.; Tsaryova, O.; Schnurpfeil, G.; Wöhrle, D. Differently substituted phthalocyanines: Comparison of calculated energy levels, singlet oxygen quantum yields, photo-oxidative stabilities, photocatalytic and catalytic activities. *J. Photochem. Photobiol., A Chem.* **2006**, *184*, 50-57.

94. Gouterman, M. Spectra of porphyrins. *J. Mol. Spectrosc.* **1961**, *6*, 138-163.

95. Gouterman, M.; Wagnière, G. H.; Snyder, L. C. Spectra of porphyrins: Part II. Four orbital model. *J. Mol. Spectrosc.* **1963**, *11*, 108-127.

96. Chidawanyika, W.; Mack, J.; Shimizu, S.; Kobayashi, N.; Nyokong, T. Effect of peripheral fused ring substitution on the optical spectroscopy and electronic structure of metal phthalocyanine complexes. *J. Porphyrins Phthalocyanines.* **2009**, *13*, 1053-1062.

97. Das, S. K.; Mahler, A.; Wilson, A. K.; D'Souza, F. High-potential perfluorinated phthalocyanine-fullerene dyads for generation of high-energy charge-separated states: formation and photoinduced electron-transfer studies. *ChemPhysChem.* **2014**, *15*, 2462-2472.

98. Lee, S. U. Influence of Exchange-Correlation Functional in the Calculations of Vertical Excitation Energies of Halogenated Copper Phthalocyanines using Time-Dependent Density Functional Theory (TD-DFT). *Bull. Korean Chem. Soc.* **2013**, *34*, 2276-2280.

99. Furche, F.; Rappoport, D. In *Computational Photochemistry*; Olivucci, M., Ed.; Elsevier: New York, **2005**; Vol. 16.

100. Fukuda, R.; Ehara, M. Excited states and electronic spectra of annulated dinuclear free-base phthalocyanines: a theoretical study on near-infrared-absorbing dyes. *J. Chem. Phys.* **2012**, *136*, 114304.

101. Zakavi, S.; Omidyan, R.; Talebzadeh, S. Porphine core saddling: Effects on the HOMO/LUMO gap and the macrocycle bond lengths and bond angles. *Polyhedron.* **2013**, *49*, 36-40.

102. Zhang, Y. H.; Zhao, W.; Jiang, P.; Zhang, L. J.; Zhang, T.; Wang, J. Structural parameters and vibrational spectra of a series of zinc meso-phenylporphyrins: a DFT and experimental study. *Spectrochim. Acta A Mol. Biomol. Spectrosc.* **2010**, *75*, 880-890.

103. Haddad, R. E.; Gazeau, S.; Pecaut, J.; Marchon, J. C.; Medforth, C. J.; Shelnutt, J. A. Origin of the red shifts in the optical absorption bands of nonplanar tetraalkylporphyrins. *J. Am. Chem. Soc.* **2003**, *125*, 1253-1268.

104. Ryeng, H.; Ghosh, A. Do Nonplanar Distortions of Porphyrins Bring about Strongly Red-Shifted Electronic Spectra? Controversy, Consensus, New Developments, and Relevance to Chelatases. *J. Am. Chem. Soc.* **2002**, *124*, 8099-8103.

105. Wertsching, A. K.; Koch, A. S.; DiMagno, S. G. On the Negligible Impact of Ruffling on the Electronic Spectra of Porphine, Tetramethylporphyrin, and Perfluoroalkylporphyrins. *J. Am. Chem. Soc.* **2001**, *123*, 3932-3939.

106. Parusel, A. B. J.; Wondimagegn, T.; Ghosh, A. Do Nonplanar Porphyrins Have Red-Shifted Electronic Spectra? A DFT/SCI Study and Reinvestigation of a Recent Proposal. *J. Am. Chem. Soc.* **2000**, *122*, 6371-6374.

107. DiMagno, S. G.; Wertsching, A. K.; Ross, C. R. Electronic Consequences of Nonplanar Core Conformations in Electron-Deficient Porphyrins: The Structure and Spectroscopic Properties of [5,10,15,20-Tetrakis(heptafluoropropyl)porphinato]cobalt(II). *J. Am. Chem. Soc.* **1995**, *117*, 8279-8280.

## Chapter 5. Bistable Photophysics in a Series of Nitro-Porphyrin Dyes[§]

### 5.1 Introduction

Functionalized porphyrins (Pors) and other tetrapyrrole derivatives have been studied extensively for decades, primarily due to their importance in biological, chemical, and optical systems.[1] These compounds possess enhanced photonic and electrochemical properties that can be finely tuned by grafting a variety of substituents to their peripheral positions,[2-4] making them very attractive as components for advanced materials and devices. In particular, nitro substituted porphyrinoids have been investigated as reduction/oxidation catalysts,[5-11] nonlinear optical materials,[4,12-15] biomedical theranostics,[14,16,17] and artificial solar energy harvesting devices.[15,18-20]

Nitro groups drastically affect the electronic properties of the Por when attached to the *β*-pyrrole position or even to the *meso*-phenyl rings. The strong electron withdrawing nature of the $NO_2$ can polarize the Por macrocycle, changing its physical and chemical properties.[4-16,22-27] On the other hand, nitro groups can also mediate the assembly of supramolecular systems by directly participating in hydrogen bonding with groups such as imidazole[29] or modulating the complexation of the Por with other species in solution.[31-35] These groups are also widely used in Por chemistry as precursors to amino groups because the latter tend to diminish the synthetic yield of the macrocycle.[36-40]

Significant attention has been paid to the excited state dynamics of Por compounds, but accurate measurement still presents a substantial challenge.[1,41,42] There are numerous reports of Pors showing appreciable aggregation in solution, which makes it difficult to extract the

[§] This chapter is adapted from a manuscript in preparation.

photophysical properties of the monomeric species *vs.* the aggregates.[2,44,45] The extent of aggregation depends on the nature of the substituents attached to the macrocycle core, the coordinated metal ion, and external conditions such as the temperature, concentration, and solvent. As mentioned, all of these factors also exert an influence on the photophysical characteristics of the molecule itself, as well as on its conformational dynamics,[47] further complicating the analysis.

The aggregation and organization of nitroporphyrins can also provide a useful strategy for making supramolecular arrays via self-assembly.[29,45] Por arrays are particularly appealing due to their rich photochemistry and ability to support electron and energy transfer processes.[28,30,34,46,48-51] Self-assembly provides efficient access to ordered architectures of Por units by a variety of mechanisms, including hydrogen bond molecular recognition, electrostatic interactions, and transition metal ion coordination, among others. Since the hierarchical structure of these assemblies will obviously depend on the number and placement of the relevant functional groups on the Por, it is important to understand how these affect the intrinsic photophysical properties of the molecules as well. For example, it has been shown that tetraphenylporphyrin (TPP) compounds with nitro groups in the *para* phenyl position have markedly different stabilities and catalytic activities from those with nitro groups in the *ortho* position.[7]

As a part of this effort to understand the role of strong electron withdrawing groups (EWGs) on Por chemistry, we present here a combined experimental and theoretical analysis of the photophysics of a series of nitroporphyrins (see **Figure 5.1**). These compounds were chosen to minimize other factors, such as conformational dynamics, different substituent group effects, and electroactivity of the central metal. We discuss the absorption and emission properties of the

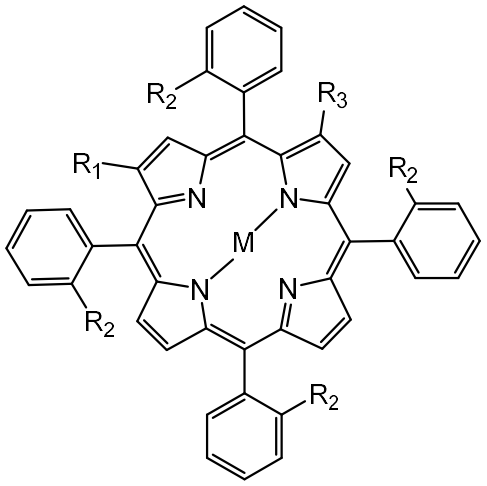


| | M | $R_1$ | $R_2$ | $R_3$ |
|---|---|---|---|---|
| **$H_2$TPP** | $2H^+$ | H | H | H |
| **ZnTPP** | $Zn^{2+}$ | H | H | H |
| **$H_2(NO_2)$TPP** | $2H^+$ | $NO_2$ | H | H |
| **$Zn(NO_2)$TPP** | $Zn^{2+}$ | $NO_2$ | H | H |
| **$H_2(NO_2)_4$TPP** | $2H^+$ | H | $NO_2$ | H |
| **$Zn(NO_2)_4$TPP** | $Zn^{2+}$ | H | $NO_2$ | H |
| **$H_2(NO_2)_5$TPP** | $2H^+$ | $NO_2$ | $NO_2$ | H |
| **$Zn(NO_2)_5$TPP** | $Zn^{2+}$ | $NO_2$ | $NO_2$ | H |
| **$Zn(NO_2)_6$TPP** | $Zn^{2+}$ | $NO_2$ | $NO_2$ | $NO_2$ |

**Figure 5.1**. Structures of the Por compounds studied in this paper. The shorthand names indicate the total number of nitro groups, but do not explicitly specify their locations.

Pors in polar and non-polar solvents (DMSO and toluene, respectively), especially in light of the electron withdrawing nature of the nitro group and its effects on the molecular orbitals and the excited state polarity.

In analyzing these compounds, we are faced with a significant body of literature[6,8,10,17,24,27,31-33,37,40,42,44,45,49-56] offering a range of descriptive frameworks that must be reconciled. These reports all describe several characteristics common to these kinds of compounds, including broad and redshifted absorbance and emission spectra, quenched fluorescence quantum yield, shortened singlet lifetimes, and strong solvent dependence. Some sources also report biexponential fluorescence decays and excitation dependent emission spectra. These observations are typically explained by invoking one of three mechanisms – (1) tautomers with distinct photophysics, (2) rotation of the nitro group modulating its conjugation into the macrocycle, or (3) interaction with a low-lying charge transfer (CT) state. To clarify the excited state dynamics and the nature of the emissive state in these porphyrins, we performed an extensive

series of DFT and TD-DFT calculations. These results are discussed in terms of the energy levels, electronic transitions and, most importantly, molecular structure. Our findings suggest that none of the three mechanisms put forth in the literature can satisfactorily explain the experimental observations. Instead, we propose that molecular distortion due to steric hindrance is the prevailing cause behind all of the unusual photophysics.

## 5.2 Experimental

### 5.2.1. Materials, Instruments, and Methods

Zinc (II) 5,10,15,20-tetraphenyl-*21H,23H*-porphyrin (ZnTPP) and 5,10,15,20-tetraphenyl-*21H,23H*-porphyrin ($H_2$TPP), toluene, and dimethylsulfoxide (DMSO) were purchased from commercial sources and used without further purification. The nitrated derivatives, 2-nitro-5,10,15,20-tetraphenylporphyrin ($H_2(NO)_2$TPP), zinc (II) 2-nitro-5,10,15,20-tetraphenylporphyrinato ($Zn(NO)_2$TPP), 2-nitro-5,10,15,20-tetrakis(2-nitrophenyl)porphyrin ($H_2(NO_2)_5$TPP), zinc (II) 2-nitro-5,10,15,20-tetrakis(2-nitrophenyl)porphyrinato ($Zn(NO_2)_5$TPP), and 2,7-dinitro-5,10,15,20-tetrakis(2-nitrophenyl)porphyrinaato zinc(II) ($Zn(NO_2)_6$TPP), were synthesized and characterized by Dr. Alexander Falber.

Mass spectrometry analyses were performed at the CUNY Mass Spectrometry Facility at Hunter College by electrospray ionization on an Agilent Technologies G6520 Q-TOF instrument and Agilent 1200 HPLC system. UV-visible absorbance spectra were obtained on a Varian Bio3 spectrophotometer. The solutions were prepared at a concentration less than 1.0 μM, and no aggregation effects were observed. Steady-state fluorescence spectra were acquired on a HORIBA Scientific FluoroLog-3 fluorescence spectrometer. The excitation wavelength ($\lambda_{ex}$) was 412 nm for DMSO solutions and 414 nm for toluene, and the emission was collected from 550 to 800 nm

for both. The excitation and emission monochromator bandwidths were both set to 2 nm. The absorbance of the solutions was 0.09 at 412 nm for DMSO solutions, and 0.10 at 414 nm for toluene solutions. For deaerated samples, the solutions were purged with $N_2$ for approximately 10 min. Fluorescence lifetimes were recorded using the FluoroHub Tau-3 time-correlated single photon counting (TCSPC) module for the same instrument. Excitation for TCSPC was provided by a pulsed diode laser source (NanoLED-405L) with a pulse duration less than 200 ps. The excitation wavelength was 405 nm, and emission was detected at 651 nm, with both monochromators set to a 2 nm bandwidth. The data collected in this manner was subjected to standard multi-exponential fitting using the Decay Analysis Software package (v. 6.4) bundled with the instrument.

DFT and TD-DFT calculations were performed with the Gaussian 09 software package using the resources of the City University of New York High Performance Computing Center based at the College of Staten Island and supported under National Science Foundation Grants CNS-0958379, CNS-0855217, ACI-1126113. Avogadro 1.1.1 was used to construct the models, generate the input files, and process and visualize the orbital surfaces. All DFT and TD-DFT calculations were performed using the B3LYP hybrid exchange-correlation functional and the 6-31G(d,p) basis set. DMSO solvent was simulated using the Polarizable Continuum Model (PCM). Ground state (GS) optimizations were performed with equilibrium PCM solvation and accompanied by frequency calculations to ensure the absence of imaginary frequency modes which would indicate a transition state. Vertical excitation (*i.e.* absorption) energies were obtained by performing single-point TD-DFT calculations of the excited electronic states (ES) at the GS optimized nuclear geometry under non-equilibrium, state-specific PCM solvation conditions.

## 5.3. Results & Discussion

### 5.3.1. UV-Vis Spectroscopy

Normalized UV-Vis absorption spectra for the compounds in DMSO and toluene are given in **Figure 5.2**, and the data is summarized in **Table 5.1**. All of the absorbance bands generally redshift with the addition of nitro groups to the molecule, similar to other reports,[23,49-52] with this effect being much more pronounced for the zinc compounds.[53] This is expected based on the electron-withdrawing nature of the nitro group, which serves to stabilize the LUMO energies relative to the HOMOs.

Looking first at the free base compounds, it is clear that the magnitude of MO stabilization is very different for nitro groups directly attached to the macrocycle at the β position and those on the *meso*-phenyl rings, consistent with other reports.[4] The absorbance data for tetrakis(*ortho*-nitrophenyl)Por, $H_2(NO_2)_4TPP$, shows only a minimal shift of at most 4 nm in the $\lambda_{max}$ values from $H_2TPP$ (**Table 5.1**, data from reference [42]). The values for the *para* isomer (not shown, data in references [57] and [55]) are nearly identical to the *ortho* isomer. However, the addition of just one nitro group to the β position instead, as in $H_2(NO_2)TPP$, induces a shift of 7-8 nm, depending on the solvent. This is often ascribed to conjugation between the nitro group and the aromatic core, which is also a function of the rotational angle of the C–N bond. In fact, early reports on β nitrated Pors[23] predicted a strong $\lambda_{max}$ dependence on the solvent polarity, with more polar solvents promoting more planar conformations of the nitro group with respect to the macrocycle. This effect is not observed in our data for the free base compounds, probably because the *meso*-phenyl groups shield the $NO_2$ from the solvent molecules, and more strongly influence the nitro C–N bond rotational position through steric interactions (*vide infra*).[52,53] When both β and phenyl nitro groups are present, as in $H_2(NO_2)_5TPP$, the total shift is not just a linear combination of the two

**Table 5.1**. UV-vis absorption peaks and extinction coefficients for Por compounds in polar vs. non-polar solvents.

| Compound | Absorption peaks, $\lambda_{max}$/nm (log ε) | | | | | |
|---|---|---|---|---|---|---|
| | **B(0,0)** | **FWHM[a]** | **$Q_x$(1,0)** | **$Q_x$(0,0)** | **$Q_y$(1,0)** | **$Q_y$(0,0)** |
| ***Free Base Porphyrins in Toluene[b]*** | | | | | | |
| $H_2$TPP | 418 (5.19) | 13 | 513 (3.85) | 547 (3.47) | 592 (3.31) | 648 (3.15) |
| $H_2(NO_2)$TPP | 426 (5.53) | 28 | 525 (4.36) | 564 (3.73)[c] | 601 (3.76) | 661 (4.03) |
| $H_2(NO_2)_4$TPP[d] | 422 (5.36) | – | 516 (4.15) | 550 (3.64) | 593 (3.61) | 652 (3.12) |
| $H_2(NO_2)_5$TPP | 434 (5.70) | 38 | 531 (4.59) | 564 (4.33) | 603 (4.32) | 676 (4.18) |
| ***Free Base Porphyrins in DMSO[e]*** | | | | | | |
| $H_2$TPP | 418 (6.39) | 13 | 514 (5.00) | 548 (4.63) | 589 (4.43) | 645 (4.37) |
| $H_2(NO_2)$TPP | 425 (6.56) | 32 | 527 (5.51) | 565 (5.14)[c] | 603 (5.05) | 663 (5.20) |
| $H_2(NO_2)_4$TPP | *–polar solvent data not available–* | | | | | |
| $H_2(NO_2)_5$TPP | 431 (5.70) | 37 | 529 (4.58) | 564 (4.29) | 608 (4.26) | 667 (4.25) |
| ***Zinc Porphyrins in Toluene[b]*** | | | | | | |
| ZnTPP[f] | 423 (5.76) | 13 | 550 (4.46) | 588 (3.74) | *n/a* | *n/a* |
| $Zn(NO_2)$TPP | 432 (5.66) | ‘25 | 558 (4.50) | 602 (4.31) | *n/a* | *n/a* |
| $Zn(NO_2)_5$TPP | 446 (5.67) | 43 | 575 (4.54) | 628 (4.50) | *n/a* | *n/a* |
| $Zn(NO_2)_6$TPP | 449 (5.33) | 45 | 573 (4.25) | 623 (4.05)[c] | *n/a* | *n/a* |
| ***Zinc Porphyrins in DMSO[e]*** | | | | | | |
| ZnTPP[g] | 428 (5.79) | 9 | 558 (4.49) | 599 (3.77) | *n/a* | *n/a* |
| $Zn(NO_2)$TPP | 432 (5.67) | 31 | 568 (4.56) | 614 (4.52) | *n/a* | *n/a* |
| $Zn(NO_2)_5$TPP | 434 (5.09) | 43 | 574 (3.89) | 629 (3.86) | *n/a* | *n/a* |
| $Zn(NO_2)_6$TPP | 449 (5.40) | 42 | 574 (4.30) | 619 (4.16) | *n/a* | *n/a* |

[a] Full-width at half-max for the Soret transition, measured in nm. [b] Toluene solvent parameters at 25 °C: η = 0.560 cP; μ = 0.36 D; $\varepsilon_r$ = 2.4; $E_T(30)$ = 33.9; DN = 0.1 kcal/mol. [c] Transition appears as a shoulder. [d] Data taken from reference [21] in benzene (solvent parameters at 25 °C: η = 0.603 cP; μ = 0.00 D; $\varepsilon_r$ = 2.3; $E_T(30)$ = 34.3; DN = 0.1 kcal/mol). [e] DMSO solvent parameters 25 °C: η = 1.996 cP; μ =3.96 D; $\varepsilon_r$ = 48.9; $E_T(30)$ = 45.1; DN = 29.8 kcal/mol. [f] Data estimated from references [28] and [43]. [g] Log(ε) values estimated from reference [46].

contributions, being greater than the sum for the Soret, $Q_x(1,0)$, $Q_y(1,0)$ and $Q_y(0,0)$ bands, but less for the $Q_x(0,0)$ band (see toluene data in **Table 5.1**). This suggests more complicated mixing of the orbitals due to interactions of the nitro groups at different positions.

The trends in the zinc compounds are slightly more complicated. Although there is no data available for the *ortho* isomer of $Zn(NO_2)_4TPP$, Wrobel *et al*. report a value of 429 nm for the Soret peak of zinc(II) tetrakis(4-nitrophenyl)porphyrin (the "*para*" isomer) in a nematic liquid crystal solution.[58] Comparing this to the $\lambda_{max}$ values for ZnTPP suggests that there is also only a small effect for the phenyl nitro groups in these compounds as well. A similar conclusion can be drawn by comparing $Zn(NO_2)_6TPP$ in toluene ($\lambda_{max}$ = 449 nm) to the literature reports of zinc(II) 2,7-dinitro-tetraphenylporphyrin in toluene ($\lambda_{max}$ = 446 nm).[52] On the other hand, the Soret is shifted 9 nm for $Zn(NO_2)TPP$ in toluene, and 23 nm for $Zn(NO_2)_5TPP$, in which both the β and phenyl nitro groups are present. The DMSO data appears to exhibit more moderate shifts across this same series, but the spectra themselves display a drastic solvent dependence, particularly for the asymmetric Soret peak of $Zn(NO_2)_5TPP$ (**Figure 5.2-D**). Since the phenyl groups will still shield the β nitro groups for the reasons discussed previously, this solvatochromism is likely a consequence of axial coordination of DMSO to the zinc center. There are many reports relating the magnitude of the Soret redshift to solvent parameters such as charge, polarity, polarizability, and donor number, with the latter being particularly important.[59-63] In addition to the

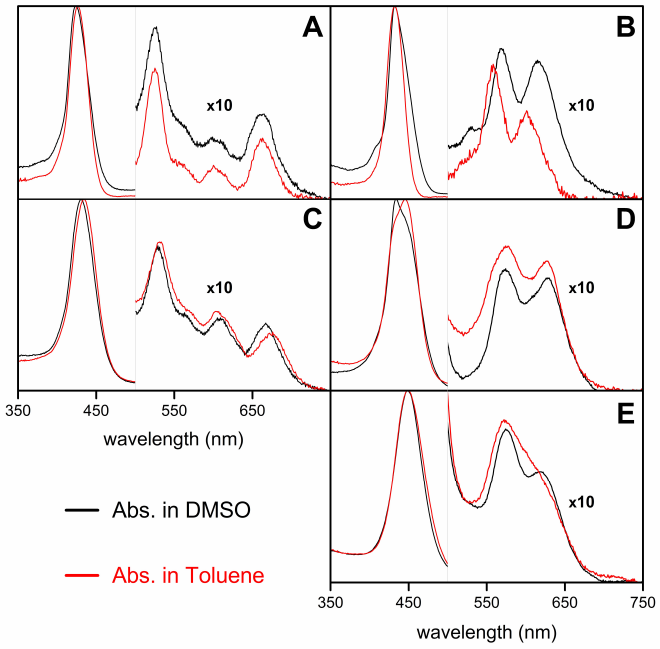


**Figure 5.2**. Normalized UV-Vis absorbance spectra of the free base (left column) and metallated (right column) nitroporphyrins in DMSO (black lines) and toluene (red lines). The Q band regions (from 500–750 nm) have been scaled by a factor of 10, as indicated in the graphs. (A) $H_2(NO_2)TPP$; (B) $Zn(NO_2)TPP$; (C) $H_2(NO_2)_5TPP$; (D) $Zn(NO_2)_5TPP$; (E) $Zn(NO_2)_6TPP$.

redshift, DMSO ligands have been reported to induce an increase in the $Q_x(0,0)/Q_x(1,0)$ intensity ratio,[61] and the development of a slight shoulder on the low-energy edge of the Soret peak,[60] both of which are observed in the spectra for $Zn(NO_2)TPP$ and $Zn(NO_2)_5TPP$.

### 5.3.2. Steady-State Fluorescence Spectroscopy

Normalized fluorescence emission spectra are shown in **Figure 5.3**, and the data is summarized in **Table 5.2**. Unsubstituted $H_2TPP$ and ZnTPP show only slight differences between emission in the non-polar, non-coordinating toluene solvent and the polar, coordinating DMSO, while the nitrated derivatives are much more solvent-dependent. The toluene solutions tend to have broad, featureless emissions while the DMSO solutions exhibit narrower, more well-defined bands. While these differences could be the result of different tendencies towards aggregation in the two solvents, we find no evidence of this under the conditions used. Although the nitro groups are known to reduce solubility and mediate intermolecular interactions,[44] we do not observe any straightforward relationship between the number of nitro groups and the shapes of the emission bands for these compounds. Furthermore, it has been reported that β-nitro-Pors exhibit a "broad and

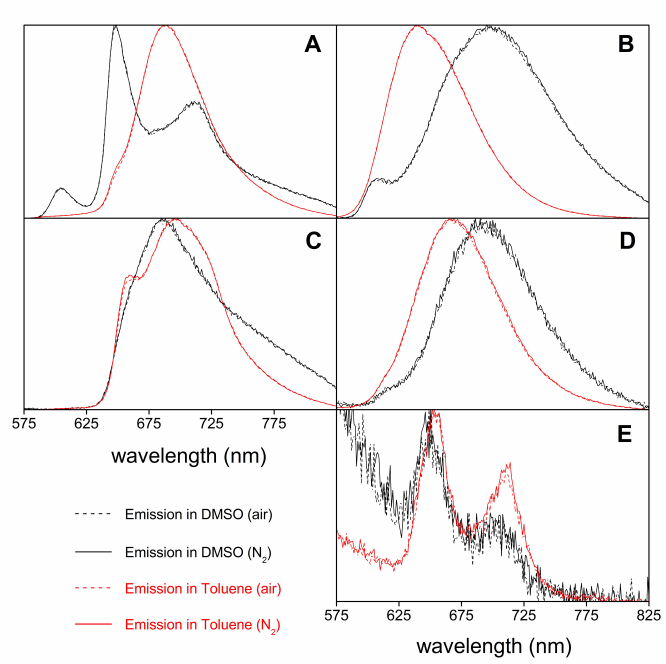


**Figure 5.3**. Normalized fluorescence emission spectra of the free base (left column) and metallated (right column) nitroporphyrins in DMSO (black lines) and toluene (red lines). Deaerated solutions under $N_2$ are denoted by solid lines, and those under ambient atmosphere are denoted by dashed lines, although they largely overlap due to normalization. (A) $H_2(NO_2)TPP$; (B) $Zn(NO_2)TPP$; (C) $H_2(NO_2)_5TPP$; (D) $Zn(NO_2)_5TPP$; (E) $Zn(NO_2)_6TPP$.

structureless"[51] fluorescence, while tetra(nitrophenyl)-Pors retain the spectral shape of the parent molecule.[51]

The strongly electron withdrawing nitro groups polarize the molecule in the GS, with this effect being even stronger in the ES. While there is some controversy over the nature and charge-transfer (CT) character of the emissive $S_1$ state of a nitro-Por, there is little doubt that it has a substantial dipole moment.[42,49-53,55] A more polar solvent like DMSO should stabilize this

**Table 5.2**. Steady state fluorescence emission and lifetime data for the Por compounds in toluene and DMSO. The steady-state excitation wavelength was $\lambda_{ex}$ = 414 nm for toluene and $\lambda_{ex}$ = 412 nm for DMSO. For lifetimes, excitation was at $\lambda_{ex}$ = 405 nm and emission was detected at $\lambda_{em}$ = 651 nm.

| Compound | Emission ($\lambda_{max}$/nm) | Quantum Yield ($\boldsymbol{\phi_F}$) | | Lifetimes under Air | | Lifetimes under $N_2$ | |
|---|---|---|---|---|---|---|---|
| | | Air | $N_2$ | $\boldsymbol{\tau_1}$/ns (%) | $\boldsymbol{\tau_2}$/ns (%) | $\boldsymbol{\tau_1}$/ns (%) | $\boldsymbol{\tau_2}$/ns (%) |
| *Free Base Porphyrins in Toluene* | | | | | | | |
| $H_2$TPP | 653, 719 | 0.110 | 0.110 | 9.53 | *n/a* | 10.9 | *n/a* |
| $H_2(NO_2)$TPP | 690 | 0.050 | 0.060 | 2.76 (76%) | 6.14 (24%) | 2.86 (82%) | 7.25 (18%) |
| $H_2(NO_2)_5$TPP | 660, 698 | 0.043 | 0.048 | 2.87 (32%) | 7.22 (68%) | 2.96 (29%) | 8.22 (71%) |
| *Free Base Porphyrins in DMSO* | | | | | | | |
| $H_2$TPP | 650, 716 | 0.110 | 0.110 | 11.2 | *n/a* | 11.1 | *n/a* |
| $H_2(NO_2)$TPP | 609, 649, 714 | 0.030 | 0.030 | 0.62 (1%) | 11.3 (99%) | 0.47 (2%) | 11.5 (98%) |
| $H_2(NO_2)_5$TPP | 685 | 0.010 | 0.010 | 0.89 (38%) | 3.49 (62%) | 0.77 (33%) | 3.39 (67%) |
| *Zinc Porphyrins in Toluene* | | | | | | | |
| ZnTPP | 596, 645[a] | – | 0.030[a,b] | – | *n/a* | 2.04[b] | *n/a* |
| $Zn(NO_2)$TPP | 641 | 0.056 | 0.061 | 1.03 (76%) | 6.63 (24%) | 1.09 (73%) | 6.90 (27%) |
| $Zn(NO_2)_5$TPP | 667 | 0.020 | 0.030 | 1.09 (79%) | 4.13 (21%) | 1.18 (83%) | 5.83 (17%) |
| $Zn(NO_2)_6$TPP | 655, 716 | 0.001 | 0.002 | 0.45 (2%) | 8.57 (98%) | 1.25 (4%) | 10.3 (96%) |
| *Zinc Porphyrins in DMSO* | | | | | | | |
| ZnTPP | 607, 660 | – | 0.033[b] | – | *n/a* | 1.93[b] | *n/a* |
| $Zn(NO_2)$TPP | 609, 699 | 0.012 | 0.012 | 0.82 (87%) | 4.40 (13%) | 0.85 (88%) | 6.72 (12%) |
| $Zn(NO_2)_5$TPP | 695 | 0.003 | 0.003 | 0.25 (33%) | 6.11 (67%) | 0.31 (20%) | 7.54 (80%) |
| $Zn(NO_2)_6$TPP | 648, 708 | 0.002 | 0.002 | 1.17 (6%) | 6.90 (94%) | 1.06 (5%) | 7.33 (95%) |

[a] Data from reference [28]. [b] Data from reference [30].

kind of polar excited state, red-shifting the emission relative to toluene. While this effect is observed for $Zn(NO_2)TPP$ and $Zn(NO_2)_5TPP$, it is much harder to see for the other compounds due to the poor resolution of the individual bands. However, it is interesting to note that there does not seem to be a redshift for $Zn(NO_2)_6TPP$ in DMSO *vs.* toluene, indicating that the electronic communication between the nitro groups and the macrocycle is somehow frustrated. The last point to note about the spectral shapes is the appearance of a third band in $H_2(NO_2)TPP$ in DMSO, which could indicate the presence of at least two separate emissive states.

The data in **Table 5.2** shows that adding nitro substituents at any position on $H_2TPP$ or ZnTPP quenches the fluorescence, consistent with a broad swath of literature.[18,23,42,49-51,54,55] This quenching has been attributed to multiple, potentially concurrent mechanisms, including mixing between $S_1$ and CT states,[49,51-53] spin-orbit coupling,[51] and enhanced vibrational or rotational relaxation. The absence of aggregation in these solutions allows us to discount collisional or static quenching mechanisms. The introduction of one nitro group on a β pyrrole position causes an approximately 50% decrease in the fluorescence quantum yield, $\phi_F$, for both the free base and zinc Pors in toluene. The effect is slightly greater for solutions under ambient atmosphere than for those under $N_2$, likely due to an enhanced association between the nitro groups and molecular oxygen in solution. For the penta-nitro derivatives in toluene, the total quenching is about 60% for the free base and 70-80% for the zinc compounds, depending on the presence of oxygen. This demonstrates that the nitro groups on the meso-phenyl rings are less efficient at depopulating the emissive $S_1$ state. The sixth nitro substituent, also attached at the β position, almost completely eliminates the remaining fluorescence in both solvents.

In more polar solvents, the quenching by the $NO_2$ substituents is much more effective. The first β nitro quenches the free base Por more than 70% and the zinc Por almost 90% in DMSO.

The additional phenyl nitro groups quench these by more than 90% and 97%, respectively. This could indicate that some of the quenching is due to $S_1$ mixing with or being in equilibrium with a highly polar state that is stabilized in polar solvents, and thus more energetically accessible.[49-54,64]

### 5.3.3. Fluorescence Lifetimes

The most salient fact about the time-resolved emission data is the appearance of two fluorescence lifetimes in each of the nitrated Pors. Similar dynamics have previously been reported for β-nitro Pors and attributed either to the slowed interconversion of tautomers with different photophysics,[24,42] or to a distribution of conformers with respect to the dihedral angle of the nitro group.[52,53] In any case, there is no reason to expect emission from higher $S_n$ states, so the two lifetimes must correspond to distinct molecular structures, whether they are tautomers, atropisomers, or some other kind of conformers. Perhaps more confounding is the fact that one of the lifetimes in each of the nitrated zinc compounds is longer than the unperturbed ZnTPP lifetime. Similar observations have been reported in the literature without explanation.[52,65]

Overall, the fluorescence lifetimes shown in **Table 5.2** are shorter under ambient conditions than under an inert $N_2$ atmosphere, with only a few exceptions close to the time resolution of the instrument (~200 ps). This is expected for a dynamic quenching mechanism between the dye and dissolved molecular oxygen. For the shorter lifetimes ($\tau \lesssim 4$ ns) of all of the compounds, there is only a very slight difference between the air and $N_2$ saturated solutions, indicating that the radiative rate constant for this state is substantially larger than the diffusion rate constant for either solvent. For the longer lifetime components of the free base dyes (including TPP), the oxygen quenching effect is large in toluene but almost absent in DMSO. The lower viscosity of the former solvent (0.59 cP *vs*. 1.996 cP) allows for better diffusion of both species,

and thus an increased likelihood for a quenching event to occur over the life of the excited fluorophore. The longer lifetimes of the zinc compounds show more sensitivity to oxygen, even in DMSO. This is likely due to an enhanced association between the dioxygen quencher and the zinc center, which would effectively increase the encounter radius and quenching efficiency of the pair.

The solvent has almost no effect on the lifetime of $H_2$TPP when oxygen is excluded, while the lifetimes of the nitrated derivatives all vary dramatically with the solvent, even under $N_2$. Since oxygen quenching is negligible, these changes can only be explained by the presence of the nitro group. The effects of the nitro group are typically attributed to the enhancement of either internal conversion (IC) or intersystem crossing (ISC), but the appearance of a separate CT interacting with $S_1$ has also been proposed.[42,49-53] There are two opposing solvent effects which dictate the singlet lifetime: (1) Solvent viscosity will make IC more important in toluene than DMSO; and (2) Solvent polarity will cause polar states to be stabilized more in DMSO than toluene, increasing non-radiative deactivation due to the Energy Gap Law. The competition between these two effects is evident in the variations of the lifetimes seen in **Table 5.2**. Most of the lifetimes are shorter in DMSO, suggesting that they have some polar or "CT-like" character, but there are a few exceptions where the other factors apparently become more important. It is important to point out that the percent contributions of each lifetime to the overall fluorescence signal cannot be directly correlated to the fractional abundances of the different structures, because there may be intrinsic differences in their emissive properties.

### 5.3.4. DFT and TD-DFT

In order to elucidate the structural factors governing the photodynamics, quantum mechanical calculations were performed on several different conformations of the compounds studied. All of the relevant nuclear geometries were optimized using DFT, and TD-DFT was used

to generate the vertical excitation energies at the fixed nuclear ground state geometry, as well as the relaxed $S_1$ geometries. TPP and ZnTPP are both known to be essentially planar macrocycles with almost perpendicular phenyl groups, and our calculations confirm this, with each phenyl group found to be at an angle of 71° ±1° with respect to the flat aromatic plane. The z-coordinate plots (*i.e.* the vertical displacements of the core atoms from the average molecular plane) for these two compounds are shown in Appendix D (Figure D1), revealing the almost perfect planarity of the macrocycles.

### 5.3.4.1. Tautomers

In their photophysical studies of $H_2(NO_2)TPP$, Chirvony *et al.*[42] found three unusual characteristics – (1) emission spectra that depend on $\lambda_{ex}$, (2) biexponential fluorescence decay, and (3) inhomogeneous broadening of the absorbance even down to 77 K. These features, which are consistent with our own experiments, were attributed to the coexistence of two tautomers (see **Figure 5.4**) with different excited state dynamics due to the different position of the nitro group with respect to the aromatic conjugation pathway. We therefore constructed these tautomers and optimized them with DFT to examine their properties. Our calculations confirmed that the "orthogonal" tautomer is more stable than the "collinear" form by almost 3 kcal/mol, indicating that the orthogonal form should predominate by more than 97% at room temperature equilibrium. As Chirvony points out,

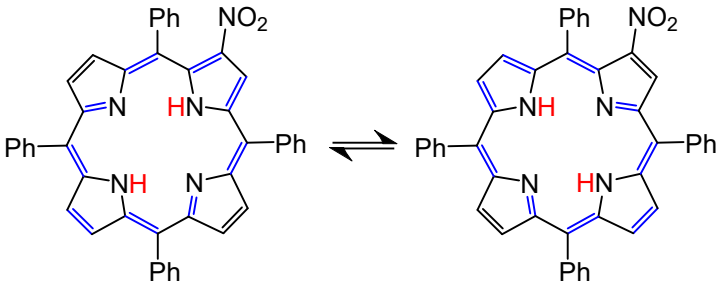


**Figure 5.4**. Inequivalent tautomers of a free base β-nitro-Por. The blue double bonds highlight the aromatic conjugation pathway.

however, NMR studies of this compound predicts a similar distribution at cryogenic temperatures.[24] Therefore the real value of $\Delta G_{taut}$ must be smaller, yielding substantial proportions of both tautomers at room temperature. In addition, TD-DFT results also indicate that the wavelength of the lowest energy transition in the orthogonal form is about 11 nm redshifted from the collinear.

However, thermodynamic considerations don't provide all of the information needed to conclusively make this case. The rate of proton exchange, in both the ground and the excited states, will determine whether or not the absorbance, emission, and lifetimes of the different tautomers can actually be kinetically resolved.[66] Since excited state proton transfer reactions can occur on the picosecond timescale and below,[67-69] the dual lifetimes cannot be unambiguously ascribed to the tautomers without independent kinetic information. Moreover, the inhomogeneous broadening of the absorbance is not due to the superposition of the two tautomers, but rather is intrinsic to each[42] and thus requires further explanation. Finally, the observation of a biexpoential decay in the *metallated* species suggests that tautomerism cannot fully account for these dynamics. We have restricted the following analysis of the other compounds to the predominant orthogonal tautomer, but when collinear tautomers were briefly investigated, similar descriptions were always found to apply.

#### 5.3.4.2. Dihedral Angle of the Nitro Group

When relatively bulky groups like $NO_2$ are added at either the *ortho*-phenyl or β-pyrrole positions, steric hindrance will cause the phenyl angles to change, and can also distort the macrocycle itself. Many different combinations of these nitro and phenyl angles were used as starting structures for the optimization of the β-nitro-Por ground states. The ground state structural data for a selection of these conformers is presented in **Table 5.3**. In each case, the final dihedral

**Table 5.3**. DFT calculated ground state structural data for β-nitro-Por conformers.

| Conformer[a] | Phenyl Group Angles[b] | | | | Nitro Angle[b] | Energy[c] (kcal/mol) | Dipole Moment[d] (D) |
|---|---|---|---|---|---|---|---|
| | $\phi_1$ | $\phi_2$ | $\phi_3$ | $\phi_4$ | $\theta$ | | |
| ***$H_2(NO_2)TPP$*** | | | | | | | |
| Ruffle | *n/a* | *n/a* | *n/a* | *n/a* | *n/a* | *n/a* | *n/a* |
| Int. 1 | 61° | 76° | 66° | 76° | 42° | 1.397 | 7.85 |
| Int. 2 | 60° | 75° | 69° | 65° | 41° | 1.024 | 7.82 |
| Int. 3 | 58° | 64° | 70° | 75° | 40° | 0.929 | 7.75 |
| **Saddle** | **57°** | **61°** | **63°** | **61°** | **37°** | **0.000** | **7.83** |
| ***$H_2(NO_2)_5TPP$*** | | | | | | | |
| ββββ | 68° | 84° | 80° | 77° | 39° | 1.619 | 19.88 |
| βββα | 67° | 84° | 79° | 78° | 38° | 1.419 | 12.716 |
| ββαα | 68° | 84° | 80° | 77° | 39° | 1.261 | 9.40 |
| βααβ | 67° | 79° | 83° | 78° | 38° | 1.163 | 7.61 |
| βαβα | 68° | 86° | 80° | 77° | 40° | 1.466 | 10.11 |
| αααα | 70° | 80° | 80° | 78° | 37° | 0.337 | 22.90 |
| αααβ | 70° | 81° | 80° | 78° | 37° | 0.223 | 13.89 |
| ααββ | 71° | 81° | 80° | 77° | 39° | 0.325 | 7.55 |
| αββα | 71° | 83° | 80° | 80° | 38° | 0.185 | 8.46 |
| **αβαβ** | **71°** | **84°** | **81°** | **77°** | **37°** | **0.000** | **6.84** |
| ***$H_2(NO_2)_6TPP$*** | | | | | | | |
| ββββ (Int.) | 82° | 67° | 77° | 81° | 38°/39° | 3.576 | 21.77 |
| αβββ (Saddle) | 66° | 66° | 78° | 79° | 35°/37° | 2.259 | 17.13 |
| βαβα (Int.) | 75° | 73° | 79° | 80° | 42°/41° | 2.373 | 14.63 |
| αβαβ (Int.) | 76° | 70° | 80° | 81° | 41°/44° | 2.111 | 8.40 |
| ββαα (Saddle) | 70° | 68° | 79° | 79° | 34°/39° | 1.098 | 6.70 |
| **βααα (Saddle)** | **69°** | **71°** | **79°** | **79°** | **33°/37°** | **0.000** | **12.55** |

[a] The conformation of the structure after optimization (Int. 1-3 are three different intermediate structures). [b] Angles measured with respect to the macrocycle plane. The first column ($\phi_1$) is the angle of the phenyl closest to the nitro group. For $H_2(NO_2)_6TPP$, the first two columns ($\phi_1$ and $\phi_2$) are the phenyls nearest the two nitro groups. [c] Ground state energy measured relative to the most stable conformer found for that particular compound, which is assigned an energy of 0.000 kcal/mol and also highlighted in **bold**. [d] Calculated dipole moment, in units of Debye (D)

angle of the nitro group ($\theta$) lies between 37° and 42° with respect to the macrocycle plane. This

angle also forces the nitro and the nearest phenyl group into a nominally coplanar arrangement, with the latter adopting a shallower angle of about $\phi_1$ = 59° ±2° with respect to the macrocycle plane. At the same time, the nitro-bearing pyrrole itself is tilted (or "pitched") upwards out of the plane by the more acute angle of $\phi_1$, significantly distorting the macrocycle. In their analysis of the tautomers, Chirvony *et al*.[42] also looked at the effect of $\theta$ on the transition energies calculated by ZINDO/S. However, these calculations began with a large initial nitro angle of $\theta$ = 80°, and left the core macrocycle geometry frozen as $\theta$ was decreased. Obviously, our results undercut the validity of that approach and the conclusions thereof.

#### 5.3.4.3. Macrocycle Distortion

Depending on the dispositions of the other phenyl groups around the ring, this distortion caused by the β-nitro group can be either enhanced or ameliorated. When the phenyls are all nominally parallel, *i.e.* tilting in the same direction, each pyrrole unit experiences repulsive forces from above and below. Since these forces are nearly balanced, there is little saddling of the Por structure, but the pyrroles will experience some twisting (or "roll"), becoming more parallel to the adjacent phenyls and resulting in a "ruffled" macrocycle. On the other hand, when the phenyls are arranged in a zig-zag pattern, the forces in the z-direction are reinforced, tilting (or "pitching") the pyrroles further out of the plane to produce a "saddled" structure. There are also conformations intermediate between these two cases, in which different pyrroles experience different environments that result in complex superpositions of saddling and ruffling distortions. **Figure 5.5** shows the intermediate and saddled $H_2(NO_2)TPP$ structures superimposed, and **Figure 5.6** shows plots of the z-coordinates for all of the optimized conformations found. These observations apply to both the free base and zinc nitro-Pors (see Appendix D, Figure D2). While the ruffled and saddled structures are uniquely determined by the orientation and position of the β-nitro group (see

**Figure 5.5**), there are obviously many different kinds of intermediate structures with slightly different properties.

Interestingly, no set of initial geometries for $H_2(NO_2)TPP$ resulted in a purely ruffled optimized structure. In other words, even when the molecular structure was initially constructed with all of the phenyl groups tilting in the same direction, which should produce a ruffled core, the final structure always had at least some of the phenyls oblique to one another, giving an intermediate or saddle type core. This suggests that a local configuration with parallel adjacent phenyls is thermodynamically disfavored. Indeed, the saddled conformation, in which no two adjacent phenyls are parallel, is calculated to be the most stable conformer by 1 kcal/mol or more (see **Table 5.3**), despite the dramatic effect it has on the planarity (see **Figure 5.6**). The nitro group, a π-acceptor, apparently draws enough electron density from the aromatic ring to cause it to violate Hückel's $4n+2$ rule, thus destabilizing the planar conformation relative to the others.

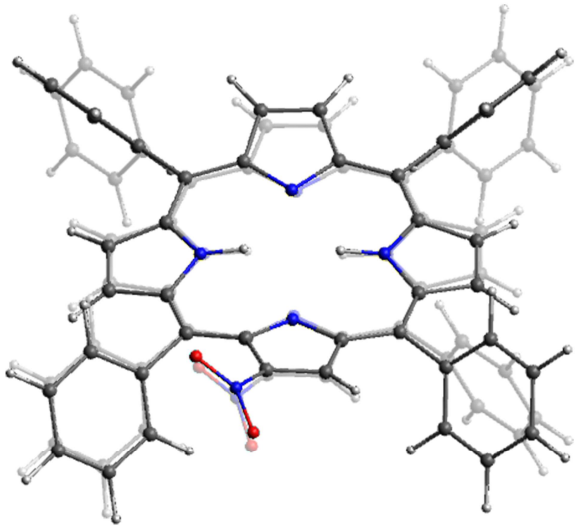

**Figure 5.5**. The two principle conformations of H2(NO2)TPP superimposed on one another to show the deviations. The opaque structure is the saddled conformation, and the transparent structure is an intermediate conformation. The nitro group and the nearest phenyl are locked into essentially the same position in all conformations, while rotation of the other phenyls pushes the other pyrrole groups above or below the plane.

The energy differences between the conformations of $Zn(NO_2)TPP$ are all slightly less, and thus a stable ruffled structure was found (see Figure D2 in Appendix D). Otherwise, the results are largely the same for the free base and zinc compounds.

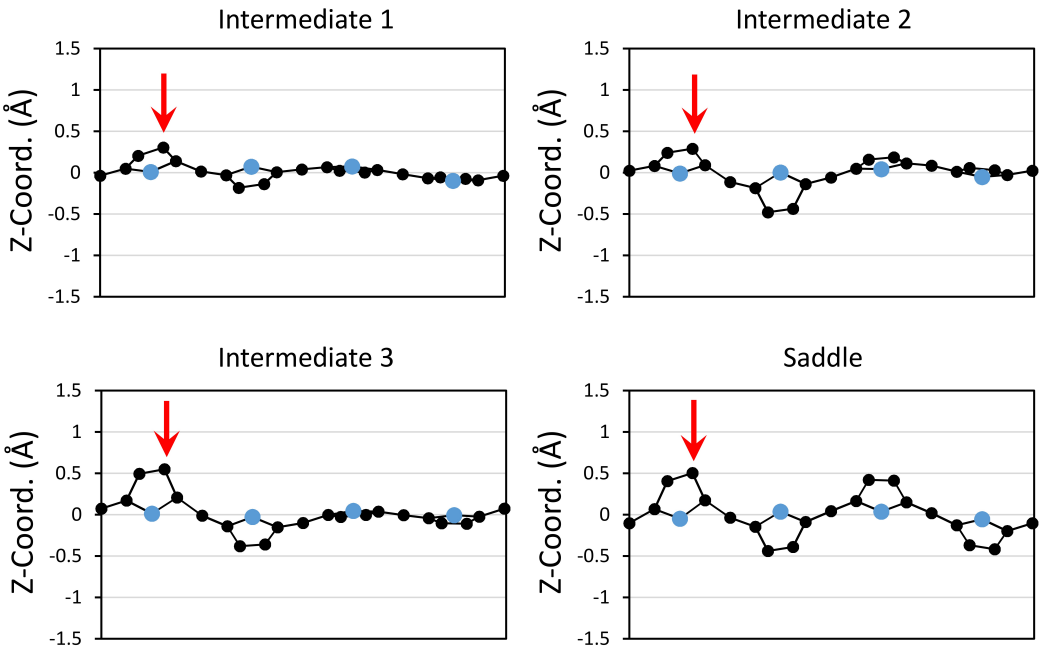


**Figure 5.6**. Z-coordinates of the core atoms for the various optimized conformations of $H_2(NO_2)TPP$. Carbon atoms are black and nitrogen atoms are blue. The red arrow points to the nitro-bearing pyrrole carbon. The horizontal axis is arbitrary. There is significantly more planar deviation throughout the entire ring for the saddle conformation.

This analysis leads to the conclusion that the mono-β-nitro-Pors exist in multiple locally stable conformations subject to thermal equilibrium. The various intermediate conformations all fall within an energy range of about 0.5 kcal/mol, which is less thank $k_BT$ at room temperate. We thus hypothesize that they are all in rapid equilibrium with one another due to low interconversion barriers. Collectively, they represent a single "upper state" with dynamics that cannot be resolved on the timescale studied at room temperature. The saddled conformation, being *ca*. 1.0 kcal/mol below the average intermediate state, accounts for about 80% of the molecular conformations according to a classical Boltzmann distribution. A significant kinetic barrier between the intermediate and saddle conformers could make interconversion between them slow on the timescale studied. Thus, if these or similar conformations persist into the excited state, they could explain both an excitation dependent emission spectrum and the dual lifetimes observed.

Moreover, this description naturally accounts for the inhomogeneous broadening of the absorbance spectra, since the macrocycle geometry is more flexible and sensitive to the phenyl positions in both conformations.

To further test this hypothesis we used another TD-DFT optimization to follow the nuclear relaxation of the two different conformations in the first excited state. These results confirm the existence of two distinct conformations, similar to the ground state, with transition wavelengths separated by about 11 nm. A schematic of these energy levels for $H_2(NO_2)TPP$ are given in **Figure 5.7**. Excitation of either ground state conformation leads to an unstable excited state geometry that can relax into either of the two local minima in the $S_1$ potential energy surface. While the higher energy conformation in the excited state would not normally be populated at room temperature under equilibrium conditions, a kinetic barrier to interconversion could make the rate of thermal equilibration slow enough for fluorescence decay to become competitive. This would result in observable fluorescence from both states, with distinct Stokes shifts, lifetimes, *etc*. for each. The differences in the dipole moments and conformational dynamics of each state could also account for the different solvent-dependent behavior observed for the two lifetimes. Since we cannot accurately account for all of the deactivation processes from the relaxed excited states, we cannot use the TD-DFT results to quantitatively predict the quantum yields or lifetimes. In particular, intersystem crossing has been shown to be an important factor in depopulating $S_1$ for nitro-Pors, and has also been shown to increase with distortion of the macrocycle.[70-72]

In contrast to the β substituted nitro-Pors, all of the surveyed initial structures for $H_2(NO_2)_4TPP$ converged to a very slight saddle conformation but remained almost completely planar (see Appendix D, Figures D3 and D4). Steric repulsion between the electron rich nitro groups and the aromatic π-system forces the phenyls into a more perpendicular orientation ($\phi_n$ =

78° ±1°, for all *n*). At the same time, this creates a significant barrier to rotation, giving rise to four distinct atropisomers, designated αααα, αααβ, ααββ, and αβαβ. While the dipole moments of these vary by about 20 D due to the orientation of the *ortho*-nitro groups, the ground state energies are all within about 0.3 kcal/mol of one another, with αβαβ being the most stable. The TD-DFT transition energies and compositions of the various atropisomers are also nearly identical, as are the relaxed excited state geometries. While there are reports of CT states in tetra(nitrophenyl)porphyrins, to our knowledge multiexponential fluorescence decay has not been observed, consistent with these results.

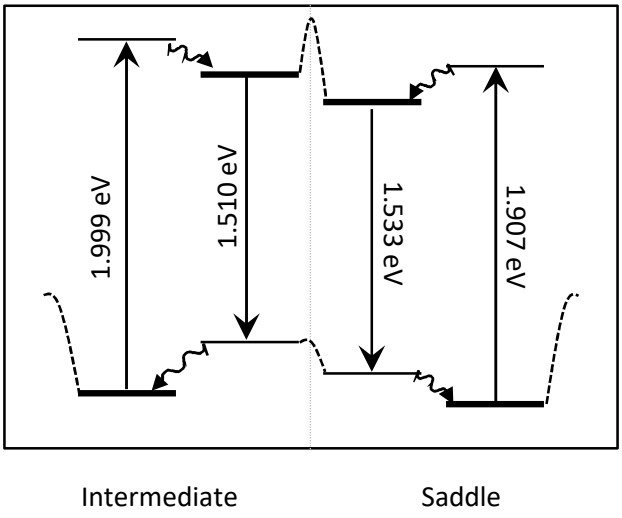


**Figure 5.7**. Schematic energy level diagram of the two principle conformations of $H_2(NO_2)TPP$. The thick lines represent optimized or relaxed nuclear geometries, and the dashed lines represent (unknown) barriers to interconversion between these relaxed geometries. The unrelaxed geometries may be able to internally convert to either stable structure (for both $S_0$ and $S_1$), potentially scrambling the populations.

When we performed a similar analysis on a set of $H_2(NO_2)_5TPP$ conformers, however, we were brought to a slightly different conclusion. The presence of the β-nitro further splits the four atropisomers of $H_2(NO_2)_4TPP$ into 16 distinct geometries in $H_2(NO_2)_5TPP$. For example, the αβαβ and βαβα isomers can be distinguished if we adopt the convention that the first character (α or β) in the string corresponds to the orientation of the nitro-phenyl group closest to the pyrrole-$NO_2$. We again surveyed a broad sample of these various conformations, and the z-coordinate plots are shown in Figure D5 in Appendix D, with the physical data given in **Table 5.3**. These conformers also tend to group into two states that are well-separated in energy, but the determining factor here

is not the distortion of the macrocycle. In fact, all of the structures sampled converged to one of the intermediate conformations – no purely ruffled or saddled type conformers were found. Rather, the orientation of the nitro-phenyl dipoles with respect to the β-nitro group dictates the overall energy. In particular, the orientation of the nitro-phenyl closest to the β-nitro has the largest influence on the energies, splitting them into higher (βxxx-type) and lower (αxxx-type) levels. The β-nitro dipole and the closest nitro-phenyl dipole are almost perfectly orthogonal in the αxxx atropisomers, but have an obtuse angle in the βxxx ones. This creates a more unfavorable dipole-dipole interaction for the latter, raising its energy almost 1.5 kcal/mol relative to the former. The other nitro-phenyl dipole orientations further modulate the molecular energies, but only slightly (< 0.5 kcal/mole). The TD-DFT results for $H_2(NO_2)_5TPP$ again show the coexistence of two stable conformations in the excited state. The energy level scheme is shown in Figure D9 of Appendix D, and has many of the same characteristics as for $H_2(NO_2)TPP$.

In $H_2(NO_2)_6TPP$, all of these complications are further exacerbated by the presence of a second β-nitro group. After surveying a range of structures, a stable saddle-type conformer once again emerged. In addition, the intermediate structures further split into the βxxx-type and αxxx-type conformers, as in the penta-nitro derivatives. Thus, there appear to be at least three separate structures that are well-resolved in terms of the energy, and possibly more. The experimental results suggest that not all of these states are populated or resolved under standard conditions.

DFT calculations on the series of nitrated zinc Pors yields results that are qualitatively similar to those just discussed. As mentioned, the energy differences between the various geometries are all slightly smaller than for the corresponding free base compounds. This lowers the ruffled conformer of $Zn(NO_2)TPP$ enough to make it an accessible, stable geometry, and confirms that the energies of the intermediate structures are about halfway between the saddled

and ruffled forms, as expected. Corresponding data for the zinc compounds is given in Appendix D.

#### 5.3.4.4. Charge Transfer States

The presence of a strongly electron withdrawing group such as $NO_2$ suggests the possibility of a CT state. If the emissive singlet is able to interact with this CT state, it will be quenched and shortened in a way consistent with the experimental spectroscopy.[42,49-54,64] Unfortunately, there seem to be contradictory, yet at times overlapping, descriptions of how this interaction is manifested, with some authors postulating a distinct CT state formed by a separate electron transfer step,[42,49-53] while others simply attribute a "CT character" to $S_1$ itself.[52,53] There is also discussion of a "twisted intramolecular charge transfer" (TICT) occurring when there is electron transfer to the nitro group followed by a rotation making it perpendicular to the macrocycle plane. While there is little doubt that nitro groups withdraw substantial electron density in the excited state, resulting in a large dipole moment, that alone is not sufficient to identify $S_1$ with an emissive CT state.

To characterize the nature of these transitions, we analyzed their composition according to the DFT and TD-DFT results. The ground state energy levels of some of these are shown in **Figure 5.8**. The levels are color coded according to the type of orbital – yellow for orbitals localized on the macrocycle core, red for nitro orbitals, and blue for phenyl orbitals. Orbitals that are delocalized among two or more regions have composite colors – orange for core/nitro, green for core/phenyl, purple for nitro/phenyl, and black for all three. The β-nitro groups mix with one of the macrocycle-centered LUMOs, lowering it in energy and breaking the degeneracy. On the other hand, the more pure nitro-localized orbitals remain relatively high in energy for these compounds. The situation for $H_2(NO_2)_4TPP$ is different because the nitro groups are not directly conjugated into the aromatic

ring. Instead, the *ortho* arrangement puts them close to the core π-system and allows them to mix equally with both LUMOs equally. This "through-space" interaction is much weaker and only shifts the orbitals about 0.1 eV in energy, explaining the much smaller redshift in their spectra.

In $H_2(NO_2)_5TPP$ and $H_2(NO_2)_6TPP$, the phenyl-nitro groups mix with the phenyl orbitals themselves more than in $H_2(NO_2)_4TPP$. This is a consequence of the structural reorganization caused by the β-nitro forcing the phenyl groups away from the more perpendicular angle attained in $H_2(NO_2)_4TPP$. This, in turn, forces the *ortho*-nitros to adopt shallower dihedral angles with respect to the phenyl, allowing more effective orbital mixing. Meanwhile, the core nitro group lowers the energy of both LUMOs enough to decouple them from the *ortho*-nitros, albeit unequally. The primary change induced by the second β-nitro in $H_2(NO_2)_6TPP$ is the lowering of the second LUMO, essentially restoring the degeneracy.

The energy levels marked with open circles in **Figure 5.8** indicate orbitals that are involved in TD-DFT transitions less than about 3.0 eV. The compositions of these same transitions, in terms of singly excited Slater determinants, is given in **Table 5.4** and Table D1. As expected, the lowering of one of the LUMOs in $H_2(NO_2)TPP$ increases the H→L contribution to the lowest energy transition, redshifting it substantially in both conformations. However, the next lowest transition present in $H_2TPP$ becomes mixed with a core→nitro excitation in both conformations of $H_2(NO_2)TPP$, raising its energy and blueshifting it from 536 nm to about 430 nm. Moreover, a new transition arises between these (at 468 nm) in the intermediate conformation, and has a 74% core→nitro excitation component. While there may be higher energy pure CT states, they would not be close enough in energy to $S_1$ for there to be a meaningful thermodynamic equilibrium between them.

In order to visualize these transitions in terms of the charge transfer, electron difference-density maps (EDDMs) were generated for each one (see Appendix D, Figures D10 to D16).[73] There is a buildup of charge on the nitro group in all of the transitions of $H_2(NO_2)TPP$ (for both conformations), but there also remains substantial electron density on the macrocycle, even in the new 468 nm transition of the intermediate conformation. Thus, none of these can be assigned to a pure CT state. A similar inspection of the wavefunctions for the relaxed excited states leads to the same conclusion. In fact, upon relaxation within the $S_1$ manifold, the β-nitro dihedral angle

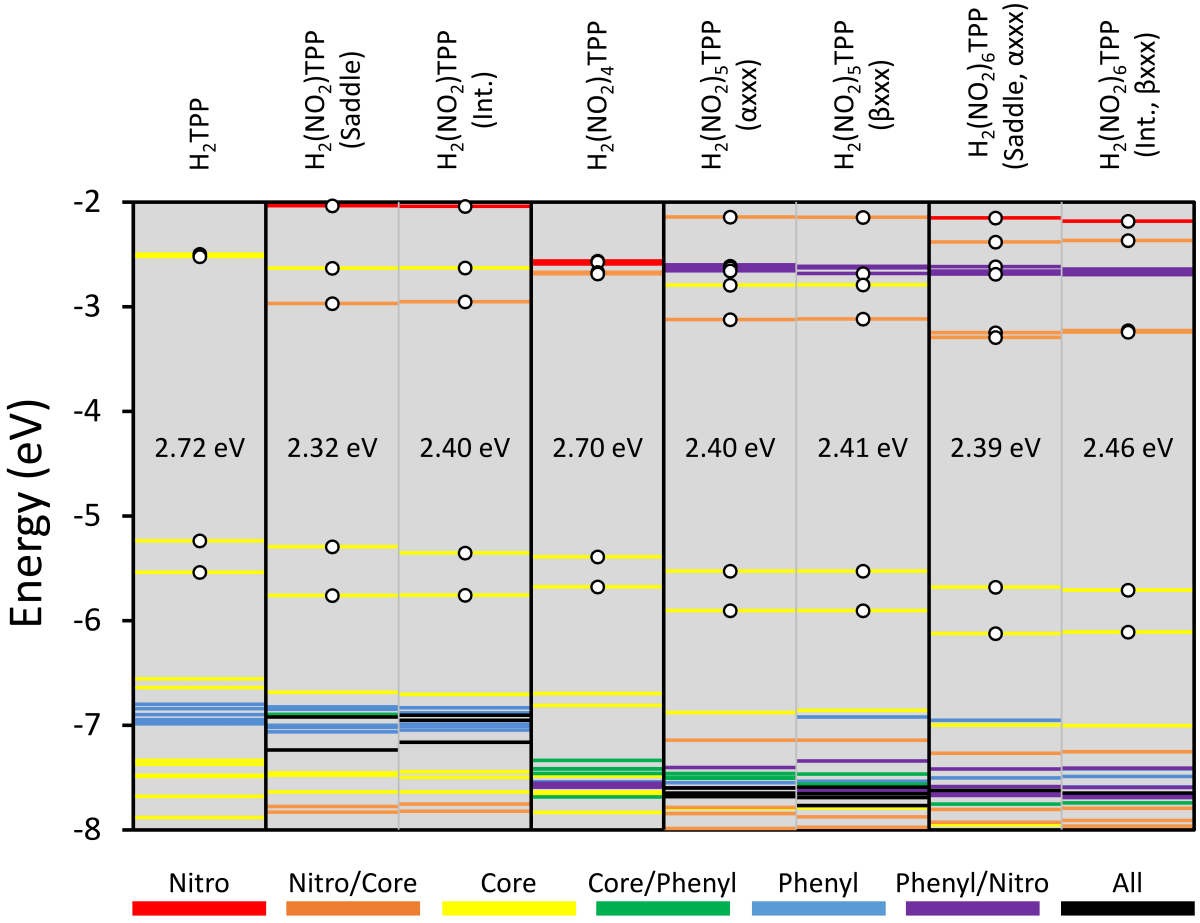


**Figure 5.8**. Ground state orbital energies for the series of free base nitro-Pors. The HOMO-LUMO gap energies are given in the gap for each compound. The energy levels are color coded according to the localization of the orbital density, as shown in the key at the bottom. Orbitals involved in the first few TD-DFT transitions are marked with open circles.

decreases by almost 30°, becoming more coplanar with the macrocycle and increasing the conjugation and thus the electron delocalization. This is in direct contradiction to the hypothesis of a TICT state, but is consistent with the results of Chirvony *et al*., who also report that $S_1$ has a transient absorbance spectrum most similar to a $^1(\pi,\pi^*)$ state.[42]

There lowest energy transitions of $H_2(NO_2)_4TPP$ have a composition similar to the same transitions in $H_2TPP$, which correspond to the $Q_x(0,0)$ and $Q_y(0,0)$ bands. The transition EDDMs for the two compounds also match very closely, with some additional charge buildup on the nitro-phenyl groups in $H_2(NO_2)_4TPP$. Visual inspection of the maps indicates that the 533 nm transition of $H_2(NO_2)_4TPP$ may be the closest to being a true CT state (see Figure D13). This is consistent with previous reports of related compounds[49-51] which analyzed the intramolecular charge transfer to an *ortho*-nitro-phenyl in terms of Marcus theory. It is worth noting, however, that the dihedral angles of the nitro groups with respect to the phenyls decrease from *ca.* 25° in the ground state to a *ca.* 17° in the relaxed excited state, contrary to the TICT hypothesis. The CT state formed here is also different in that it is actually delocalized over all four nitro groups. This will affect factors such as the solvent reorganization energy and the CT lifetime, and may have important implications for harnessing the state to use in specific applications.

In $H_2(NO_2)_5TPP$, the transitions share features of the mono- and tetra-nitro derivatives. For both the αxxx and βxxx type atropisomers, transitions corresponding to the $Q_x(0,0)$ and $Q_y(0,0)$ bands are present. These are perturbed by the β-nitro in a manner almost identical to the intermediate conformation of $H_2(NO_2)TPP$, resulting in bands near 630 and 430 nm. There are also new bands that arise between these with significant CT character, but these are formed by the mixing of multiple nitro groups simultaneously, as in $H_2(NO_2)_4TPP$. The αxxx-type atropisomers apparently have more pure CT transitions at 449 and 442 nm, but both of these are formed by

**Table 5.4**. TD-DFT transitions for the series of free base nitro-Pors.

| ΔE (eV)[a] | λ (nm)[b] | *f*[c] | Wavefunction[d] |
|---|---|---|---|
| | | | ***$H_2$TPP*** |
| 2.164 | 573 | 0.023 | **34% (H-1→L+1)** + **65% (H→L)** + … |
| 2.314 | 536 | 0.030 | **38% (H-1→L)** + **62% (H→L+1)** + … |
| | | | ***$H_2(NO_2)$TPP (Saddle)*** |
| 1.908 | 650 | 0.099 | **13% (H-1→L+1)** + **86% (H→L)** + … |
| 2.858 | 434 | 0.748 | **39% (H-1s→L)** + 27% (H-1→L+2) + **30% (H→L+1)** + … |
| | | | ***$H_2(NO_2)$TPP (Intermediate)*** |
| 1.966 | 631 | 0.080 | **15% (H-1→L+1)** + **83% (H→L)** + … |
| 2.650 | 468 | 0.014 | **22% (H-1→L+1)** + 74% (H→L+2) + … |
| 2.884 | 430 | 0.639 | **34% (H-1→L)** + 32% (H-1→L+2) + **29% (H→L+1)** + … |
| | | | ***$H_2(NO_2)_4$TPP*** |
| 2.149 | 577 | 0.017 | **26% (H-1→L+1)** + **61% (H→L)** + **6% (H→L+1)** + … |
| 2.325 | 533 | 0.014 | **26% (H-1→L)** + **16% (H→L+1)** + 21% (H→L+4) + 30% (H→L+5) + … |
| | | | ***$H_2(NO_2)_5$TPP (αxxx)*** |
| 1.959 | 633 | 0.070 | **14% (H-1→L+1)** + **84% (H→L)** + … |
| 2.694 | 460 | 0.036 | **33% (H-1→L+1)** + 9% (H-1→L+2) + 53% (H→L+6) + … |
| 2.763 | 449 | 0.042 | 5% (H-1→L+2) + 86% (H-1→L+3) + … |
| 2.803 | 442 | 0.011 | 95% (H-1→L+4) + … |
| 2.915 | 425 | 0.618 | **29% (H-1→L)** + 5% (H-1→L+3) + 26% (H-1→L+6) + 25% (H→L+1) + … |
| | | | ***$H_2(NO_2)_5$TPP (βxxx)*** |
| 1.967 | 630 | 0.069 | **14% (H-1→L+1)** + **83% (H→L)** + … |
| 2.683 | 462 | 0.021 | **24% (H-1→L+1)** + 57% (H-1→L+2) + 15% (H→L+6) + … |
| 2.712 | 457 | 0.032 | **10% (H-1→L+1)** + 34% (H-1→L+2) + 52% (H→L+6) + … |
| 2.933 | 423 | 0.663 | **32% (H-1→L)** + 30% (H-1→L+6) + **25% (H→L+1)** + … |

[a] Energy of the transition in electron volts. Only transitions with energies below 3.0 eV are given. [b] Transition wavelength in nanometers. [c] Calculated oscillator strengths. Only transitions with oscillator strengths greater than 0.01 are given. [d] Excited state wavefunction, in terms of the contributions of single excitations of the ground state Slater determinant. Only single excitations with contributions greater than 5% are given. The HOMO is designated "H", the second HOMO is "H-1", *etc*. The LUMO is designated "L", the second LUMO is "L+1", *etc*. Excitations involving only orbitals corresponding to Gouterman's four-orbital model are shown in **bold**. Excitations which populate a nitro or nitro-like orbital are underlined.

transfer to the *ortho*-nitros with the β-nitro actually losing electron density. The transitions of $H_2(NO_2)_6$TPP are even further complicated by the second β-nitro, the four *ortho*-nitros, and the coexistence of two or more conformations. The two examples in **Table 5.4** (see Figure D16 and

D17 in Appendix D for EDDMs) show the extreme variation in the number and character of the transitions.

The relaxed $S_1$ geometries of the penta- and hexa-nitro derivatives are more complicated than the other cases. For $H_2(NO_2)_5TPP$, they again display shallower angles for both the *ortho*- and β-nitro groups, but for $H_2(NO_2)_6TPP$ one of the β-nitros becomes slightly more perpendicular by about 5°. Moreover, the wavefunction compositions have a different character after nuclear reorganization, with more pure CT states developing. This could indicate the potential for efficient charge separation, although the transition probabilities between the states are unknown.

### 5.4. Conclusion

The strong electron withdrawing nature of the nitro group makes it very useful for modulating the ground state properties and excited state dynamics of porphyrinoids and other organic dyes. It can be tempting to try to explain all of the properties of a nitrated compound strictly in terms of electronic effects, but our results indicate that structural factors related to the presence of an $NO_2$ group can be just as important, if not more so. Taken together, our spectroscopic and quantum chemical studies point to three principle conclusions: (1) a nitro group at a β-pyrrole position can interact with a nearby bulky *meso*-substituent to significantly distort the macrocycle; (2) increased conformational dynamics can lead to multiple stable minima in both the ground and excited state potential energy surfaces, each with different photophysical characteristics; and (3) the position of the nitro group in a TPP molecule will significantly modify the excited state dynamics and dictate the existence and energy of a CT state.

In addition, there are many subtle effects that the detailed molecular structure can have on the photodynamics, especially when both *ortho*- and β-nitro groups are present in the same

molecule. Given the important role of atropisomerism these compounds, for example, it may be possible to use an external field to switch between two states with distinguishable excited state dynamics. Depending on the specific interconversion barriers between states, this could manifest as electrochromic or photochromic behavior, although we have not observed any evidence for this to date. The rate of intersystem crossing is another important factor to consider, as the triplet state population can be crucial to applications in photodynamic therapy, photovoltaics, and organic light emitting diodes.

These results also have implications for organic dyes other than nitrated porphyrins. The nitro group itself has some electronic effect on the photophysics, but many of the more significant changes are due to the distortion of the macrocycle. The structural changes induced by the nitro group can also be brought about by the presence of other bulky substituents. There is at least one example of anomalous biexponential decay of distorted Pors reported in the literature,[74] but while the authors discuss the possibility of multiple stable excited state conformations, they do not explicitly cite this as the reason for the dual lifetimes. This framework may be useful for interpreting other results in the literature, and should also help point to new directions for future progress.

### 5.5. References


1. Seybold, P. G.; Gouterman, M. Porphyrins : XIII: Fluorescence spectra and quantum yields. *Journal of Molecular Spectroscopy.* **1969**, *31*, 1-13.
2. Hosomizu, K.; Oodoi, M.; Umeyama, T.; Matano, Y.; Yoshida, K.; Isoda, S.; Isosomppi, M.; Tkachenko, N. V.; Lemmetyinen, H.; Imahori, H. Substituent Effects of Porphyrins on Structures and Photophysical Properties of Amphiphilic Porphyrin Aggregates. *The Journal of Physical Chemistry B.* **2008**, *112*, 16517-16524.
3. Mathew, S.; Iijima, H.; Toude, Y.; Umeyama, T.; Matano, Y.; Ito, S.; Tkachenko, N. V.; Lemmetyinen, H.; Imahori, H. Optical, Electrochemical, and Photovoltaic Effects of an Electron-Withdrawing Tetrafluorophenylene Bridge in a Push–Pull Porphyrin Sensitizer

Used for Dye-Sensitized Solar Cells. *The Journal of Physical Chemistry C.* **2011**, *115*, 14415-14424.

4. Grover, N.; Sankar, M.; Song, Y.; Kadish, K. M. Asymmetrically Crowded "Push-Pull" Octaphenylporphyrins with Modulated Frontier Orbitals: Syntheses, Photophysical, and Electrochemical Redox Properties. *Inorganic chemistry.* **2016**, *55*, 584-597.
5. Wang, L.; She, Y.; Zhong, R.; Ji, H.; Zhang, Y.; Song, X. A Green Process for Oxidation of p-Nitrotoluene Catalyzed by Metalloporphyrins under Mild Conditions. *Organic Process Research & Development.* **2006**, *10*, 757-761.
6. Schiavon, M. A.; Iamamoto, Y.; Nascimento, O. R.; Assis, M. d. D. Catalytic activity of nitro- and carboxy-substituted iron porphyrins in hydrocarbon oxidation. *Journal of Molecular Catalysis A: Chemical.* **2001**, *174*, 213-222.
7. Zakavi, S.; Heidarizadi, F.; Rayati, S. Comparative study of catalytic activity of some biomimetic models of cytochrome P450 in oxidation of olefins with tetra-n-butylammonium periodate: Electron-rich Mn-porphyrins versus the electron-deficient ones. *Inorganic Chemistry Communications.* **2011**, *14*, 1010-1013.
8. Gong, L.-C.; Dolphin, D. Nitrooctaethylporphyrins: synthesis, optical and redox properties. *Canadian Journal of Chemistry.* **1985**, *63*, 401-405.
9. Ozette, K.; Leduc, P.; Palacio, M.; Bartoli, J.-F.; Barkigia, K. M.; Fajer, J.; Battioni, P.; Mansuy, D. New Metalloporphyrins with Extremely Altered Redox Properties: Synthesis, Structure, and Facile Reduction to Air-Stable π-Anion Radicals of Zinc and Nickel β-Heptanitroporphyrins. *Journal of the American Chemical Society.* **1997**, *119*, 6442-6443.
10. Bartoli, J. F.; Battioni, P.; De Foor, W. R.; Mansuy, D. Synthesis and remarkable properties of iron β-polynitroporphyrins as catalysts for monooxygenation reactions. *Journal of the Chemical Society, Chemical Communications.* **1994**, 23-24.
11. Sun, B.; Ou, Z.; Yang, S.; Meng, D.; Lu, G.; Fang, Y.; Kadish, K. M. Synthesis and electrochemistry of beta-pyrrole nitro-substituted cobalt(II) porphyrins. The effect of the NO(2) group on redox potentials, the electron transfer mechanism and catalytic reduction of molecular oxygen in acidic media. *Dalton Transactions.* **2014**, *43*, 10809-10815.
12. Suslick, K. S.; Chen, C. T.; Meredith, G. R.; Cheng, L. T. Push-pull porphyrins as nonlinear optical materials. *Journal of the American Chemical Society.* **1992**, *114*, 6928-6930.
13. Sen, A.; Krishnan, V. Synthesis, spectral and electrochemical properties of donor/acceptor substituted fluoroarylporphyrins. *Tetrahedron Letters.* **1996**, *37*, 5421-5424.
14. Senge, M. O.; Ryppa, C.; Fazekas, M.; Zawadzka, M.; Dahms, K. 5,10-A2B2-type meso-substituted porphyrins-a unique class of porphyrins with a realigned dipole moment. *Chemistry.* **2011**, *17*, 13562-13573.
15. Chou, J.-h.; Kosal, M. E.; Nalwa, H. S.; Rakow, N. A.; Suslick, K. S. In *The Porphyrin Handbook*; Academic Press: New York, **2000**; Vol. 6, p 43-131.
16. Schiavon, M. A.; Iwamoto, L. S.; Ferreira, A. G.; Iamamoto, Y.; Zanoni, M. V. B.; Assis, M. d. D. Synthesis and characterization of a novel series of meso (nitrophenyl) and meso (carboxyphenyl) substituted porphyrins. *Journal of the Brazilian Chemical Society.* **2000**, *11*, 458-466.

17. Gros, C. P.; Desbois, N.; Michelin, C.; Demilly, E.; Tilkin-Mariamé, A.-F.; Mariamé, B.; Gallardo, F. Synthesis and Antiviral Activity Evaluation of Nitroporphyrins and Nitrocorroles as Potential Agents against HumanCytomegalovirusInfection. *ACS Infectious Diseases.* **2015**, *1*, 350-356.

18. Maiya, G. B.; Krishnan, V. Intramolecular electron transfer in donor-acceptor systems. Porphyrins bearing trinitroaryl acceptor group. *The Journal of Physical Chemistry.* **1985**, *89*, 5225-5235.

19. Kim, H.-S.; Kim, C.-H.; Ha, C.-S.; Lee, J.-K. Organic solar cell devices based on PVK/porphyrin system. *Synthetic Metals.* **2001**, *117*, 289-291.

20. Tingting, X.; He, H.; Wang, Q.; Dubey, M.; Xingzhong, Y.; Galipeau, D.; Ropp, M. In *Photovoltaic Specialists Conference, 33rd IEEE*; IEEE: San Diego, CA, 2008, p 1-3.

21. Kim, J. B.; Leonard, J. J.; Longo, F. R. Mechanistic study of the synthesis and spectral properties of meso-tetraarylporphyrins. *Journal of the American Chemical Society.* **1972**, *94*, 3986-3992.

22. Karki, L.; Vance, F. W.; Hupp, J. T.; LeCours, S. M.; Therien, M. J. Electronic Stark Effect Studies of a Porphyrin-Based Push−Pull Chromophore Displaying a Large First Hyperpolarizability: State-Specific Contributions to β. *Journal of the American Chemical Society.* **1998**, *120*, 2606-2611.

23. Karelson, M.; Pihlaja, K.; Tamm, T.; Uri, A.; Zerner, M. C. UV-visible spectra of some nitro-substituted porphyrins. *Journal of Photochemistry and Photobiology A: Chemistry.* **1995**, *85*, 119-126.

24. Crossley, M. J.; Harding, M. M.; Sternhell, S. Tautomerism in 2-substituted 5,10,15,20-tetraphenylporphyrins. *Journal of the American Chemical Society.* **1986**, *108*, 3608-3613.

25. Yang, S.; Sun, B.; Ou, Z.; Meng, D.; Lu, G.; Fang, Y.; Kadish, K. M. β-Nitro-substituted free-base, iron(III) and manganese(III) tetraarylporphyrins: synthesis, electrochemistry and effect of the NO2substituent on spectra and redox potentials in non-aqueous media. *Journal of Porphyrins and Phthalocyanines.* **2013**, *17*, 857-869.

26. Siri, O.; Jaquinod, L.; Smith, K. M. Coplanar conjugated β-nitroporphyrins and some aspects of nitration of porphyrins with N2O4. *Tetrahedron Letters.* **2000**, *41*, 3583-3587.

27. Vicente, M. G. H.; Neves, M. G. P. M. S.; Cavaleiro, J. S.; Hombrecher, H. K.; Koll, D. Electrochemical and spectroscopic properties of Cu(II) β-nitro meso-tetra(pentafluorophenyl)porphyrins. *Tetrahedron Letters.* **1996**, *37*, 261-262.

28. Hindin, E.; Kirmaier, C.; Diers, J. R.; Tomizaki, K.-y.; Taniguchi, M.; Lindsey, J. S.; Bocian, D. F.; Holten, D. Photophysical Properties of Phenylethyne-Linked Porphyrin and Oxochlorin Dyads. *The Journal of Physical Chemistry B.* **2004**, *108*, 8190-8200.

29. Barkigia, K. M.; Renner, M. W.; Senge, M. O.; Fajer, J. Interplay of Axial Ligation, Hydrogen Bonding, Self-Assembly, and Conformational Landscapes in High-Spin Ni(II) Porphyrins. *The Journal of Physical Chemistry B.* **2004**, *108*, 2173-2180.

30. Hsiao, J.-S.; Krueger, B. P.; Wagner, R. W.; Johnson, T. E.; Delaney, J. K.; Mauzerall, D. C.; Fleming, G. R.; Lindsey, J. S.; Bocian, D. F.; Donohoe, R. J. Soluble Synthetic

Multiporphyrin Arrays. 2. Photodynamics of Energy-Transfer Processes. *Journal of the American Chemical Society.* **1996**, *118*, 11181-11193.

31. Pukhovskaya, S. G.; Ivanova, Y. B.; Nam, D. T.; Vashurin, A. S. Dependence of the basic properties of meso-nitro-substituted derivatives of β-octaethylporphyrin on the nature of substituents. *Russian Journal of Physical Chemistry A.* **2014**, *88*, 1670-1676.
32. Ivanova, Y. B.; Nam, D. T.; Chizhova, N. V.; Mamardashvili, N. Z. Spectrophotometric study of acid-base and complexing properties of 5,10,15-trinitro-2,3,7,8,12,13,17,18-octaethylporphyrin in acetonitrile. *Russian Journal of General Chemistry.* **2014**, *84*, 1207-1211.
33. Ivanova, Y. B.; Chizhova, N. V.; Mamardashvili, N. Z. Spectrophotometric study of the complexing properties of 2,3,7,8,12,13,17,18-Octaethyl-5,10,15-trinitroporphyrin and its dianion toward Zn(OAc)2 in acetonitrile. *Russian Journal of General Chemistry.* **2014**, *84*, 1394-1398.
34. Dey, S.; Ikbal, S. A.; Rath, S. P. Self-assembly of cobalt(ii) and zinc(ii) tetranitrooctaethylporphyrin via bidentate axial ligands: synthesis, structure, surface morphology and effect of axial coordination. *New Journal of Chemistry.* **2014**, *38*, 1458-1470.
35. Kleij, A. W.; Kuil, M.; Tooke, D. M.; Spek, A. L.; Reek, J. N. Template-assisted ligand encapsulation; the impact of an unusual coordination geometry on a supramolecular pyridylphosphine-Zn(II)porphyrin assembly. *Inorganic chemistry.* **2005**, *44*, 7696-7698.
36. Weimin, S.; Qi, S.; Yucheng, W.; Lihong, L.; Jingchao, T. An alternative approach to amino porphyrins. *Journal of Heterocyclic Chemistry.* **2010**, *47*, 1221-1224.
37. Luguya, R.; Jaquinod, L.; Fronczek, F. R.; Vicente, M. G. H.; Smith, K. M. Synthesis and reactions of meso-(p-nitrophenyl)porphyrins. *Tetrahedron.* **2004**, *60*, 2757-2763.
38. Ormond, A. B.; Freeman, H. S. Effects of substituents on the photophysical properties of symmetrical porphyrins. *Dyes and Pigments.* **2013**, *96*, 440-448.
39. Rose, E.; Cardon-Pilotaz, A.; Quelquejeu, M.; Bernard, N.; Kossanyi, A.; Desmazieres, B. Efficient Preparation of the .alpha.,.alpha.,.beta.,.beta.-Atropoisomer of meso-Tetrakis(o-aminophenyl)porphyrin. *The Journal of Organic Chemistry.* **1995**, *60*, 3919-3920.
40. Serra, V. I. V.; Pires, S. M. G.; Alonso, C. M. A.; Neves, M. G. P. M. S.; Tomé, A. C.; Cavaleiro, J. A. S. Meso-Tetraarylporphyrins Bearing Nitro or Amino Groups: Synthetic Strategies and Reactivity Profiles. *Topics in Heterocyclic Chemistry.* **2014**, *33*, 35-78.
41. Karolczak, J.; Kowalska, D.; Lukaszewicz, A.; Maciejewski, A.; Steer, R. P. Photophysical Studies of Porphyrins and Metalloporphyrins: Accurate Measurements of Fluorescence Spectra and Fluorescence Quantum Yields for Soret Band Excitation of Zinc Tetraphenylporphyrin. *The Journal of Physical Chemistry A.* **2004**, *108*, 4570-4575.
42. Chirvony, V. S.; van Hoek, A.; Schaafsma, T. J.; Pershukevich, P. P.; Filatov, I. V.; Avilov, I. V.; Shishporenok, S. I.; Terekhov, S. N.; Malinovskii, V. L. On the Nature of the Fluorescent State in β-Nitrotetraarylporphyrins. *The Journal of Physical Chemistry B.* **1998**, *102*, 9714-9724.

43. Barnett, G. H.; Hudson, M. F.; Smith, K. M. Concerning meso-tetraphenylporphyrin purification. *Journal of the Chemical Society, Perkin Transactions 1.* **1975**, 1401-1403.

44. Senge, M. O.; Eigenbrot, C. W.; Brennan, T. D.; Shusta, J.; Scheidt, W. R.; Smith, K. M. Aggregation properties of nitroporphyrins: comparisons between solid-state and solution structures. *Inorganic chemistry.* **1993**, *32*, 3134-3142.

45. Ono, N.; Muratani, E.; Fumoto, Y.; Ogawa, T.; Tazima, K. Synthesis of 2,7,12,17-tetraaryl-3,8,13,18-tetranitroporphyrins; electronic effects on aggregation properties of porphyrins. *Journal of the Chemical Society, Perkin Transactions 1.* **1998**, 3819-3824.

46. Zhao, Z.; Nyokong, T.; Maree, M. D. Synthesis and photochemical characterization of a zinc phthalocyanine–zinc porphyrin heterotrimer and heterononamer. *Dalton Transactions.* **2005**, 3732-3737.

47. Drain, C. M.; Kirmaier, C.; Medforth, C. J.; Nurco, D. J.; Smith, K. M.; Holten, D. Dynamic Photophysical Properties of Conformationally Distorted Nickel Porphyrins. 1. Nickel(II) Dodecaphenylporphyrin. *The Journal of Physical Chemistry.* **1996**, *100*, 11984-11993.

48. Hwang, I. W.; Kamada, T.; Ahn, T. K.; Ko, D. M.; Nakamura, T.; Tsuda, A.; Osuka, A.; Kim, D. Porphyrin boxes constructed by homochiral self-sorting assembly: optical separation, exciton coupling, and efficient excitation energy migration. *J Am Chem Soc.* **2004**, *126*, 16187-16198.

49. Knyukshto, V.; Zenkevich, E.; Sagun, E.; Shulga, A.; Bachilo, S. Pathways for photoinduced electron transfer in meso-nitro-phenyl-octaethylporphyrins and their chemical dimers. *Chemical Physics Letters.* **1999**, *304*, 155-166.

50. Knyukshto, V. N.; Zen'kevich, É. I.; Sagun, E. I.; Shul'ga, A. M.; Bachilo, S. M. Photophysical properties of mesonitrophenyl-substituted porphyrins and their dimers at 295 K. *Journal of Applied Spectroscopy.* **1999**, *66*, 588-592.

51. Knyukshto, V. N.; Sagun, E. I.; Shul'ga, A. M.; Bachilo, S. M.; Zen'kevich, É. I. Photoinduced electron transfer in meso-nitrophenyl-substituted porphyrins and their chemical dimers. *Optics and Spectroscopy.* **2000**, *88*, 205-216.

52. Dahal, S.; Krishnan, V. Charge transfer excited states of zinc(II) derivatives of β-substituted dinitrotetraphenylporphyrin. *Journal of Photochemistry and Photobiology A: Chemistry.* **1995**, *89*, 105-112.

53. Dahal, S.; Krishnan, V. Excited singlet state intramolecular charge transfer in di and trinitrotetraphenylporphyrins. *Chemical Physics Letters.* **1997**, *274*, 390-395.

54. Gust, D.; Moore, T. A.; Luttrull, D. K.; Seely, G. R.; Bittersmann, E.; Bensasson, R. V.; Rougée, M.; Land, E. J.; Schryver, F. C. D.; Auweraer, M. V. d. Photophysical properties of 2-nitro-5,10,15,20-tetra-p-tolylporphyrins. *Photochemistry and Photobiology.* **1990**, *51*, 419-426.

55. Harriman, A.; Hosie, R. J. Luminescence of porphyrins and metalloporphyrins. Part 4.—Fluorescence of substituted tetraphenylporphyrins. *Journal of the Chemical Society, Faraday Transactions 2.* **1981**, *77*, 1695-1702.

56. Wickramasinghe, A.; Jaquinod, L.; Nurco, D. J.; Smith, K. M. Investigations on the directive effects of a single meso-substituent via nitration of 5,12,13,17,18-pentasubstituted porphyrins: syntheses of conjugated β-nitroporphyrins. *Tetrahedron.* **2001**, *57*, 4261-4269.

57. Lan, M.; Zhao, H.; Yuan, H.; Jiang, C.; Zuo, S.; Jiang, Y. Absorption and EPR spectra of some porphyrins and metalloporphyrins. *Dyes and Pigments.* **2007**, *74*, 357-362.

58. Wróbel, D.; Łukasiewicz, J.; Goc, J.; Waszkowiak, A.; Ion, R. Photocurrent generation in an electrochemical cell with substituted metalloporphyrins. *Journal of Molecular Structure.* **2000**, *555*, 407-417.

59. Vogel, G. C.; Stahlbush, J. R. Thermodynamic study of the adduct formation of zinc tetraphenylporphine with several neutral donors in cyclohexane. *Inorganic chemistry.* **1977**, *16*, 950-953.

60. Cole, S. J.; Curthoys, G. C.; Magnusson, E. A.; Phillips, J. N. Ligand binding by metalloporphyrins. III. Thermodynamic functions for the addition of substituted pyridines to nickel(II) and zinc(II) porphyrins. *Inorganic chemistry.* **1972**, *11*, 1024-1028.

61. Nappa, M.; Valentine, J. S. The influence of axial ligands on metalloporphyrin visible absorption spectra. Complexes of tetraphenylporphinatozinc. *Journal of the American Chemical Society.* **1978**, *100*, 5075-5080.

62. Kolling, O. W. Soret red shift for zinc tetraphenylporphine in the presence of uncharged Lewis bases. *Inorganic chemistry.* **1979**, *18*, 1175-1176.

63. Kolling, O. W. Comparison of donor-acceptor parameters in nonaqueous solvents. *Analytical Chemistry.* **1982**, *54*, 260-264.

64. Takahashi, K.; Hase, S.; Komura, T.; Imanaga, H.; Ohno, O. The Fluorescence Properties of (2-Nitro-5,10,15,20-tetraphenylporphyrinato)zinc. *Bulletin of the Chemical Society of Japan.* **1992**, *65*, 1475-1481.

65. Krishnan, V. Supramolecular assemblies for molecular scale information transport processes. *Journal of the Indian Institute of Science.* **1999**, *79*, 3-16.

66. Taylor, P. J.; van der Zwan, G.; Antonov, L. In *Tautomerism: Methods and Theories*; Antonov, L., Ed.; Wiley-VCH Verlag GmbH & Co. KGaA: Weinheim, Germany, **2014**.

67. Elsaesser, T.; Schmetzer, B.; Lipp, M.; Bäuerle, R. J. Excited-state proton transfer in 2-(2′-hydroxyphenyl)benzothiazole: Transient electronic absorption measured on the picosecond time scale. *Chemical Physics Letters.* **1988**, *148*, 112-118.

68. Laermer, F.; Elsaesser, T.; Kaiser, W. Femtosecond spectroscopy of excited-state proton transfer in 2-(2′-hydroxyphenyl)benzothiazole. *Chemical Physics Letters.* **1988**, *148*, 119-124.

69. Elsaesser, T.; Schmetzer, B. Excited-state proton transfer in 2-(2'-hydroxyphenyl)benzothiazole: formation of the anion in polar solvents. *Chemical Physics Letters.* **1987**, *140*, 293-299.

70. Gentemann, S.; Medforth, C. J.; Forsyth, T. P.; Nurco, D. J.; Smith, K. M.; Fajer, J.; Holten, D. Photophysical Properties of Conformationally Distorted Metal-Free Porphyrins.

Investigation into the Deactivation Mechanisms of the Lowest Excited Singlet State. *Journal of the American Chemical Society.* **1994**, *116*, 7363-7368.

71. Roder, B.; Buchner, M.; Ruckmann, I.; Senge, M. O. Correlation of photophysical parameters with macrocycle distortion in porphyrins with graded degree of saddle distortion. *Photochemical & photobiological sciences : Official journal of the European Photochemistry Association and the European Society for Photobiology.* **2010**, *9*, 1152-1158.
72. Regev, A.; Galili, T.; Medforth, C. J.; Smith, K. M.; Barkigia, K. M.; Fajer, J.; Levanon, H. Triplet Dynamics of Conformationally Distorted Porphyrins: Time-Resolved Electron Paramagnetic Resonance. *The Journal of Physical Chemistry.* **1994**, *98*, 2520-2526.
73. Steiner, E. Density-difference maps in quantum chemistry. *Theoretica Chimica Acta.* **1982**, *60*, 561-572.
74. Sazanovich, I. V.; Galievsky, V. A.; van Hoek, A.; Schaafsma, T. J.; Malinovskii, V. L.; Holten, D.; Chirvony, V. S. Photophysical and Structural Properties of Saddle-Shaped Free Base Porphyrins: Evidence for an "Orthogonal" Dipole Moment. *The Journal of Physical Chemistry B.* **2001**, *105*, 7818-7829.

## Appendix A. Supporting Information for Chapter 2

### A1. Synthesis

#### A1.1. Porphyrin 1b

Pyrrole (69.5 µL, 1.0 mmol) and 5-Formyl-6-methyluracil **1** (158 mg, 1.0 mmol) and zinc acetate (109.8 mg, 0.50 mmol) were added to a boiling mixture of acetic acid (7.5 mL) and nitrobenzene (5.0 mL). The reaction mixture was refluxed for 10 h while monitoring the yields spectroscopically, and then taken to dryness under vacuum. The resulting solid was purified by column chromatography, eluting with ethyl acetate/ methanol/ acetic acid (7:3:1) to yield 17 mg (8%) of **1**. Chromatographic purification enriches the $\alpha^4$ and $\alpha^3\beta$ atropisomers. $^1$H NMR (DMSO-$d_6$) δ11.5 (br, d, 8H), 9.50 (s, 8H), 2.50 (s, 12 H); $^{13}$C (DMSO-$d_6$) δ 41.84, 110.60, 113.38, 113.41, 131.70, 150.77, 150.81, 152.26, 166.25. HRMS calcd. for $C_{40}H_{28}N_{12}O_8Zn$ (M+H)+ 869.1523, found 869.1514.

#### A1.2. Porphyrin 2b

Aldehyde **4** was synthesized according to the previous literature. Pyrrole (69.5 µL, 1.0 mmol) and 1-Ethoxymethyl-5-formyl-6-methyluracil **4** (212 mg, 1.0 mmol) and zinc acetate (109.8 mg, 0.50 mmol) were added to a boiling mixture of acetic acid (7.5 mL) and nitrobenzene (5.0 mL). The reaction mixture was refluxed for 10 h while monitoring the yields spectroscopically, and then taken to dryness under vaccum. The resulting solid was purified by column chromatography, eluting with ethyl acetate/ methanol (9:1) to yield 15 mg (5 %) of **2**. Chromatographic purification enriches somewhat the $\alpha^4$ and $\alpha^3\beta$ atropisomers. $^1$H NMR (MeOD-$d_4$) δ 9.22 (s, 8H), 5.65 (m, 8H), 3.86 (m, 8H), 2.51 (m, 12H), 1.31(m, 12H). $^{13}$C NMR (MeOD-

$d_4$) δ 12.83, 14.48, 54.63, 63.24, 71.86, 129.61, 149.23, 163.24, 189.5. HRMS calcd. for $C_{52}H_{52}N_{12}O_{12}Zn$ $(M)^{+\cdot}$ 1100.3119, found 1100.3112.

### A1.3. Porphyrins 1a and 2a (Free Base)

Porphyrin **2b** (15 mg, 13 μmol) was dissolved in a THF, water and concentrated HCl mixture. This was stirred for 30 min and then poured into water, after which $(NH_4)_2CO_3$ was added to reach a pH of 6. The porphyrin products were extracted with ethyl acetate. The combined organic extract was washed with water and brine, and then dried over $Na_2SO_4$. Porphyrin **2a** was precipitated from this solution with ethyl acetate/hexane to give 12 mg of product (90% yield). The same procedure was performed with 15 mg of porphyrin **1b** (17 μmol) to give 12 mg of porphyrin **1a** (90% yield).

### A1.4. 2,4-di(*n*-decylamino)-6-amino-1,3,5-triazine (bis(decyl)melamine)

Bis(decyl)melamine, was prepared similarly to literature methods[1-3] from 2-amino-4,6-dichloro-1,3,5-triazine, which was prepared from cyanuric chloride (Scheme A1). [4]

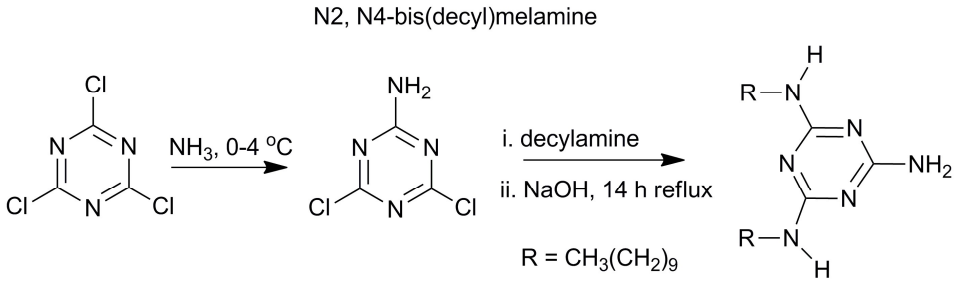


**Scheme A1**. Synthesis of 2-amino-4,6-dichloro-1,3,5-triazine from cyanuric chloride.

## A2. Spectroscopy

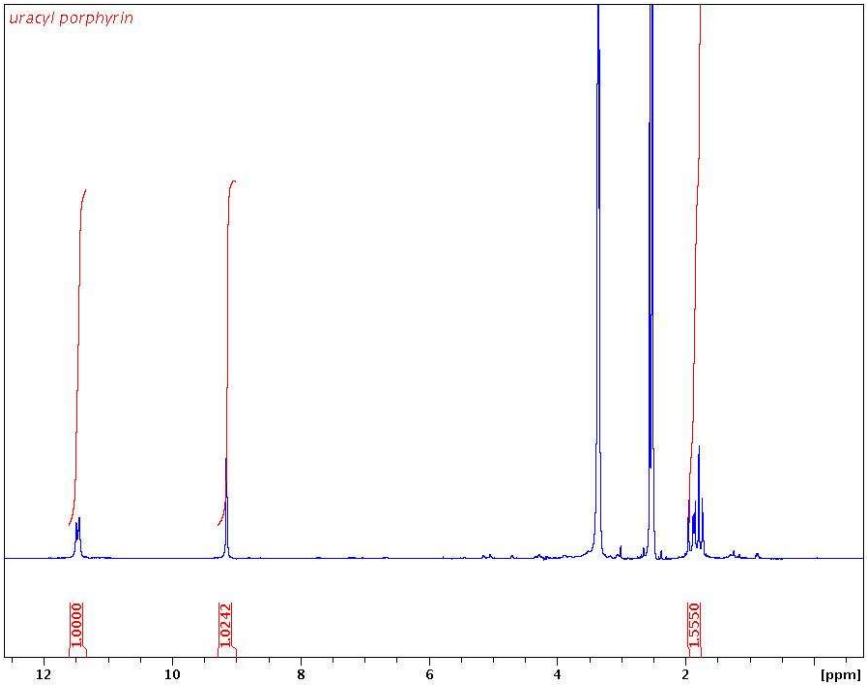


**Figure A1**. $^{1}H$ NMR of porphyrin **1b** in DMSO-$d_6$.

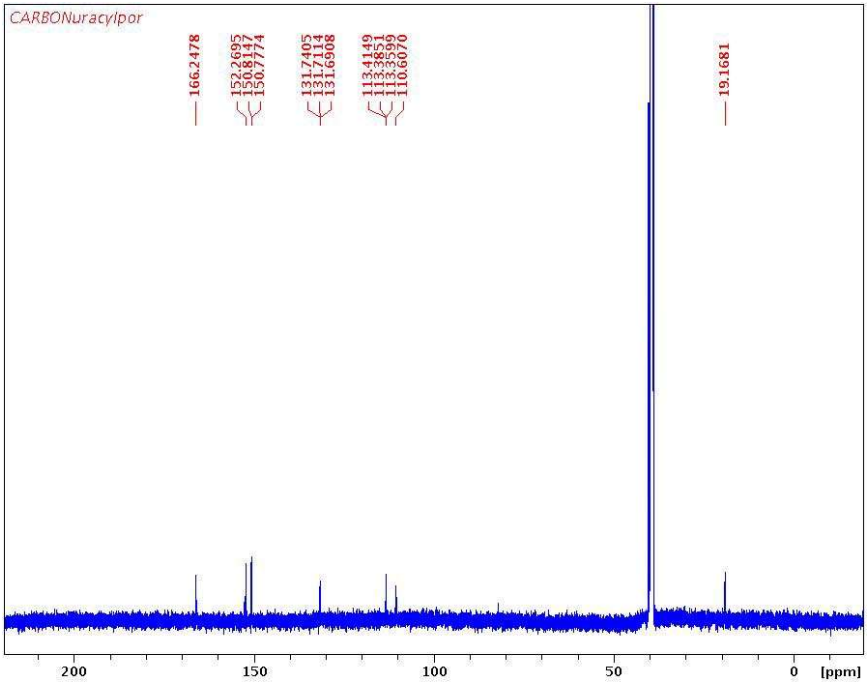


**Figure A2**. $^{13}C$ NMR of Porphyrin **1b** in DMSO-$d_6$.

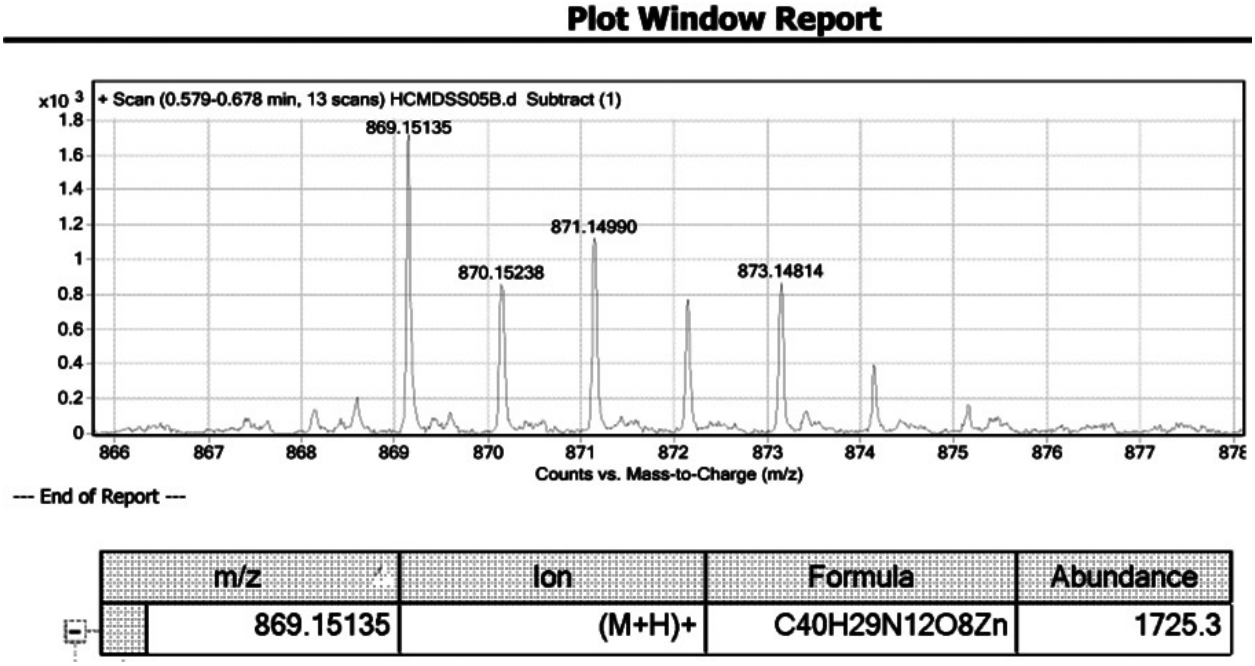


**Figure A3**. Mass spectrum of Porphyrin **1b**

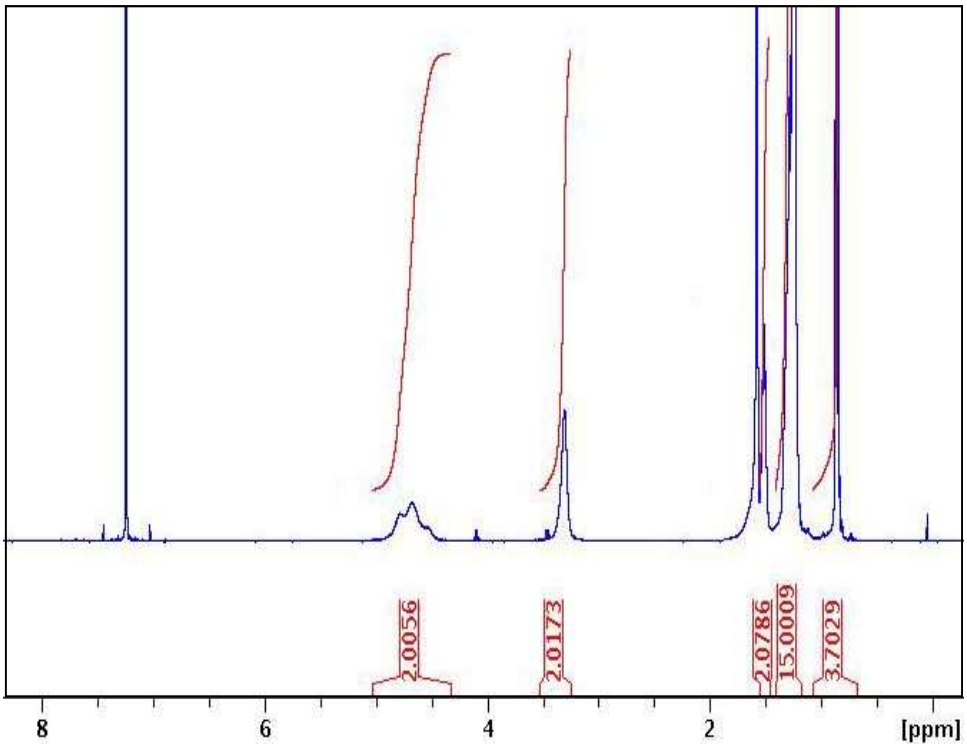


**Figure A4**. NMR of bis(decyl)melamine in $CDCl_3$.

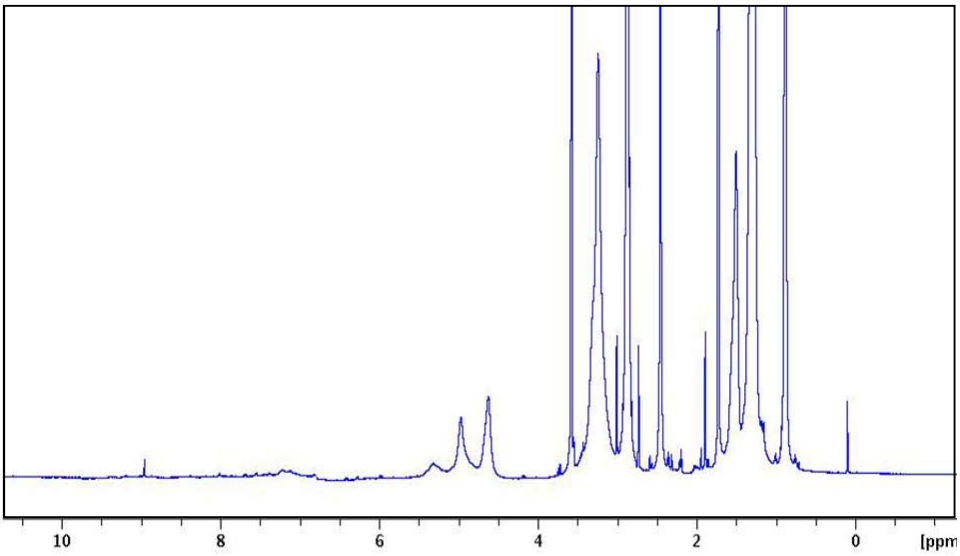


**Figure A5**. Day 1 NMR of melamine and porphyrin **1b** in dry THF in ratio 4:2 respectively.

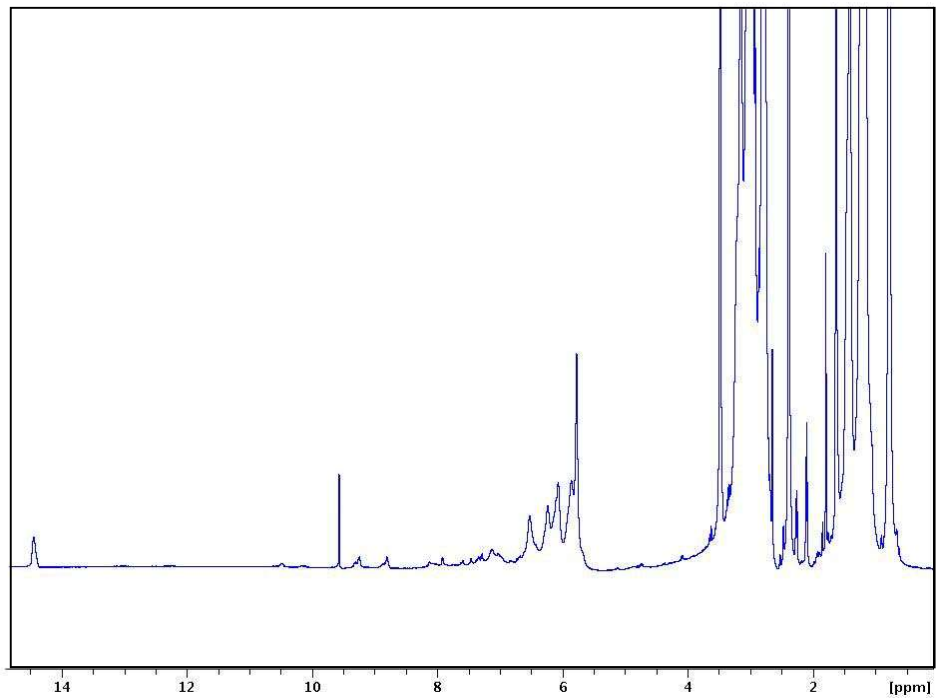


**Figure A6**. Day 14 NMR of melamine and porphyrin **1b** in dry THF in a ratio of 4:2 respectively.

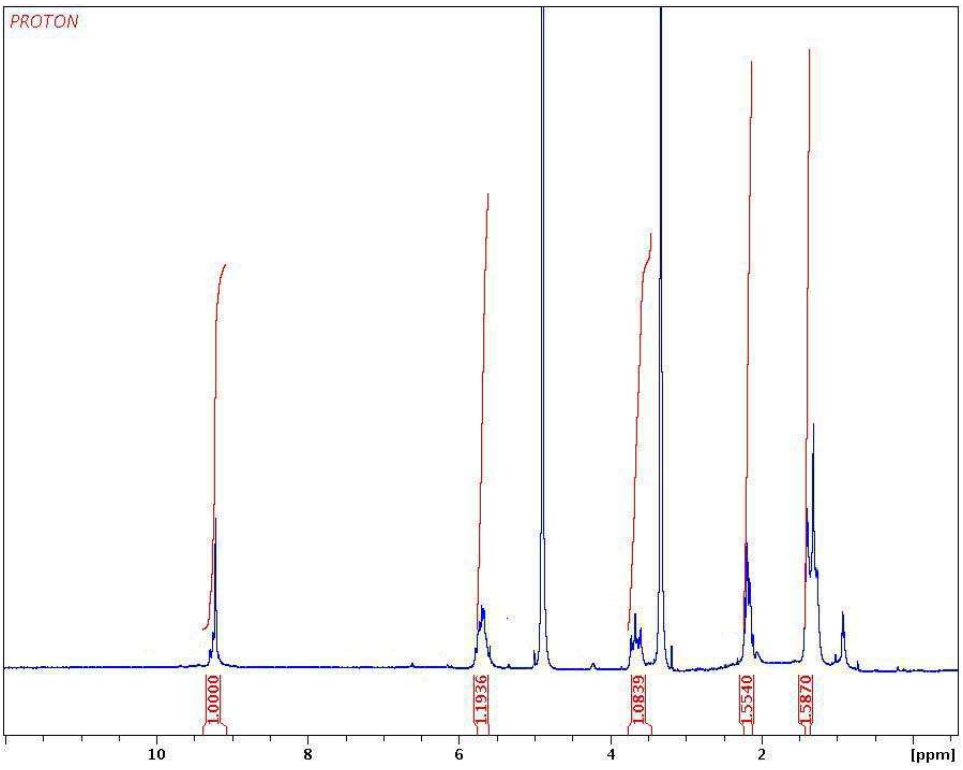


**Figure A7**. $^{1}H$ NMR of porphyrin **2b** in MeOD-$d_4$ solvent.

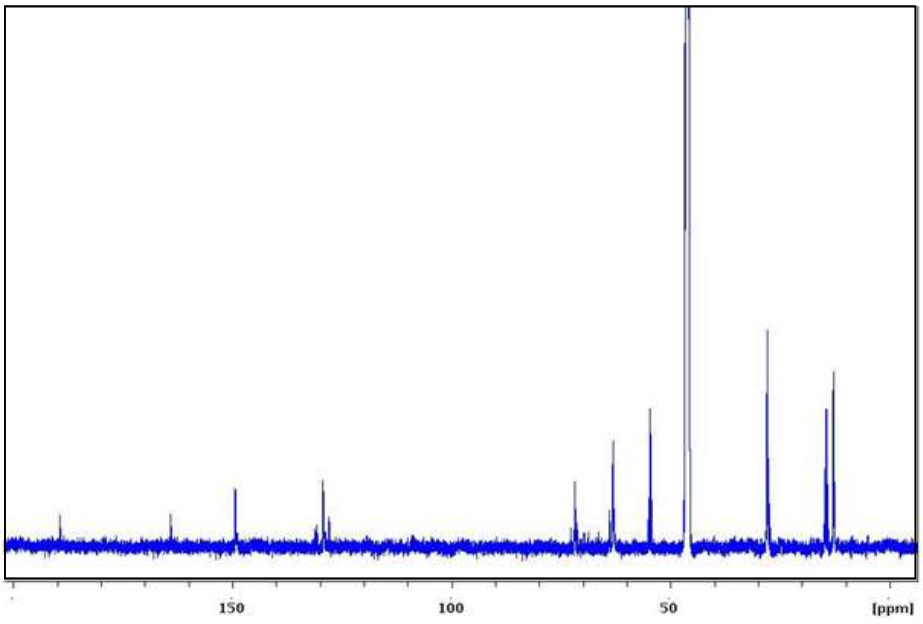


**Figure A8**. $^{13}C$ NMR of porphyrin **2b** in MeOD-$d_4$ solvent.

| Compound Label | RT | Mass | Abund | Formula | Tgt Mass | Diff (ppm) |
|---|---|---|---|---|---|---|
| Cpd 1: C52H52N12O12Zn | 0.264 | 1100.3122 | 2913 | C52H52N12O12Zn | 1100.3119 | 0.24 |

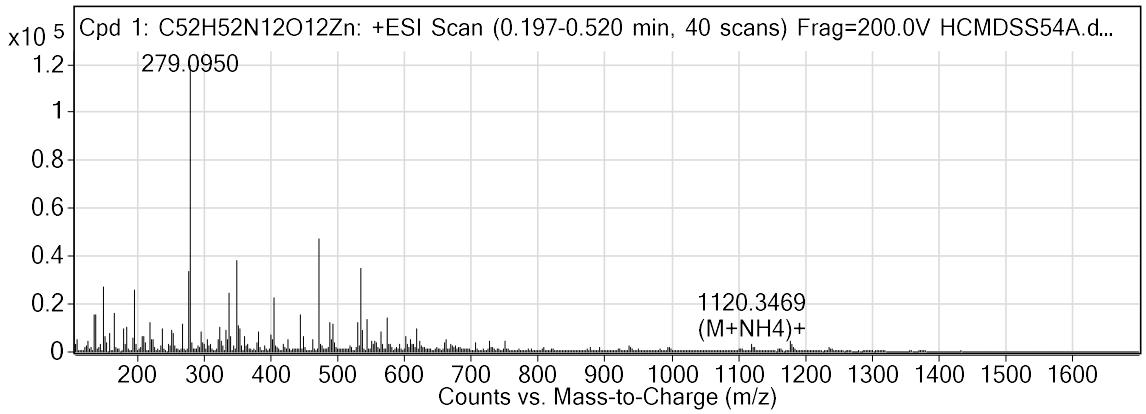


**Figure A9**. Mass spectrum of porphyrin **2b**.

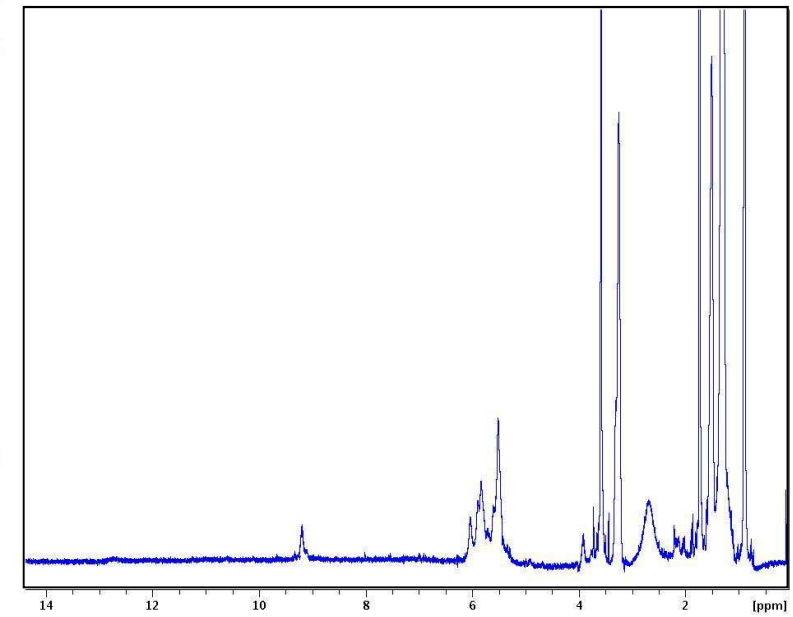


**Figure A10**. $^{1}H$ NMR of Porphyrin **2b** + melamine; day 1 in THF-$d_8$.

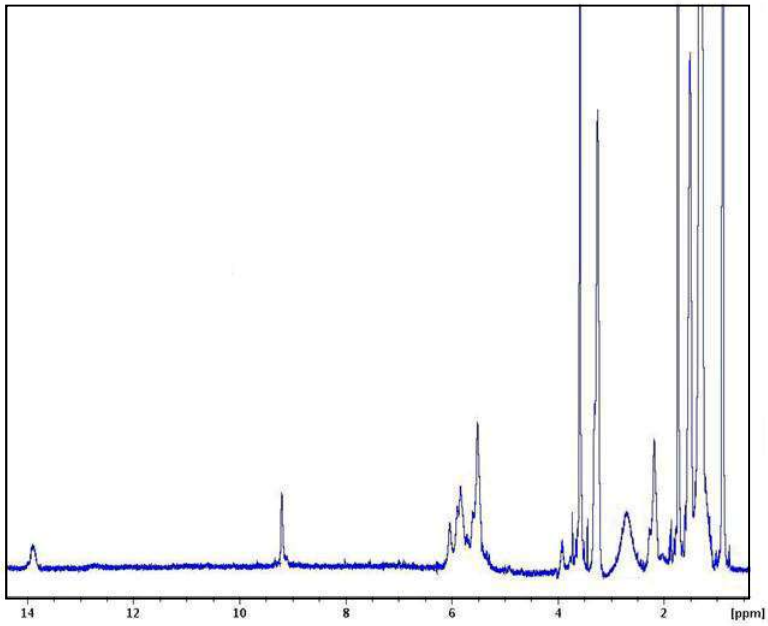


**Figure A11**. $^{1}H$ NMR of Porphyrin **2b** + melamine; day 10 in THF-$d_8$.

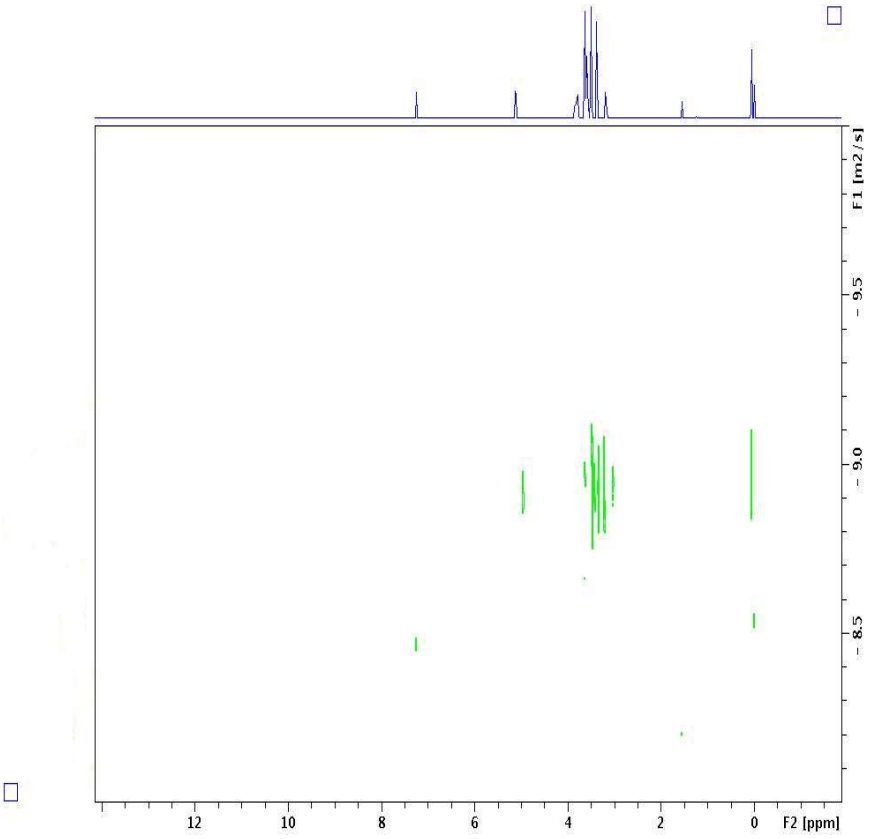


**Figure A12**. 2D DOSY spectrum of cyclodextrin in $CDCl_3$.

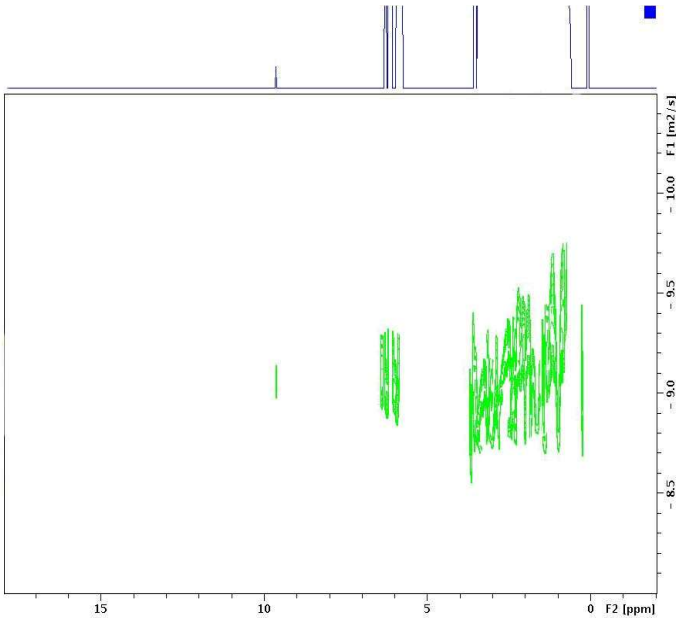


**Figure A13**. 2D DOSY spectrum of porphyrin **1b** + melamine in THF as

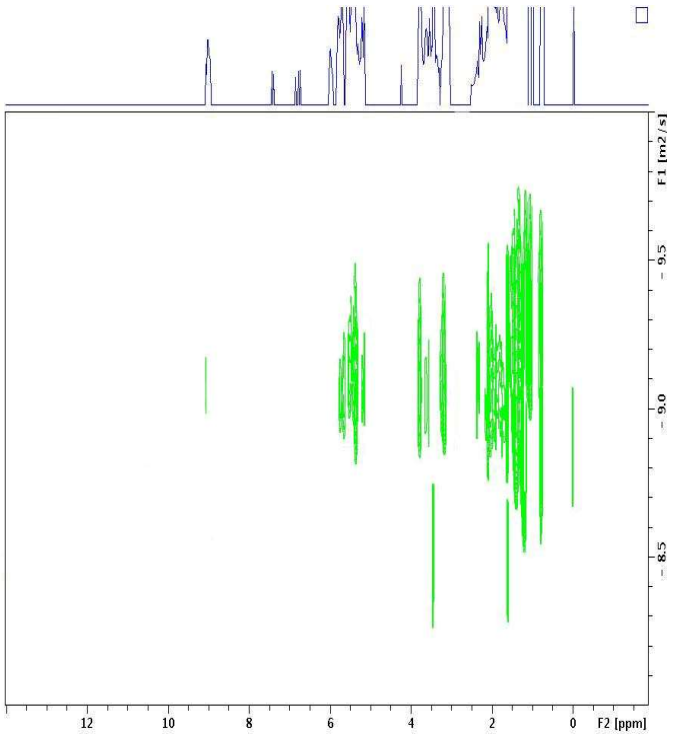


**Figure A14**. 2D DOSY spectrum of Porphyrin **2b** + melamine in THF as the solvent.

| Compound Label | RT | Mass | Abund | Formula | Tgt Mass | Diff (ppm) |
|---|---|---|---|---|---|---|
| Compound 1 | 0.6 | 406.37921 | 46202 | C23H46N6 | 406.3784 | 2.01 |

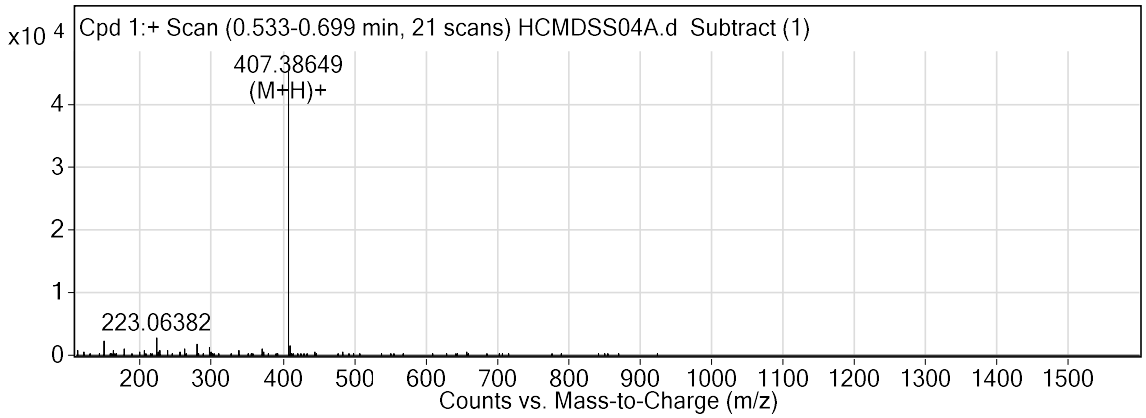


**Figure A15**. Mass spectrum of bis(decyl)melamine.

## A3. References


1. Vollhardt, D.; Fainerman, V. B.; Liu, F. Thermodynamic and Structural Characterization of Amphiphilic Melamine-type Monolayers. *J. Phys. Chem. B.* **2005**, *109*, 11706.
2. Fainerman, V. B.; Vollhardt, D.; Aksenenko, E. V.; Liu, F. Molecular Recognition Kinetics of Nonsurface Active Pyrimidine Derivatives Dissolved in the Aqueous Subphase by an Amphiphilic Melamine Type Monolayer: A Theoretical Approach. *J. Phys. Chem. B.* **2005**, *109*, 14137.
3. Kimizuka, N.; Kawasaki, T.; Hirata, K.; Kunitake, T. Supramolecular Membranes. Spontaneous Assembly of Aqueous Bilayer Membrane via Formation of Hydrogen Bonded Pairs of Melamine and Cyanuric Acid Derivatives. *J. Am. Chem. Soc.* **1998**, *120*, 4094.
4. Baliani, A.; Bueno, G. J.; Stewart, M. L.; Yardley, V.; Brun, R.; Barrett, M. P.; Gilbert, I. H. Design and Synthesis of a Series of Melamine-based Nitroheterocycles with Activity against Trypanosomatid Parasites. *J. Med. Chem.* **2005**, *48*, 5570.

## Appendix B. Supporting Information for Chapter 3

### B1. UV-Visible Spectra

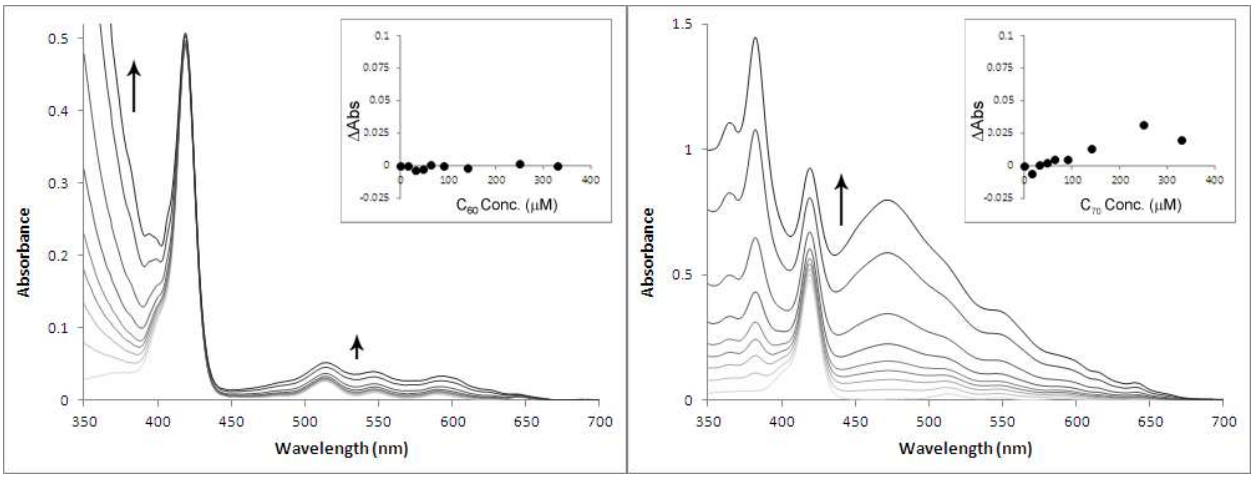


**Figure B1**. UV-Visible absorbances of a titration of $C_{60}$ (left) or $C_{70}$ (right) into 10.0 μM solutions of **$1H_2$**. The inset shows the difference between the calculated sum of the absorbance of the two components (at 419 nm) and the experimentally observed absorbance for the mixed solutions, as function of the quencher concentration.

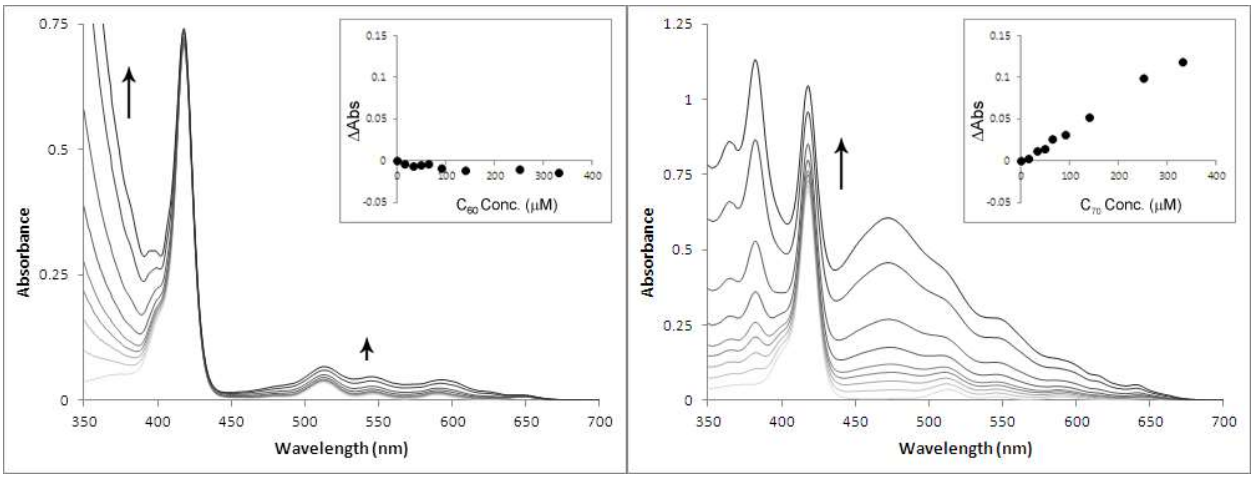


**Figure B2**. UV-Visible absorbances of a titration of $C_{60}$ (left) or $C_{70}$ (right) into 20.0 μM solutions of **$TPPF_5$**. The inset shows the difference between the calculated sum of the absorbance of the two components (at 418 nm) and the experimentally observed absorbance for the mixed solutions, as function of the quencher concentration.

## B2. Fluorescence Spectra

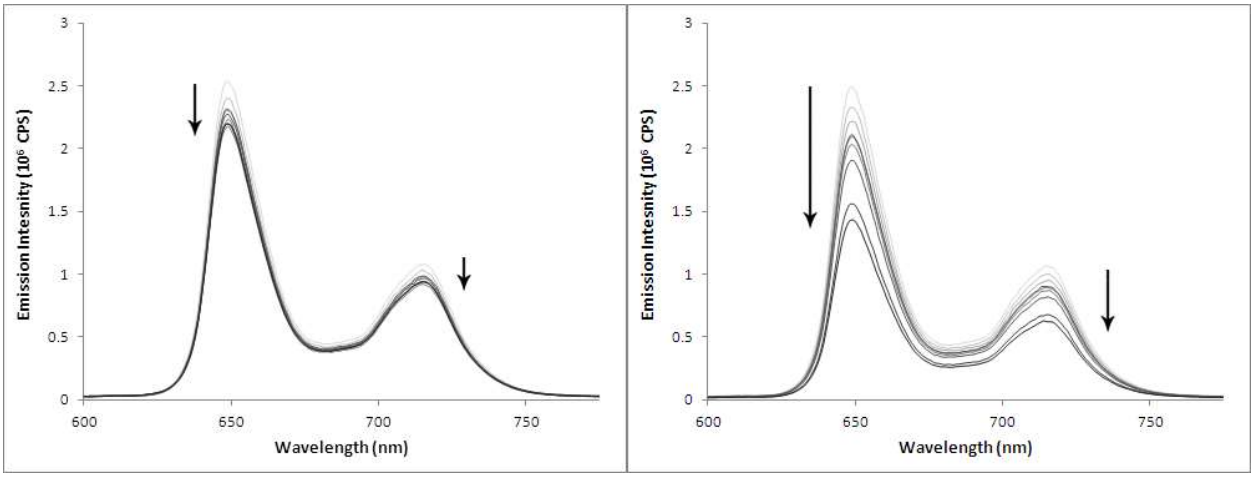


**Figure B3**. Fluorescence emission spectra of a titration of (left) $C_{60}$ and (right) $C_{70}$ into a 10.0 μM solution of **1H₂**. Both graphs show quenching, but the effect of $C_{70}$ is again more pronounced. The solutions were excited at a wavelength of 414 nm, a near-isosbestic point, and the emission was further corrected for the absorbance at the excitation wavelength.

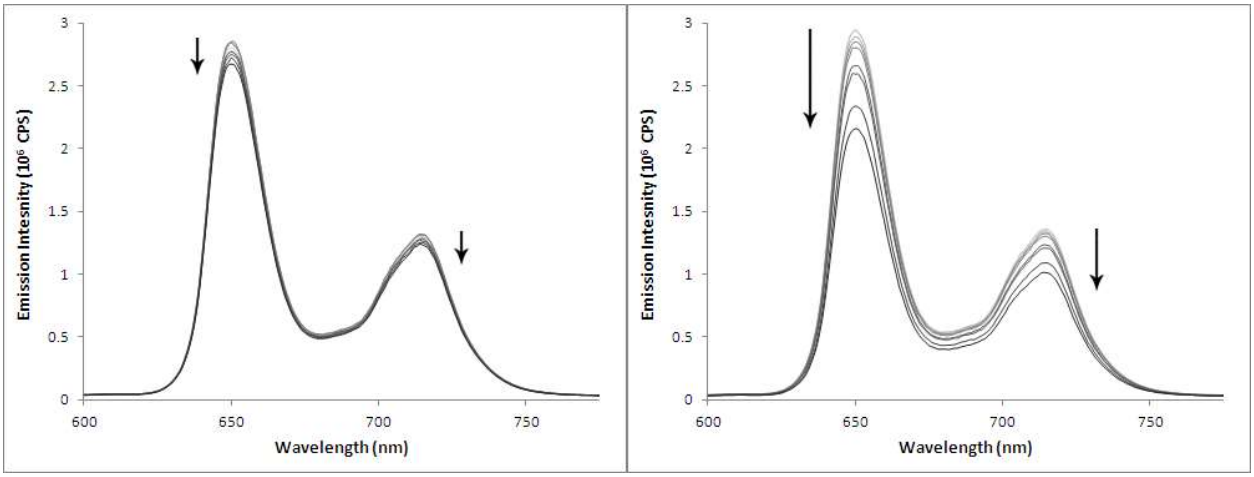


**Figure B4**. Fluorescence emission spectra of a titration of (left) $C_{60}$ and (right) $C_{70}$ into a 20.0 μM solution of **$TPPF_5$** solution. The solutions were excited at a wavelength of 414 nm, a near-isosbestic point, and the emission was further corrected for the absorbance at the excitation wavelength.

## B3. Carbon Nanotube Studies

Portions (3 mL) of an 85 μM solution of **1Zn** in DMF were sonicated with 1.0 mg single walled carbon nanotubes (SWCNT) for 20 minutes. The solutions were then centrifuged to remove insoluble SWCNT and its complexes with the dimer. The supernatants were analyzed by fluorescence and UV-vis spectroscopy.

## B3.1. Fluorescence Spectra

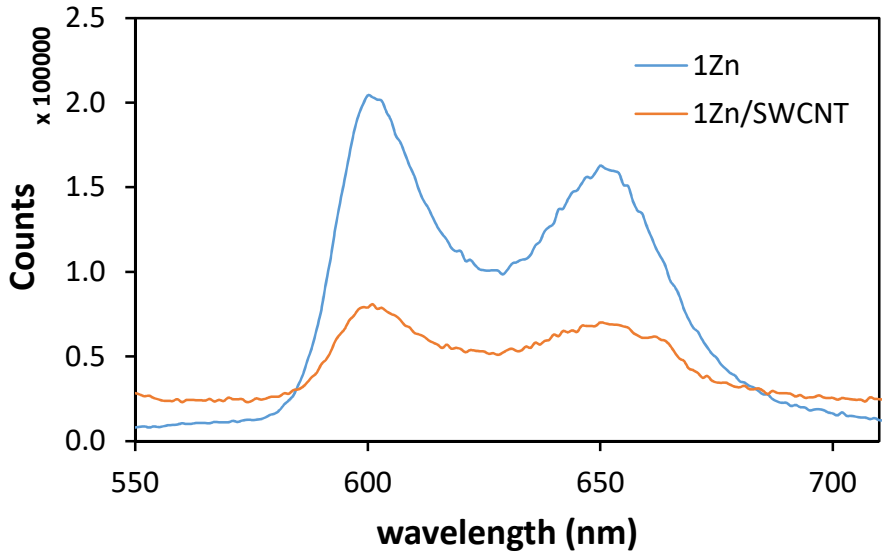


**Figure B5**. Fluorescence spectra of a typical nanotube experiment before and after treatment with nanotubes.

## B3.2. UV-visible Spectra

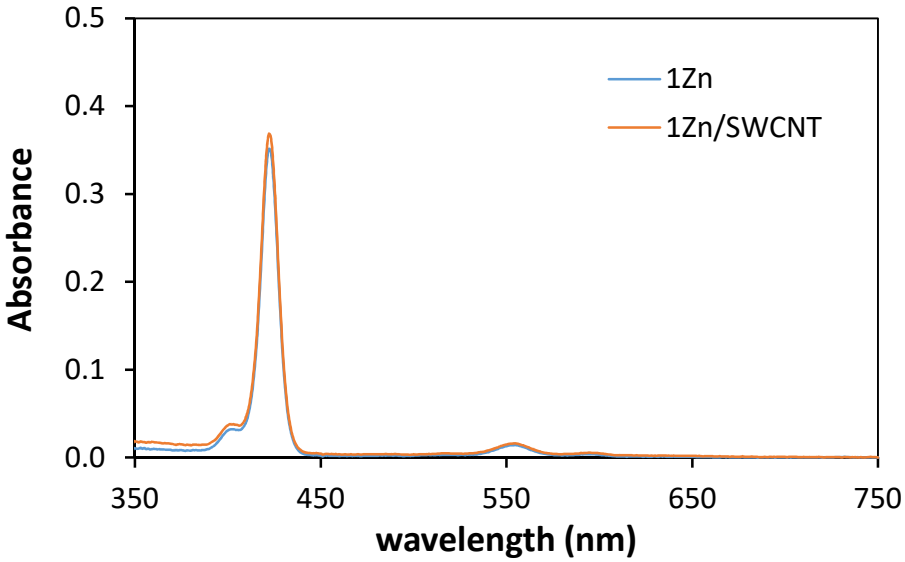


**Figure B6**. UV-vis. spectra of a typical nanotube experiment before and after treatment with nanotubes.

## B4. AFM

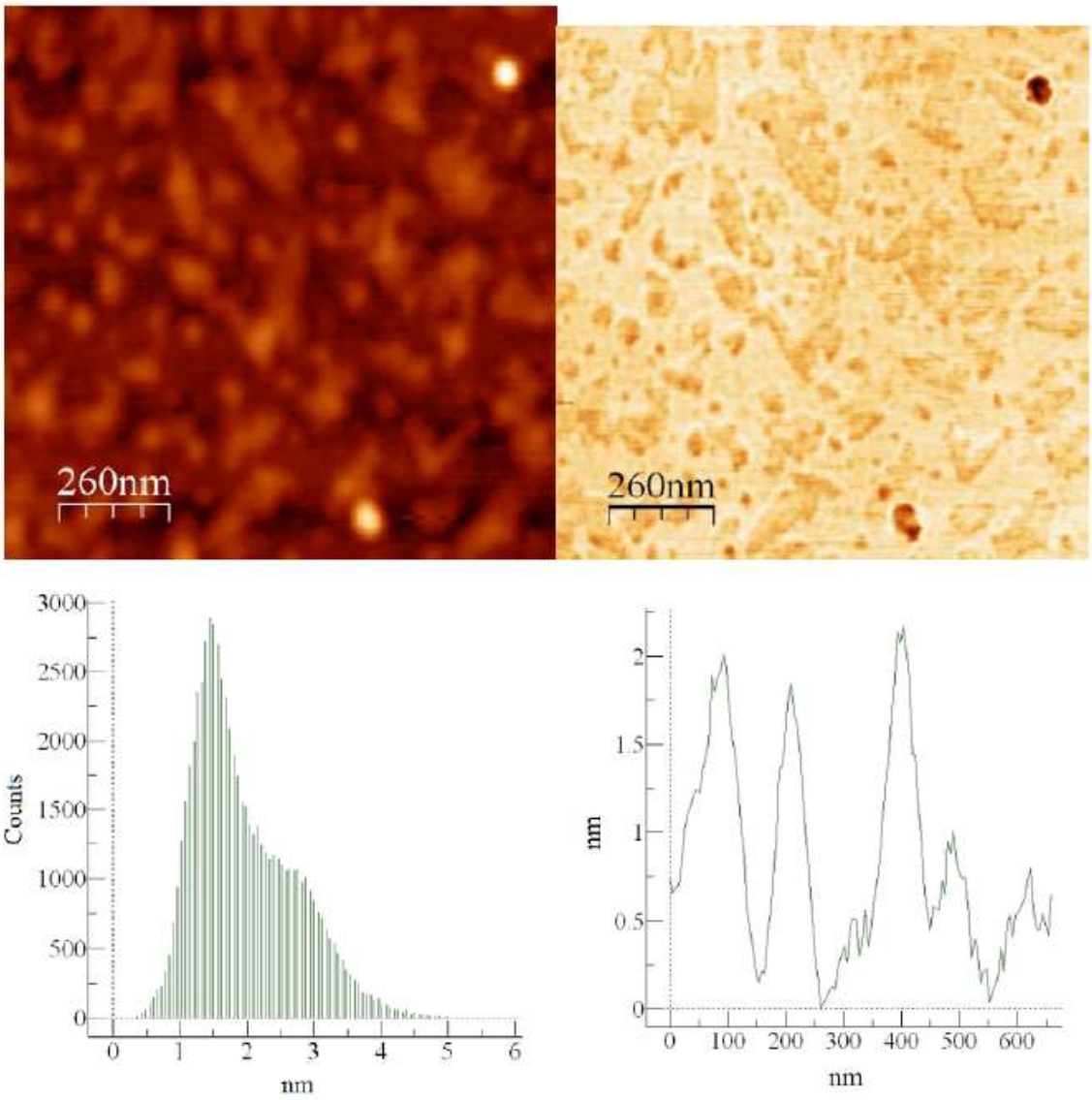


**Figure B7**. AFM of films deposited from a 1.0 mM solution of $C_{70}$. Top-left: height image. Top-right: phase image. Bottom-left: histogram of particle sizes (~1.1 nm corresponds to the diameter of $C_{70}$). Bottom-right: height profile.

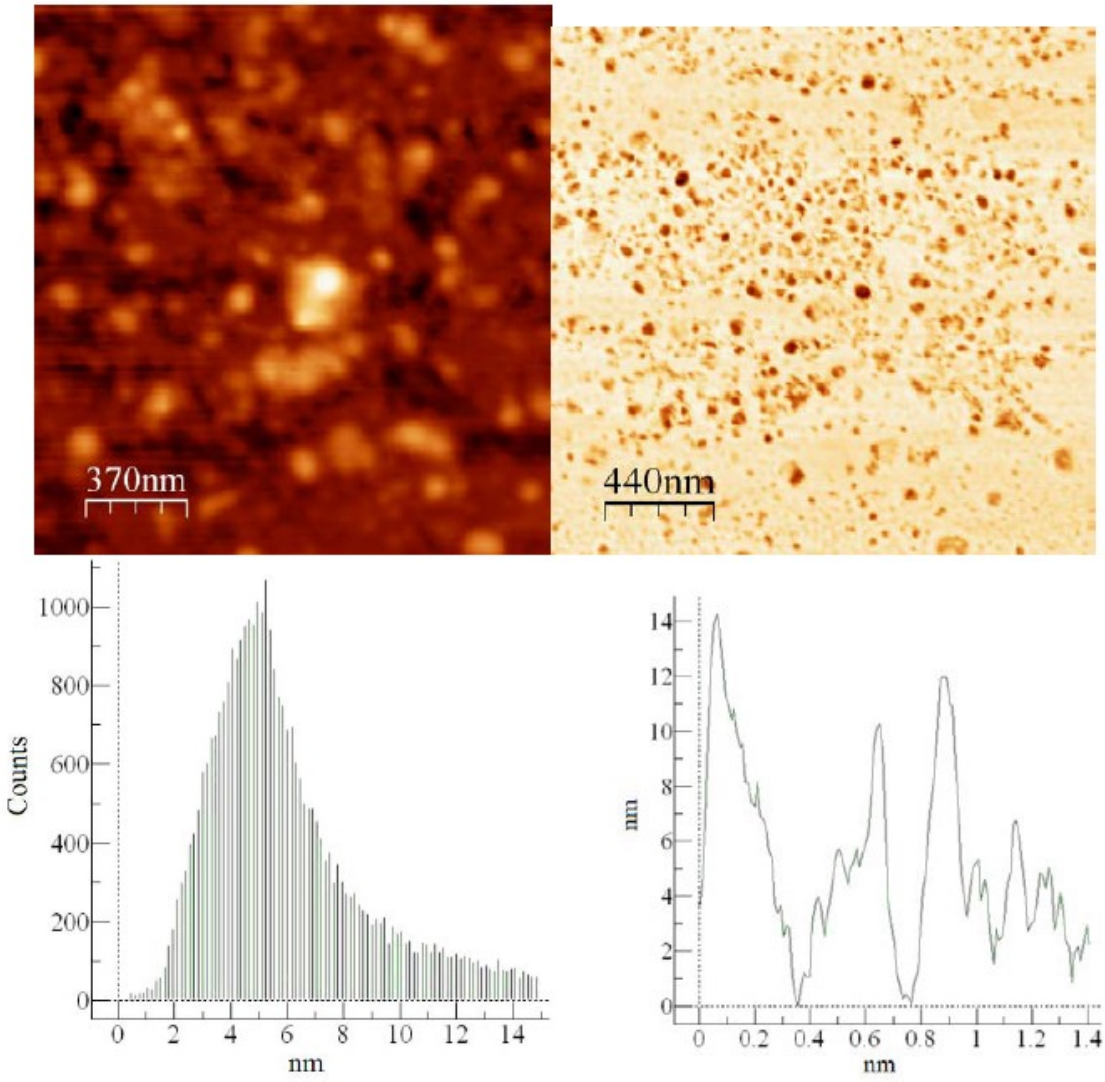


**Figure B8**. Films deposited from a 10 μM solution of **1H$_2$**. Top-left: height image. Top-right: phase image. Bottom-left: histogram of particle sizes (mean ~5 nm). Bottom-right: height profile of larger aggregates.

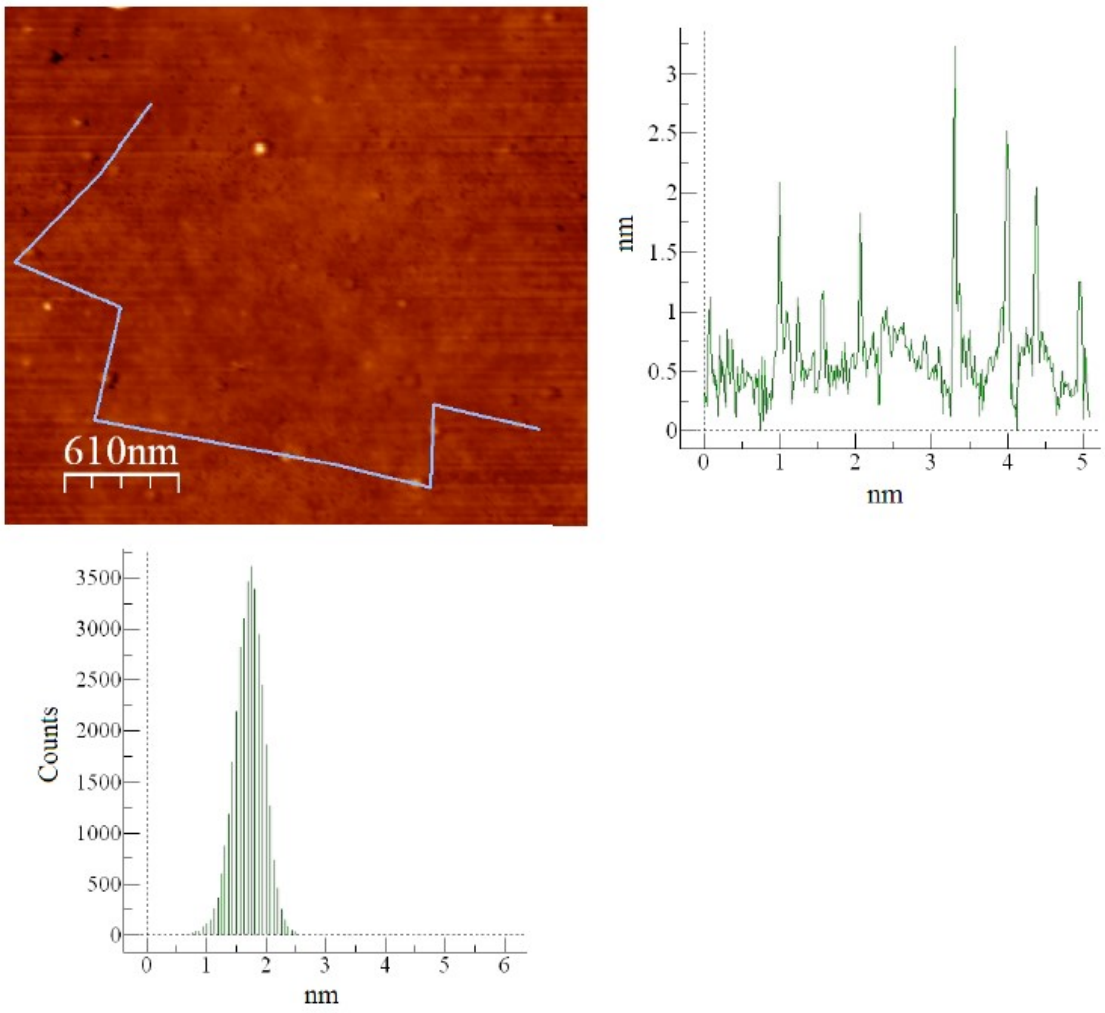


**Figure B9**. Films deposited from a 10 μM solutions of $C_{70}$. Top-left: height image. Top-right: height profile. Bottom: histogram of particle sizes (~1.1 nm corresponds to the diameter of $C_{70}$).

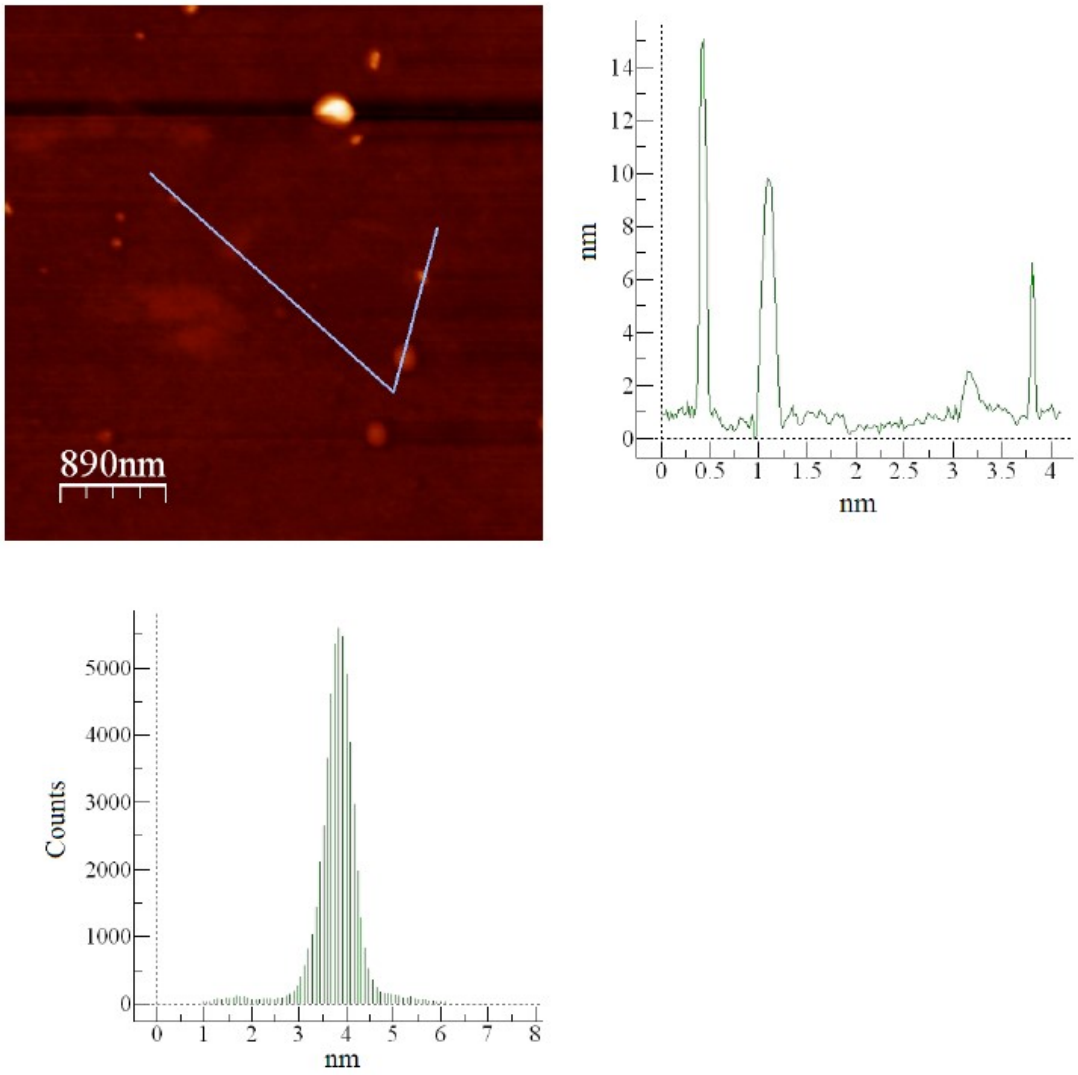


**Figure B10**. Films deposited from equimolar solutions of $C_{70}$ and dimer **1H$_2$**, 10 μM each. Top-left: height image. Top-right: height profile trace. Bottom: histogram of particle sizes. A mean of ~3.8 nm corresponds to diameter of $C_{70}$ complexed with two porphyrins (~1.1 nm for the $C_{70}$ and ~1.4 nm for each porphyrin).

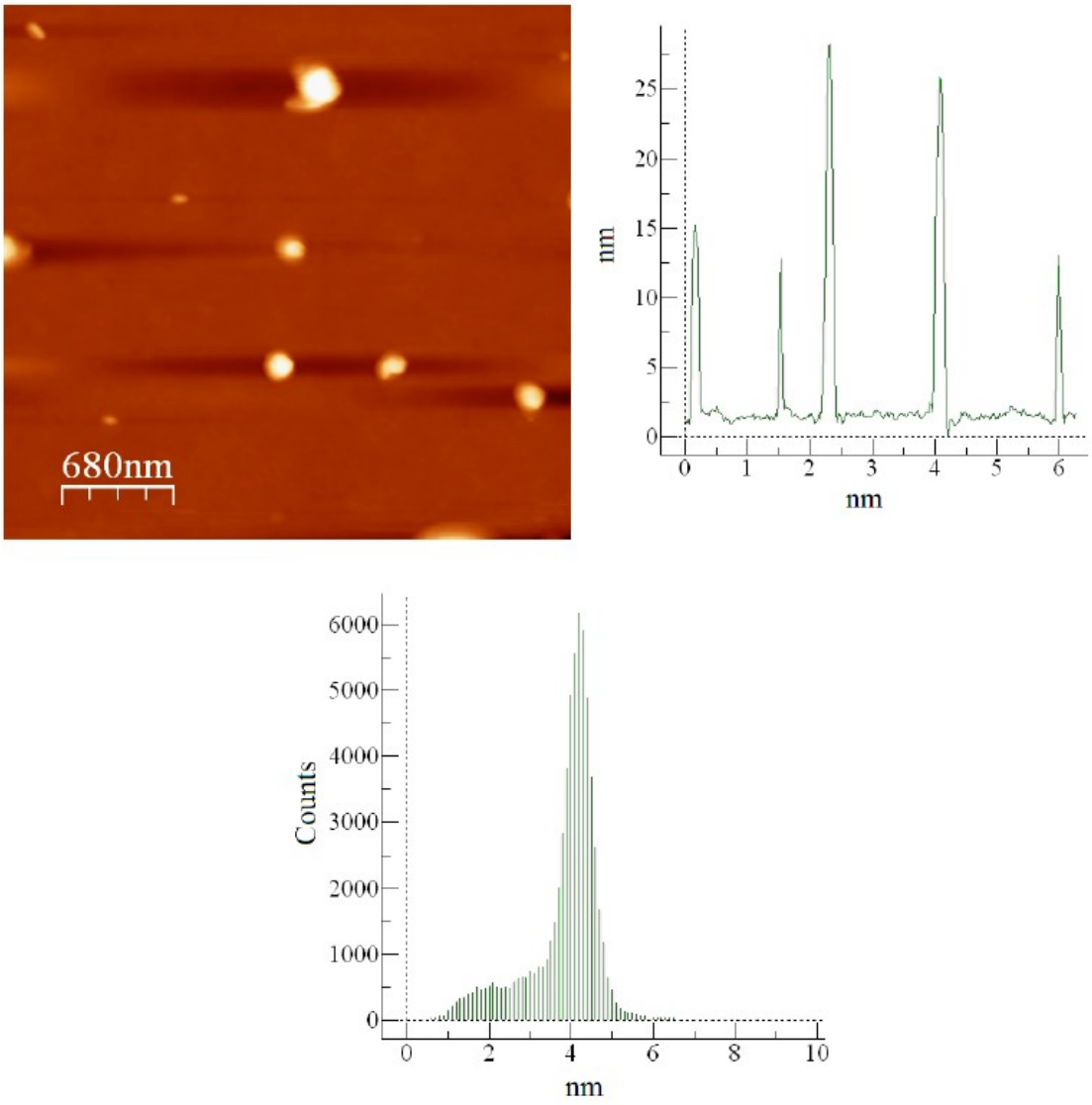


**Figure B11**. Films deposited from equimolar solutions of $C_{70}$ and dimer **1Zn** (10 μM each). Top-left: height image showing a few large islands interspersed in the ~4 nm thick film. Top-right: height profile trace. Bottom: histogram of particle sizes in the films. A mean of ~4 nm corresponds to diameter of $C_{70}$ complexed with two porphyrins.

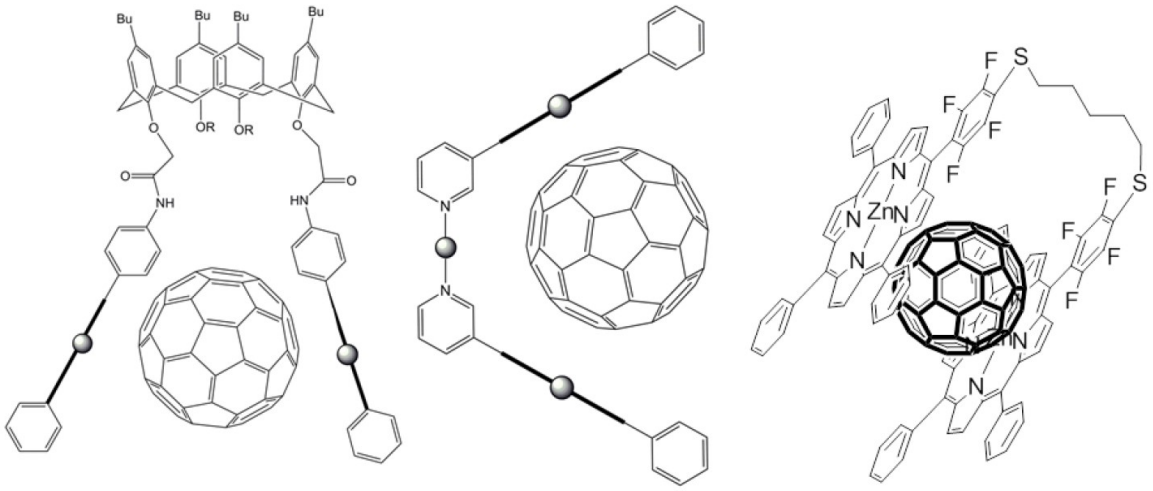


Calixarene $H_2$Por and ZnPor  Jaws $H_2$Por and ZnPor  Porphyrins $\mathbf{1H_2}$ and **1Zn**

**Figure B12**. The structures of the dimers listed in **Table 3.1** in the main text.

## Appendix C. Supporting Information for Chapter 4

### C1. Distribution of Positional Isomers

In order to analyze how the positional isomers are distributed among the members of the series studied, a custom PHP program was written to enumerate the possibilities. The code first prompts the user to enter the number of positions available for substitution, the number of substituted positions being considered, and the order of the principal axis of rotation. While the code assumes only one kind of substituent and a dihedral, achiral prismatic symmetry ($D_{nh}$, where $n$ is input by the user), it can be easily modified to account for multiple substituent types and other molecular point groups. Conceptually, the code consists of two parts. First, it finds every possible permutation of the specified number of substitutions over the specified number of positions. Second, it takes each permutation, applies all of the relevant operations of the symmetry group specified, and checks each result to see if it is duplicated somewhere else in the list. If found, the redundant isomer is deleted, and the program moves on to check the next item in the list.

The process of enumerating every permutation is accomplished by representing the substitution pattern as a binary string (or array, in practice) and applying a previously published algorithm.[1] This can obviously be extended to any number of different types of substituents simply by assigning each substituent type a different numerical value, in which case the string would no longer be binary. The advantage of using an array over a string is that each position in an array can hold an arbitrarily large number, rather than being limited to the ten decimal digits 0 through 9. This allows for a potentially unlimited number of possible substituents, and the search algorithm is general enough to be applied without modification. The only changes necessary would be to prompt the user to enter the numbers of each possible substituent, and to find an alternate

way to generate the initial, “non-increasing” multiset array that begins the search. Both of these modifications are trivial.

Modifying the code to account for other molecular point groups is somewhat more challenging. First, the proper symmetry subgroup must be identified. This is the subgroup consisting of all orientation-preserving operations. Thus, it excludes reflections, improper rotations, and other operations that do not correspond to real physical transformations of the molecule. For metallophthalocyanines with $D_{4h}$ symmetry, the proper symmetry subgroup comprises only the rotations about the principal $C_4$ axis and the four $C_2$ axes perpendicular to it. For other symmetry groups, this list of operations would need to be modified accordingly. Moreover, each of these operations is implemented in the code as a transformation acting on a matrix representation of a given isomer. This means that any additional symmetry operations would need to be interpreted in terms of such matrix transformations before being incorporated into the program. While this is less trivial than the other modifications discussed, it is certainly possible given the limited number of point groups that exist.

The following code was written and executed on a Lenovo Yoga 3 Pro with an Intel® 5Y70 1.30 GHz processor and 8 GB RAM, running a 64-Bit version of the Windows 10 Home Operating System. A local Apache HTTP Server (v. 2.4.16) running PHP v. 5.6.12 was implemented via the XAMPP (Control Panel v. 3.2.1) stack. The PHP program was accessed through an HTML form interface embedded in a page named “isomers.php” (identified by the action attribute of the HTML form element), using the Firefox (v. 42) web browser.

```
/*-------Begin code-------*/
<?php
if ( $_SERVER['REQUEST_METHOD'] == 'POST' )
   $posted = true;
else
   $posted = false;
?>

<!DOCTYPE html>
<html>
   <head></head>
   <body>
      <form action="isomers.php" method="post">
         No. of Positions:
         <input type="text" name="positions"
         value="<?php echo $posted ? $_POST['positions'] : ''; ?>"><br>

         No. of Substitutions:
         <input type="text" name="substitutions"
         value="<?php echo $posted ? $_POST['substitutions'] : ''; ?>"><br>

         Order of Principal Axis of Rotation:
         <input type="text" name="n"
         value="<?php echo $posted ? $_POST['n'] : ''; ?>"><br>

         <input type="submit" value="Submit">
      </form>
      <br>
<?php
if (  ($posted == true) AND
      (  !isset($_POST['positions']) OR
         !isset($_POST['substitutions']) OR
         !isset($_POST['n']) )  )
   echo "Bad Data Passed!";
elseif ( $posted == true )
{
   $places = $_POST['positions'];
   $subs = $_POST['substitutions'];
   $n = $_POST['n'];

   /*
   Create the "non-increasing" binary multiset list (actually an array)
   1 = substituted position
   0 = unsubstituted position */
   $array = array();
   for ($i = 0; $i <= $places-1; $i++) {
      if ($i < $subs)
         $array[] = 1;
      else
         $array[] = 0;
   }

   /*
   Initialize values for positions that require comparison
   (counting starts at 0 for arrays) */
   $i = $places - 2;    // Second-to-last position in the array
   $j = $places - 1;    /* last position in the array */
```

```
   /*
   Initialize the master array of all permutations
   (without regard to symmetry) */
   $permutations[0] = $array;

   /*
   Loop will stop when 2 conditions are BOTH met:
    1. $j has reached the final bit position
    2. The value of the bit in $j is greater than or equal to
       the head bit value ($array[0]) */
   while ( ($j < $places-1) OR ($array[$j] < $array[0]) )
   {
      if ( ($j < $places-1) AND ($array[$i] >= $array[$j+1]) )
         $k = $j + 1;
      else
         $k = $i + 1;

      /*
      "beforek.next <-- k.next"
      First rearrangement of actual multiset array
      Store the bit in position k first */
      $kvalue = $array[$k];

      /* Also store the head bit for later comparison */
      $headvalue = $array[0];

      /* Then remove the kth bit and reindex the following bits */
      unset($array[$k]);
      $array = array_values($array);

      /*
      "k.next <-- head"
      Then push the k value onto the beginning of the stack
      and reset the $k variable */
      array_unshift($array,$kvalue);
      $k = 0;

      /* This also requires pushing up the i index */
      $i++;

      if ($kvalue < $headvalue)
         $i = $k;
      $j = $i + 1;

      /* Push this binary representation onto the master array */
      $permutations[] = $array;
   }
   echo "Done. ".count($permutations)." total permutations, including
duplicate structures.<br>\r\n";

   /*
   We will need to split each array representation into n segments,
   where n is the order of the principal axis, defined by the user
   $groupNo will be the length of each segment */
   $groupNo = $places/$n;
```

```
   /*
   Set the begin and end points for the search
   through the master $permutations array */
   $key = 0;
   $number = count($permutations);

   set_time_limit(500);
   while ($key < $number)
   {
      if (isset($permutations[$key]))
      {
         /* Create a 2 dimensional array of n rows, each $groupNo long */
         for ($i = 0; $i <= $n-1; $i++)
            $isomer[$i] = array_slice($permutations[$key], $groupNo*$i,
$groupNo);

         /* $isomer now holds a matrix representation of the isomer that we
are testing, which will need to be manipulated to check if it is identical to
any other isomers in the list. Since we are considering the proper symmetry
subgroup, we only need to deal with rotations that are relevant to the
molecular point group. We are here assuming a dihedral, achiral point group,
D_nh, where the user supplies the order of the principal rotational axis, n
(n=4 for metallophthalocyanines). We will need to step through n rotations
about the principal axis, and for each, we also need to take a 180 degree
rotation about a single C2 axis within the symmetry plane. This is equivalent
to taking separate 180 degree rotations of the original isomer about each of
the n C2 axes perpendicular to Cn. */
         for ($rotation = 1; $rotation <= $n; $rotation++) {
            /*
            Apply a (360/n) degree rotation by cycling the
            rows of the $isomer array */
            $lastrow = array_pop($isomer);
            array_unshift($isomer, $lastrow);

            /*
            Rebuild a one line array to compare to other entries
            in the master permutations list */
            $isoarray = array();
            foreach ($isomer as $isokey=>$row)
                  $isoarray = array_merge($isoarray,$row);

            /*
            check if isoarray matches any other values in the master
            permutations list */
            $foundkeys = array_keys($permutations, $isoarray, TRUE);
            if ( (count($foundkeys) > 1) OR
                 ( (count($foundkeys) == 1) AND ($foundkeys[0] != $key) )  )
            {
                  /*
                  Delete the duplicate entries in the $permutations array */
                  foreach ($foundkeys as $duplicatekey)
                        unset($permutations[$duplicatekey]);
            }

            /*
            And check a 180 degree rotation of this about a C2 axis,
            just by reversing the array */
```

```
            $isoarray = array_reverse($isoarray);

            /*
            check if isoarray matches any other values in the
            master permutations list */
            $foundkeys = array_keys($permutations, $isoarray, TRUE);
            if ( (count($foundkeys) > 1) OR
                 ( (count($foundkeys) == 1) AND ($foundkeys[0] != $key) ) )
            {
                  /* Delete duplicate entries in the $permutations array */
                  foreach ($foundkeys as $duplicatekey)
                        unset($permutations[$duplicatekey]);
            }
         }
         unset($isomer);
      }

      /* Move on to the next permutation */
      $key++;
   }

   /*
   Quote the results and list the binary representations
   of the isomers found */
   echo "Done filtering. ".count($permutations)." unique structures
found.<br>\r\n";
   foreach ($permutations as $row) {
      foreach ($row as $bit)
         echo $bit;

      echo "<br>\r\n";
   }
}
?>
   </body>
</html>
/*-------End code-------*/
```

Figure C1 shows plots of the results obtained from running the program for two different cases. The total number of permutations and the number of unique isomers are plotted as functions of the number of substituents. If all sixteen fluorines on the $ZnF_{16}Pc$ can be substituted with equal probability, the distribution will resemble that in Figure C1(A), with $ZnF_8(SR)_8Pc$ having the maximum number (1,654) of unique isomers. In order to determine the distribution for the restricted case, in which the β fluorines are substituted first, we ignore the α fluorines and input "8" as the number of possible positions into the program prompt, while retaining the $D_{4h}$ symmetry.

This data is shown in Figure C1(B), with two maxima occurring at just 13 unique isomers for both $ZnF_{12}(SR)_4Pc$ and $ZnF_4(SR)_{12}Pc$. As one check of the validity of the program, we note that the total number of permutations for any given number of substituents, $n$, should be ${}_{16}C_n = 16!/[n!\,(16-n)!]$ for the unrestricted case, and ${}_{8}C_n = 8!/[n!\,(8-n)!]$ for the restricted case, and these calculated values match the program output exactly.

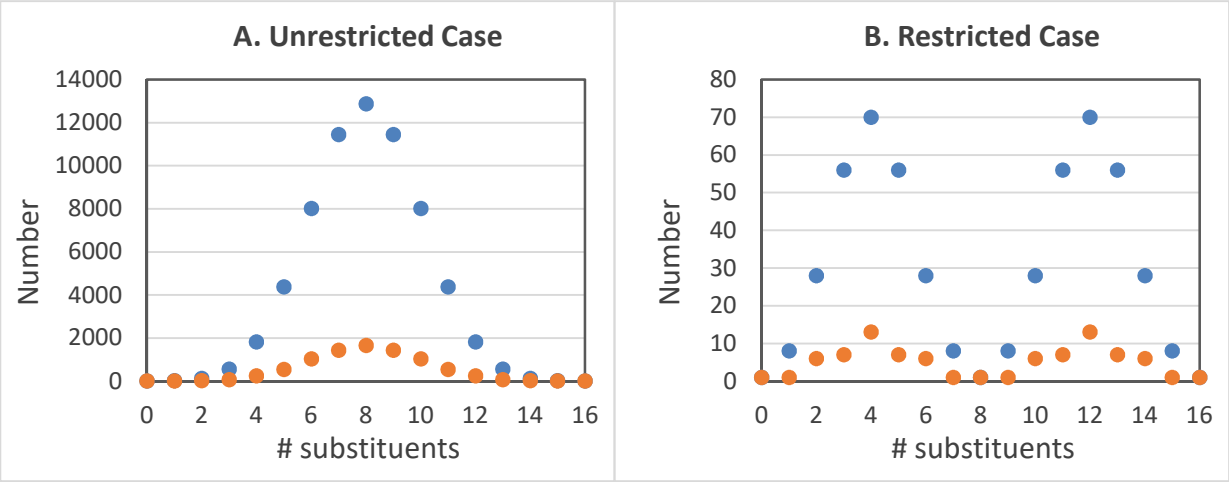


**Figure C1**. The total number of permutations (•) and the number unique isomers (•) as a function of the number of substituents, for two different mechanistic assumptions: (A) The unrestricted case assumes that all sixteen positions react with equal probability, and (B) The restricted case assumes that all eight β positions react with equal probability, before any of the eight α positions react. Note the difference in the vertical scales.

## C2. Oxidative Decomposition

Purification and separation of the crude reaction mixtures proved to be difficult, due primarily to the ease with which thioethers can oxidize into sulfoxides and sulfones. This is indicated by the differences in TLCs of purified products upon standing in air, wherein the $R_f$, were reduced essentially to zero, indicating near quantitative conversion into a highly polar product. The UV-Vis absorbance spectra of these spots also showed distinct changes, including a splitting of the Q-band and an increase in the band at the blue edge near 640 nm. To verify this

conclusion, a small sample of $ZnF_{13}(SR)_3Pc$ was freshly purified by TLC and then subjected to oxidative conditions by dissolving in glacial acetic acid with four equivalents of 30% hydrogen peroxide per thioalkane group, and the solution was stirred at room temperature. These conditions were reported to convert alkyl phenyl sulfides into the corresponding sulfoxides in high yield.[2] After two hours, UV-Vis spectroscopy of the reaction mixture was almost identical to those observed in the unknown polar products, confirming that they were indeed sulfoxides. Consequently, TLC was used for most separations, and the compounds were kept under nitrogen at low temperatures.

**C3. UV-Vis Spectroscopy**

Solution phase UV-Vis absorbance spectra were obtained on a Lambda 35 spectrophotometer operating in single beam mode. The monochromator bandwidth was set to 1 nm to match the excitation monochromator settings of the fluorescence spectrometer. All spectra were obtained from dilute solutions in either quartz or special optical glass cuvettes using freshly distilled or spectroscopic grade solvents. For extinction coefficient measurements, samples of each Pc were accurately weighed and dissolved into a known volume of distilled THF. This solution was then titrated into a THF blank to record spectra at multiple concentrations and construct calibration curves according to the Beer-Lambert equation.

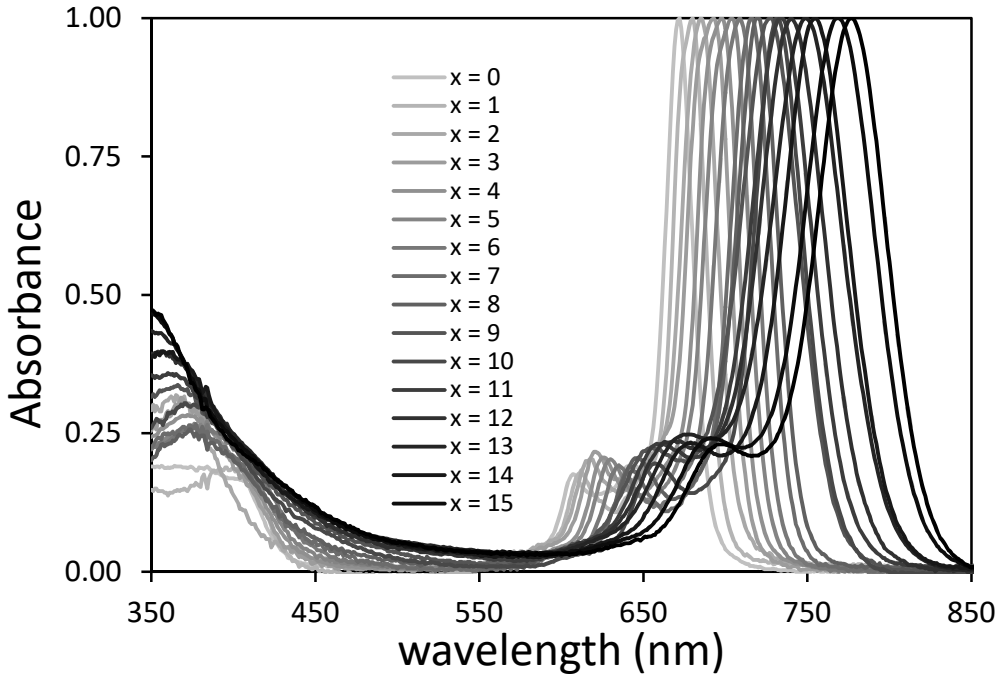


**Figure C2**. Expanded, normalized UV-Vis spectra of all compounds $ZnF_{16-x}(SR)_xPc$ (x = 0 to 16) in freshly distilled THF. The arrow indicates the increase in the high energy absorbance with increasing thioalkyl substitution and the corresponding changes in the molecular orbitals as described in the text.

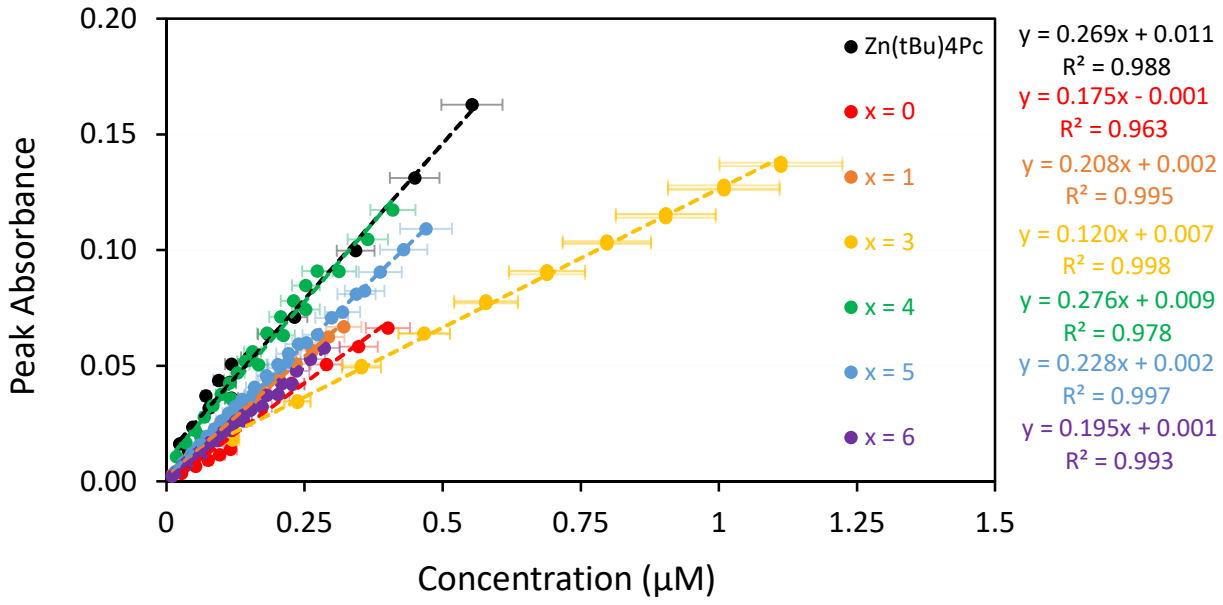


**Figure C3**. Calibration curves of the compounds $Zn(tBu)_4Pc$ and $ZnF_{16-x}(SR)_xPc$ for x = 0, 1, 3, 4, 5 and 6. Linearity over the concentration range is consistent with the application of the Beer-Lambert Law. The slopes given on the right are the extinction coefficients in units of $(\mu M \cdot cm)^{-1}$.

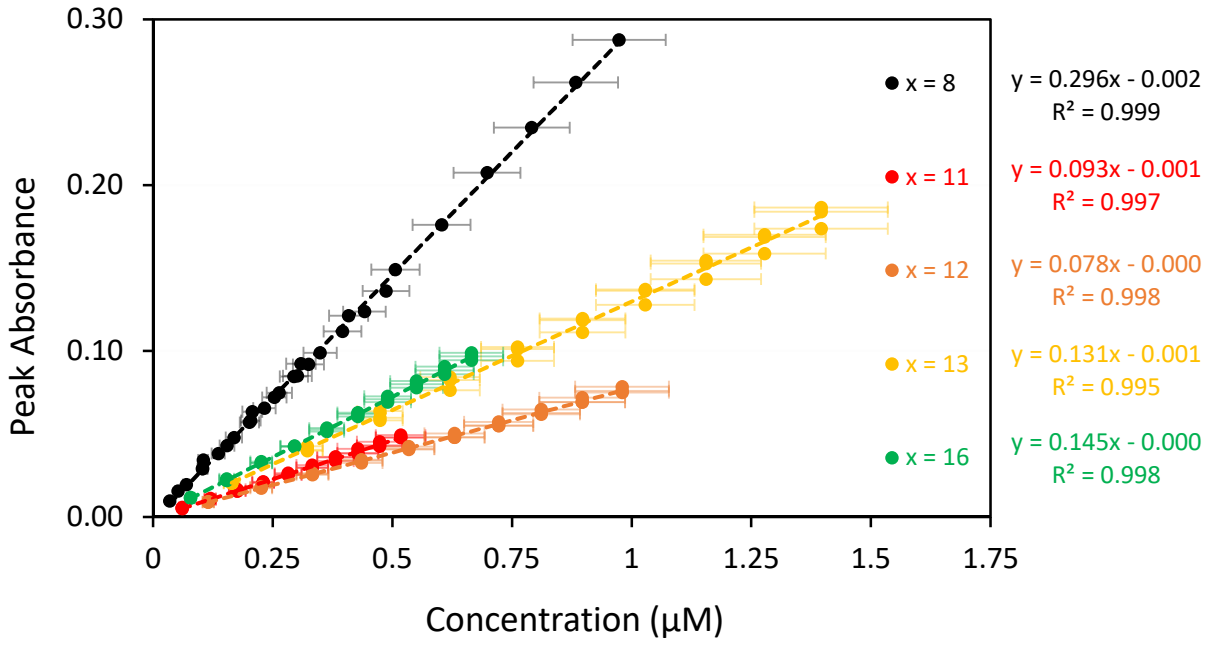


**Figure C4**. Calibration curves of the compounds $ZnF_{16-x}(SR)_xPc$ for x = 8, 11, 12, 13 and 16. Linearity over the concentration range is consistent with the application of the Beer-Lambert Law. The slopes given on the right are the extinction coefficients in units of $(\mu M \cdot cm)^{-1}$.

## C4. Fluorescence Spectroscopy

Steady state fluorescence emission spectra, quantum yield comparisons, and fluorescence lifetime measurements were made using right-angle detection mode with the excitation monochromator bandwidth set to 1 nm. Excitation spectra were obtained in the same configuration with the monochromator bandwidths reversed. For both steady state and lifetime experiments, all solutions were degassed with dry nitrogen for 2 to 3 minutes immediately prior to data collection. Monochromator bandwidths were sometimes increased as necessary to improve signal-to-noise ratios, but were always kept consistent between samples and standards for comparison purposes and quantum yield calculations. In order to minimize inner filter effects, solutions for right angle measurement were diluted so that the absorbance remained below 0.1 for all wavelengths. Quantum yields, $\phi_f$, were calculated using a relative gradient method according to the equation

$\phi_f = \phi_r \left(\frac{\nabla F}{\nabla F_r}\right)\left(\frac{n}{n_r}\right)^2$. The $\nabla F$ term is the gradient of a plot of integrated fluorescence intensity vs. absorbance at the excitation wavelength for each compound. The last term is a correction for the respective indices of refraction, *n*, of the solvents used for the sample and reference solutions. The subscript, *r*, indicates a quantity corresponding to the reference solution. Thus, $\phi_r$ is the quantum yield of the standard obtained from the literature. To obtain the $\nabla F$ values, multiple solutions of each compound were prepared at varying concentrations, and emission spectra were taken for each. Zn(*t*Bu)$_4$Pc in deaerated toluene was used as standard, with $\phi_r$ = 0.081.[3]

It is not clear why there is an anomalously high value for the quantum yield of ZnF$_{16}$Pc in the literature (see main text).[4] The higher concentration reported would tend to increase aggregation and thus decrease the apparent quantum yield by artificially inflating the measured absorbance at the excitation wavelength quoted (660 nm). Indeed, the authors cite this as the reason for the reduction of the quantum yield between ZnPc and ZnF$_{16}$Pc, stating that aggregation prevails in the latter. However, our own studies indicate that there is a real decrease by the same factor between these two for a series of dilute THF solutions in which there is no evidence of aggregation. It is thus much more likely that the inflated literature value for ZnF$_{16}$Pc is a consequence of the artificially high value of the ZnPc quantum yield they used as a standard.

Linearity of the plots of florescence intensity *vs*. absorbance at $\lambda_{ex}$ was used as a criteria to judge the extent of aggregation. For compounds ZnF$_{16}$Pc, ZnF$_{15}$(SR)Pc, ZnF$_{14}$(SR)$_2$Pc, and ZnF$_{13}$(SR)$_3$Pc, there was a noticeable curvature in these plots. This was accompanied by the observation of increasing absorbance bands near 635, 642, 649, and 655 nm, respectively. These bands are commonly attributed to the absorbance of dark (*i.e.* non-emissive) aggregates. Since they overlap the excitation wavelengths used for fluorescence, their contribution needed to be subtracted from the absorbance used to calculate the quantum yield. To account for this, the

lineshape of the most dilute, least aggregated solution of each compound was scaled to the peak maximum of the spectra for the other concentrations, and the absorbance of the newly scaled spectra at the excitation wavelength was used in calculating the quantum yield. Performing this correction on these four compounds effectively restored the linear relationship between fluorescence intensity and absorbance in all cases.

For lifetime measurements a dilute solution of colloidal silica (LUDOX, Sigma) in deionized water was used to produce the instrument response function (IRF). Dilute samples and narrow slit bandwidths were preferred to give slower collection rates over longer periods of time. This reduces the so-called "pulse pile-up effect" that would otherwise skew the counting statistics towards earlier photon detection events and therefore shorter lifetimes. All of the measured decays were fit reasonably well with a single lifetime parameter, except as noted in **Table 4.1** n the main text. The only exceptions to this required a minor second lifetime parameter very close to the IRF width, which is likely to be a scattering artifact. The fits obtained were judged based on a combination of the $\chi^2$ value and visual inspection of the plotted residuals. Lifetimes were recorded for each compound at several different concentrations over the range studied, and multiple fits were performed on each decay spectrum using different boundaries to ensure numerical stability. The separate numerical fits for each concentration were averaged together and then plotted as a function of concentration (Figure C5) to ensure that they remained constant over the range of interest. Finally, the results for each compound were averaged together over all fits and all concentrations to give the lifetime values quoted in **Table 4.1**.

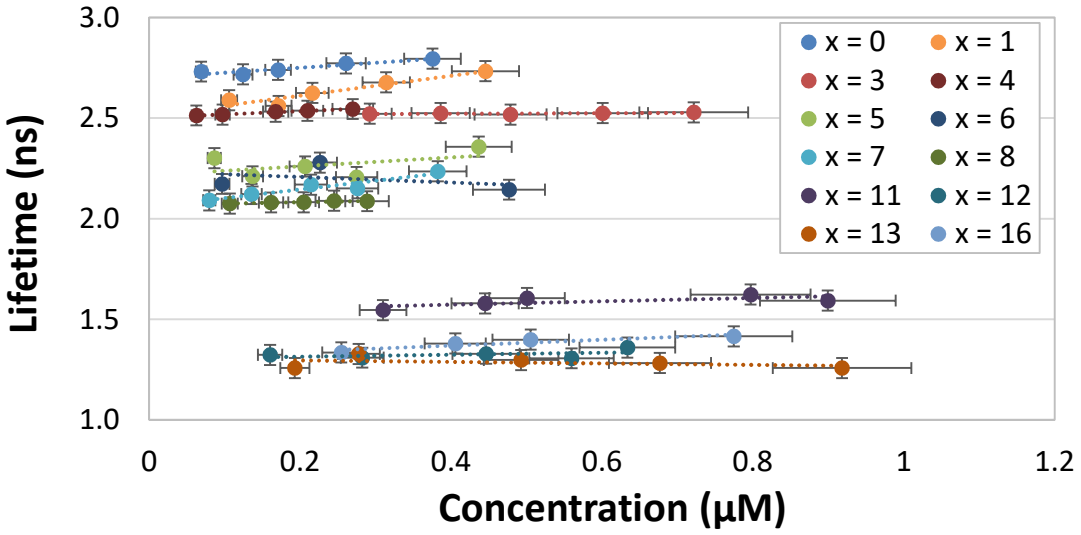


**Figure C5**. Lifetimes for each compound $ZnF_{16-x}(SR)_xPc$ (x = 0 to 16) *vs*. concentration, demonstrating that they remain constant over the range investigated. Concentrations were calculated from the absorbance spectra of the solutions and the extinction coefficients that were obtained in a separate set of experiments. Horizontal error bars indicate a ±10% uncertainty in the concentration as a consequence of the uncertainty in the extinction coefficient. Vertical error bars correspond to instrumental uncertainties of ±50 ps.

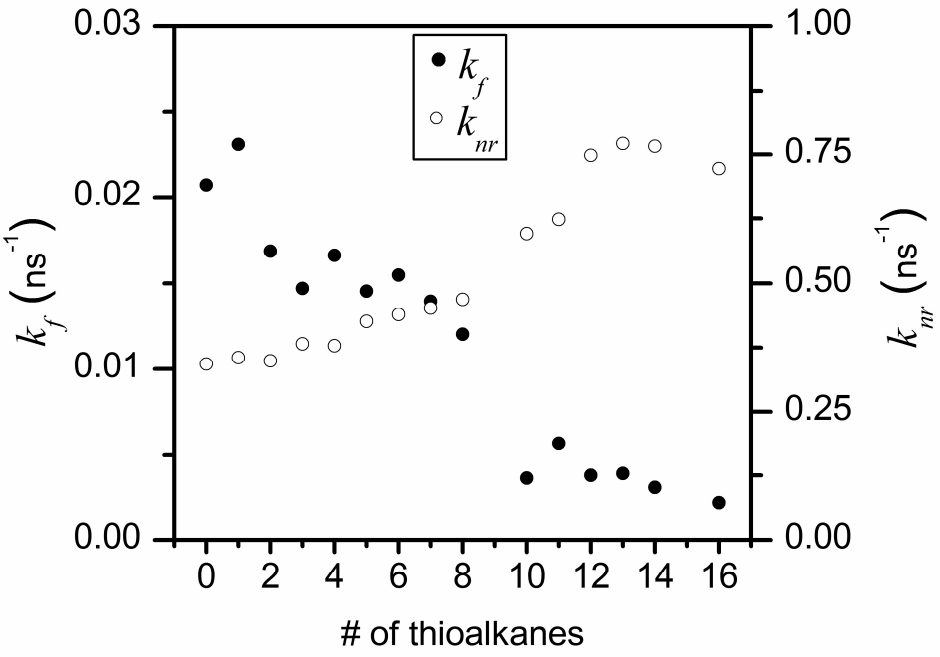


**Figure C6**. Fluorescence and non-radiative rate constants ($k_f$ and $k_{nr}$, respectively) for compounds $ZnF_{16-x}(SR)_xPc$ (x = 0 to 16) in THF. Note the different scales of the left and right axes for the different constants.

## C5. Synthesis & Characterization

### octylthiopentadecafluorophthalocyaninato zinc(II), $ZnF_{15}(SR)Pc$

$ZnF_{15}(SR)Pc$ was synthesized according to the above procedure using 30 mg $ZnF_{16}Pc$ (0.035 mmol), 0.1 mL 1-octanethiol (0.58 mmol), and 100 mg $K_2CO_3$ (0.72 mmol) in 10 mL dry THF. The reaction was run at 50° C for 1 hour. The blue-green solid Pc mixture obtained from the column was separated by TLC using a 6:4 mixture of hexanes to ethyl acetate. Yield: 43% (15 mg, 0.015 mmol). $^1H$ NMR ($(CD_3)_2CO$, 500 MHz): δ 0.82-0.97 (m, 3H, $CH_3$), 1.17-1.83 (m, 12H, $CH_2$), 2.51-2.73 (m, 2H, $SCH_2$). $^{19}F$ NMR ($(CD_3)_2CO$, 376.5 MHz): δ -141.90 (br, 7F, β), -153.46 (br, 8F, α). MALDI-TOF MS: m/z 990.96 (65%, $[M+H]^+$), 877.71 (100%, $[M-(CH_2)_7CH_3]^+$); calculated for $[ZnF_{15}(SR)Pc+H]^+$ 991.04. UV-Vis (in THF): $\lambda_{max}$/nm 679 (log ε 5.32), 612 (4.58), 401 (4.58).

### bis(octylthio)tetradecafluorophthalocyaninato zinc(II), $ZnF_{14}(SR)_2Pc$

UV-Vis (in THF): $\lambda_{max}$/nm 686, 618, 369.

### tris(octylthio)triskadecafluorophthalocyaninato zinc(II), $ZnF_{13}(SR)_3Pc$

$ZnF_{13}(SR)_3Pc$ was synthesized according to the above procedure using 65.5 mg $ZnF_{16}Pc$ (0.076 mmol), 0.04 mL 1-octanethiol (0.23 mmol), and 165 mg NaH (6.88 mmol) in 2 mL dry THF. The reaction was run at room temperature for 10 min. The green solid Pc mixture obtained from the column was separated by TLC using a 8:2 mixture of hexanes to ethyl acetate. MALDI-TOF MS: m/z 1244.88 (100%, $[M+H]^+$), 1146.70 (8%, $[M-(CH_2)_7CH_3+O]^+$); calculated for $[ZnF_{13}(SR)_3Pc+H]^+$ 1244.24. UV-Vis (in THF): $\lambda_{max}$/nm 692 (log ε 5.08), 620 (4.41), 369 (4.57).

**tetrakis(octylthio)dodecafluorophthalocyaninato zinc(II), $ZnF_{12}(SR)_4Pc$**

$ZnF_{12}(SR)_4Pc$ was synthesized according to the above procedure using 60 mg $ZnF_{16}Pc$ (0.069 mmol), 0.4 mL 1-octanethiol (2.3 mmol), and 200 mg $K_2CO_3$ (1.4 mmol) in 20 mL dry THF. The reaction was run at 50° C for 4 hours. The green solid Pc mixture obtained from the column was separated by TLC using a 9:1 mixture of hexanes to ethyl acetate. Yield: 24% (22.4 mg, 0.016 mmol). $^1$H NMR ($CDCl_3$, 500 MHz): δ 0.81-0.91 (m, 12H, $CH_3$), 1.18-1.57 (m, 48H, $CH_2$), 3.17-3.36 (m, 8H, $SCH_2$). $^{19}$F NMR ($CDCl_3$, 376.5 MHz): δ -108.86 (br, 4F, β), -122.65 (br, 4F, α), -142.47 (br, 4F, α). MALDI-TOF MS: m/z 1370.29 (100%, $[M]^+$), 1496.38 (10%, $[ZnF_{11}(SR)_5Pc]^+$); calculated for $[ZnF_{12}(SR)_4Pc]^+$ 1370.35. UV-Vis (in THF): $\lambda_{max}$/nm 698 (log ε 5.44), 626 (4.75), 372 (4.89).

**pentakis(octylthio)undecafluorophthalocyaninato zinc(II), $ZnF_{11}(SR)_5Pc$**

$ZnF_{11}(SR)_5$ was isolated from the same reaction as $ZnF_{12}(SR)_4Pc$ above. Yield: 26% (27.0 mg, 0.018 mmol). $^1$H NMR ($CDCl_3$, 500 MHz): δ 0.83-0.91 (m, 15H, $CH_3$), 1.17-1.67 (m, 60H, $CH_2$), 3.25-3.70 (m, 10H, $SCH_2$). $^{19}$F NMR ($CDCl_3$, 376.5 MHz): δ -109.09 (br, 6F, α), -123.07 (br, 3F, β), -142.57 (br, 2F, α). MALDI-TOF MS: m/z 1496.37 (100%, $[M]^+$), 1622.47 (15%, $[ZnF_{10}(SR)_6Pc]^+$); calculated for $[ZnF_{11}(SR)_5Pc]^+$ 1496.46. UV-Vis (in THF): $\lambda_{max}$/nm 704 (log ε 5.36), 630 (4.67), 378 (4.77).

**hexakis(octylthio)decafluorophthalocyaninato zinc(II), $ZnF_{10}(SR)_6$**

$ZnF_{10}(SR)_6$ was isolated from the same reaction mixture as $ZnF_{12}(SR)_4Pc$ above. Yield: 19% (21.1 mg, 0.013 mmol). $^1$H NMR ($CDCl_3$, 500 MHz): δ 0.82-0.95 (m, 18H, $CH_3$), 1.18-1.57 (m, 72H, $CH_2$), 3.17-3.36 (m, 12H, $SCH_2$). $^{19}$F NMR ($CDCl_3$, 376.5 MHz): δ -109.13 (bs, 4F, α), -123.22 (bs, 2F, β), -142.38 (bs, 4F, α). MALDI-TOF MS: m/z 1623.44 (100%, $[M]^+$), 1749.52

(7%, $[ZnF_9(SR)_7Pc]^+$); calculated for $[ZnF_{10}(SR)_6Pc]^+$ 1623.57. UV-Vis (in THF): $\lambda_{max}$/nm 708 (log ε 5.29), 635 (4.57), 382 (4.69).

**heptakis(octylthio)nonafluorophthalocyaninato zinc(II), $ZnF_9(SR)_7Pc$**

$ZnF_9(SR)_7Pc$ was synthesized according to the above procedure using 60 mg $ZnF_{16}Pc$ (0.069 mmol), 0.6 mL 1-octanethiol (3.5 mmol), and 200 mg $K_2CO_3$ (1.4 mmol) in 20 mL dry THF. The reaction was refluxed for 8 hours. The green solid Pc mixture obtained from the column was separated by TLC using a 9.4:0.6 mixture of hexanes to ethyl acetate. Yield: 17% (21.4 mg, 0.012 mmol). $^1$H NMR ($CDCl_3$, 500 MHz): δ 0.75-0.85 (m, 21H, $CH_3$), 1.19-1.65 (m, 84H, $CH_2$), 3.00-3.50 (m, 14H, $SCH_2$). $^{19}$F NMR ($CDCl_3$, 376.5 MHz): δ -91.10 (s, 1F, α), -91.85-92.05 (m, 2F, α/ β), -93-93.5 (m, 6F, α). MALDI-TOF MS: m/z 1749.54 (100%, $[M]^+$), 1875.64 (17%, $[ZnF_8(SR)_8Pc]^+$); calculated for $[ZnF_9(SR)_7Pc]^+$ 1749.68. UV-Vis (in THF): $\lambda_{max}$/nm 716 (log ε 5.46), 642 (4.73), 372 (4.87).

**octakis(octylthio)octafluorophthalocyaninato zinc(II), $ZnF_8(SR)_8Pc$**

$ZnF_8(SR)_8Pc$ was isolated from the same reaction mixture as $ZnF_9(SR)_7Pc$ above. Yield: 25% (31.4 mg, 0.017 mmol). $^1$H NMR ($CDCl_3$, 500 MHz): δ 0.75-0.85 (m, 24H, $CH_3$), 1.15-1.92 (m, 96H, $CH_2$), 3.27-3.51 (m, 16H, $SCH_2$). $^{19}$F NMR ($CDCl_3$, 376.5 MHz): δ -91.17 (s, 1F, β), -92.06 (s, 4F, α), -92.34-93.74 (m, 3F, α). MALDI-TOF MS: m/z 2002.11 (6%, $[ZnF_7(SR)_9Pc]^+$), 1876.01 (100%, $[M]^+$), 1779.86 (17%, $[M-(CH_2)_7CH_3+O]^+$), 1763.84 (14%, $[M-(CH_2)_7CH_3]^+$), 1749.87 (11%, $[ZnF_9(SR)_7Pc]^+$); calculated for $[ZnF_8(SR)_8Pc]^+$ 1875.78. UV-Vis (in THF): $\lambda_{max}$/nm 720 (log ε 5.47), 645 (4.78), 374 (4.88).

**nonakis(octylthio)heptafluorophthalocyaninato zinc(II), $ZnF_7(SR)_9Pc$**

UV-Vis (in THF): $\lambda_{max}$/nm 727, 656, 366.

**decakis(octylthio)hexafluorophthalocyaninato zinc(II), $ZnF_6(SR)_{10}Pc$**

MALDI-TOF MS: m/z 2129.72 (100%, $[M]^+$); calculated for $[ZnF_6(SR)_{10}Pc]^+$ 2129.99. UV-Vis (in THF): $\lambda_{max}$/nm 731, 657, 371.

**undecakis(octylthio)pentafluorophthalocyaninato zinc(II), $ZnF_5(SR)_{11}Pc$**

MALDI-TOF MS: m/z 2255.28 (100%, $[M+H]^+$), 2160.12 (16%, $[M-(CH_3)_7CH_3+O+H]^+$); calculated for $[ZnF_5(SR)_{11}Pc+H]^+$ 2255.10. UV-Vis (in THF): $\lambda_{max}$/nm 733 (log ε 4.97), 660 (4.33), 364 (4.52).

**dodecakis(octylthio)tetrafluorophthalocyaninato zinc(II), $ZnF_4(SR)_{12}Pc$**

MALDI-TOF MS: m/z 2382.28 (100%, $[M+H]^+$), 2255.13 (37%, $[ZnF_5(SR)_{11}+H]^+$); calculated for $[ZnF_4(SR)_{12}Pc+H]^+$ 2382.21. UV-Vis (in THF): $\lambda_{max}$/nm 740 (log ε 4.89), 669 (4.27), 358 (4.49).

**triskadecakis(octylthio)trifluorophthalocyaninato zinc(II), $ZnF3(SR)_{13}Pc$**

$^1H$ NMR ($CDCl_3$, 500 MHz): δ 0.78-0.92 (m, 39H, $CH_3$), 0.95-1.85 (m, 156H, $CH_2$), 3.15-3.58 (m, 26H, $SCH_2$). MALDI-TOF MS: m/z 2634.40 (24%, $[ZnF_2(SR)_{14}Pc+H]^+$), 2508.29 (100%, $[M+H]^+$), 2382.18 (38%, $[ZnF_4(SR)_{12}Pc+H]^+$), 2254.06 (10%, $[ZnF_5(SR)_{11}Pc+H]^+$); calculated for $[ZnF_3(SR)_{13}Pc+H]^+$ 2508.31. UV-Vis (in THF): $\lambda_{max}$/nm 749(log ε 5.12), 677 (4.51).

**tetradecakis(octylthio)difluorophthalocyaninato zinc(II), $ZnF_2(SR)_{14}Pc$**

$^1H$ NMR ($CDCl_3$, 500 MHz): δ 0.75-0.85 (m, 42H, $CH_3$), 1.05-1.90 (m, 168H, $CH_2$), 3.15-3.55 (m, 28H, $SCH_2$). MALDI-TOF MS: m/z 2633.97 (100%, $[M]^+$), 2507.86 (28%, $[ZnF_3(SR)_{13}Pc]^+$); calculated for $[ZnF_2(SR)_{14}Pc]^+$ 2633.41. UV-Vis (in THF): $\lambda_{max}$/nm 755, 679, 357.

**pentadecakis(octylthio)monofluorophthalocyaninato zinc(II), $ZnF(SR)_{15}Pc$**

UV-Vis (in THF): $\lambda_{max}$/nm 768, 691.

**hexadecakis(octylthio)phthalocyaninato zinc(II), $Zn(SR)_{16}Pc$**

Sodium metal (300 mg) was added to 25 mg of $ZnF_{16}Pc$ (0.029 mmol) in 40 mL of diglyme and stirred until the Na dissolved. Then, 3.5 mL of 1-octanethiol (0.013 mol) was added under $N_2$ at room temperature. The resulting mixture was heated to 100 °C and stirred for 16 hours. The reaction was then cooled to room temperature and poured into 300 mL of water. The product was extracted with diethyl ether (3 × 20 mL), dried over $Na_2SO_4$, and concentrated under reduced pressure. Silica gel chromatography (2 × 8 in) with hexane followed by hexane/ethyl acetate (30:1 v:v) yielded 50 mg (0.013 mmol) of the product (44% yield). MALDI-TOF MS: m/z 2887.16 (100%, $[M]^+$), 2793.12 (18%, $[ZnF_3(SR)_{13}Pc]^+$); calculated for $[Zn(SR)_{16}Pc]^+$ 2887.64. UV-Vis (in THF): $\lambda_{max}$/nm 777 (log ε 5.16), 697 (4.52).

**C6. MALDI-TOF Mass Spectrometry**

After being separated chromatographically, each individual Pc was prepared for MALDI-TOF analysis using a DHB matrix and a THF/water/TFA mixture as the solvent. The MALDI spectra obtained are shown in Figure C7 through C20 For each compound there is a strong peak corresponding to the intact molecular cation, either protonated ($[M+H]^+$) or oxidized ($[M]^+$). In some cases additional minor peaks are observed. These are attributed to either contamination by a small amount of a different substitution product, oxidized byproducts of the expected Pc, fragment ions in which one or more sulfide chains have been cleaved, or some combination of these three. In some spectra we observed small peaks between 600 and 800 amu which are likely due to fragmentation of the Pc macrocycle itself. Increasing the laser power generally caused these peaks

to become more significant, confirming that they are due to fragmentation occurring during the laser ablation.

All of the mass spectra obtained are shown below along with tables listing the assignments of the most prominent peaks. For some of the sample, there is a cluster of small molecular weight fragments around 600 Daltons. This cluster likely corresponds to ionic fragments of the parent molecule, and has been cut out of most of the given spectra for clarity. The x-axis (m/z) is scaled differently for each compound in order to show all of the observed peaks in as much detail as possible, but no higher mass fragments have been excluded from the data shown.

Except for the $ZnF_{16}Pc$ standard, each spectrum is followed by a table of peak assignments. Each peak cluster in the spectrum is labelled by the most abundant mass, and the table gives a proposed structure and the corresponding observed and expected mass ranges. In each chart, the structure of the primary intact molecular ion is given in red. The abbreviated notation includes the number of fluorine atoms, $F_n$, followed by $(16 - n)$ different possible substituents. $(SR)_x$ indicates $x$ octylthio chains, while $(SH)_y$ indicates $y$ chains in which the octyl portion has been cleaved off, leaving behind a thiol. $H_z$ denotes $z$ similar cleavages, except that the sulfur atom has been removed with the octyl chain, the entire group being replaced by an H attached directly to the Pc core. $O_m$ may also be included to indicate that one or more of the sulfur groups has been oxidized. Although it is not possible to establish the precise nature or locus of oxidation through MALDI, a pattern emerges in which an oxygen is almost always accompanied by the presence of a thiol group. This suggests that oxidation occurs by the conversion of thiol (–SH) to sulfenic acid (–SOH) subsequent to fragmentation.

For every possible proposed structure, $n + x + y + z = 16$, necessarily, and $m \leq 2(x + y)$ since only sulfur atoms can be oxidized in this case. Finally, the "-H" or "+H" terms are used when the mass more closely corresponds to a deprotonated anion or protonated cation, depending on the detection mode. However, given the resolution of the instrument, the usage is somewhat arbitrary. As an example, the structure denoted $[ZnF_9(SR)_3(SH)_4Pc+H]^+$ refers to a protonated fragment of a $ZnF_9(SR)_7Pc$ molecule in which four octyl chains have been cleaved, leaving behind four thiols and three intact octylthio groups.

From the UV-Vis spectroscopy and TLC analysis, it appears that all of these compounds are stable in solution over the timescale of the mass spec analysis. Thus, it is likely that these fragmentations occur during the laser ablation. This is further corroborated by the fact that the relative intensity of the fragmentation peaks was observed to increase with increasing laser power.

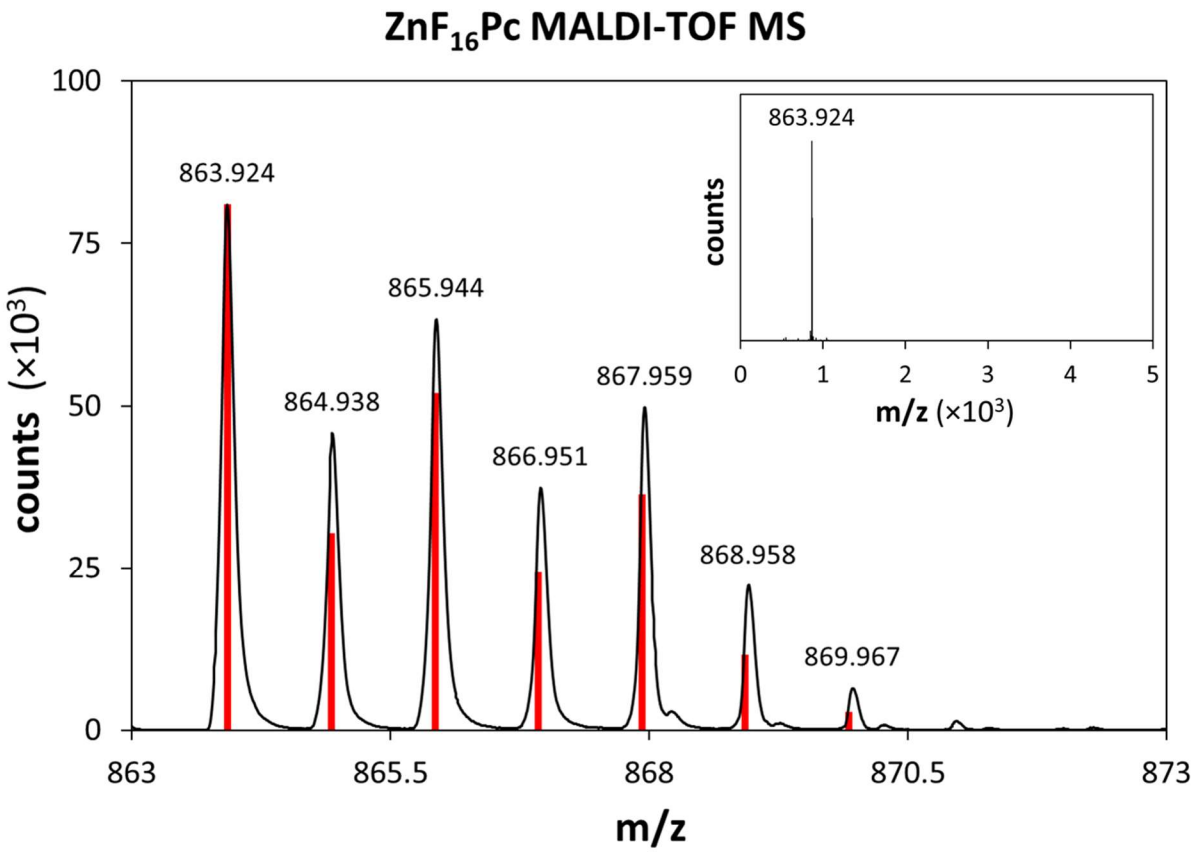


**Figure C7**. Mass spectrum of $ZnF_{16}Pc$ in a DHB matrix. An expanded view of the region immediately surrounding the detected ion peak $[ZnF_{16}Pc]^+$. The black trace is the experimental data obtained in positive ion detection mode. The vertical red lines correspond to the expected theoretical isotopic distribution, calculated using ChemBioDraw Ultra 14.0 and scaled to the highest observed peak. The inset shows the full spectrum over the entire mass range observed, from 0 to 5000 Daltons, with no other ions or fragments visible.

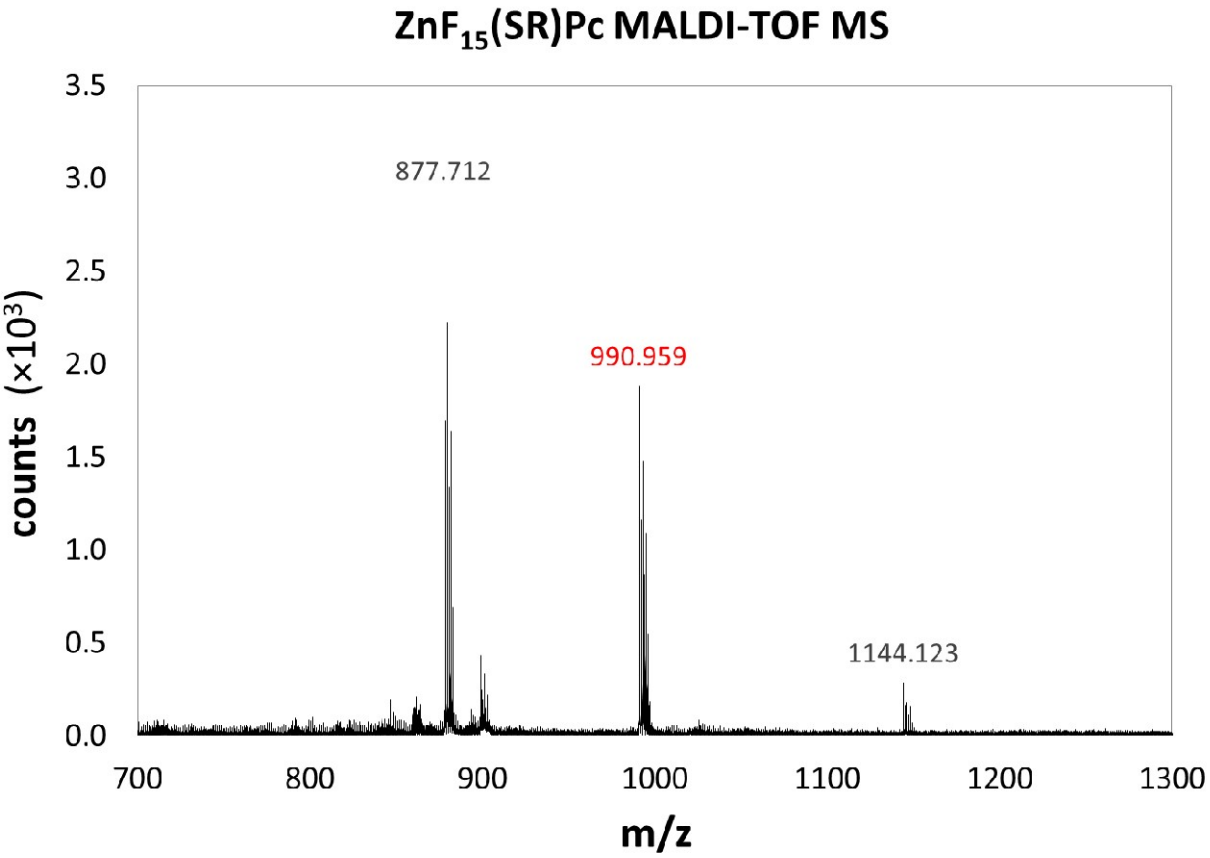


| Structure | Observed Mass Range | | Expected Mass Range | |
|---|---|---|---|---|
| $[ZnF_{15}(SH)Pc]^+$ | 877.71 | 883.77 | 877.91 | 883.90 |
| $[ZnF_{15}(SR)Pc+H]^+$ | 990.96 | 997.04 | 991.04 | 997.04 |
| $[ZnF_{12}(SR)_2(SH)_2Pc]^+$ | 1144.12 | 1150.12 | 1144.10 | 1150.10 |

**Figure C8**. Mass spectrum of zinc (II) octylthiopentadecafluorophthalocyanine ($ZnF_{15}(SR)Pc$) in a DHB matrix. A very small amount of fragmented tetra-substituted Pc also appears to be present, as well as significant fragmentation of the primary compound. The structural notation is described in detail above.

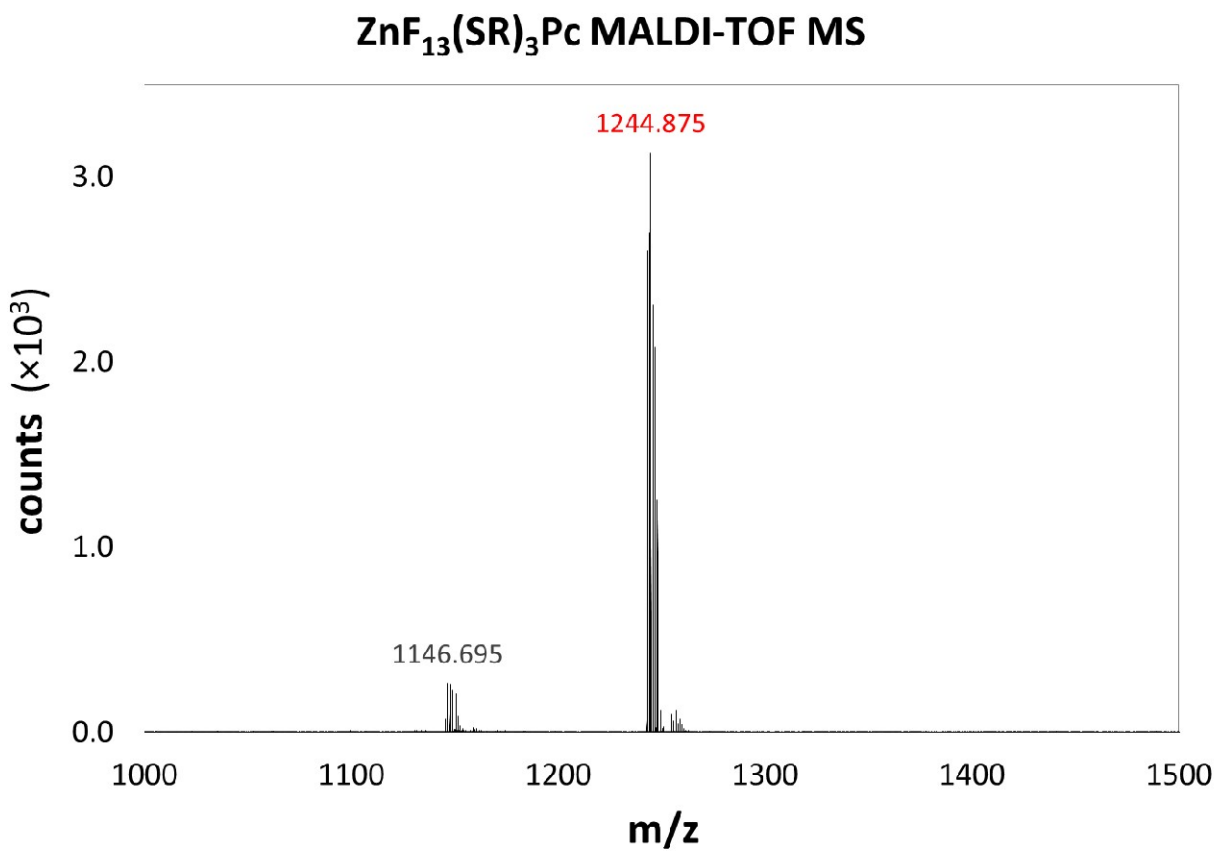


| Structure | Observed Mass Range | | Expected Mass Range | |
|---|---|---|---|---|
| $[ZnF_{13}(SH)_2(SH)OPc]^+$ | 1145.70 | 1153.74 | 1146.12 | 1153.11 |
| $[ZnF_{13}(SR)_3Pc+H]^+$ | 1242.88 | 1249.90 | 1243.26 | 1250.25 |

**Figure C9**. Mass spectrum of zinc (II) tris(octylthio)tridecafluorophthalocyanine ($ZnF_{13}(SR)_3Pc$) in a DHB matrix. A small amount of an oxidized fragment ion is also present. The structural notation is described in detail above.

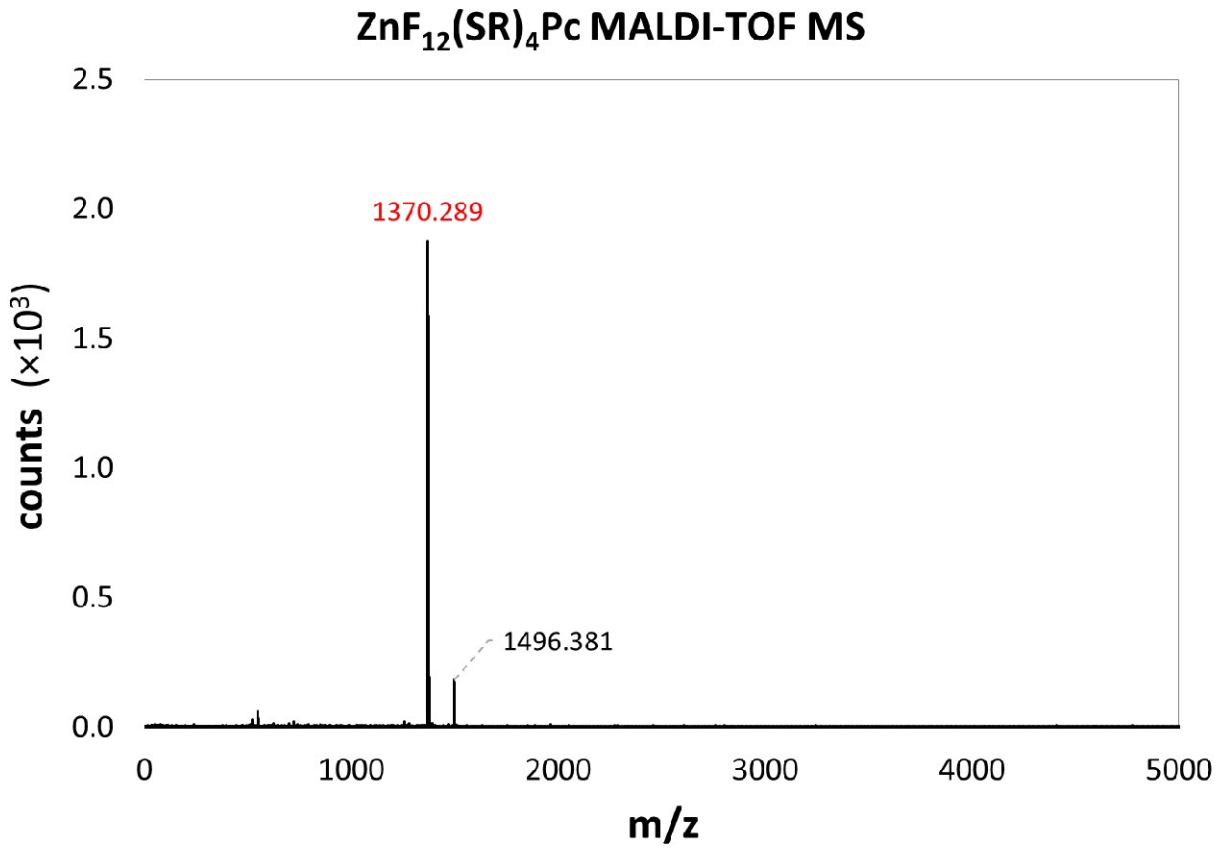


| Structure | Observed Mass Range | | Expected Mass Range | |
|---|---|---|---|---|
| $[ZnF_{12}(SR)_4Pc]^+$ | 1368.28 | 1376.31 | 1368.35 | 1376.35 |
| $[ZnF_{11}(SR)_5Pc]^+$ | 1494.39 | 1501.37 | 1494.46 | 1501.47 |

**Figure C10**. Mass spectrum of zinc (II) tetrakis(octylthio)dodecafluorophthalocyanine ($ZnF_{12}(SR)_4Pc$) in a DHB matrix. A very small amount of the pentakis- substituted product is also present. The structural notation is described in detail above.

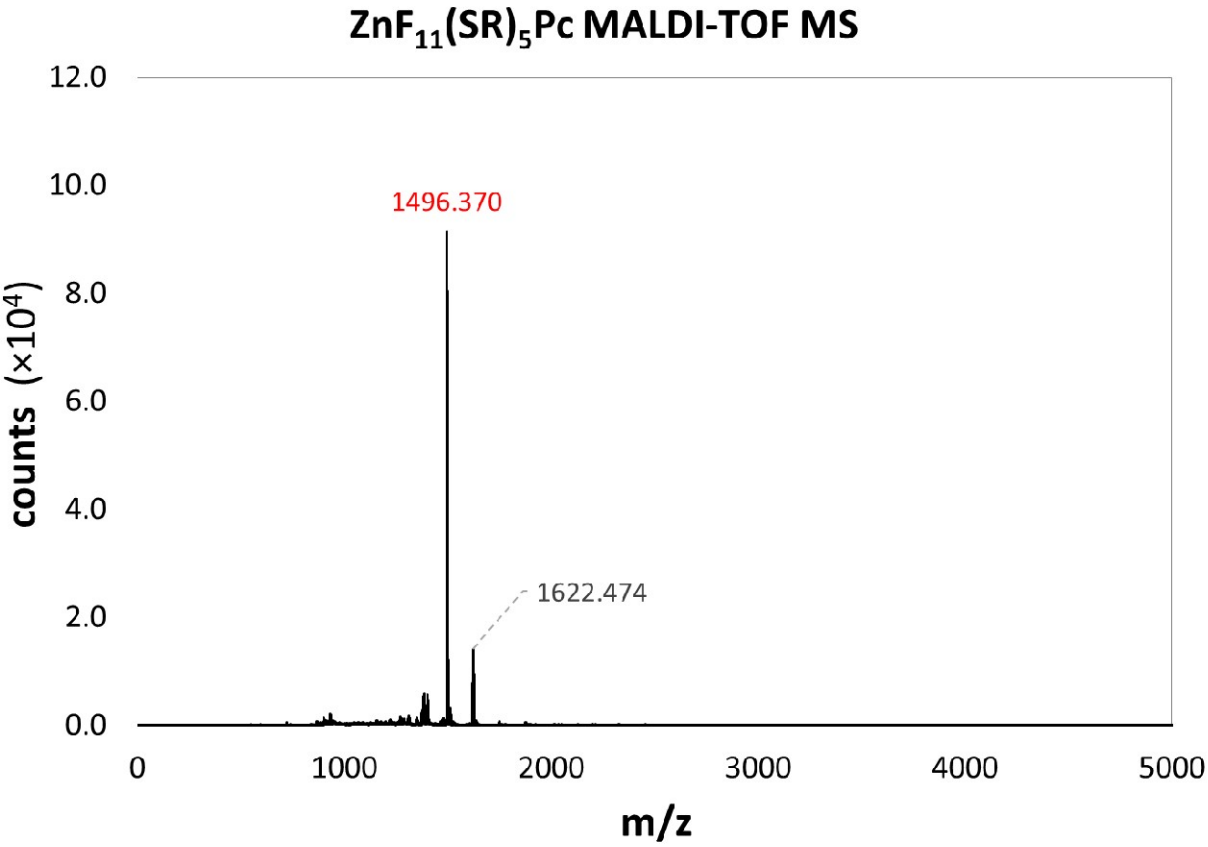


| Structure | Observed Mass Range | | Expected Mass Range | |
|---|---|---|---|---|
| $[ZnF_{11}(SR)_5Pc]^+$ | 1494.35 | 1503.42 | 1494.46 | 1501.47 |
| $[ZnF_{10}(SR)_6Pc]^+$ | 1620.47 | 1628.48 | 1620.57 | 1629.57 |

**Figure C11**. Mass spectrum of Zinc (II) pentakis(octylthio)undecafluorophthalocyanine ($ZnF_{11}(SR)_5Pc$) in a DHB matrix. A very small amount of the hexakis- substituted product is also present. The structural notation is described in detail above.

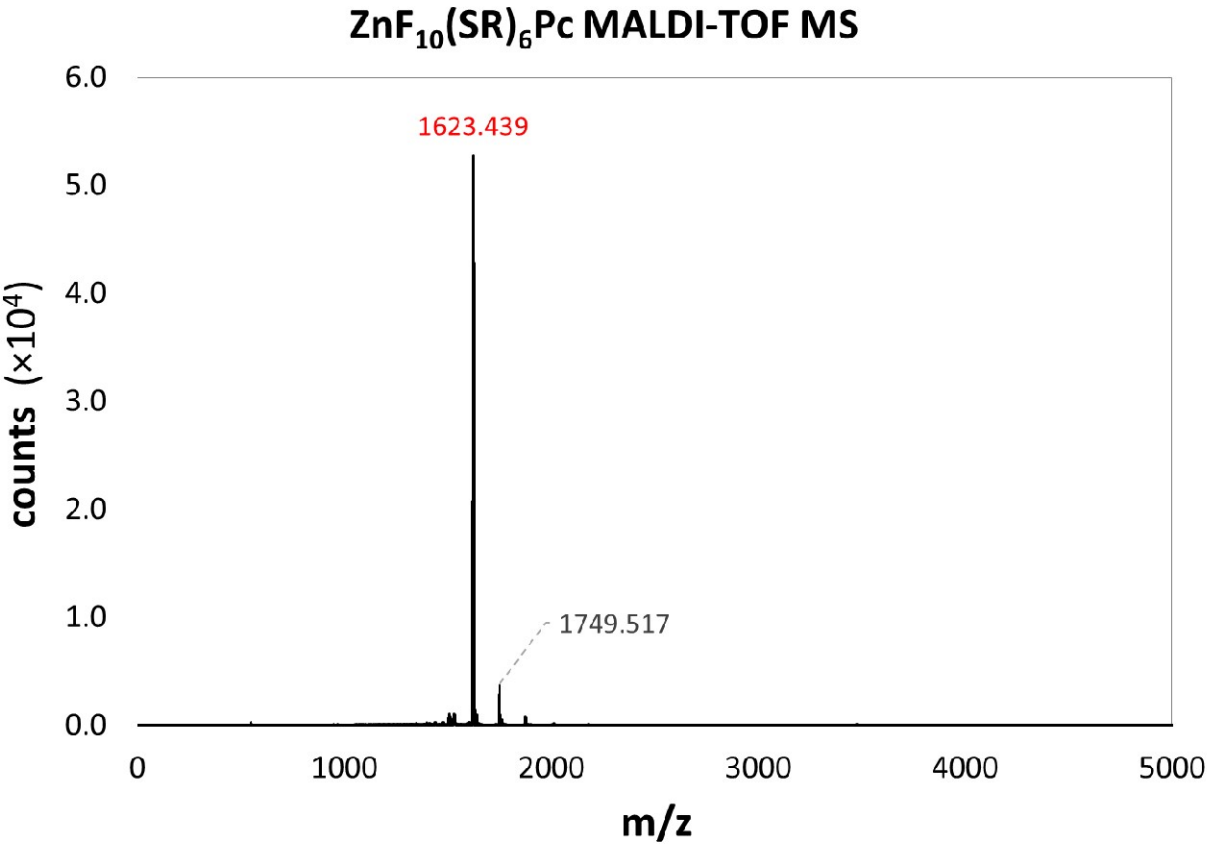


| Structure | | | | Observed Mass Range | | Expected Mass Range | |
|---|---|---|---|---|---|---|---|
| $[ZnF_{10}(SR)_6Pc]^+$ | | | | 1620.43 | 1629.44 | 1620.57 | 1629.57 |
| $[ZnF_9(SR)_7Pc]^+$ | 1745.54 | 1754.51 | 1746.68 | 1755.68 | | | |

**Figure C12**. Mass spectrum of Zinc (II) hexakis(octylthio)decafluorophthalocyanine ($ZnF_{10}(SR)_6Pc$) in a DHB matrix. A very small amount of the heptakis- substituted product is also present. The structural notation is described in detail above.

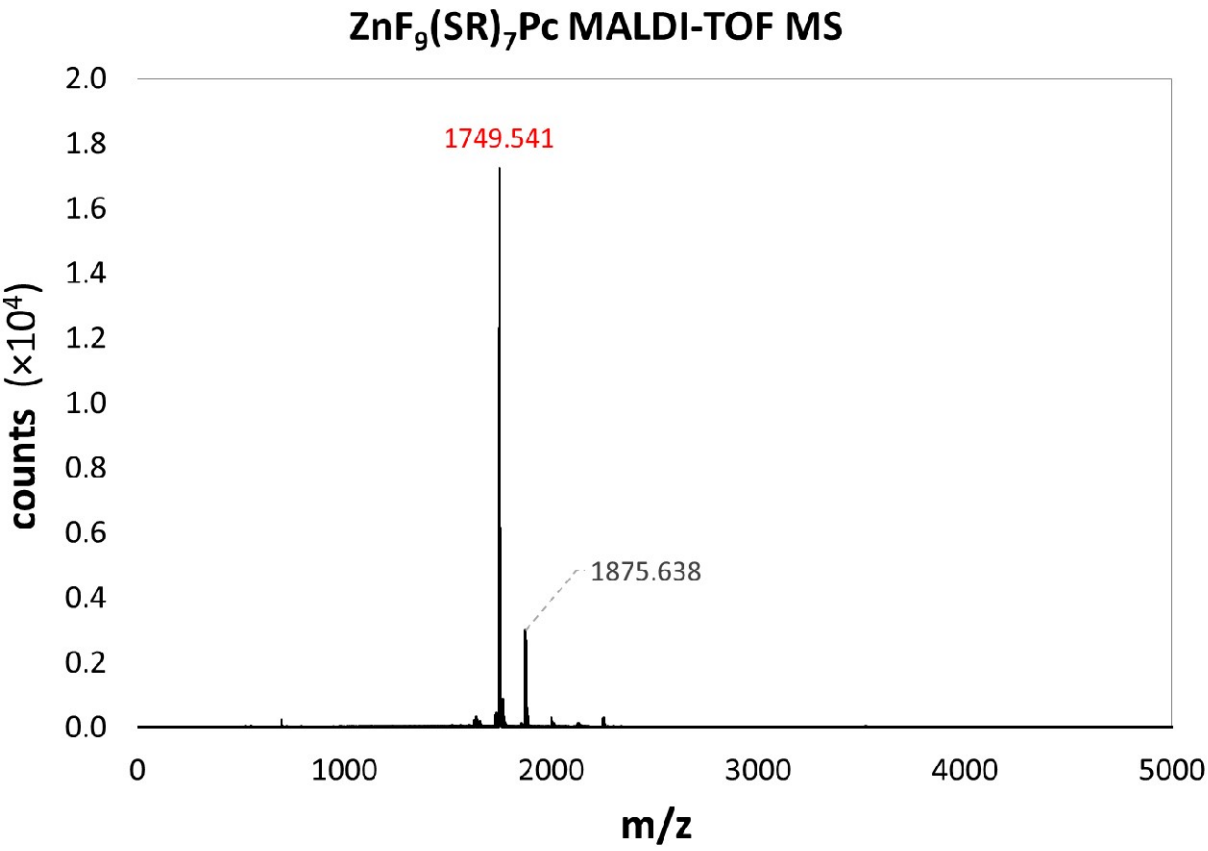


| Structure | Observed Mass Range | | Expected Mass Range | |
|---|---|---|---|---|
| $[ZnF_9(SR)_7Pc]^+$ | 1746.54 | 1755.56 | 1746.68 | 1755.68 |
| $[ZnF_8(SR)_8Pc]^+$ | 1872.63 | 1881.64 | 1872.78 | 1882.78 |

**Figure C13**. Mass spectrum of Zinc (II) heptakis(octylthio)nonafluorophthalocyanine ($ZnF_9(SR)_7Pc$) in a DHB matrix. A very small amount of the octakis- substituted product is also present. The structural notation is described in detail above.

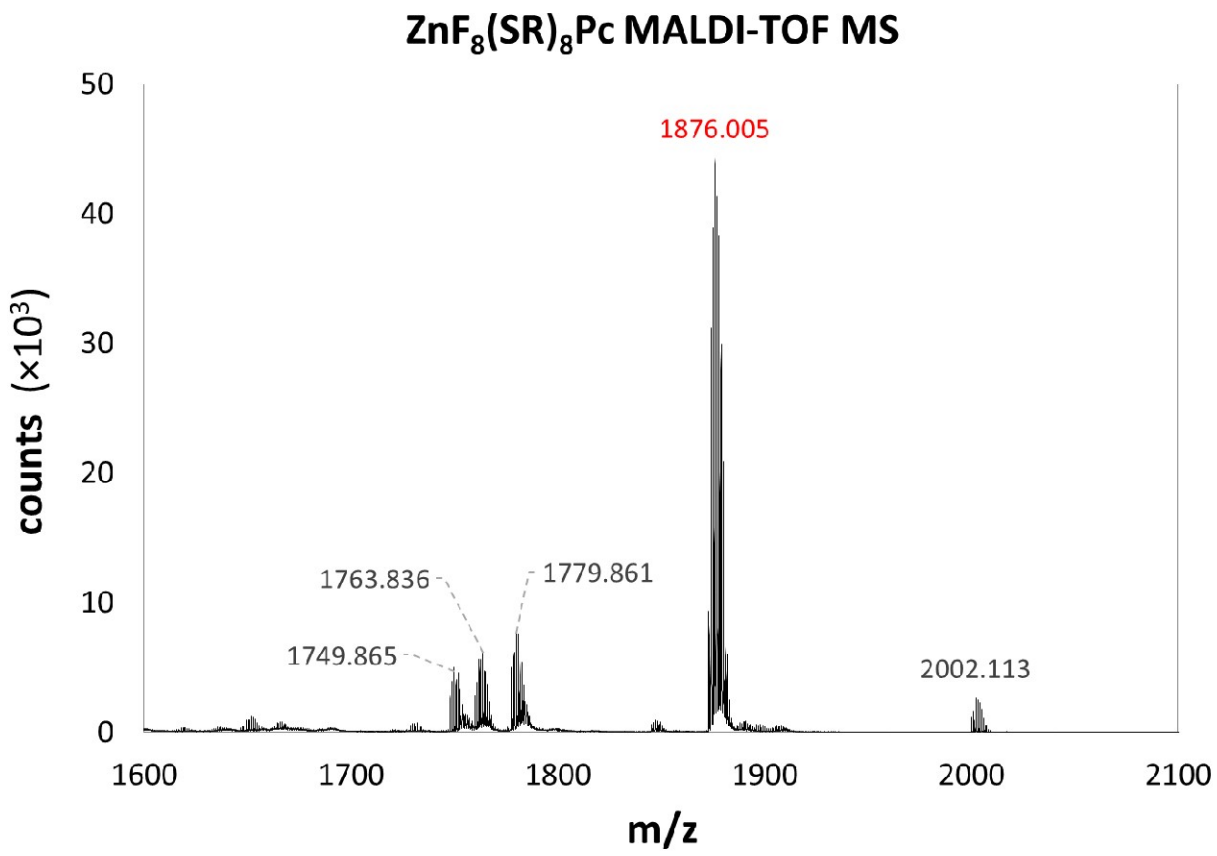


| Structure | Observed Mass Range | | Expected Mass Range | |
|---|---|---|---|---|
| $[ZnF_9(SR)_7Pc]^+$ | 1747.87 | 1755.06 | 1746.68 | 1755.68 |
| $[ZnF_8(SR)_7(SH)Pc]^+$ | 1759.87 | 1767.88 | 1760.66 | 1769.66 |
| $[ZnF_8(SR)_7(SH)OPc]^+$ | 1776.88 | 1784.86 | 1776.65 | 1785.65 |
| $[ZnF_8(SR)_8Pc]^+$ | 1872.99 | 1882.98 | 1872.78 | 1882.78 |
| $[ZnF_7(SR)_9Pc]^+$ | 2000.10 | 2009.14 | 1998.89 | 2008.88 |

**Figure C14**. Mass spectrum of Zinc (II) octakis(octylthio)octafluorophthalocyanine ($ZnF_8(SR)_8Pc$) in a DHB matrix. Some fragmentation and oxidation products are present, as well as very small amounts of the heptakis- and nonakis- substituted products. The structural notation is described in detail above.

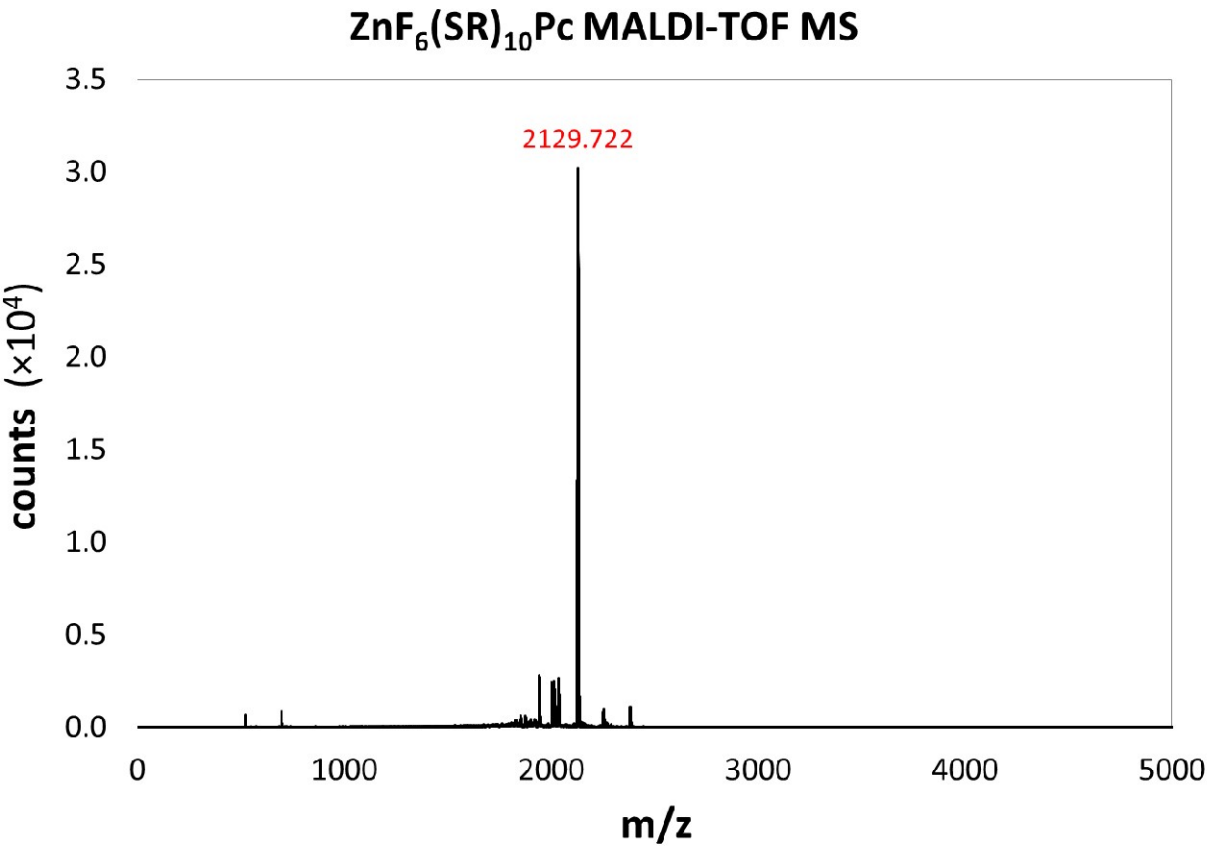


| Structure | Observed Mass Range | | Expected Mass Range | |
|---|---|---|---|---|
| $[ZnF_6(SR)_{10}Pc]^+$ | 2125.72 | 2135.74 | 2125.00 | 2134.00 |

**Figure C15**. Mass spectrum of Zinc (II) decakis(octylthio)hexafluorophthalocyanine ($ZnF_6(SR)_{10}Pc$) in a DHB matrix. Very small amounts of oxidized fragment ions are also present. The structural notation is described in detail above.

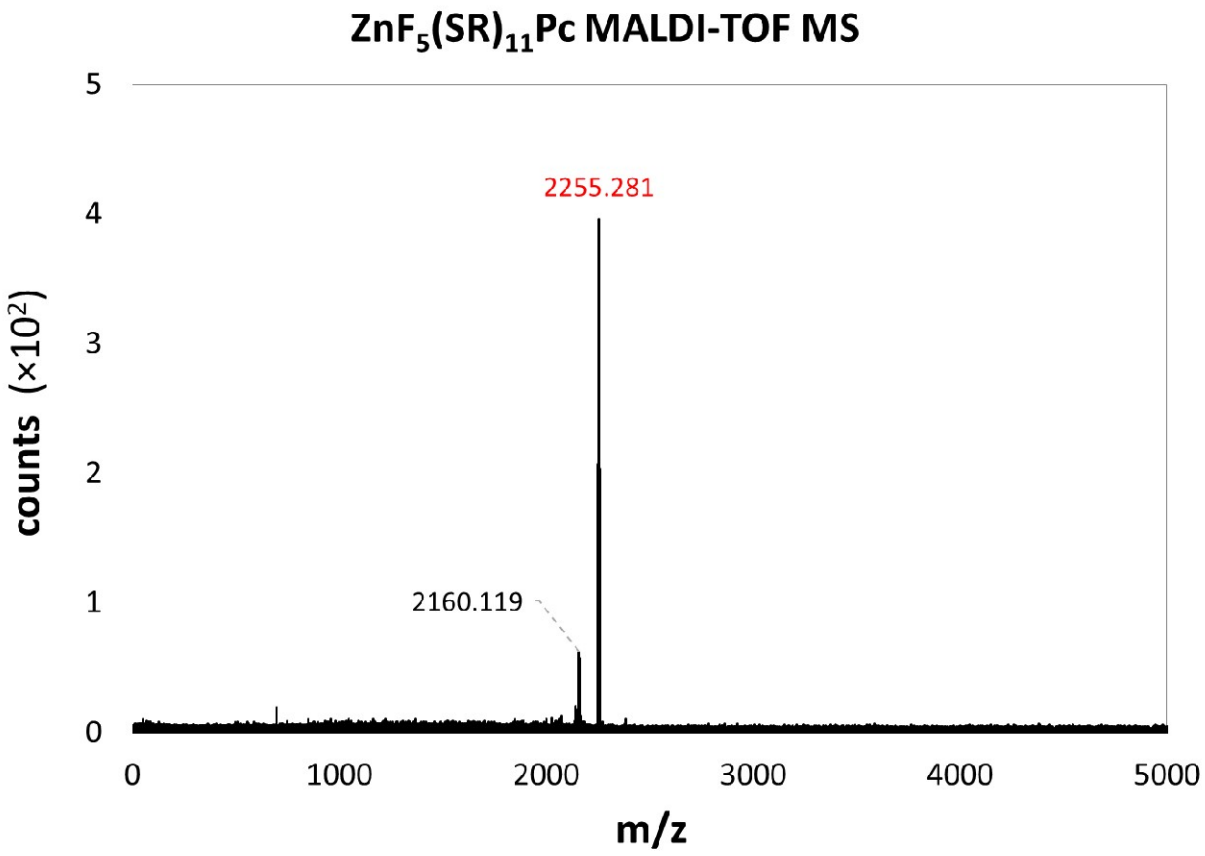


| Structure | Observed Mass Range | | Expected Mass Range | |
|---|---|---|---|---|
| $[ZnF_5(SR)_{10}(SH)OPc+H]^+$ | 2156.13 | 2165.22 | 2155.98 | 2165.97 |
| $[ZnF_5(SR)_{11}Pc+H]^+$ | 2252.26 | 2260.27 | 2252.11 | 2262.10 |

**Figure C16**. Mass spectrum of Zinc (II) undecakis(octylthio)pentafluorophthalocyanine ($ZnF_5(SR)_{11}Pc$) in a DHB matrix. A small amount of an oxidized fragment ion is also present. The structural notation is described in detail above.

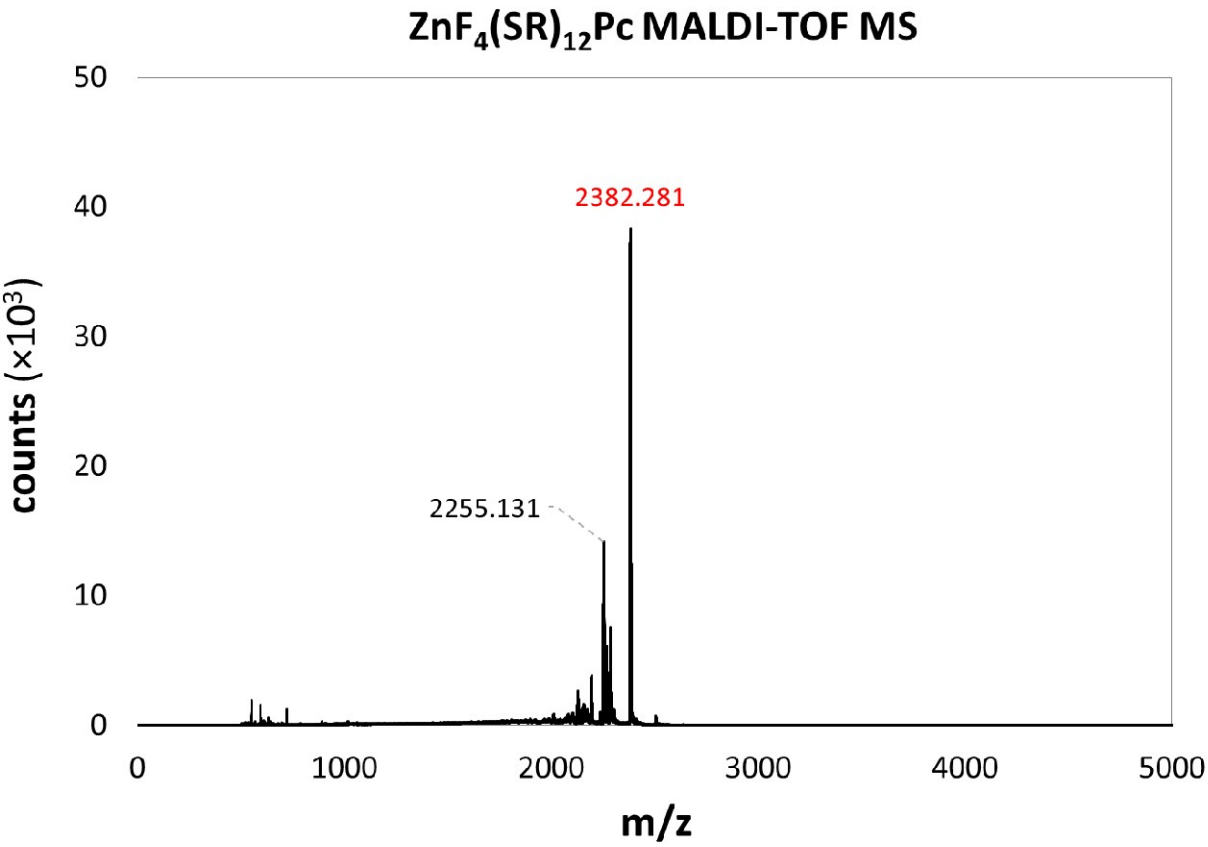


| Structure | Observed Mass Range | | Expected Mass Range | |
|---|---|---|---|---|
| $[ZnF_5(SR)_{11}Pc+H]^+$ | 2252.16 | 2262.19 | 2252.11 | 2262.10 |
| $[ZnF_4(SR)_{12}Pc+H]^+$ | 2378.27 | 2388.29 | 2378.21 | 2388.21 |

**Figure C17**. Mass spectrum of Zinc (II) dodecakis(octylthio)tetrafluorophthalocyanine ($ZnF_4(SR)_{12}Pc$) in a DHB matrix. A small amount of the undecakis- substituted product is also present. The structural notation is described in detail above.

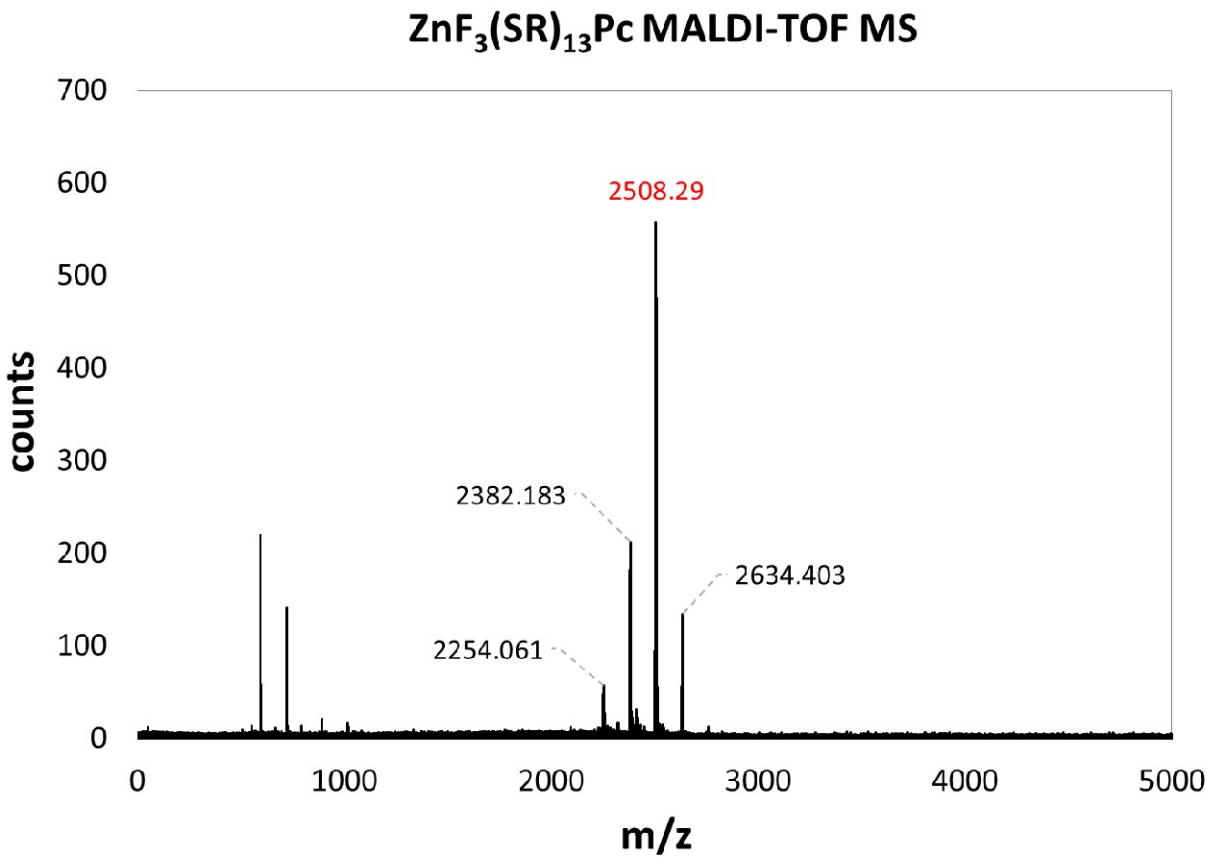


| Structure | Observed Mass Range | | Expected Mass Range | |
|---|---|---|---|---|
| $[ZnF_5(SR)_{11}Pc+H]^+$ | 2252.04 | 2261.16 | 2252.11 | 2262.10 |
| $[ZnF_4(SR)_{12}Pc+H]^+$ | 2378.20 | 2388.15 | 2378.21 | 2389.22 |
| $[ZnF_3(SR)_{13}Pc+H]^+$ | 2504.29 | 2513.27 | 2504.32 | 2515.31 |
| $[ZnF_2(SR)_{14}Pc+H]^+$ | 2630.39 | 2639.42 | 2630.43 | 2642.42 |

**Figure C18**. Mass spectrum of Zinc (II) triskadecakis(octylthio)trifluorophthalocyanine ($ZnF_3(SR)_{13}Pc$) in a DHB matrix. Small amounts of the undecakis-, dodecakis-, and tetradecakis- substituted products are also present, as well as some unidentified smaller fragments. The structural notation is described in detail above.

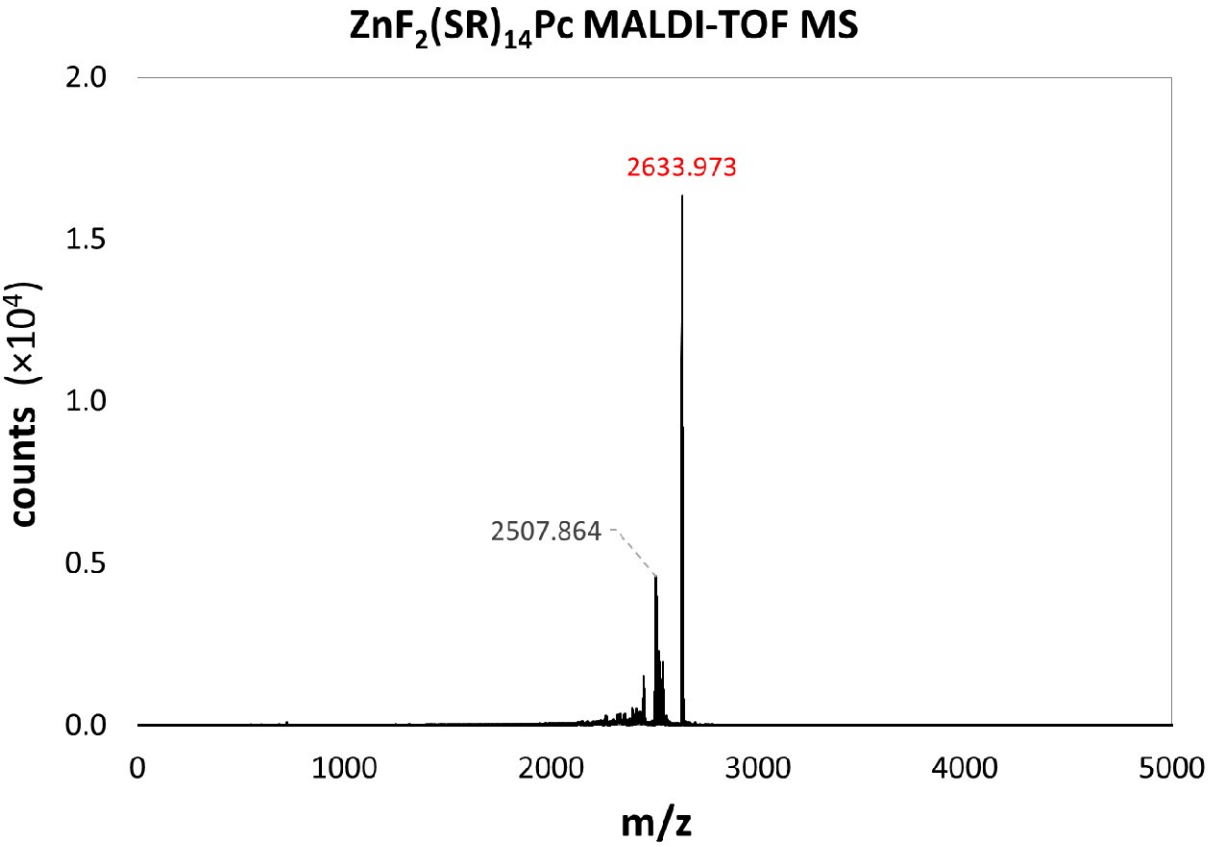


| Structure | Observed Mass Range | | Expected Mass Range | |
|---|---|---|---|---|
| $[ZnF_3(SR)_{13}Pc]^+$ | 2503.85 | 2513.86 | 2503.32 | 2514.31 |
| $[ZnF_2(SR)_{14}Pc]^+$ | 2629.98 | 2640.98 | 2629.42 | 2641.42 |

**Figure C19**. Mass spectrum of Zinc (II) tetradecakis(octylthio)difluorophthalocyanine ($ZnF_2(SR)_{14}Pc$) in a DHB matrix. A small amount of the triskadecakis- substituted product is also presents. The structural notation is described in detail above.

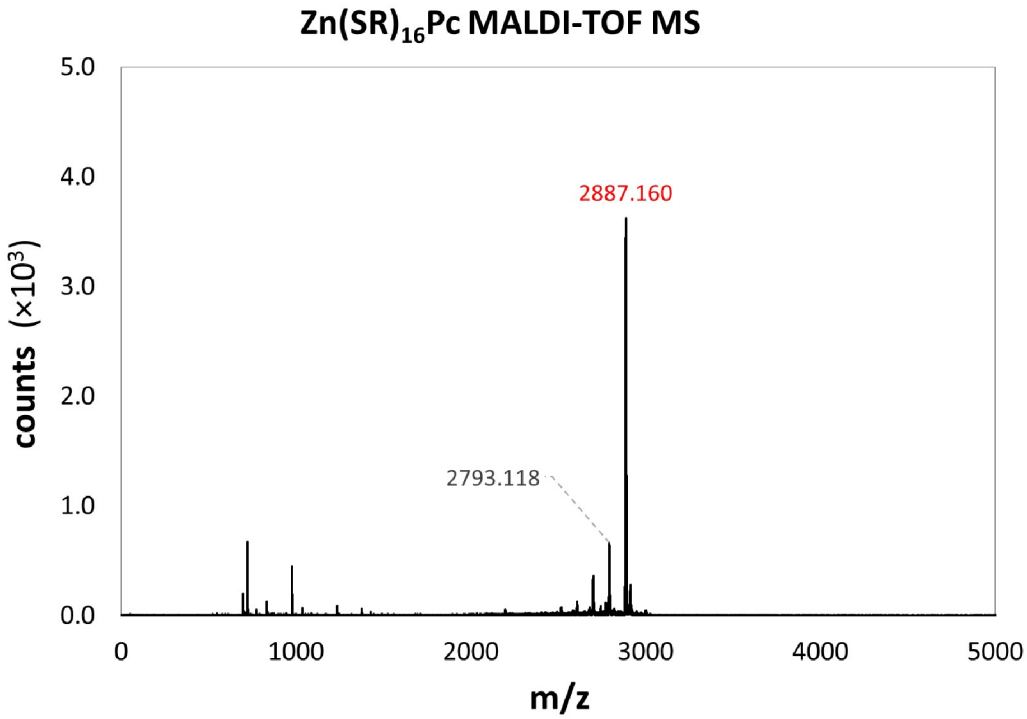


| Structure | Observed Mass Range | | Expected Mass Range | |
|---|---|---|---|---|
| $[Zn(SR)_{15}(SH)OPc]^+$ | 2789.12 | 2797.12 | 2786.50 | 2797.51 |
| $[Zn(SR)_{16}Pc]^+$ | 2882.19 | 2894.17 | 2881.64 | 2893.64 |

**Figure C20**. Mass spectrum of Zinc (II) hexadecakis(octylthio)phthalocyanine ($Zn(SR)_{16}Pc$) in a DHB matrix. Small amounts of some oxidized fragments are also present. The structural notation is described in detail above.

## C7. References


1. Williams, A. Loopless Generation of Multiset Permutations using a Constant Number of Variables by Prefix Shifts. *Proceedings of the Twentieth Annual ACM-SIAM Symposium on Discrete Algorithms* **2009**, 987.
2. Golchoubian, H.; Hosseinpoor, F. Effective Oxidation of Sulfides to Sulfoxides with Hydrogen Peroxide under Transition-Metal-Free Conditions. *Molecules* **2007**, *12*, 304.
3. Chidawanyika, W.; Nyokong, T. The synthesis and photophysicochemical properties of low-symmetry zinc phthalocyanine analogues. *J. Photochem. Photobiol., A Chem.* **2009**, *206*, 169.
4. Garcia, A. M.; Alarcon, E.; Munoz, M.; Scaiano, J. C.; Edwards, A. M.; Lissi, E. Photophysical behaviour and photodynamic activity of zinc phthalocyanines associated to liposomes. *Photochem. Photobiol. Sci.* **2011**, *10*, 507.

# Appendix D. Supporting Information for Chapter 5

## D1. Z-Coordinate Plots

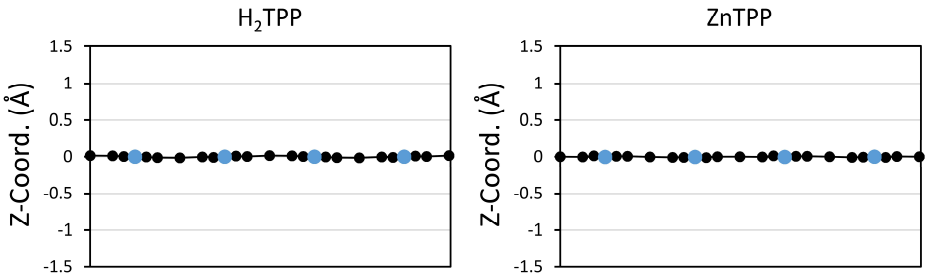


**Figure D2**. Z-coordinates of the core atoms of $H_2$TPP (left) and ZnTPP (right). Carbon atoms are black and nitrogen atoms are blue.

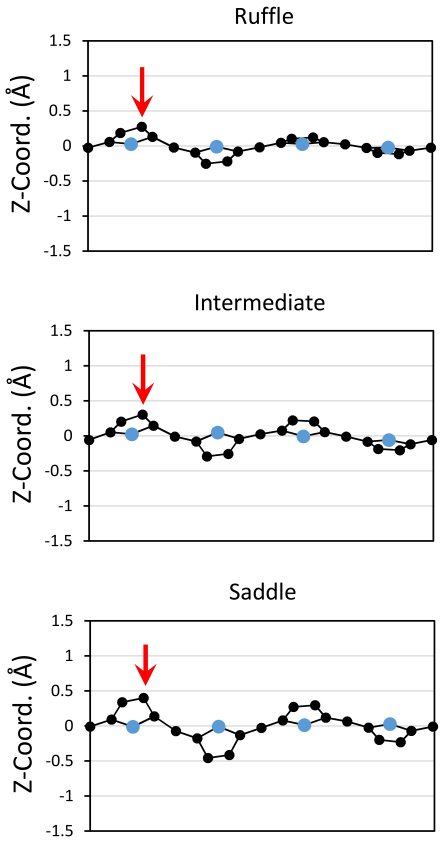


**Figure D1**. Z-coordinates of the core atoms for the three principle conformations of Zn($NO_2$)TPP. The red arrow points to the nitro-bearing pyrrole carbon. The horizontal axis is arbitrary. The planar deviations increase on going from the ruffled to intermediate to saddled conformations. Carbon atoms are black and nitrogen atoms are blue.

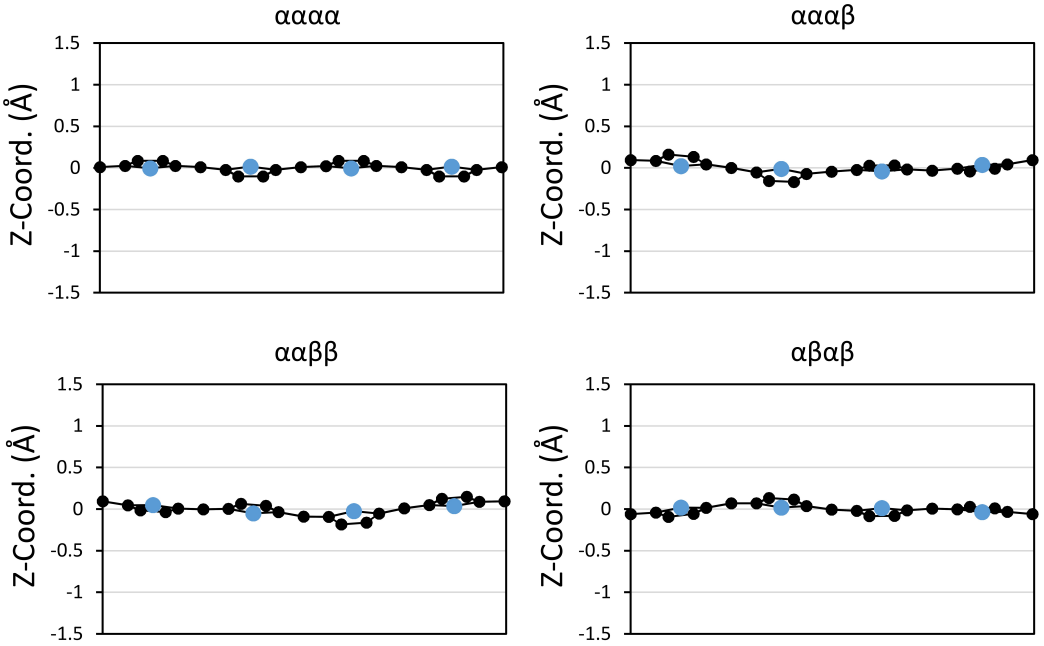


**Figure D3**. Z-coordinates of the core atoms for the four atropisomers of $H_2(NO_2)_4TPP$. The horizontal axis is arbitrary. Carbon atoms are black and nitrogen atoms are blue.

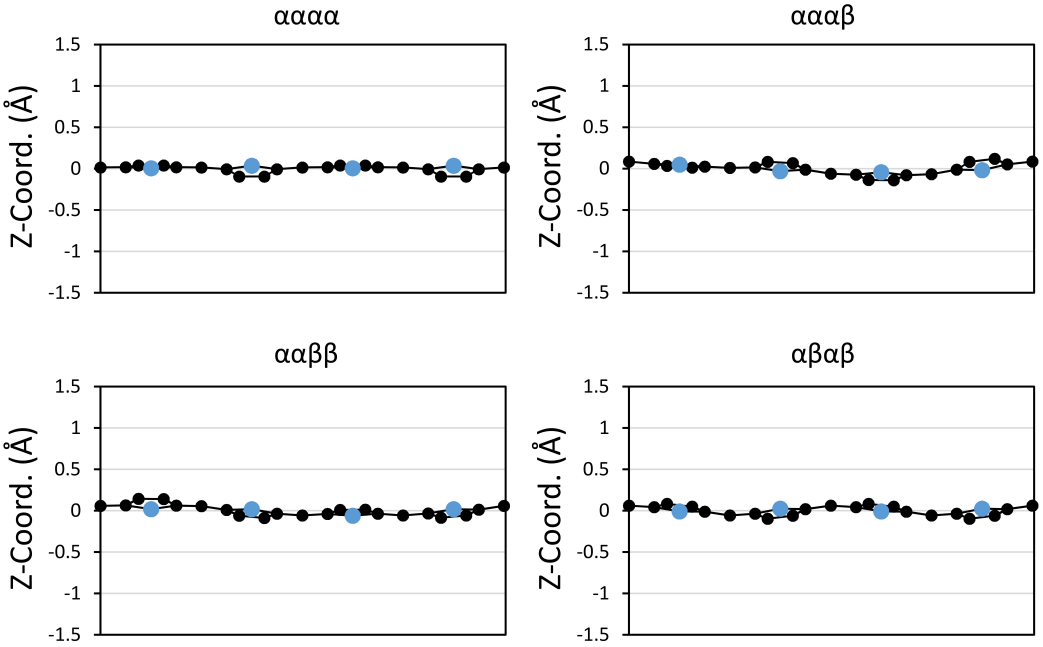


**Figure D4**. Z-coordinates of the core atoms for the four atropisomers of $Zn(NO_2)_4TPP$. The horizontal axis is arbitrary. Carbon atoms are black and nitrogen atoms are blue.

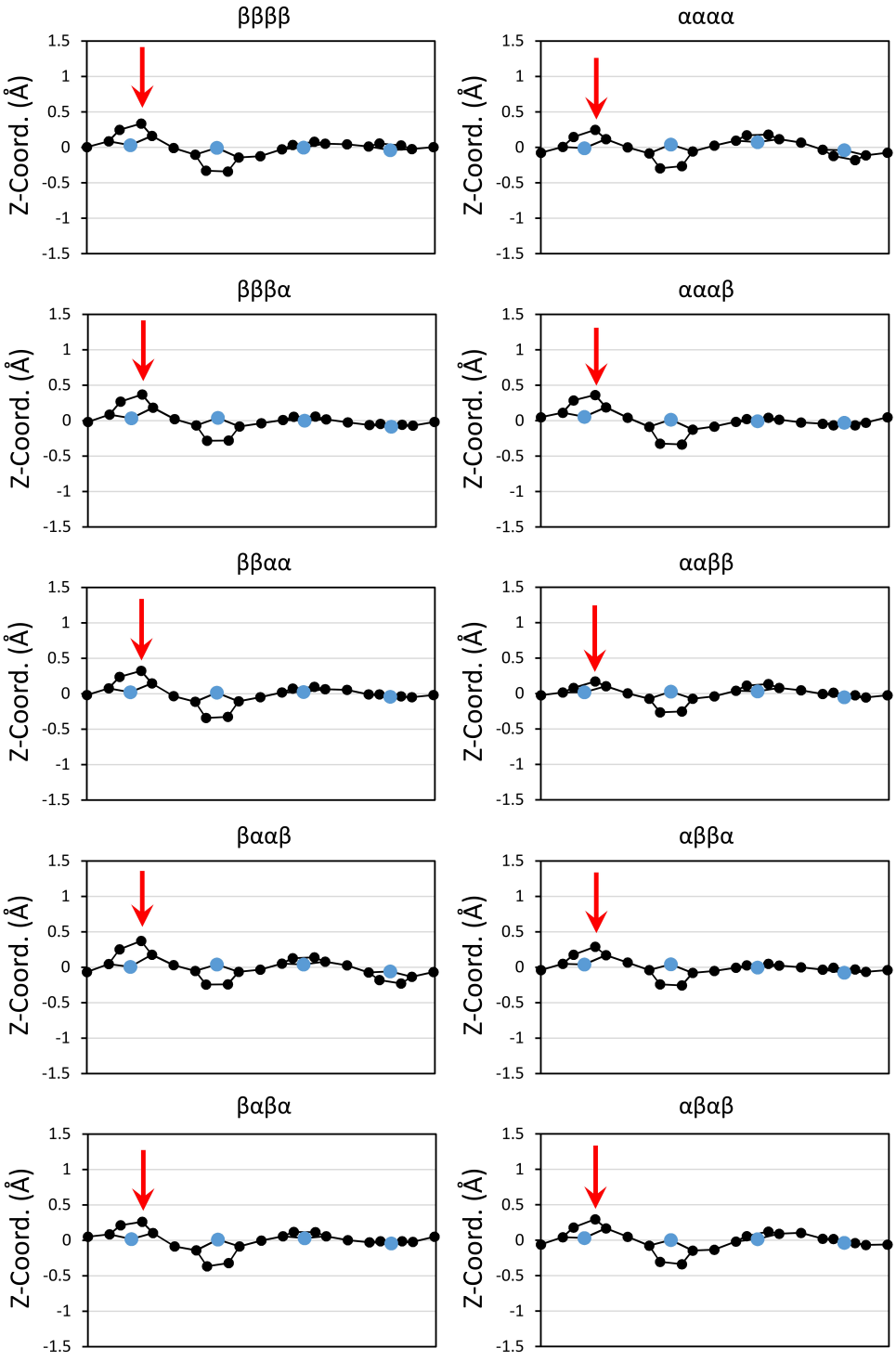


**Figure D5**. Z-coordinates of the core atoms for some of the conformers of $H_2(NO_2)_5TPP$. The red arrow points to the nitro-bearing pyrrole carbon. The horizontal axis is arbitrary. All of the atropisomers adopt an intermediate conformation. Carbon atoms are black and nitrogen atoms are blue.

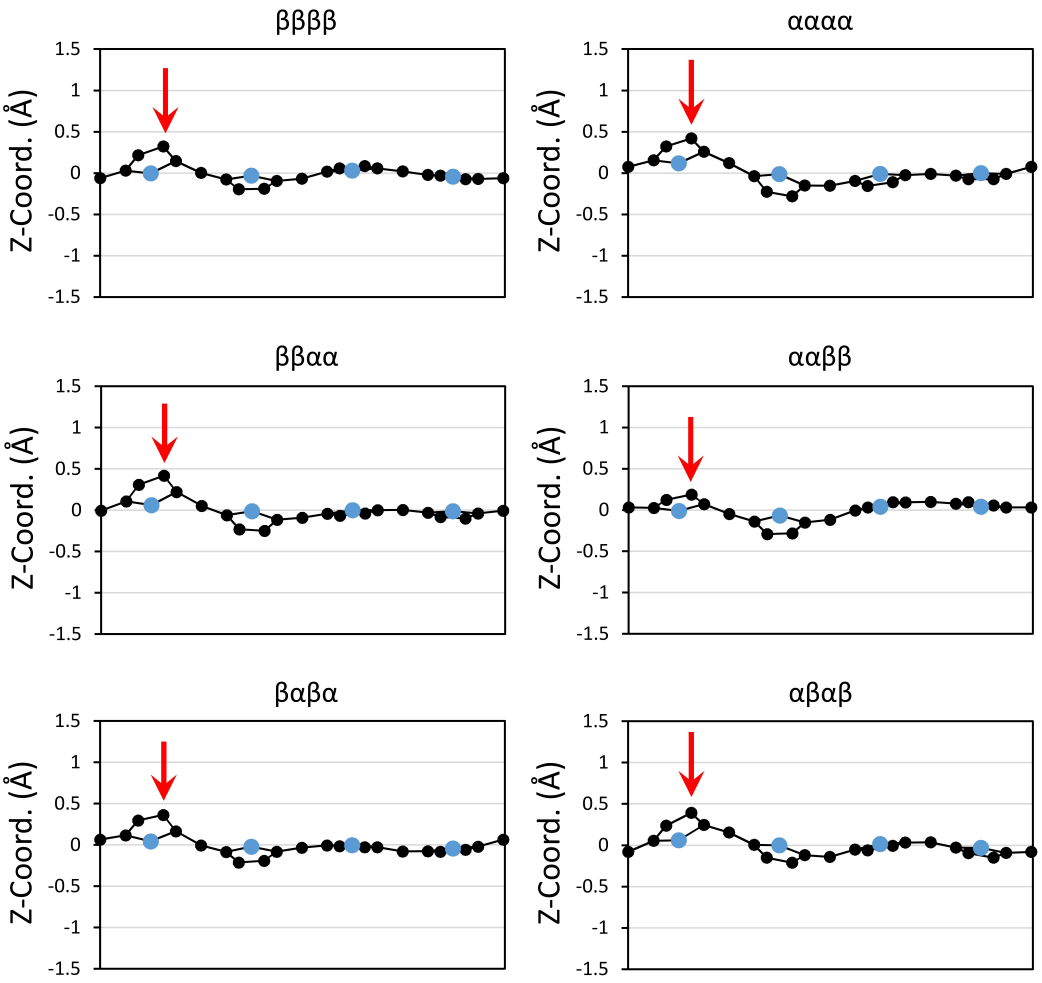


**Figure D6**. Z-coordinates of the core atoms for some of the conformers of $Zn(NO_2)_5TPP$. The red arrow points to the nitro-bearing pyrrole carbon. The horizontal axis is arbitrary. Carbon atoms are black and nitrogen atoms are blue.

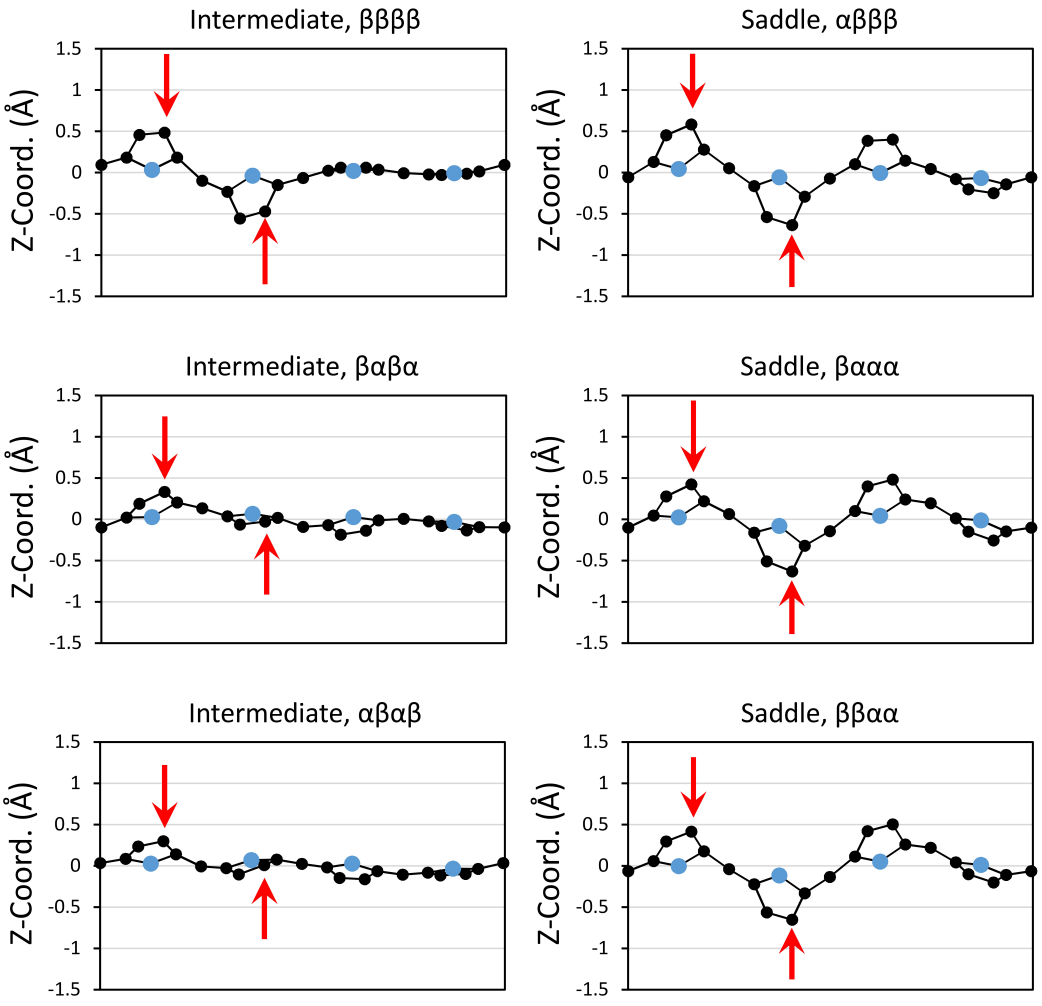


**Figure D7**. Z-coordinates of the core atoms for some of the conformers of $H_2(NO_2)_6TPP$. The red arrows point to the nitro-bearing pyrrole carbons. The horizontal axis is arbitrary. Carbon atoms are black and nitrogen atoms are blue.

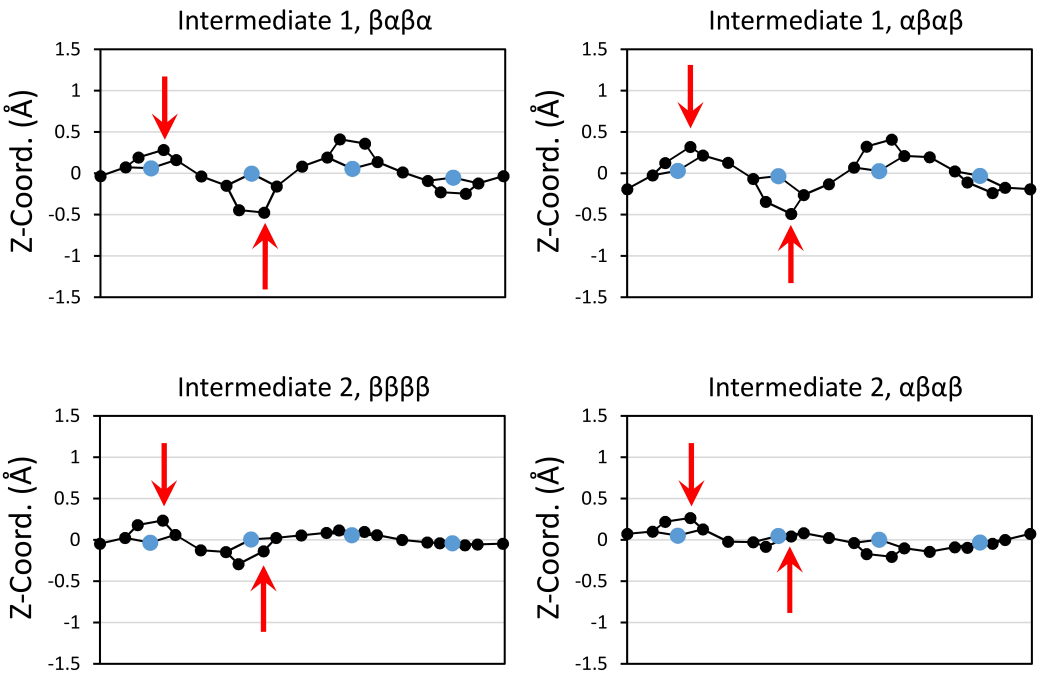


**Figure D8**. Z-coordinates of the core atoms for some of the conformers of $Zn(NO_2)_6TPP$. The red arrows point to the nitro-bearing pyrrole carbons. The horizontal axis is arbitrary. Carbon atoms are black and nitrogen atoms are blue.

## D2. Molecular Energy Level Diagram for $H_2(NO_2)_5TPP$

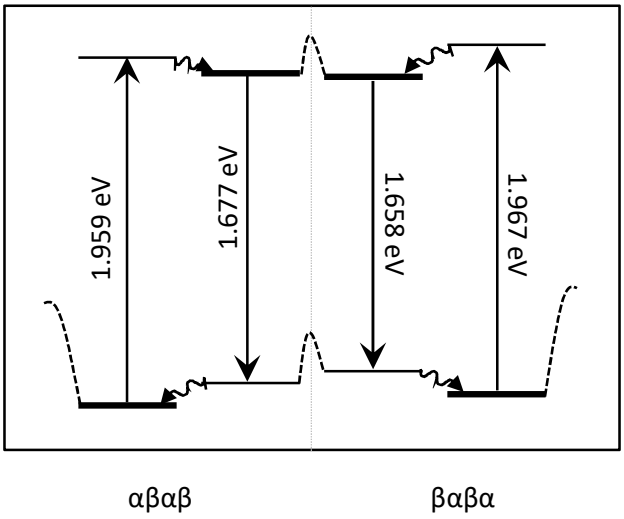


**Figure D9**. Schematic energy level diagram of the two principle conformations of $H_2(NO_2)_5TPP$. The thick lines represent optimized or relaxed nuclear geometries, and the dashed lines represent (unknown) barriers to interconversion between these relaxed geometries. The unrelaxed geometries may be able to internally convert to either stable structure (for both $S_0$ and $S_1$), potentially scrambling the populations.

## D3. Ground State Orbital Energies for the Zinc Nitro-Porphyrins

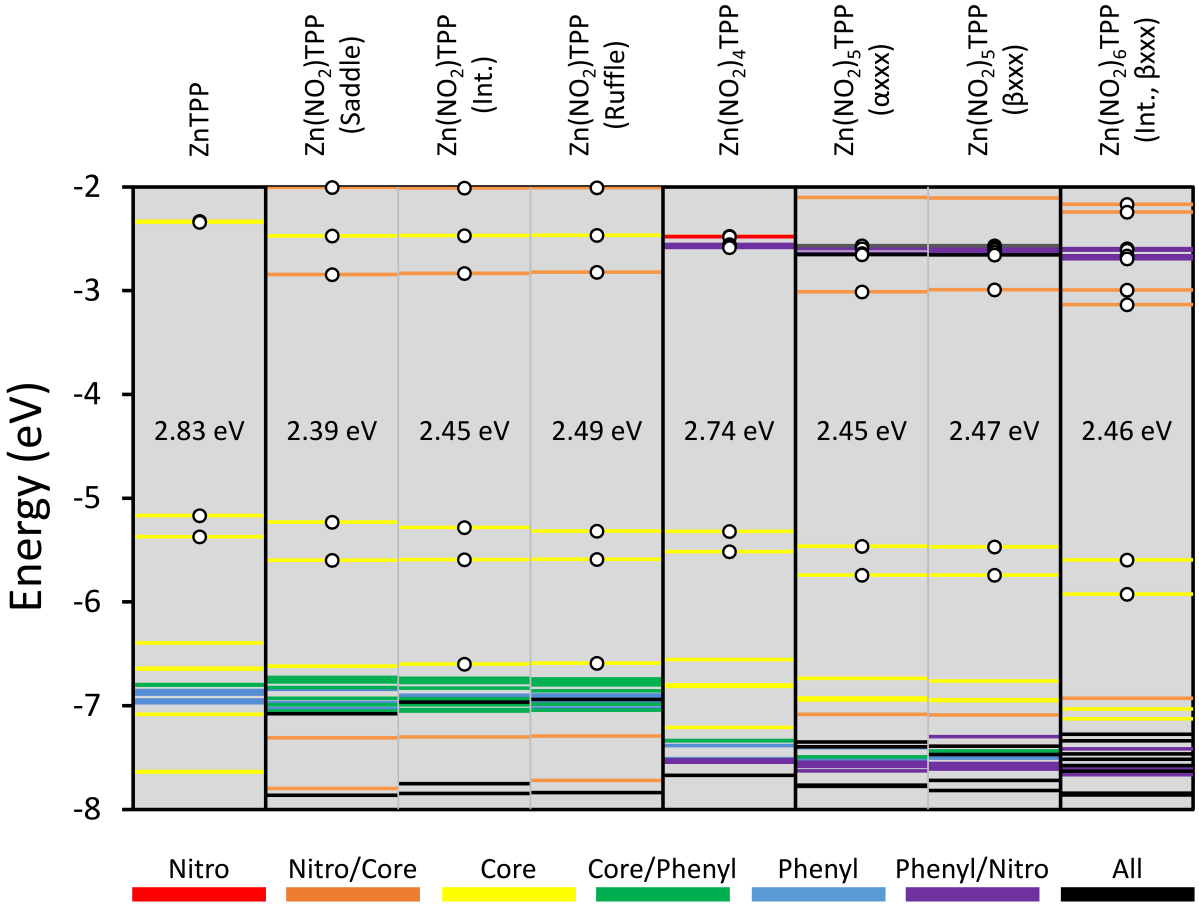


**Figure D10**. Ground state orbital energies for the series of zinc nitro-Pors. The HOMO-LUMO gap energies are given in the gap for each compound. The energy levels are color coded according to the localization of the orbital density, as shown in the key at the bottom. Orbitals involved in the first few TD-DFT transitions are marked with open circles.

## D4. TD-DFT Results for the Free Base Nitro-Porphyrin

**Table D1**. TD-DFT transitions for two conformations of $H_2(NO_2)_6TPP$.

| ΔE (eV)[a] | λ (nm)[b] | *f*[c] | Wavefunction[d] |
|---|---|---|---|
| | | | ***$H_2(NO_2)_6$TPP (Intermediate, αxxx)*** |
| 1.987 | 624 | 0.033 | **12% (H-1→L)** + **13% (H-1→L+1)** + **37% (H→L)** + **37% (H→L+1)** + … |
| 2.087 | 594 | 0.041 | **13% (H-1→L)** + **10% (H-1→L+1)** + **40% (H→L)** + **36% (H→L+1)** + … |
| 2.659 | 466 | 0.160 | **37% (H-1→L+1)** + **9% (H→L)** + 47% (H→L+6) + … |
| 2.709 | 458 | 0.419 | **48% (H-1→L)** + **6% (H-1→L+1)** + **15% (H→L+1)** + 23% (H→L+7) + … |
| | | | ***$H_2(NO_2)_6$TPP (Saddle, βxxx)*** |
| 1.954 | 635 | 0.034 | **24% (H-1→L)** + **74% (H→L+1)** + … |
| 2.017 | 615 | 0.059 | **18% (H-1→L+1)** + **81% (H→L)** + … |
| 2.608 | 475 | 0.138 | **9% (H-1→L)** + **36% (H-1→L+1)** + 44% (H→L+6) + … |
| 2.672 | 464 | 0.427 | **46% (H-1→L)** + **12% (H-1→L+1)** + **12% (H→L+1)** + 17% (H→L+7) + … |
| 2.917 | 425 | 0.021 | 94% (H-1→L+2) + … |
| 3.000 | 413 | 0.017 | 83% (H-1→L+5) + 8% (H→L+7) + … |

[a] Energy of the transition in electron volts. Only transitions with energies below 3.0 eV are given. [b] Transition wavelength in nanometers. [c] Calculated oscillator strengths. Only transitions with oscillator strengths greater than 0.01 are given. [d] Excited state wavefunction, in terms of the contributions of single excitations of the ground state Slater determinant. Only single excitations with contributions greater than 5% are given. The HOMO is designated "H", the second HOMO is "H-1", *etc*. The LUMO is designated "L", the second LUMO is "L+1", *etc*. Excitations involving only orbitals corresponding to Gouterman's four-orbital model are shown in **bold**. Excitations which populate a nitro or nitro-like orbital are underlined.

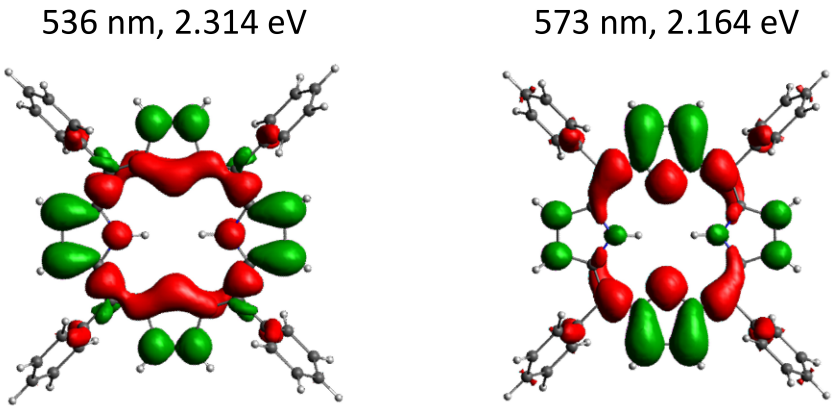


**Figure D11**. Electron density-difference maps for the lowest energy transitions of $H_2TPP$. The red regions are areas that lose electron density in the transition, and the green areas gain electron density.

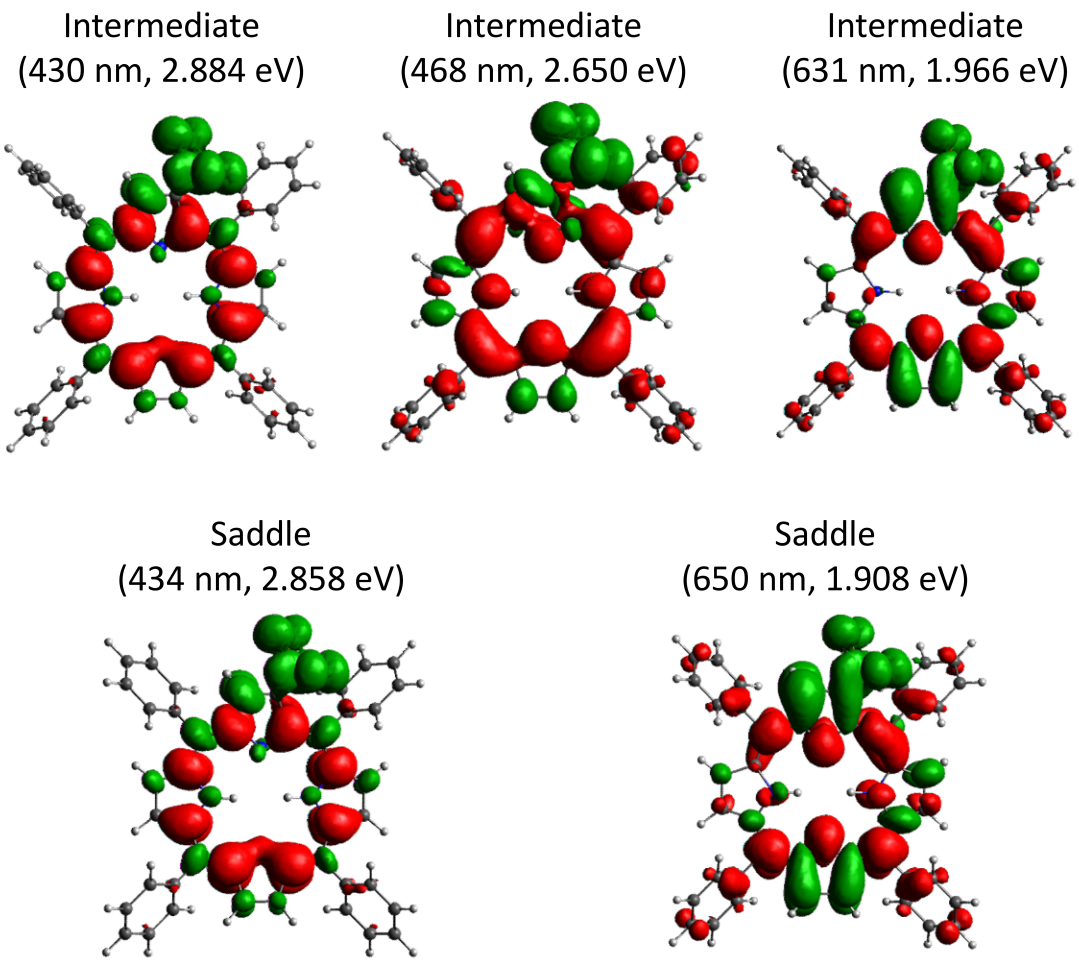


**Figure D13**. Electron density-difference maps for the lowest energy transitions of the intermediate (top row) and saddle (bottom row) conformations of $H_2(NO_2)TPP$. The red regions are areas that lose electron density in the transition, and the green areas gain electron density.

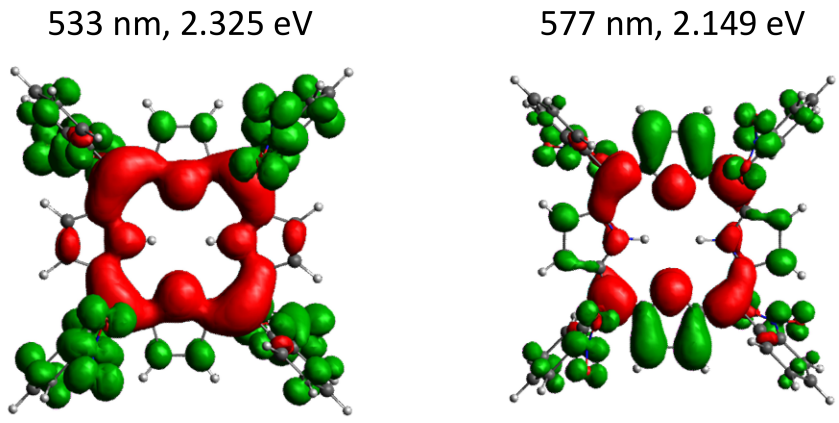


**Figure D12**. Electron density-difference maps for the lowest energy transitions of the αβαβ atropisomer of $H_2(NO_2)_4TPP$. The red regions are areas that lose electron density in the transition, and the green areas gain electron density.

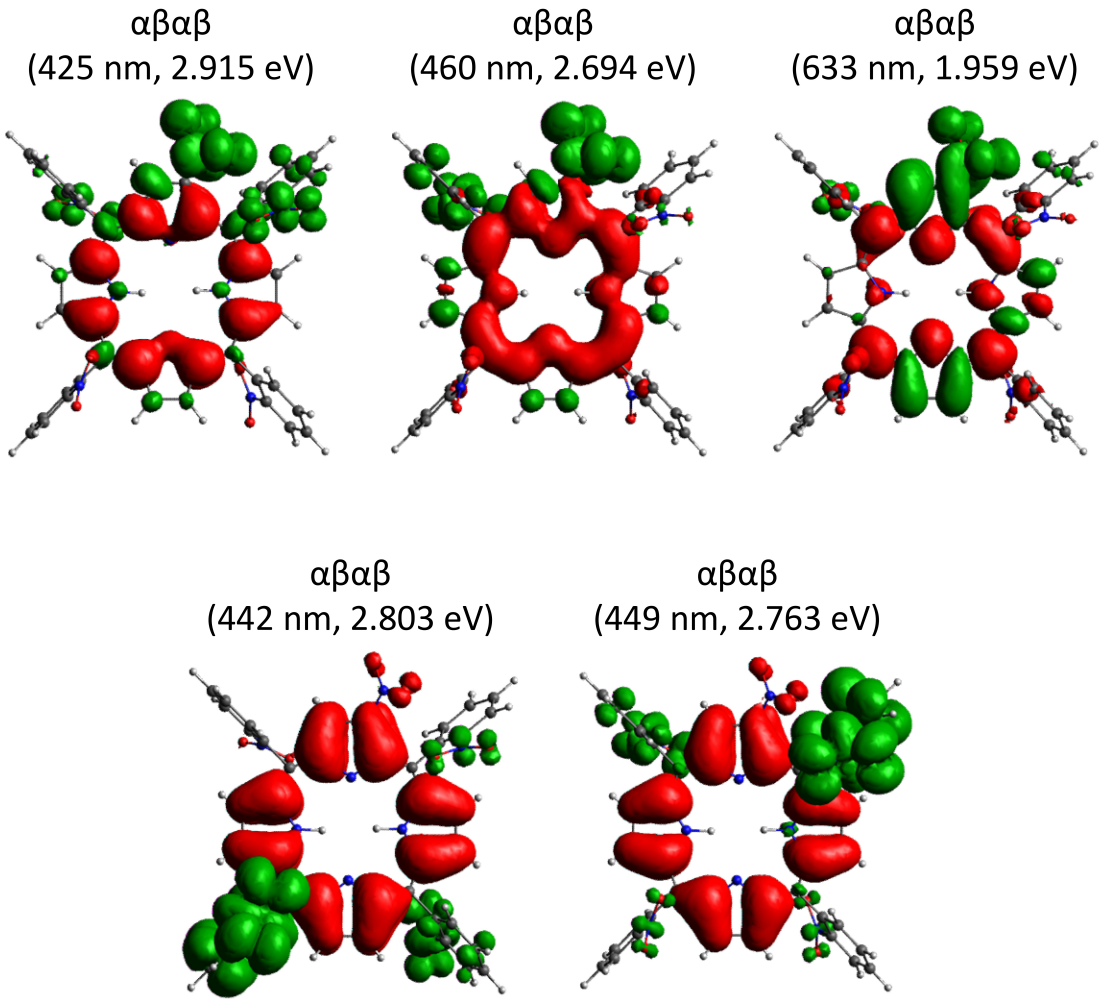


**Figure D14**. Electron density-difference maps for the lowest energy transitions of the αβαβ atropisomer of $H_2(NO_2)_5TPP$. The red regions are areas that lose electron density in the transition, and the green areas gain electron density.

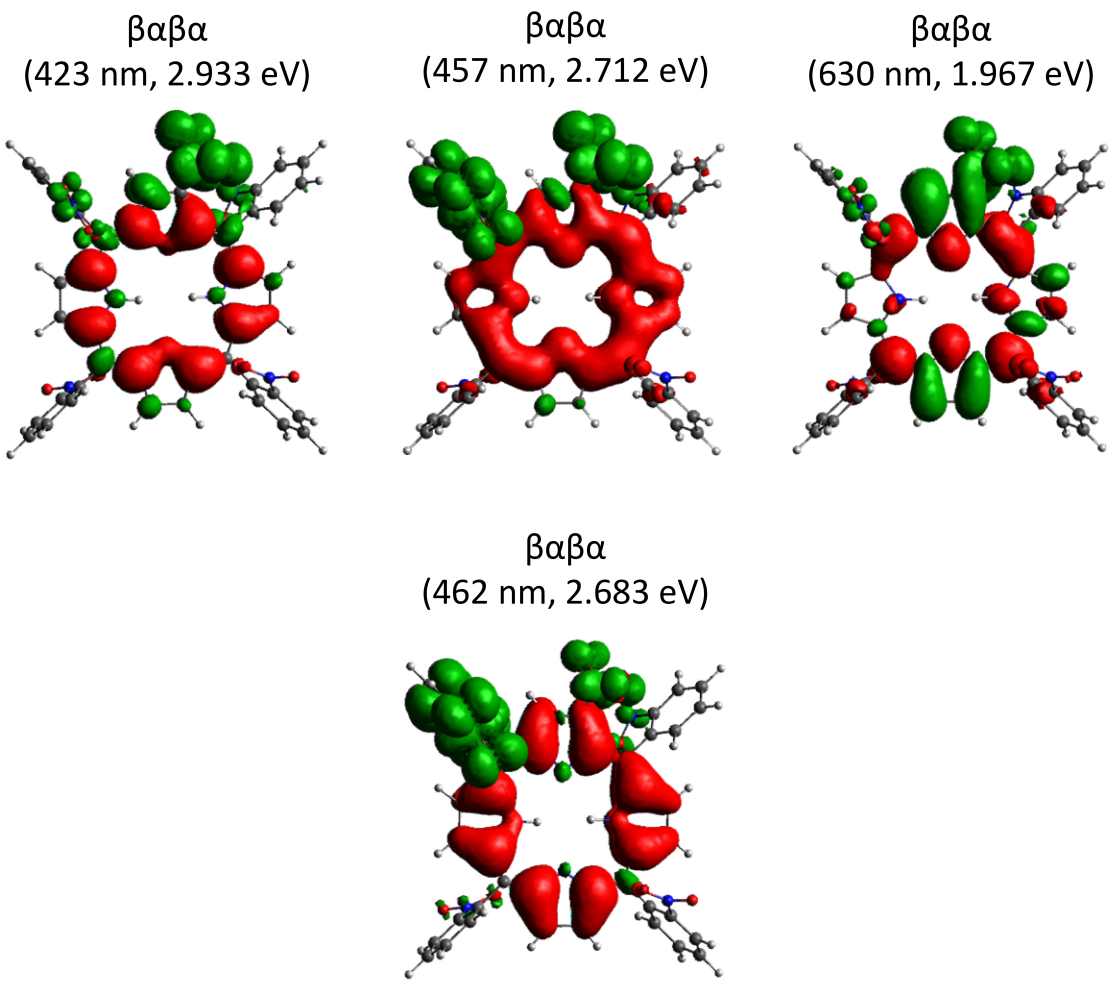


**Figure D15**. Electron density-difference maps for the lowest energy transitions of the βαβα atropisomer of $H_2(NO_2)_5TPP$. The red regions are areas that lose electron density in the transition, and the green areas gain electron density.

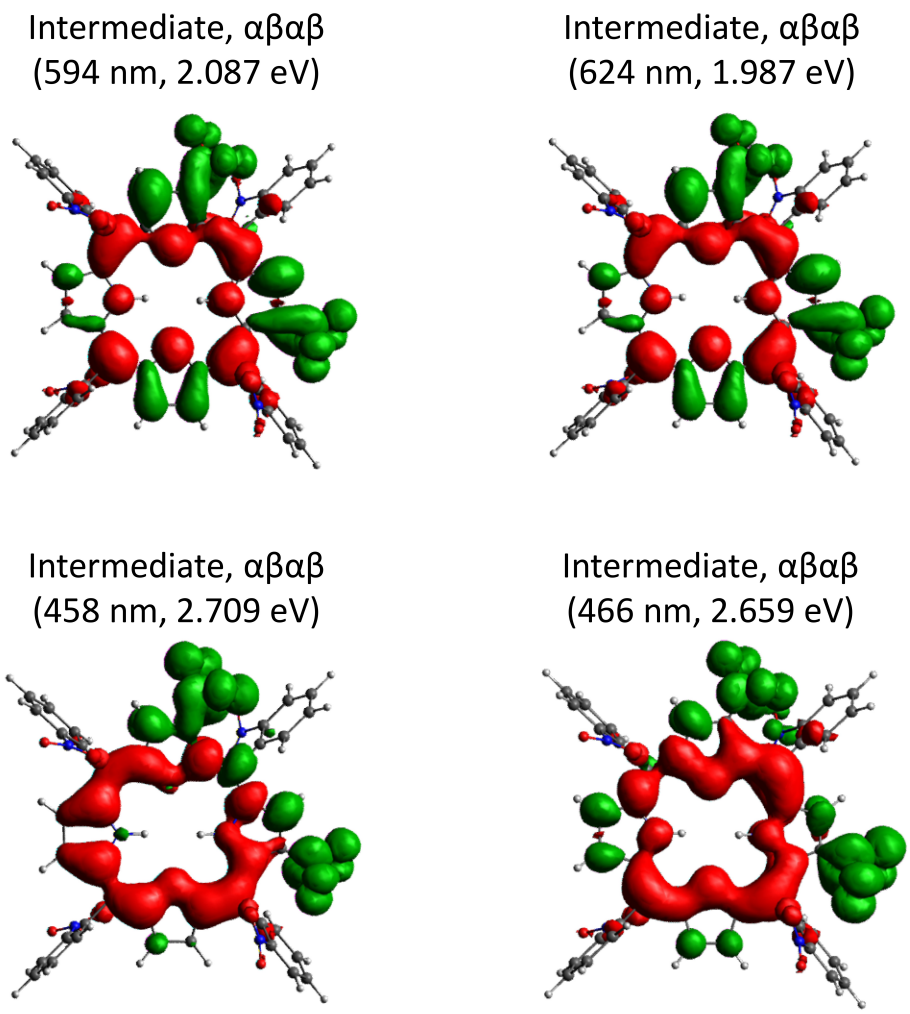


**Figure D16**. Electron density-difference maps for the lowest energy transitions of the αβαβ atropisomer of the intermediate structure of $H_2(NO_2)_6TPP$. The red regions are areas that lose electron density in the transition, and the green areas gain electron density.

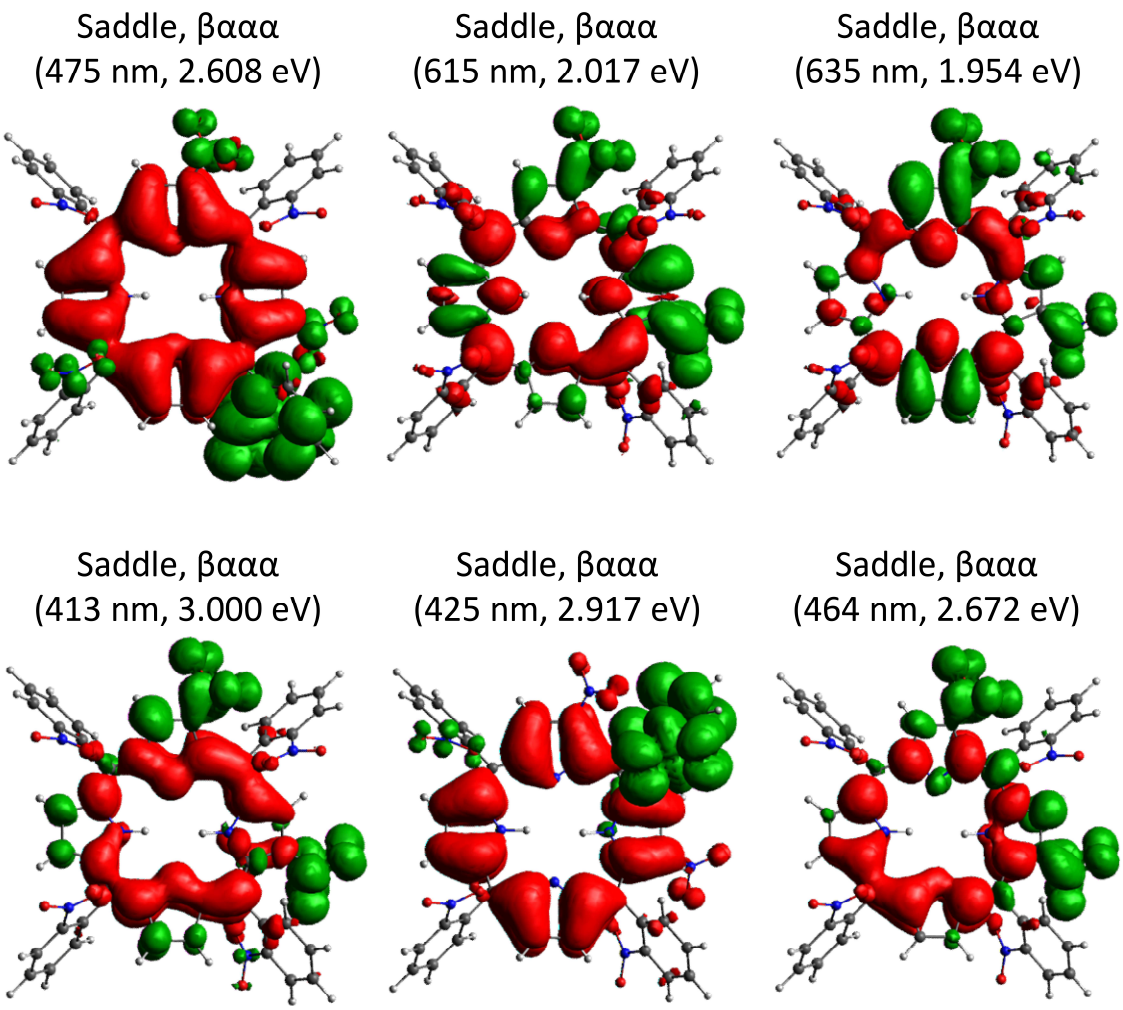


**Figure D17**. Electron density-difference maps for the lowest energy transitions of the βααα atropisomer of the saddle structure of $H_2(NO_2)_6TPP$. The red regions are areas that lose electron density in the transition, and the green areas gain electron density.

## Bibliography

### Chapter 1.


1. Radivojevic, I.; Varotto, A.; Farley, C.; Drain, C. M. Commercially viable porphyrinoid dyes for solar cells. *Energy Environ. Sci.* **2010**, *3*, 1897.
2. Farley, C.; Ferreira, J. T.; Aggarwal, A.; Bhupathiraju, N. V. S. D. K.; Singh, S.; Drain, C. M.; Tomé, J. P. C. In *Handbook of Porphyrin Science*; Kadish, K. M., Smith, K. M., Guilard, R., Eds.; World Scientific Publishing Co., Pte. Ltd.: Singapore, **2016**; Vol. 41 (forthcoming).
3. Service, R. F. Solar energy. Is it time to shoot for the sun? *Science* **2005**, *309*, 548.
4. Kalowekamo, J.; Baker, E. Estimating the manufacturing cost of purely organic solar cells. *Solar Energy* **2009**, *83*, 1224.
5. Drain, C. M.; Christensen, B.; Mauzerall, D. Photogating of ionic currents across a lipid bilayer. *Proc. Natl. Acad. Sci. U.S.A.* **1989**, *86*, 6959.
6. Drain, C. M. Self-organization of self-assembled photonic materials into functional devices: photo-switched conductors. *Proc. Natl. Acad. Sci. U.S.A.* **2002**, *99*, 5178.
7. Drain, C. M.; Nifiatis, F.; Vasenko, A.; Batteas, J. D. Porphyrin Tessellation by Design: Metal-Mediated Self-Assembly of Large Arrays and Tapes. *Angew. Chem. Int. Ed.* **1998**, *37*, 2344.
8. Drain, C. M.; Varotto, A.; Radivojevic, I. Self-organized porphyrinic materials. *Chem. Rev.* **2009**, *109*, 1630.
9. Drain, C. M.; Hupp, J. T.; Suslick, K. S.; Wasielewski, M. R.; Chen, X. A perspective on four new porphyrin-based functional materials and devices. *J. Porphyrins Phthalocyanines* **2002**, *06*, 243.
10. Ariga, K.; Hill, J. P.; Wakayama, Y.; Akada, M.; Barrena, E.; de Oteyza, D. G. New aspects of porphyrins and related compounds: self-assembled structures in two-dimensional molecular arrays. *J. Porphyrins Phthalocyanines* **2009**, *13*, 22.
11. Cheng, K. F.; Thai, N. A.; Teague, L. C.; Grohmann, K.; Drain, C. M. Supramolecular squares of porphyrazines. *Chem. Commun.* **2005**, 4678.
12. Lee, S. J.; Hupp, J. T. Porphyrin-containing molecular squares: Design and applications. *Coord. Chem. Rev.* **2006**, *250*, 1710.
13. Drain, C. M.; Smeureanu, G.; Patel, S.; Gong, X.; Garno, J.; Arijeloye, J. Porphyrin nanoparticles as supramolecular systems. *New J. Chem.* **2006**, *30*, 1834.
14. Gong, X.; Milic, T.; Xu, C.; Batteas, J. D.; Drain, C. M. Preparation and Characterization of Porphyrin Nanoparticles. *J. Am. Chem. Soc.* **2002**, *124*, 14290.
15. Smeureanu, G.; Aggarwal, A.; Soll, C. E.; Arijeloye, J.; Malave, E.; Drain, C. M. Enhanced catalytic activity and unexpected products from the oxidation of cyclohexene by organic nanoparticles of 5,10,15,20-tetrakis-(2,3,4,5,6-pentafluorophenyl)porphyrinatoiron(III) in water by using O2. *Chem. Eur. J.* **2009**, *15*, 12133.

16. Nitschke, C.; O'Flaherty, S. M.; Kröll, M.; Doyle, J. J.; Blau, W. J. Optical properties of zinc phthalocyanine nanoparticle dispersions. *Chem. Phys. Lett.* **2004**, *383*, 555.

17. Van Keuren, E.; Bone, A.; Ma, C. Phthalocyanine nanoparticle formation in supersaturated solutions. *Langmuir* **2008**, *24*, 6079.

18. Rangel-Rojo, R.; Matsuda, H.; Kasai, H.; Nakanishi, H. Irradiance dependence of the resonant nonlinearities in an organic material. *Journal of the Optical Society of America B* **2000**, *17*, 1376.

19. Dixon, J. M.; Taniguchi, M.; Lindsey, J. S. PhotochemCAD 2: A Refined Program with Accompanying Spectral Databases for Photochemical Calculations. *Photochem. Photobiol.* **2007**, *81*, 212.

20. Kadish, K. M.; Smith, K. M.; Guilard, R., Eds.; *Handbook of Porphyrin Science*, Academic Press: San Diego, CA, **2010-2011**; Vol. 1-15.

21. de la Torre, G.; Claessens, C. G.; Torres, T. Phthalocyanines: old dyes, new materials. Putting color in nanotechnology. *Chem. Commun.* **2007**, 2000.

22. Claessens, C. G.; Hahn, U.; Torres, T. Phthalocyanines: from outstanding electronic properties to emerging applications. *Chem. Rec.* **2008**, *8*, 75.

23. Gust, D.; Moore, T. A.; Moore, A. L. Mimicking photosynthetic solar energy transduction. *Acc. Chem. Res.* **2001**, *34*, 40.

24. Guldi, D. M. Fullerene-porphyrin architectures; photosynthetic antenna and reaction center models. *Chem. Soc. Rev.* **2002**, *31*, 22.

25. Li, X.; Sinks, L. E.; Rybtchinski, B.; Wasielewski, M. R. Ultrafast aggregate-to-aggregate energy transfer within self-assembled light-harvesting columns of zinc phthalocyanine tetrakis(perylenediimide). *J. Am. Chem. Soc.* **2004**, *126*, 10810.

26. Vail, S. A.; Krawczuk, P. J.; Guldi, D. M.; Palkar, A.; Echegoyen, L.; Tomé, J. P. C.; Fazio, M. A.; Schuster, D. I. Energy and electron transfer in polyacetylene-linked zinc-porphyrin-[60]fullerene molecular wires. *Chem. Eur. J.* **2005**, *11*, 3375.

27. Gonzalez-Rodriguez, D.; Claessens, C. G.; Torres, T.; Liu, S.; Echegoyen, L.; Vila, N.; Nonell, S. Tuning photoinduced energy- and electron-transfer events in subphthalocyanine-phthalocyanine dyads. *Chem. Eur. J.* **2005**, *11*, 3881.

28. Wasielewski, M. R. Energy, charge, and spin transport in molecules and self-assembled nanostructures inspired by photosynthesis. *J. Org. Chem.* **2006**, *71*, 5051.

29. El-Khouly, M. E.; Ju, D. K.; Kay, K. Y.; D'Souza, F.; Fukuzumi, S. Supramolecular tetrad of subphthalocyanine-triphenylamine-zinc porphyrin coordinated to fullerene as an "antenna-reaction-center" mimic: formation of a long-lived charge-separated state in nonpolar solvent. *Chem. Eur. J.* **2010**, *16*, 6193.

30. Bottari, G.; Trukhina, O.; Ince, M.; Torres, T. Towards artificial photosynthesis: Supramolecular, donor–acceptor, porphyrin- and phthalocyanine/carbon nanostructure ensembles. *Coord. Chem. Rev.* **2012**, *256*, 2453.

31. Li, J.; Diers, J. R.; Seth, J.; Yang, S. I.; Bocian, D. F.; Holten, D.; Lindsey, J. S. Synthesis and Properties of Star-Shaped Multiporphyrin−Phthalocyanine Light-Harvesting Arrays. *J. Org. Chem.* **1999**, *64*, 9090.

32. Miller, M. A.; Lammi, R. K.; Prathapan, S.; Holten, D.; Lindsey, J. S. A tightly coupled linear array of perylene, bis(porphyrin), and phthalocyanine units that functions as a photoinduced energy-transfer cascade. *J. Org. Chem.* **2000**, *65*, 6634.

33. Jacobs, R.; Stranius, K.; Maligaspe, E.; Lemmetyinen, H.; Tkachenko, N. V.; Zandler, M. E.; D'Souza, F. Syntheses and excitation transfer studies of near-orthogonal free-base porphyrin-ruthenium phthalocyanine dyads and pentad. *Inorg. Chem.* **2012**, *51*, 3656.

34. KC, C. B.; Ohkubo, K.; Karr, P. A.; Fukuzumi, S.; D'Souza, F. A 'two-point' bound zinc porphyrin-zinc phthalocyanine-fullerene supramolecular triad for sequential energy and electron transfer. *Chem. Commun.* **2013**, *49*, 7614.

35. Beletskaya, I.; Tyurin, V. S.; Tsivadze, A. Y.; Guilard, R.; Stern, C. Supramolecular chemistry of metalloporphyrins. *Chem. Rev.* **2009**, *109*, 1659.

36. Ozoemena, K. I.; Zhao, Z.; Nyokong, T. Immobilized cobalt(II) phthalocyanine–cobalt(II) porphyrin pentamer at a glassy carbon electrode: Applications to efficient amperometric sensing of hydrogen peroxide in neutral and basic media. *Electrochem. Commun.* **2005**, *7*, 679.

37. Purrello, R.; Gurrieri, S.; Lauceri, R. Porphyrin assemblies as chemical sensors. *Coord. Chem. Rev.* **1999**, *190-192*, 683.

38. Souto, J.; RodrÍGuez, M. L.; Desaja, J. A.; Aroca, R. Langmuir-Blodgett films of lanthanide bysphthalocyanines: applications as gas sensors. *Int. J. Electron.* **1994**, *76*, 763.

39. Bassoul, P.; Toupance, T.; Simon, J. Semiconductivity and gas-sensing properties of crown-ether-substituted lutetium bisphthalocyanines. *Sens. Actuators, B Chem.* **1995**, *26*, 150.

40. Álvarez, J.; Souto, J.; Rodríguez-Méndez, M. L.; de Saja, J. A. Response of a sensor based on ytterbium bisphthalocyanine Langmuir–Blodgett films to selected herbicides. *Sens. Actuators, B Chem.* **1998**, *48*, 339.

41. Amao, Y.; Asai, K.; Miyakawa, K.; Okura, I. Oxygen sensing using palladium porphyrin with long alkyl chain self-assembled film. *J. Porphyrins Phthalocyanines* **2000**, *04*, 19.

42. Kadish, K. M.; Fremond, L.; Shen, J.; Chen, P.; Ohkubo, K.; Fukuzumi, S.; El Ojaimi, M.; Gros, C. P.; Barbe, J. M.; Guilard, R. Catalytic activity of biscobalt porphyrin-corrole dyads toward the reduction of dioxygen. *Inorg. Chem.* **2009**, *48*, 2571.

43. Kadish, K. M.; Fremond, L.; Ou, Z.; Shao, J.; Shi, C.; Anson, F. C.; Burdet, F.; Gros, C. P.; Barbe, J. M.; Guilard, R. Cobalt(III) corroles as electrocatalysts for the reduction of dioxygen: reactivity of a monocorrole, biscorroles, and porphyrin-corrole dyads. *J. Am. Chem. Soc.* **2005**, *127*, 5625.

44. Oliveri, C. G.; Gianneschi, N. C.; Nguyen, S. T.; Mirkin, C. A.; Stern, C. L.; Wawrzak, Z.; Pink, M. Supramolecular allosteric cofacial porphyrin complexes. *J. Am. Chem. Soc.* **2006**, *128*, 16286.

45. Lee, S. J.; Cho, S. H.; Mulfort, K. L.; Tiede, D. M.; Hupp, J. T.; Nguyen, S. T. Cavity-tailored, self-sorting supramolecular catalytic boxes for selective oxidation. *J. Am. Chem. Soc.* **2008**, *130*, 16828.

46. Fruhbeisser, S.; Grohn, F. Catalytic activity of macroion-porphyrin nanoassemblies. *J. Am. Chem. Soc.* **2012**, *134*, 14267.

47. Jérôme, F.; Gros, C. P.; Tardieux, C.; Barbe, J.-M.; Guilard, R. Synthesis of a 'face-to-face' porphyrin-corrole. A potential precursor of a catalyst for the four-electron reduction of dioxygen. *New J. Chem.* **1998**, *22*, 1327.

48. Kadish, K. M.; Fremond, L.; Burdet, F.; Barbe, J. M.; Gros, C. P.; Guilard, R. Cobalt(IV) corroles as catalysts for the electroreduction of O2: reactions of heterobimetallic dyads containing a face-to-face linked Fe(III) or Mn(III) porphyrin. *J. Inorg. Biochem.* **2006**, *100*, 858.

49. Slagt, V. F.; van Leeuwen, P. W. N. M.; Reek, J. N. H. Multicomponent Porphyrin Assemblies as Functional Bidentate Phosphite Ligands for Regioselective Rhodium-Catalyzed Hydroformylation. *Angew. Chem.* **2003**, *115*, 5777.

50. de la Torre, G.; Vazquez, P.; Agullo-Lopez, F.; Torres, T. Role of structural factors in the nonlinear optical properties of phthalocyanines and related compounds. *Chem. Rev.* **2004**, *104*, 3723.

51. Chen, L.; Hu, R.; Xu, J.; Wang, S.; Li, X.; Li, S.; Yang, G. Third-order nonlinear optical properties of a series of porphyrin-appended europium(III) bis(phthalocyaninato) complexes. *Spectrochim. Acta A Mol. Biomol. Spec.* **2013**, *105*, 577.

52. Ke, H.; Li, W.; Zhang, T.; Zhu, X.; Tam, H. L.; Hou, A.; Kwong, D. W. J.; Wong, W. K. Acetylene bridged porphyrin-monophthalocyaninato ytterbium(III) hybrids with strong two-photon absorption and high singlet oxygen quantum yield. *Dalton Trans.* **2012**, *41*, 4536.

53. Morisue, M.; Ogawa, K.; Kamada, K.; Ohta, K.; Kobuke, Y. Strong two-photon and three-photon absorptions in the antiparallel dimer of a porphyrin-phthalocyanine tandem. *Chem. Commun.* **2010**, *46*, 2121.

54. Soares, A. R. M.; Tomé, J. P. C.; Neves, M. G. P. M. S.; Tomé, A. C.; Cavaleiro, J. A. S.; Torres, T. Synthesis of water-soluble phthalocyanines bearing four or eight D-galactose units. *Carbohydr. Res.* **2009**, *344*, 507.

55. Silva, S.; Pereira, P. M. R.; Silva, P.; Paz, F. A. A.; Faustino, M. A. F.; Cavaleiro, J. A. S.; Tomé, J. P. C. Porphyrin and phthalocyanine glycodendritic conjugates: synthesis, photophysical and photochemical properties. *Chem. Commun.* **2012**, *48*, 3608.

56. Bonnett, R. Photosensitizers of the porphyrin and phthalocyanine series for photodynamic therapy. *Chem. Soc. Rev.* **1995**, *24*, 19.

57. Pereira, J. B.; Carvalho, E. F. A.; Faustino, M. A. F.; Fernandes, R.; Neves, M. G. P. M. S.; Cavaleiro, J. A. S.; Gomes, N. C. M.; Cunha, A.; Almeida, A.; Tomé, J. P. C. Phthalocyanine thio-pyridinium derivatives as antibacterial photosensitizers. *Photochem. Photobiol.* **2012**, *88*, 537.

58. Gomes, M. C.; Woranovicz-Barreira, S. M.; Faustino, M. A. F.; Fernandes, R.; Neves, M. G. P. M. S.; Tomé, A. C.; Gomes, N. C. M.; Almeida, A.; Cavaleiro, J. A. S.; Cunha, A.; Tomé,

J. P. C. Photodynamic inactivation of Penicillium chrysogenum conidia by cationic porphyrins. *Photochem. Photobiol. Sci.* **2011**, *10*, 1735.

59. Tavares, A.; Dias, S. R. S.; Carvalho, C. M. B.; Faustino, M. A. F.; Tomé, J. P. C.; Neves, M. G. P. M. S.; Tomé, A. C.; Cavaleiro, J. A. S.; Cunha, A.; Gomes, N. C. M.; Alves, E.; Almeida, A. Mechanisms of photodynamic inactivation of a gram-negative recombinant bioluminescent bacterium by cationic porphyrins. *Photochem. Photobiol. Sci.* **2011**, *10*, 1659.

60. Silva, J. N.; Bosca, F.; Tomé, J. P. C.; Silva, E. M. P.; Neves, M. G. P. M. S.; Cavaleiro, J. A. S.; Patterson, L. K.; Filipe, P.; Maziere, J. C.; Santus, R.; Morliere, P. Tricationic porphyrin conjugates: evidence for chain-structure-dependent relaxation of excited singlet and triplet States. *J. Phys. Chem. B* **2009**, *113*, 16695.

61. Agirtas, S.; Ion, R. M.; Bekaroglu, O. Spectral study of the supramolecular assemblies porphyrins-phthalocyanines. *Mater. Sci. Eng., C* **2000**, *7*, 105.

62. Bao, G.; Wang, W.; Mao, Y.; Lu, F. Raman spectroscopic characteristics of phthalocyanine in mixed [5-(4-hydroxyphenyl)-10,15,20-tris(4-octyloxyphenyl)porphyrinato]-(phthalocyaninato) rare earth triple-deckers. *Spectrochim. Acta A Mol. Biomol. Spec.* **2013**, *102*, 275.

63. Bian, Y.; Chen, X.; Wang, D.; Choi, C. F.; Zhou, Y.; Zhu, P.; Ng, D. K. P.; Jiang, J.; Weng, Y.; Li, X. Porphyrin-appended europium(III) bis(phthalocyaninato) complexes: synthesis, characterization, and photophysical properties. *Chem. Eur. J.* **2007**, *13*, 4169.

64. Zhao, Z.; Ozoemena, K. I.; Maree, D. M.; Nyokong, T. Synthesis and electrochemical studies of a covalently linked cobalt(II) phthalocyanine-cobalt(II) porphyrin conjugate. *Dalton Trans.* **2005**, 1241.

65. Zhao, Z.; Poon, C.-T.; Wong, W.-K.; Wong, W.-Y.; Tam, H.-L.; Cheah, K.-W.; Xie, T.; Wang, D. Synthesis, Photophysical Characterization, and Surface Photovoltage Spectra of Windmill-Shaped Phthalocyanine–Porphyrin Heterodimers and Heteropentamers. *Eur. J. Inorg. Chem.* **2008**, *2008*, 119.

66. Leng, X.; Choi, C. F.; Lo, P. C.; Ng, D. K. P. Assembling a mixed phthalocyanine-porphyrin array in aqueous media through host-guest interactions. *Org. Lett.* **2007**, *9*, 231.

67. Berber, G.; Cammidge, A. N.; Chambrier, I.; Cook, M. J.; Hough, P. W. Controlled synthesis of ruthenium phthalocyanines and their use in the construction of supramolecular arrays. *Tetrahedron Lett.* **2003**, *44*, 5527.

68. Cammidge, A. N.; Berber, G.; Chambrier, I.; Hough, P. W.; Cook, M. J. Octaalkylphthalocyaninato ruthenium(II) complexes with mixed axial ligands and supramolecular porphyrin : phthalocyanine structures derived from them. *Tetrahedron* **2005**, *61*, 4067.

69. Chabach, D.; DeCian, A.; Fischer, J.; Weiss, R.; Bibout, M. E. M. induce. *Angew. Chem. Int. Ed.* **1996**, *35*, 898.

70. Chabach, D.; Tahiri, M.; DeCian, A.; Fischer, J.; Weiss, R.; Bibout, M. E. M. Tervalent-Metal Porphyrin-Phthalocyanine Heteroleptic Sandwich-Type Complexes - Synthesis, Structure, and Spectroscopic Characterization of Their Neutral, Singly-Oxidized, and Singly-Reduced States. *J. Am. Chem. Soc.* **1995**, *117*, 8548.

71. Gusev, A. V.; Danilov, E. O.; Rodgers, M. A. J. Association Complexes between Cationic Metallophthalocyanines and Anionic Metalloporphyrins II: Ultrafast Studies of Excited State Dynamics. *J. Phys. Chem. A* **2002**, *106*, 1993.

72. Gusev, A. V.; Rodgers, M. A. J. Association Complexes between Cationic Metallophthalocyanines and Anionic Metalloporphyrins I: Spectrometric Studies of Electronic Interactions. *J. Phys. Chem. A* **2002**, *106*, 1985.

73. Jiang, J. Z.; Lau, R. L. C.; Chan, T. W. D.; Mak, T. C. W.; Ng, D. K. P. Synthesis and spectroscopic properties of heteroleptic sandwich-type (phthalocyaninato)(porphyrinato)lanthanide(III) complexes. *Inorg. Chim. Acta* **1997**, *255*, 59.

74. Jiang, J. Z.; Liu, W.; Law, W. F.; Ng, D. K. P. Heteroleptic triple-decker (phthalocyaninato)(porphyrinato)europium(III) complexes: synthesis and electrochemical study. *Inorg. Chim. Acta* **1998**, *268*, 49.

75. Jiang, J.; Xie, J.; Choi, M. T. M.; Yan, Y.; Sun, S.; Ng, D. K. P. Double-decker Yttrium(III) Complexes with Phthalocyaninato and Porphyrinato Ligands. *J. Porphyrins Phthalocyanines* **1999**, *03*, 322.

76. Kandhadi, J.; Kanaparthi, R. K.; Giribabu, L. Germanium(IV) phthalocyanine-porphyrin based hetero trimers: synthesis, spectroscopy and photochemistry. *J. Porphyrins Phthalocyanines* **2012**, *16*, 282.

77. Kwag, G.; Park, E.; Kim, S. Self-assembled and alternative porphyrin-phthalocyanine array. *Bull. Korean Chem. Soc.* **2004**, *25*, 298.

78. Li, X. Y.; Ng, D. K. P. Self-assembly of meso-pyridylporphyrins and zinc phthalocyanines through axial coordination. *Eur. J. Inorg. Chem.* **2000**, *2000*, 1845.

79. Liu, J. X.; Xu, L. G.; Shen, S. Y.; Zhou, Q. F.; Li, T. K.; Xu, H. J. Novel Langmuir-Blodgett-Films, Consisting of Amphiphilic Zinc Phthalocyanine and Hydrophobic Porphyrin. *J. Photochem. Photobiol., A Chem.* **1993**, *71*, 275.

80. Maligaspe, E.; Kumpulainen, T.; Lemmetyinen, H.; Tkachenko, N. V.; Subbaiyan, N. K.; Zandler, M. E.; D'Souza, F. Ultrafast singlet-singlet energy transfer in self-assembled via metal-ligand axial coordination of free-base porphyrin-zinc phthalocyanine and free-base porphyrin-zinc naphthalocyanine dyads. *J. Phys. Chem. A* **2010**, *114*, 268.

81. Morisue, M.; Kobuke, Y. Tandem cofacial stacks of porphyrin-phthalocyanine dyads through complementary coordination. *Chem. Eur. J.* **2008**, *14*, 4993.

82. Pereira, A. M. V. M.; Hausmann, A.; Tomé, J. P. C.; Trukhina, O.; Urbani, M.; Neves, M. G. P. M. S.; Cavaleiro, J. A. S.; Guldi, D. M.; Torres, T. Porphyrin-phthalocyanine/pyridylfullerene supramolecular assemblies. *Chem. Eur. J.* **2012**, *18*, 3210.

83. Sun, Y. P.; Zhang, X.; Sun, C. Q.; Wang, Z. Q.; Shen, J. C.; Wang, D. J.; Li, T. J. Supramolecular assembly of alternating porphyrin and phthalocyanine layers based on electrostatic interactions. *Chem. Commun.* **1996**, 2379.

84. Ali, H.; van Lier, J. E. An efficient method for the synthesis of C–C connected phthalocyanine–porphyrin oligomers. *Tetrahedron Lett.* **2009**, *50*, 1113.

85. Bartelmess, J.; Soares, A. R. M.; Martinez-Diaz, M. V.; Neves, M. G. P. M. S.; Tomé, A. C.; Cavaleiro, J. A. S.; Torres, T.; Guldi, D. M. Panchromatic light harvesting in single wall carbon nanotube hybrids-immobilization of porphyrin-phthalocyanine conjugates. *Chem. Commun.* **2011**, *47*, 3490.

86. Calvete, M. J. F.; Tomé, J. P. C.; Cavaleiro, J. A. S. Synthesis and Characterization of New Cross-like Porphyrin-Naphthalocyanine and Porphyrin-Phthalocyanine Pentads. *J. Heterocycl. Chem.* **2014**, *51*, E202.

87. Enes, R. F.; Cid, J. J.; Hausmann, A.; Trukhina, O.; Gouloumis, A.; Vazquez, P.; Cavaleiro, J. A. S.; Tomé, A. C.; Guldi, D. M.; Torres, T. Synthesis and photophysical properties of fullerene-phthalocyanine-porphyrin triads and pentads. *Chem. Eur. J.* **2012**, *18*, 1727.

88. Ermilov, E. A.; Leng, X.; Roder, B.; Ng, D. K. P. Preparation and photophysical properties of a tetraethylene glycol-linked phthalocyanine-porphyrin dyad and triad. *New J. Chem.* **2013**, *37*, 1746.

89. Ermilov, E. A.; Tannert, S.; Werncke, T.; Choi, M. T. M.; Ng, D. K. P.; Röder, B. Photoinduced electron and energy transfer in a new porphyrin–phthalocyanine triad. *Chem. Phys.* **2006**, *328*, 428.

90. Fortage, J.; Goransson, E.; Blart, E.; Becker, H. C.; Hammarstrom, L.; Odobel, F. Strongly coupled zinc phthalocyanine-tin porphyrin dyad performing ultra-fast single step charge separation over a 34 A distance. *Chem. Commun.* **2007**, 4629.

91. Fournier, T.; Liu, Z.; Tran-Thi, T. H.; Houde, D.; Brasseur, N.; La Madeleine, C.; Langlois, R.; van Lier, J. E.; Lexa, D. Influence of molecular oxygen on the charge transfer properties of a Co(II)porphyrin-Al(III)phthalocyanine aggregate. Excited states dynamics and photobiological activities. *J. Phys. Chem. A* **1999**, *103*, 1179.

92. Gaspard, S.; Giannotti, C.; Maillard, P.; Schaeffer, C.; Tran-Thi, T.-H. The first synthesis of covalently linked mixed dimer complexes containing phthalocyanine and porphyrin. *J. Chem. Soc., Chem. Commun.* **1986**, 1239.

93. Hausmann, A.; Soares, A. R. M.; Martinez-Diaz, M. V.; Neves, M. G. P. M. S.; Tomé, A. C.; Cavaleiro, J. A. S.; Torres, T.; Guldi, D. M. Transduction of excited state energy between covalently linked porphyrins and phthalocyanines. *Photochem. Photobiol. Sci.* **2010**, *9*, 1027.

94. Yang, S. I.; Li, J.; Cho, H. S.; Kim, D.; Bocian, D. F.; Holten, D.; Lindsey, J. S. Synthesis and excited-state photodynamics of phenylethyne-linked porphyrin–phthalocyanine dyads. *J. Mater. Chem.* **2000**, *10*, 283.

95. Kameyama, K.; Satake, A.; Kobuke, Y. Light-harvesting composites of directly connected porphyrin–phthalocyanine dyads and their coordination dimers. *Tetrahedron Lett.* **2004**, *45*, 7617.

96. Ito, F.; Ishibashi, Y.; Khan, S. R.; Miyasaka, H.; Kameyama, K.; Morisue, M.; Satake, A.; Ogawa, K.; Kobuke, Y. Photoinduced electron transfer and excitation energy transfer in directly linked zinc porphyrin/zinc phthalocyanine composite. *J. Phys. Chem. A* **2006**, *110*, 12734.

97. KC, C. B.; Stranius, K.; D'Souza, P.; Subbaiyan, N. K.; Lemmetyinen, H.; Tkachenko, N. V.; D'Souza, F. Sequential Photoinduced Energy and Electron Transfer Directed Improved

Performance of the Supramolecular Solar Cell of a Zinc Porphyrin-Zinc Phthalocyanine Conjugate Modified TiO2 Surface. *J. Phys. Chem. C* **2013**, *117*, 763.

98. Li, J. Z.; Lindsey, J. S. Efficient synthesis of light-harvesting arrays composed of eight porphyrins and one phthalocyanine. *J. Org. Chem.* **1999**, *64*, 9101.
99. Li, L.; Shen, S. Y.; Yu, Q.; Zhou, Q. F.; Xu, H. J. Photoinduced Electron-Transfer and Charge Separation in Anthraquinone-Substituted Porphyrin Phthalocyanine Heterodimer. *J. Chem. Soc., Chem. Commun.* **1991**, 619.
100. Li, X. Y.; Zhou, Q. F.; Tian, H. J.; Xu, H. J. Synthesis and photophysical properties of porphyrin-phthalocyanine heterodimer linked by piperazine. *Chin. J. Chem* . **1998**, *16*, 97.
101. Liu, M. O.; Hu, A. T. Microwave-assisted synthesis of phthalocyanine–porphyrin complex and its photoelectric conversion properties. *J. Organomet. Chem.* **2004**, *689*, 2450.
102. Osati, S.; Safari, N.; Jamaat, P. R. Synthesis and characterization of three covalently linked porphyrin-phthalocyanine pentamers with nucleophilic substitution. *Inorg. Chim. Acta* **2010**, *363*, 2180.
103. Pereira, A. M. V. M.; Soares, A. R. M.; Hausmann, A.; Neves, M. G. P. M. S.; Tomé, A. C.; Silva, A. M. S.; Cavaleiro, J. A. S.; Guldi, D. M.; Torres, T. Distorted fused porphyrin-phthalocyanine conjugates: synthesis and photophysics of supramolecular assembled systems with a pyridylfullerene. *Phys. Chem. Chem. Phys.* **2011**, *13*, 11858.
104. Soares, A. R. M.; Martinez-Diaz, M. V.; Bruckner, A.; Pereira, A. M. V. M.; Tomé, J. P. C.; Alonso, C. M. A.; Faustino, M. A. F.; Neves, M. G. P. M. S.; Tomé, A. C.; Silva, A. M. S.; Cavaleiro, J. A. S.; Torres, T.; Guldi, D. M. Synthesis of novel N-linked porphyrin-phthalocyanine dyads. *Org. Lett.* **2007**, *9*, 1557.
105. Sutton, J. M.; Boyle, R. W. First synthesis of porphyrin-phthalocyanine heterodimers with a direct ethynyl linkage. *Chem. Commun.* **2001**, 2014.
106. Tannert, S.; Ermilov, E. A.; Vogel, J. O.; Choi, M. T. M.; Ng, D. K. P.; Roder, B. The influence of solvent polarity and metalation on energy and electron transfer in porphyrin-phthalocyanine heterotrimers. *J. Phys. Chem. B* **2007**, *111*, 8053.
107. Tasso, T. T.; Moreira, W. C. Heteroarray of cobalt(II) tetrasulfophthalocyanine and cobalt(II) tetrakis(N-methyl-4-pyridyl)porphyrin: synthesis, isolation and electronic properties. *J. Porphyrins Phthalocyanines* **2012**, *16*, 244.
108. Tomé, J. P. C.; Pereira, A. M. V. M.; Alonso, C. M. A.; Neves, M. G. P. M. S.; Tomé, A. C.; Silva, A. M. S.; Cavaleiro, J. A. S.; Martínez-Díaz, M. V.; Torres, T.; Rahman, G. M. A.; Ramey, J.; Guldi, D. M. Synthesis and Photophysical Studies of New Porphyrin-Phthalocyanine Dyads with Hindered Rotation. *Eur. J. Org. Chem.* **2006**, *2006*, 257.
109. Tran-Thi, T. H.; Lipskier, J. F.; Simoes, M.; Palacin, S. Photoinduced charge transfer in semi-amphiphilic porphyrin-phthalocyanine mixed dimers. *Thin Solid Films* **1992**, *210-211*, 150.
110. Zhao, Z.; Cammidge, A. N.; Cook, M. J. Towards black chromophores: mu-oxo linked phthalocyanine-porphyrin dyads and phthalocyanine-subphthalocyanine dyad and triad arrays. *Chem. Commun.* **2009**, 7530.

111. Zhao, Z.; Cammidge, A. N.; Hughes, D. L.; Cook, M. J. Modular face-to-face assembly of multichromophore arrays that absorb across the complete UV-visible spectrum and into the near-IR. *Org. Lett.* **2010**, *12*, 5138.

112. Zhao, Z.; Nyokong, T.; Maree, M. D. Synthesis and photochemical characterization of a zinc phthalocyanine-zinc porphyrin heterotrimer and heterononamer. *Dalton Trans.* **2005**, 3732.

113. Zhao, Z. X.; Ogunsipe, A. O.; Maree, M. D.; Nyokong, T. Synthesis and photophysical properties of a covalently linked porphyrin-phthalocyanine conjugate. *J. Porphyrins Phthalocyanines* **2005**, *9*, 186.

114. Wei, L.; Padmaja, K.; Youngblood, W. J.; Lysenko, A. B.; Lindsey, J. S.; Bocian, D. F. Diverse redox-active molecules bearing identical thiol-terminated tripodal tethers for studies of molecular information storage. *J. Org. Chem.* **2004**, *69*, 1461.

115. Yamada, Y.; Okamoto, M.; Furukawa, K.; Kato, T.; Tanaka, K. Switchable intermolecular communication in a four-fold rotaxane. *Angew. Chem. Int. Ed.* **2012**, *51*, 709.

116. Drain, C. M.; Varotto, A.; Radivojevic, I. Self-organized porphyrinic materials. *Chem. Rev.* **2009**, *109*, 1630.

117. Moan, J.; Peng, Q. An Outline of the History of PDT. *Photodynamic Therapy* **2006**, *2*, 1.

118. Ormond, A. B.; Freeman, H. Dye Sensitizers for Photodynamic Therapy. *Materials* **2013**, *6*, 817.

119. Vinodh, M.; Alipour, F. H.; Mohamod, A. A.; Al-Azemi, T. F. Molecular assemblies of porphyrins and macrocyclic receptors: recent developments in their synthesis and applications. *Molecules* **2012**, *17*, 11763.

120. Lo, P. C.; Leng, X. B.; Ng, D. K. P. Hetero-arrays of porphyrins and phthalocyanines. *Coord. Chem. Rev.* **2007**, *251*, 2334.

121. Lu, G. F.; Ou, Z. P.; Jiang, J. Z.; Bian, Y. Z. Nanoscale Hollow Spheres of an Amphiphilic Mixed (Phthalocyaninato)(porphyrinato)europium Double-Decker Complex. *Eur. J. Inorg. Chem.* **2010**, *2010*, 753.

122. Lipskier, J. F.; Tran-Thi, T. H. Supramolecular assemblies of porphyrins and phthalocyanines bearing oppositely charged substituents. First evidence of heterotrimer formation. *Inorg. Chem.* **1993**, *32*, 722.

123. Radivojevic, I.; Bazzan, G.; Burton-Pye, B. P.; Ithisuphalap, K.; Saleh, R.; Durstock, M. F.; Francesconi, L. C.; Drain, C. M. Zirconium((IV)) and Hafnium((IV)) Porphyrin and Phthalocyanine Complexes as New Dyes for Solar Cell Devices. *J. Phys. Chem. C* **2012**, *116*, 15867.

124. Milic, T.; Garno, J. C.; Batteas, J. D.; Smeureanu, G.; Drain, C. M. Self-organization of self-assembled tetrameric porphyrin arrays on surfaces. *Langmuir* **2004**, *20*, 3974.

125. Jurow, M.; Varotto, A.; Manichev, V.; Travlou, N. A.; Giannakoudakis, D. A.; Drain, C. M. Self-organized nanostructured materials of alkylated phthalocyanines and underivatized C60 on ITO. *RSC Advances* **2013**, *3*, 21360.

126. Singh, S.; Aggarwal, A.; Farley, C.; Hageman, B. A.; Batteas, J. D.; Drain, C. M. Hierarchical organization of a robust porphyrin cage self-assembled by hydrogen bonds. *Chem. Commun.* **2011**, *47*, 7134.

127. Chan, Y. H.; Schuckman, A. E.; Perez, L. M.; Vinodu, M.; Drain, C. M.; Batteas, J. D. Synthesis and characterization of a thiol-tethered tripyridyl porphyrin on Au(111). *J. Phys. Chem. C* **2008**, *112*, 6110.

128. Jurow, M.; Schuckman, A. E.; Batteas, J. D.; Drain, C. M. Porphyrins as Molecular Electronic Components of Functional Devices. *Coord. Chem. Rev.* **2010**, *254*, 2297.

129. Garno, J. C.; Xu, C.; Bazzan, G.; Batteas, J. D.; Drain, C. M. In *Metal-Containing and Metallosupramolecular Polymers and Materials*; American Chemical Society: **2006**; Vol. 928, p 168.

130. Schuckman, A. E.; Ewers, B. W.; Yu, L. H.; Tomé, J. P. C.; Pérez, L. M.; Drain, C. M.; Kushmerick, J. G.; Batteas, J. D. Utilizing Nearest-Neighbor Interactions To Alter Charge Transport Mechanisms in Molecular Assemblies of Porphyrins on Surfaces. *J. Phys. Chem. C* **2015**, *119*, 13569.

131. Gryko, D.; Li, J. Z.; Diers, J. R.; Roth, K. M.; Bocian, D. F.; Kuhr, W. G.; Lindsey, J. S. Studies related to the design and synthesis of a molecular octal counter. *J. Mater. Chem.* **2001**, *11*, 1162.

132. Lysenko, A. B.; Malinovskii, V. L.; Padmaja, K.; Wei, L. Y.; Diers, J. R.; Bocian, D. F.; Lindsey, J. S. Multistate molecular information storage using S-acetylthio-derivatized dyads of triple-decker sandwich coordination compounds. *J. Porphyrins Phthalocyanines* **2005**, *9*, 491.

133. Padmaja, K.; Youngblood, W. J.; Wei, L.; Bocian, D. F.; Lindsey, J. S. Triple-decker sandwich compounds bearing compact triallyl tripods for molecular information storage applications. *Inorg. Chem.* **2006**, *45*, 5479.

134. Schweikart, K. H.; Malinovskii, V. L.; Diers, J. R.; Yasseri, A. A.; Bocian, D. F.; Kuhr, W. G.; Lindsey, J. S. Design, synthesis, and characterization of prototypical multistate counters in three distinct architectures. *J. Mater. Chem.* **2002**, *12*, 808.

135. Schweikart, K. H.; Malinovskii, V. L.; Yasseri, A. A.; Li, J.; Lysenko, A. B.; Bocian, D. F.; Lindsey, J. S. Synthesis and characterization of bis(S-acetylthio)-derivatized europium triple-decker monomers and oligomers. *Inorg. Chem.* **2003**, *42*, 7431.

136. Ambroise, A.; Wagner, R. W.; Rao, P. D.; Riggs, J. A.; Hascoat, P.; Diers, J. R.; Seth, J.; Lammi, R. K.; Bocian, D. F.; Holten, D.; Lindsey, J. S. Design and synthesis of porphyrin-based optoelectronic gates. *Chem. Mater.* **2001**, *13*, 1023.

137. Engelkamp, H.; Middelbeek, S.; Nolte, R. J. Self-assembly of disk-shaped molecules to coiled-coil aggregates with tunable helicity. *Science* **1999**, *284*, 785.

138. Gao, J.; Li, D.; Chen, Y. Controllable Self-assembly of Sandwich-type Mixed (phthalocyaninato)(porphyrinato) Rare Earth Triple-Decker Complexes. *J. Inorg. Organomet. P.* **2011**, *21*, 876.

139. Lu, G.; Chen, Y.; Zhang, Y.; Bao, M.; Bian, Y.; Li, X.; Jiang, J. Morphology controlled self-assembled nanostructures of sandwich mixed (phthalocyaninato)(porphyrinato) europium

triple-deckers. Effect of hydrogen bonding on tuning the intermolecular interaction. *J. Am. Chem. Soc.* **2008**, *130*, 11623.

140. Balakumar, A.; Lysenko, A. B.; Carcel, C.; Malinovskii, V. L.; Gryko, D. T.; Schweikart, K. H.; Loewe, R. S.; Yasseri, A. A.; Liu, Z.; Bocian, D. F.; Lindsey, J. S. Diverse redox-active molecules bearing O-, S-, or Se-terminated tethers for attachment to silicon in studies of molecular information storage. *J. Org. Chem.* **2004**, *69*, 1435.

141. Goransson, E.; Boixel, J.; Fortage, J.; Jacquemin, D.; Becker, H. C.; Blart, E.; Hammarstrom, L.; Odobel, F. Long-range electron transfer in zinc-phthalocyanine-oligo(phenylene-ethynylene)-based donor-bridge-acceptor dyads. *Inorg. Chem.* **2012**, *51*, 11500.

142. Zhu, P.; Zhang, X.; Wang, H.; Zhang, Y.; Bian, Y.; Jiang, J. Ferrocene-decorated (phthalocyaninato)(porphyrinato) double- and triple-decker rare earth complexes: synthesis, structure, and electrochemical properties. *Inorg. Chem.* **2012**, *51*, 5651.

143. Cheng, K. F.; Thai, N. A.; Grohmann, K.; Teague, L. C.; Drain, C. M. Tessellation of porphyrazines with porphyrins by design. *Inorg. Chem.* **2006**, *45*, 6928.

144. Smeureanu, G.; Aggarwal, A.; Soll, C. E.; Arijeloye, J.; Malave, E.; Drain, C. M. Enhanced catalytic activity and unexpected products from the oxidation of cyclohexene by organic nanoparticles of 5,10,15,20-tetrakis-(2,3,4,5,6-pentafluorophenyl)porphyrinatoiron(III) in water by using O2. *Chem. Eur. J.* **2009**, *15*, 12133.

145. Meunier, B. Metalloporphyrins as versatile catalysts for oxidation reactions and oxidative DNA cleavage. *Chem. Rev.* **1992**, *92*, 1411.

146. Nam, W.; Lim, M. H.; Oh, S.-Y.; Lee, J. H.; Lee, H. J.; Woo, S. K.; Kim, C.; Shin, W. Remarkable Anionic Axial Ligand Effects of Iron(III) Porphyrin Complexes on the Catalytic Oxygenations of Hydrocarbons by H2O2 and the Formation of Oxoiron(IV) Porphyrin Intermediates bym-Chloroperoxybenzoic Acid. *Angew. Chem. Int. Ed.* **2000**, *39*, 3646.

147. Sheldon, R. A., Ed.; *Metalloporphyrins in Catalytic Oxidations*, Marcel Dekker: New York, NY, **1994**.

148. Collman, J. P.; Wagenknecht, P. S.; Hutchison, J. E. Molecular Catalysts for Multielectron Redox Reactions of Small Molecules: The“Cofacial Metallodiporphyrin” Approach. *Angew. Chem. Int. Ed.* **1994**, *33*, 1537.

149. Kadish, K. M.; Shao, J.; Ou, Z.; Fremond, L.; Zhan, R.; Burdet, F.; Barbe, J. M.; Gros, C. P.; Guilard, R. Electrochemistry, spectroelectrochemistry, chloride binding, and O2 catalytic reactions of free-base porphyrin-cobalt corrole dyads. *Inorg. Chem.* **2005**, *44*, 6744.

150. Menting, R.; Lau, J. T. F.; Xu, H.; Ng, D. K. P.; Roder, B.; Ermilov, E. A. Formation and photoinduced processes of a self-assembled subphthalocyanine-porphyrin-phthalocyanine supramolecular complex. *Chem. Commun.* **2012**, *48*, 4597.

151. *Web of Science*; Thomson Reuters: New York, NY, **2015**; http://www.webofknowledge.com.

**Chapter 2.**


1. Singh, S.; Aggarwal, A.; Farley, C.; Hageman, B. A.; Batteas, J. D.; Drain, C. M. Hierarchical organization of a robust porphyrin cage self-assembled by hydrogen bonds. *Chem. Commun.* **2011**, *47*, 7134-7136.
2. Balaban, T. S.; Berova, N.; Drain, C. M.; Hauschild, R.; Huang, X.; Kalt, H.; Lebedkin, S.; Lehn, J. M.; Nifaitis, F.; Pescitelli, G.; Prokhorenko, V. I.; Riedel, G.; Smeureanu, G.; Zeller, J. Syntheses and energy transfer in multiporphyrinic arrays self-assembled with hydrogen-bonding recognition groups and comparison with covalent steroidal models. *Chem. Eur. J.* **2007**, *13*, 8411-8427.
3. Arai, S.; Niwa, D.; Nishide, H.; Takeoka, S. Atropisomers of meso-Conjugated Uracyl Porphyrin Derivatives and Their Assembling Structures. *Org. Lett.* **2007**, *9*, 17-20.
4. Arai, S.; Okamura, T.; Takeoka, S. Synthesis and self-assembling behavior of a porphyrin bearing multiple meso-conjugated barbiturates. *Tetrahedron Lett.* **2010**, *51*, 5177-5180.
5. Drain, C. M.; Russell, K. C.; Lehn, J.-M. Self-assembly of a multi-porphyrin supramolecular macrocycle by hydrogen bond molecular recognition. *Chem. Commun.* **1996**, 337.
6. Drain, C. M.; Fischer, R. d.; Nolen, E. G.; Lehn, J.-M. Self-assembly of a bisporphyrin supramolecular cage induced by molecular recognition between complementary hydrogen bonding sites. *J. Chem. Soc., Chem. Commun.* **1993**, 243.
7. Drain, C. M.; Shi, X.; Milic, T.; Nifiatis, F. Self-assembled multiporphyrin arrays mediated by self-complementary quadruple hydrogen bond motifs. *Chem. Commun.* **2001**, 287-288.
8. Shi, X.; Barkigia, K. M.; Fajer, J.; Drain, C. M. Design and Synthesis of Porphyrins Bearing Rigid Hydrogen Bonding Motifs: Highly Versatile Building Blocks for Self-Assembly of Polymers and Discrete Arrays. *J. Org. Chem.* **2001**, *66*, 6513-6522.
9. González-Rodríguez, D.; Schenning, A. P. H. J. Hydrogen-bonded Supramolecular π-Functional Materials. *Chem. Mater.* **2011**, *23*, 310-325.
10. Ligthart, G. B.; Ohkawa, H.; Sijbesma, R. P.; Meijer, E. W. Complementary quadruple hydrogen bonding in supramolecular copolymers. *J. Am. Chem. Soc.* **2005**, *127*, 810-811.
11. Steed, J. W. Supramolecular gel chemistry: developments over the last decade. *Chem. Commun.* **2011**, *47*, 1379-1383.
12. Wessendorf, F.; Hirsch, A. Self-assembly of supramolecular oligo-phenylene-ethynylene wires consisting of double Hamilton receptor modified OPE rods and a tetraphenylporphyrin cyanurate. *Tetrahedron* **2008**, *64*, 11480-11489.
13. Arai, S.; Ohshiro, H.; Nishide, H.; Takeoka, S. Synthesis of porphyrins bearing uracyl groups and their assembly induced by melamine derivatives. *Polym. Adv. Technol.* **2007**, *18*, 497-501.
14. Hwang, D. R.; Helquist, P.; Shekhani, M. S. Total synthesis of (+)-sparsomycin. Approaches using cysteine and serine inversion. *J. Org. Chem.* **1985**, *50*, 1264-1271.

15. Petersen, L.; Pedersen, E. B.; Nielsen, C. Three Routes for the Synthesis of 6-Benzyl-1-ethoxymethyl-2,4-dioxo-1,2,3,4-tetrahydropyrimidine-5-carbaldehyde. *Synthesis* **2001**, *2001*, 0559-0564.

16. Kimizuka, N.; Kawasaki, T.; Hirata, K.; Kunitake, T. Supramolecular Membranes. Spontaneous Assembly of Aqueous Bilayer Membrane via Formation of Hydrogen Bonded Pairs of Melamine and Cyanuric Acid Derivatives. *J. Am. Chem. Soc.* **1998**, *120*, 4094-4104.

17. Vollhardt, D.; Fainerman, V. B.; Liu, F. Thermodynamic and structural characterization of amphiphilic melamine-type monolayers. *J. Phys. Chem. B* **2005**, *109*, 11706-11711.

18. Gellman, S. H.; Dado, G. P.; Liang, G. B.; Adams, B. R. Conformation-directing effects of a single intramolecular amide-amide hydrogen bond: variable-temperature NMR and IR studies on a homologous diamide series. *J. Am. Chem. Soc.* **1991**, *113*, 1164-1173.

19. Plieger, P. G.; Burrell, A. K.; Jameson, G. B.; Officer, D. L. Metallation effects on the thermal interconversion of atropisomers of di(orthomethylarene)-substituted porphyrins. *Dalton Trans.* **2004**, 319-326.

20. Freitag, R. A.; Whitten, D. G. Thermal and photo-induced atropisomerization of picket-fence porphyrins, metalloporphyrins, and diacids: a means for examining porphyrin solution properties. *J. Phys. Chem.* **1983**, *87*, 3918-3925.

21. Freitag, R. A.; Whitten, D. G. Thermal and photo-induced atropisomerization of picket-fence porphyrins, metalloporphyrins, and diacids: a means for examining porphyrin solution properties. *J. Phys. Chem.* **1983**, *87*, 3918-3925.

22. Kottas, G. S.; Clarke, L. I.; Horinek, D.; Michl, J. Artificial molecular rotors. *Chem. Rev.* **2005**, *105*, 1281-1376.

23. Plieger, P. G.; Burrell, A. K.; Jameson, G. B.; Officer, D. L. Metallation effects on the thermal interconversion of atropisomers of di(orthomethylarene)-substituted porphyrins. *Dalton Trans.* **2004**, 319-326.

24. Lindsey, J. Increased yield of a desired isomer by equilibriums displacement on binding to silica gel, applied to meso-tetrakis(o-aminophenyl)porphyrin. *J. Org. Chem.* **1980**, *45*, 5215-5215.

25. Gouterman, M. In *The Porphyrins*; Dolphin, D., Ed.; Academic Press: New York, **1979**; Vol. III.

26. Tran Thi, T. H.; Desforge, C.; Thiec, C.; Gaspard, S. Singlet-singlet and triplet-triplet intramolecular transfer processes in a covalently linked porphyrin-phthalocyanine heterodimer. *J. Phys. Chem.* **1989**, *93*, 1226-1233.

27. Cohen, Y.; Avram, L.; Frish, L. Diffusion NMR spectroscopy in supramolecular and combinatorial chemistry: an old parameter--new insights. *Angew. Chem. Int. Ed.* **2005**, *44*, 520-554.

28. Ohkawa, H.; Arai, S.; Takeoka, S.; Shibue, T.; Nishide, H. A Duplex of Tetra(2-pyridyl)porphyrin and Tetrahydroxylcalix[4]arene. *Chem. Lett.* **2003**, *32*, 1052-1053.

29. Ohkawa, H.; Takayama, A.; Nakajima, S.; Nishide, H. Cyclic tetramer of a metalloporphyrin based on a quadruple hydrogen bond. *Org. Lett.* **2006**, *8*, 2225-2228.

30. Zhao, T.; Beckham, H. W.; Gibson, H. W. Quantitative Determination of Threading in Rotaxanated Polymers by Diffusion-Ordered NMR Spectroscopy. *Macromolecules* **2003**, *36*, 4833-4837.

31. Yang, Y.; Wang, C. Hierarchical construction of self-assembled low-dimensional molecular architectures observed by using scanning tunneling microscopy. *Chem. Soc. Rev.* **2009**, *38*, 2576-2589.

32. Milic, T.; Garno, J. C.; Batteas, J. D.; Smeureanu, G.; Drain, C. M. Self-Organization of Self-Assembled Tetrameric Porphyrin Arrays on Surfaces. *Langmuir* **2004**, *20*, 3974-3983.

**Chapter 3.**

1. Jurow, M.; Farley, C.; Pabon, C.; Hageman, B.; Dolor, A.; Drain, C. M. Facile synthesis of a flexible tethered porphyrin dimer that preferentially complexes fullerene C70. *Chem. Commun.* **2012**, *48*, 4731-4733.

2. Mulliken, R. S.; Person, W. B. Donor-Acceptor Complexes. *Annu. Rev. Phys. Chem.* **1962**, *13*, 107-126.

3. Williams, F. Donor-acceptor pairs in semiconductors. *Physica Status Solidi B.* **1968**, *25*, 493-512.

4. Foster, R. Electron donor-acceptor complexes. *J. Phys. Chem.* **1980**, *84*, 2135-2141.

5. Sapsford, K. E.; Berti, L.; Medintz, I. L. Materials for fluorescence resonance energy transfer analysis: beyond traditional donor-acceptor combinations. *Angew. Chem. Int. Ed.* **2006**, *45*, 4562-4589.

6. Emmett, L.; Prentice, G. M.; Pantoş, G. D. Donor–acceptor interactions in chemistry. *Annu. Rep. Prog. Chem., Sect. B: Org. Chem.* **2013**, *109*, 217.

7. Kularatne, R. S.; Magurudeniya, H. D.; Sista, P.; Biewer, M. C.; Stefan, M. C. Donor-acceptor semiconducting polymers for organic solar cells. *J. Polym. Sci.* **2013**, *51*, 743-768.

8. Mullen, K.; Pisula, W. Donor-Acceptor Polymers. *J. Am. Chem. Soc.* **2015**, *137*, 9503-9505.

9. Kc, C. B.; D'Souza, F. Design and photochemical study of supramolecular donor–acceptor systems assembled via metal–ligand axial coordination. *Coord. Chem. Rev.* **2016**, *322*, 104-141.

10. Rudolf, M.; Kirner, S. V.; Guldi, D. M. A multicomponent molecular approach to artificial photosynthesis - the role of fullerenes and endohedral metallofullerenes. *Chem. Soc. Rev.* **2016**, *45*, 612-630.

11. Boyd, P. D. W.; Reed, C. A. Fullerene−Porphyrin Constructs. *Acc. Chem. Res.* **2004**, *38*, 235-242.

12. Echegoyen, L.; Echegoyen, L. E. Electrochemistry of Fullerenes and Their Derivatives. *Acc. Chem. Res.* **1998**, *31*, 593-601.

13. Baran, P. S.; Monaco, R. R.; Khan, A. U.; Schuster, D. I.; Wilson, S. R. Synthesis and Cation-Mediated Electronic Interactions of Two Novel Classes of Porphyrin−Fullerene Hybrids. *J. Am. Chem. Soc.* **1997**, *119*, 8363-8364.

14. Bhattacharya, S.; Tominaga, K.; Kimura, T.; Uno, H.; Komatsu, N. A new metalloporphyrin dimer: Effective and selective molecular tweezers for fullerenes. *Chem. Phys. Lett.* **2007**, *433*, 395-402.

15. Boyd, P. D. W.; Hodgson, M. C.; Rickard, C. E. F.; Oliver, A. G.; Chaker, L.; Brothers, P. J.; Bolskar, R. D.; Tham, F. S.; Reed, C. A. Selective Supramolecular Porphyrin/Fullerene Interactions. *J. Am. Chem. Soc.* **1999**, *121*, 10487-10495.

16. D'Souza, F.; Chitta, R.; Gadde, S.; Zandler, M. E.; Sandanayaka, A. S.; Araki, Y.; Ito, O. Supramolecular porphyrin-fullerene via 'two-point' binding strategy: axial-coordination and cation-crown ether complexation. *Chem. Commun.* **2005**, 1279-1281.

17. D'Souza, F.; Ito, O. Supramolecular donor-acceptor hybrids of porphyrins/phthalocyanines with fullerenes/carbon nanotubes: electron transfer, sensing, switching, and catalytic applications. *Chem. Commun.* **2009**, 4913-4928.

18. Liddell, P. A.; Kodis, G.; Kuciauskas, D.; Andreasson, J.; Moore, A. L.; Moore, T. A.; Gust, D. Photoinduced electron transfer in a symmetrical diporphyrin-fullerene triad. *Phys. Chem. Chem. Phys.* **2004**, *6*, 5509-5515.

19. Mulholland, A. R.; Woodward, C. P.; Langford, S. J. Fullerene-templated synthesis of a cyclic porphyrin trimer using olefin metathesis. *Chem. Commun.* **2011**, *47*, 1494-1496.

20. Sessler, J. L.; Jayawickramarajah, J.; Gouloumis, A.; Torres, T.; Guldi, D. M.; Maldonado, S.; Stevenson, K. J. Synthesis and photophysics of a porphyrin-fullerene dyad assembled through Watson-Crick hydrogen bonding. *Chem. Commun.* **2005**, 1892-1894.

21. Sun, D.; Tham, F. S.; Reed, C. A.; Chaker, L.; Burgess, M.; Boyd, P. D. W. Porphyrin−Fullerene Host−Guest Chemistry. *J. Am. Chem. Soc.* **2000**, *122*, 10704-10705.

22. Wilson, S. R.; MacMahon, S.; Tat, F. T.; Jarowski, P. D.; Schuster, D. I. Synthesis and photophysics of a linear non-covalently linked porphyrin–fullerene dyad. *Chem. Commun.* **2003**, 226-227.

23. Zhang, Y.; Yu, Y.; Jiang, Z.; Xu, H.; Wang, Z.; Zhang, X.; Oda, M.; Ishizuka, T.; Jiang, D.; Chi, L.; Fuchs, H. Single-Molecule Study on Intermolecular Interaction between C60 and Porphyrin Derivatives: Toward Understanding the Strength of the Multivalency. *Langmuir* **2009**, *25*, 6627-6632.

24. Dudic, M.; Lhotak, P.; Stibor, I.; Petrickova, H.; Lang, K. (Thia)calix[4]arene-porphyrin conjugates: novel receptors for fullerene complexation with C70 over C60 selectivity. *New J. Chem.* **2004**, *28*.

25. He, L.; Zhu, Y.-Z.; Zheng, J.-Y.; Ma, Y.-F.; Chen, Y.-S. Meso-meso linked diporphyrin functionalized single-walled carbon nanotubes. *J. Photochem. Photobiol.* **2010**, *216*, 15-23.

26. Mukherjee, S.; Bauri, A. K.; Bhattacharya, S. Photophysical investigations and binding strength in supramolecular interaction of a newly designed diporphyrin tweezer with fullerenes C60 and C70 in solution. *Chem. Phys. Lett.* **2010**, *500*, 128-139.

27. Shoji, Y.; Tashiro, K.; Aida, T. Selective Extraction of Higher Fullerenes Using Cyclic Dimers of Zinc Porphyrins. *J. Am. Chem. Soc.* **2004**, *126*, 6570-6571.

28. Tamaki, K.; Imahori, H.; Sakata, Y.; Nishimura, Y.; Yamazaki, I. Synthesis and photophysical properties of a diporphyrin-fullerene triad. *Chem. Commun.* **1999**, 625-626.

29. Umeyama, T.; Tezuka, N.; Kawashima, F.; Seki, S.; Matano, Y.; Nakao, Y.; Shishido, T.; Nishi, M.; Hirao, K.; Lehtivuori, H.; Tkachenko, N. V.; Lemmetyinen, H.; Imahori, H. Carbon Nanotube Wiring of Donor–Acceptor Nanograins by Self-Assembly and Efficient Charge Transport. *Angew. Chem. Int. Ed.* **2011**, *50*, 4615-4619.

30. Wu, Z.-Q.; Shao, X.-B.; Li, C.; Hou, J.-L.; Wang, K.; Jiang, X.-K.; Li, Z.-T. Hydrogen-Bonding-Driven Preorganized Zinc Porphyrin Receptors for Efficient Complexation of C60, C70, and C60 Derivatives. *J. Am. Chem. Soc.* **2005**, *127*, 17460-17468.

31. Vilmercati, P.; Cudia, C. C.; Larciprete, R.; Cepek, C.; Zampieri, G.; Sangaletti, L.; Pagliara, S.; Verdini, A.; Cossaro, A.; Floreano, L.; Morgante, A.; Petaccia, L.; Lizzit, S.; Battocchio, C.; Polzonetti, G.; Goldoni, A. Molecular orientations, electronic properties and charge transfer timescale in a Zn-porphyrin/C70 donor–acceptor complex for solar cells. *Surf. Sci.* **2006**, *600*, 4018-4023.

32. Coates, G. W.; Dunn, A. R.; Henling, L. M.; Ziller, J. W.; Lobkovsky, E. B.; Grubbs, R. H. Phenyl−Perfluorophenyl Stacking Interactions: Topochemical [2+2] Photodimerization and Photopolymerization of Olefinic Compounds. *J. Am. Chem. Soc.* **1998**, *120*, 3641-3649.

33. Li, H.; Zhou, B.; Lin, Y.; Gu, L.; Wang, W.; Fernando, K. A. S.; Kumar, S.; Allard, L. F.; Sun, Y.-P. Selective Interactions of Porphyrins with Semiconducting Single-Walled Carbon Nanotubes. *J. Am. Chem. Soc.* **2004**, *126*, 1014-1015.

34. Sgobba, V.; Rahman, G. M. A.; Guldi, D. M.; Jux, N.; Campidelli, S.; Prato, M. Supramolecular Assemblies of Different Carbon Nanotubes for Photoconversion Processes. *Adv. Mater.* **2006**, *18*, 2264-2269.

35. Tasis, D.; Tagmatarchis, N.; Bianco, A.; Prato, M. Chemistry of Carbon Nanotubes. *Chem. Rev.* **2006**, *106*, 1105-1136.

36. Cheng, F.; Zhu, J.; Adronov, A. Supramolecular Functionalization of Single-Walled Carbon Nanotubes with Triply Fused Porphyrin Dimers: A Study of Structure–Property Relationships. *Chem. Mater.* **2011**, *23*, 3188-3194.

**Chapter 4.**

1. Farley, C.; Bhupathiraju, N. V.; John, B. K.; Drain, C. M. Tuning the Structure and Photophysics of a Fluorous Phthalocyanine Platform. *J. Phys. Chem. A.* **2016**, *(in press)*.

2. Chidawanyika, W.; Nyokong, T. The synthesis and photophysicochemical properties of low-symmetry zinc phthalocyanine analogues. *J. Photochem. Photobiol., A Chem.* **2009**, *206*, 169-176.

3. Braun, A.; Tcherniac, J. Über die Produkte der Einwirkung von Acetanhydrid auf Phthalamid. *Ber. Dtsch. Chem. Ges.* **1907**, *40*, 2709-2714.

4. de Diesbach, H.; von der Weid, E. Quelques sels complexes des o-dinitriles avec le cuivre et la pyridine. *Helv. Chim. Acta.* **1927**, *10*, 886-888.

5. Ogunsipe, A.; Maree, D.; Nyokong, T. Solvent effects on the photochemical and fluorescence properties of zinc phthalocyanine derivatives. *J. Mol. Struct.* **2003**, *650*, 131-140.

6. Löbbert, G. In *Ullmann's Encyclopedia of Industrial Chemistry, Electronic Release*; Wiley-VCH: Weinheim, **2000**; Vol. 27.

7. Varotto, A.; Nam, C. Y.; Radivojevic, I.; Tome, J. P.; Cavaleiro, J. A.; Black, C. T.; Drain, C. M. Phthalocyanine blends improve bulk heterojunction solar cells. *J. Am. Chem. Soc.* **2010**, *132*, 2552-2554.

8. Walter, M. G.; Rudine, A. B.; Wamser, C. C. Porphyrins and phthalocyanines in solar photovoltaic cells. *J. Porphyrins Phthalocyanines.* **2010**, *14*, 759-792.

9. Jurow, M. J.; Hageman, B. A.; Dimasi, E.; Nam, C. Y.; Pabon, C.; Black, C. T.; Drain, C. M. Controlling Morphology and Molecular Packing of Alkane Substituted Phthalocyanine Blend Bulk Heterojunction Solar Cells. *J. Mater. Chem. A.* **2013**, *1*, 1557-1565.

10. Ragoussi, M.-E.; Ince, M.; Torres, T. Recent Advances in Phthalocyanine-Based Sensitizers for Dye-Sensitized Solar Cells. *Eur. J. Org. Chem.* **2013**, *2013*, 6475-6489.

11. Ince, M.; Yum, J.-H.; Kim, Y.; Mathew, S.; Grätzel, M.; Torres, T.; Nazeeruddin, M. K. Molecular Engineering of Phthalocyanine Sensitizers for Dye-Sensitized Solar Cells. *J. Phys. Chem. C.* **2014**, *118*, 17166-17170.

12. Martín-Gomis, L.; Fernández-Lázaro, F.; Sastre-Santos, Á. Advances in phthalocyanine-sensitized solar cells (PcSSCs). *J. Mater. Chem. A.* **2014**, *2*, 15672-15682.

13. Debnath, A. K.; Kumar, A.; Samanta, S.; Prasad, R.; Singh, A.; Chauhan, A. K.; Veerender, P.; Singh, S.; Basu, S.; Aswal, D. K.; Gupta, S. K. Fluorinated copper-phthalocyanine/cobalt-phthalocyaine organic heterojunctions: Charge transport and Kelvin probe studies. *Appl. Phys. Lett.* **2012**, *100*, 142104.

14. Wang, H.; Liu, Z.; Fai Lo, M.; Wai Ng, T.; Yan, D.; Lee, C.-S. Electron depletion and accumulation regions in n-type copper-hexadecafluoro-phthalocyanine and their effects on electronic properties. *Appl. Phys. Lett.* **2012**, *100*, 103302.

15. Komolov, A. S.; Lazneva, E. F.; Komolov, S. A.; Repin, P. S.; Gavrikov, A. A. Potential barrier and photovoltage at interfaces of hexadecafluoro-copper-phthalocyanine and copper phthalocyanine films on the surface of tin dioxide. *Semiconductors.* **2012**, *46*, 988-992.

16. Gao, Y. L.; Ding, H. J.; Wang, H. B.; Yan, D. H. Electronic structure of interfaces between copper-hexadecafluoro-phthalocyanine and 2,5-bis(4-biphenylyl) bithiophene. *Appl. Phys. Lett.* **2007**, *91*, 142112.

17. Jiang, H.; Ye, J.; Hu, P.; Wei, F.; Du, K.; Wang, N.; Ba, T.; Feng, S.; Kloc, C. Fluorination of metal phthalocyanines: single-crystal growth, efficient N-channel organic field-effect transistors, and structure-property relationships. *Sci. Rep.* **2014**, *4*, 7573.

18. Jurow, M. J.; Schuckman, A. E.; Batteas, J. D.; Drain, C. M. Porphyrins as Molecular Electronic Components of Functional Devices. *Coord. Chem. Rev.* **2010**, *254*, 2297-2310.

19. Decreau, R.; Richard, M.-J.; Julliard, M. Photodynamic therapy against achromic M6 melanocytes: phototoxicity of lipophilic axially substituted aluminum phthalocyanines and hexadecahalogenated zinc phthalocyanines. *J. Porphyrins Phthalocyanines.* **2001**, *05*, 390-396.

20. Stanley, C. F., Durham University, 1997.

21. Boyle, R. W.; Rousseau, J.; Kudrevich, S. V.; Obochi, M. O. K.; van Lier, J. E. Hexadecafluorinated zinc phthalocyanine: photodynamic properties against the EMT-6 tumour in mice and pharmacokinetics using 65Zn as a radiotracer. *Br. J. Cancer.* **1996**, *73*, 49-53.

22. Allémann, E.; Rousseau, J.; Brasseur, N.; Kudrevich, S. V.; Lewis, K.; van Lier, J. E. Photodynamic therapy of tumours with hexadecafluoro zinc phthalocyanine formulated in PEG-coated poly(lactic acid) nanoparticles. *Int. J. Cancer.* **1996**, *66*, 821-824.

23. Allémann, E.; Brasseur, N.; Kudrevich, S. V.; La Madeleine, C.; van Lier, J. E. Photodynamic activities and biodistribution of fluorinated zinc phthalocyanine derivatives in the murine EMT-6 tumour model. *Int. J. Cancer.* **1997**, *72*, 289-294.

24. Sekkat, N.; van den Bergh, H.; Nyokong, T.; Lange, N. Like a bolt from the blue: phthalocyanines in biomedical optics. *Molecules.* **2012**, *17*, 98-144.

25. Leznoff, C. C.; Hiebert, A.; Ok, S. Titration syntheses of polyaminosubstituted phthalocyanines via nucleophilic aromatic substitutions on zinc(II) 1,2,3,4,8,9,10,11,15,16,17,18,22,23,24,25-hexadecafluorophthalocyanine. *J. Porphyrins Phthalocyanines.* **2007**, *11*, 537-546.

26. Alonso, M. I.; Garriga, M.; Ossó, J. O.; Schreiber, F.; Barrena, E.; Dosch, H. Strong optical anisotropies of F[sub 16]CuPc thin films studied by spectroscopic ellipsometry. *J. Chem. Phys.* **2003**, *119*, 6335.

27. Leznoff, C. C.; Sosa-Sanchez, J. L. Polysubstituted phthalocyanines by nucleophilic substitution reactions on hexadecafluorophthalocyanines. *Chem. Commun.* **2004**, 338-339.

28. Jurow, M. J.; Varotto, A.; Manichev, V.; Travlou, N. A.; Giannakoudakis, D. A.; Drain, C. M. Self-organized nanostructured materials of alkylated phthalocyanines and underivatized C60 on ITO. *RSC Adv.* **2013**, *3*, 21360.

29. Garcia, A. M.; Alarcon, E.; Munoz, M.; Scaiano, J. C.; Edwards, A. M.; Lissi, E. Photophysical behaviour and photodynamic activity of zinc phthalocyanines associated to liposomes. *Photochem. Photobiol. Sci.* **2011**, *10*, 507-514.

30. Bartoli, G.; Ciminale, F.; Todesco, P. E. Electronic and steric effects in nucleophilic aromatic substitution. Reaction by phenoxides as nucleophiles in dimethyl sulfoxide. *J. Org. Chem.* **1975**, *40*, 872-874.

31. Wang, J.; Khanamiryan, A. K.; Leznoff, C. C. Multisubstituted phthalonitriles for phthalocyanine synthesis. *J. Porphyrins Phthalocyanines.* **2004**, *08*, 1293-1299.

32. Bhupathiraju, N. V.; Rizvi, W.; Batteas, J. D.; Drain, C. M. Fluorinated porphyrinoids as efficient platforms for new photonic materials, sensors, and therapeutics. *Org. Biomol. Chem.* **2016**, *14*, 389-408.

33. Chambrier, I.; J. Cook, M.; T. Wood, P. Conformationally stressed phthalocyanines: the non-planarity of the 1,4,8,11,15,18,22,25-octaisopentyl derivative. *Chem. Commun.* **2000**, 2133-2134.

34. Zorlu, Y.; Kumru, U.; Isci, U.; Divrik, B.; Jeanneau, E.; Albrieux, F.; Dede, Y.; Ahsen, V.; Dumoulin, F. 1,4,8,11,15,18,22,25-Alkylsulfanyl phthalocyanines: effect of macrocycle distortion on spectroscopic and packing properties. *Chem. Commun.* **2015**, *51*, 6580-6583.

35. Honda, T.; Kojima, T.; Kobayashi, N.; Fukuzumi, S. Crystal structures and electronic properties of saddle-distorted and protonated phthalocyanines. *Angew. Chem. Int. Ed.* **2011**, *50*, 2725-2728.

36. Furuyama, T.; Satoh, K.; Kushiya, T.; Kobayashi, N. Design, synthesis, and properties of phthalocyanine complexes with main-group elements showing main absorption and fluorescence beyond 1000 nm. *J. Am. Chem. Soc.* **2014**, *136*, 765-776.

37. Kobayashi, N.; Fukuda, T.; Ueno, K.; Ogino, H. Extremely Non-Planar Phthalocyanines with Saddle or Helical Conformation: Synthesis and Structural Characterizations. *J. Am. Chem. Soc.* **2001**, *123*, 10740-10741.

38. Cammidge, A. N.; Tseng, C.-H.; Chambrier, I.; Hughes, D. L.; Cook, M. J. Phthalocyanines bearing bulky cycloalkylmethyl substituents on non-peripheral sites. *Tetrahedron Lett.* **2009**, *50*, 5254-5256.

39. Kobayashi, N.; Furuyama, T.; Satoh, K. Rationally designed phthalocyanines having their main absorption band beyond 1000 nm. *J. Am. Chem. Soc.* **2011**, *133*, 19642-19645.

40. Isago, H. In *Optical Spectra of Phthalocyanines and Related Compounds*; Springer: New York, **2015**, p 107-131.

41. Golchoubian, H.; Hosseinpoor, F. Effective Oxidation of Sulfides to Sulfoxides with Hydrogen Peroxide under Transition-Metal-Free Conditions. *Molecules.* **2007**, *12*, 304-311.

42. Taniguchi, M.; Du, H.; Lindsey, J. S. Virtual libraries of tetrapyrrole macrocycles. Combinatorics, isomers, product distributions, and data mining. *J. Chem. Inf. Model.* **2011**, *51*, 2233-2247.

43. Taniguchi, M.; Soares, A. R. M.; Chandrashaker, V.; Lindsey, J. S. A tandem combinatorial model for the prebiogenesis of diverse tetrapyrrole macrocycles. *New J. Chem.* **2012**, *36*, 1057.

44. Taniguchi, M.; Lindsey, J. S. Diversity, isomer composition, and design of combinatorial libraries of tetrapyrrole macrocycles. *J. Porphyrins Phthalocyanines.* **2012**, *16*, 1-13.

45. Taniguchi, M.; Lindsey, J. S. In *Handbook of Porphyrin Science*; World Scientific: Singapore, **2012**; Vol. 23, p 1-80.

46. Drain, C. M.; Singh, S. In *Handbook of Porphyrin Science*; Kadish, K. M., Smith, K. M., Guilard, R., Eds.; World Scientific: Singapore, **2011**; Vol. 3, p 485-530.

47. Berlin, K.; Jain, R. K.; Tetzlaff, C.; Steinbeck, C.; Richert, C. Spectrometrically monitored selection experiments: quantitative laser desorption mass spectrometry of small chemical libraries. *Chem. Biol.* **1997**, *4*, 63-77.

48. Stulz, E.; Scott, S. M.; Bond, A. D.; Teat, S. J.; Sanders, J. K. Selection and amplification of mixed-metal porphyrin cages from dynamic combinatorial libraries. *Chem. Eur. J.* **2003**, *9*, 6039-6048.

49. Ding, S.; Gray, N. S.; Wu, X.; Ding, Q.; Schultz, P. G. A Combinatorial Scaffold Approach toward Kinase-Directed Heterocycle Libraries. *J. Am. Chem. Soc.* **2002**, *124*, 1594-1596.

50. Drain, C. M.; Gong, X.; Ruta, V.; Soll, C. E.; Chicoineau, P. F. Combinatorial Synthesis and Modification of Functional Porphyrin Libraries: Identification of New, Amphipathic Motifs for Biomolecule Binding. *J. Comb. Chem.* **1999**, *1*, 286-290.

51. Samaroo, D.; Vinodu, M.; Chen, X.; Drain, C. M. meso-Tetra(pentafluorophenyl)porphyrin as an efficient platform for combinatorial synthesis and the selection of new photodynamic therapeutics using a cancer cell line. *J. Comb. Chem.* **2007**, *9*, 998-1011.

52. Read, R. C. Pólya's Theorem and Its Progeny. *Math. Mag.* **1987**, *60*, 275.

53. Pólya, G. Kombinatorische Anzahlbestimmungen für Gruppen, Graphen und chemische Verbindungen. *Acta Math.* **1937**, *68*, 145-254.

54. Redfield, J. H. The Theory of Group-Reduced Distributions. *Am. J. Math.* **1927**, *49*, 433.

55. Williams, A. Loopless Generation of Multiset Permutations using a Constant Number of Variables by Prefix Shifts. *Proceedings of the Twentieth Annual ACM-SIAM Symposium on Discrete Algorithms.* **2009**, 987-996.

56. Iagatti, A.; Doria, S.; Marcelli, A.; Angelini, N.; Notarantonio, S.; Paoletti, A. M.; Pennesi, G.; Rossi, G.; Zanotti, G.; Calogero, G.; Foggi, P. Photophysical Processes Occurring in a Zn-phthalocyanine in Ethanol Solution and on TiO2 Nanostructures. *J. Phys. Chem. C.* **2015**, *119*, 20256-20264.

57. Dick, S.; Peisert, H.; Dini, D.; Hanack, M.; Cook, M. J.; Chambrier, I.; Chassé, T. Influence of the alkyl-chains length on the electronic structure and interface properties of 1,4-octasubstituted zinc phthalocyanines on gold. *J. Appl. Phys.* **2005**, *97*, 073715.

58. Mack, J.; Kobayashi, N.; Stillman, M. J. Re-examination of the emission properties of alkoxy- and thioalkyl-substituted phthalocyanines. *J. Inorg. Biochem.* **2010**, *104*, 310-317.

59. Gorun, S. M.; Rathke, J. W.; Chen, M. J. Long-range solid-state ordering and high geometric distortions induced in phthalocyanines by small fluoroalkyl groups. *Dalton Trans.* **2009**, 1095-1097.

60. Gao, Y.; Chen, Y.; Li, R.; Bian, Y.; Li, X.; Jiang, J. Nonperipherally octa(butyloxy)-substituted phthalocyanine derivatives with good crystallinity: effects of metal-ligand coordination on the molecular structure, internal structure, and dimensions of self-assembled nanostructures. *Chem. Eur. J.* **2009**, *15*, 13241-13252.

61. Gunaratne, T. C.; Gusev, A. V.; Peng, X.; Rosa, A.; Ricciardi, G.; Baerends, E. J.; Rizzoli, C.; Kenney, M. E.; Rodgers, M. A. Photophysics of octabutoxy phthalocyaninato-Ni(II) in

toluene: ultrafast experiments and DFT/TDDFT studies. *J. Phys. Chem. A.* **2005**, *109*, 2078-2089.

62. Bishop, S. M.; Beeby, A.; Parker, A. W.; Foley, M. S. C.; Phillips, D. The preparation and photophysical measurements of perdeutero zinc phthalocyanine. *J. Photochem. Photobiol., A Chem.* **1995**, *90*, 39-44.

63. Alberto, M. E.; De Simone, B. C.; Mazzone, G.; Sicilia, E.; Russo, N. The heavy atom effect on Zn(II) phthalocyanine derivatives: a theoretical exploration of the photophysical properties. *Phys. Chem. Chem. Phys.* **2015**, *17*, 23595-23601.

64. Azenha, E. l. G.; Serra, A. C.; Pineiro, M.; Pereira, M. M.; Seixas de Melo, J.; Arnaut, L. G.; Formosinho, S. J.; Rocha Gonsalves, A. M. d. A. Heavy-atom effects on metalloporphyrins and polyhalogenated porphyrins. *Chem. Phys.* **2002**, *280*, 177-190.

65. Bonnett, R.; Harriman, A.; Kozyrev, A. N. Photophysics of halogenated porphyrins. *J. Chem. Soc., Faraday Trans.* **1992**, *88*, 763.

66. Makhseed, S.; Ghazal, B.; Abdelmoniem, A. M.; Novakova, V.; Zimcik, P. Photophysical and theoretical studies of peripherally halogenated octaphenoxyphthalocyanines. *RSC Adv.* **2015**, *5*, 58854-58864.

67. Lo, P.-C.; Wang, S.; Zeug, A.; Meyer, M.; Röder, B.; Ng, D. K. P. Preparation and photophysical properties of halogenated silicon(IV) phthalocyanines substituted axially with poly(ethylene glycol) chains. *Tetrahedron Lett.* **2003**, *44*, 1967-1970.

68. Kobayashi, N.; Ogata, H.; Nonaka, N.; Luk'yanets, E. A. Effect of peripheral substitution on the electronic absorption and fluorescence spectra of metal-free and zinc phthalocyanines. *Chem. Eur. J.* **2003**, *9*, 5123-5134.

69. Bixon, M.; Jortner, J.; Cortes, J.; Heitele, H.; Michel-Beyerle, M. E. Energy Gap Law for Nonradiative and Radiative Charge Transfer in Isolated and in Solvated Supermolecules. *J. Phys. Chem.* **1994**, *98*, 7289-7299.

70. Gutierrez-Meza, E.; Noria, R.; Granados, G.; Gomez-Vidales, V.; Ramirez, J. Z.; Beltran, H. I.; Peon, J. Photophysics of a cis axially disubstituted macrocycle: rapid intersystem crossing in a tin(IV) phthalocyanine with a half-domed geometry. *J. Phys. Chem. B.* **2012**, *116*, 14107-14114.

71. Peceli, D.; Hu, H.; Fishman, D. A.; Webster, S.; Przhonska, O. V.; Kurdyukov, V. V.; Slominsky, Y. L.; Tolmachev, A. I.; Kachkovski, A. D.; Gerasov, A. O.; Masunov, A. E.; Hagan, D. J.; Van Stryland, E. W. Enhanced intersystem crossing rate in polymethine-like molecules: sulfur-containing squaraines versus oxygen-containing analogues. *J. Phys. Chem. A.* **2013**, *117*, 2333-2346.

72. Orchin, M.; Macomber, R. S.; Pinhas, A. R.; Wilson, R. M. *The Vocabulary and Concepts of Organic Chemistry*; Second ed.; John Wiley & Sons, Inc.: Hoboken, NJ, **2005**.

73. Zander, M. The Intra-annular Internal Heavy-atom Effect on the Fluorescence and Phosphorescence Properties of Oxygen, Sulphur or Selenium Containing Heterocyclic Systems Related to Dibenzo [b,n] perylene. *Zeitschrift für Naturforschung A.* **1989**, *44*.

74. Goldacker, W.; Schweitzer, D.; Zimmermann, H. Electronic properties of the triplet state of fluorene, carbazole, dibenzofuran and dibenzothiophene (X-traps). *Chem. Phys.* **1979**, *36*, 15-26.

75. Wróbel, D.; Graja, A. Photoinduced electron transfer processes in fullerene–organic chromophore systems. *Coord. Chem. Rev.* **2011**, *255*, 2555-2577.

76. Turro, N. J.; Ramamurthy, V.; Scaiano, J. C. *Principles of Molecular Photochemistry: An Introduction*; University Science Books: Sausalito, CA, **2009**.

77. Ravikanth, M.; Reddy, D.; Chandrashekar, T. K. Fluorescence properties of distorted short-chain basket handle porphyrins. *J. Photochem. Photobiol., A Chem.* **1993**, *72*, 61-67.

78. Maiti, N. C.; Ravikanth, M. Photophysical properties of structurally deformed basket-handle prophyrins. *J. Chem. Soc., Faraday Trans.* **1995**, *91*, 4369.

79. Senge, M. O. In *The Porphyrin Handbook*; Kadish, K. M., Smith, K. M., Guilard, R., Eds.; Academic Press: New York, **2000**; Vol. 1, p 239-348.

80. Ivashin, N. V.; Shchupak, E. E.; Panarin, A. Y.; Sagun, E. I. Photophysical properties of porphyrins with sterically distorted and partially screened macrocycles. *Opt. Spectrosc.* **2015**, *118*, 882-892.

81. Sazanovich, I. V.; Galievsky, V. A.; van Hoek, A.; Schaafsma, T. J.; Malinovskii, V. L.; Holten, D.; Chirvony, V. S. Photophysical and Structural Properties of Saddle-Shaped Free Base Porphyrins: Evidence for an "Orthogonal" Dipole Moment. *J. Phys. Chem. B.* **2001**, *105*, 7818-7829.

82. Nifiatis, F.; Su, W.; Haley, J. E.; Slagle, J. E.; Cooper, T. M. Comparison of the photophysical properties of a planar, PtOEP, and a nonplanar, PtOETPP, porphyrin in solution and doped films. *J. Phys. Chem. A.* **2011**, *115*, 13764-13772.

83. Gentemann, S.; Medforth, C. J.; Forsyth, T. P.; Nurco, D. J.; Smith, K. M.; Fajer, J.; Holten, D. Photophysical Properties of Conformationally Distorted Metal-Free Porphyrins. Investigation into the Deactivation Mechanisms of the Lowest Excited Singlet State. *J. Am. Chem. Soc.* **1994**, *116*, 7363-7368.

84. Röder, B.; Büchner, M.; Rückmann, I.; Senge, M. O. Correlation of photophysical parameters with macrocycle distortion in porphyrins with graded degree of saddle distortion. *Photochem. Photobiol. Sci.* **2010**, *9*, 1152-1158.

85. Lebedev, A. Y.; Filatov, M. A.; Cheprakov, A. V.; Vinogradov, S. A. Effects of structural deformations on optical properties of tetrabenzoporphyrins: free-bases and Pd complexes. *J. Phys. Chem. A.* **2008**, *112*, 7723-7733.

86. Drain, C. M.; Kirmaier, C.; Medforth, C. J.; Nurco, D. J.; Smith, K. M.; Holten, D. Dynamic Photophysical Properties of Conformationally Distorted Nickel Porphyrins. 1. Nickel(II) Dodecaphenylporphyrin. *J. Phys. Chem.* **1996**, *100*, 11984-11993.

87. Drain, C. M.; Gentemann, S.; Roberts, J. A.; Nelson, N. Y.; Medforth, C. J.; Jia, S.; Simpson, M. C.; Smith, K. M.; Fajer, J.; Shelnutt, J. A.; Holten, D. Picosecond to Microsecond Photodynamics of a Nonplanar Nickel Porphyrin: Solvent Dielectric and Temperature Effects. *J. Am. Chem. Soc.* **1998**, *120*, 3781-3791.

88. Retsek, J. L.; Drain, C. M.; Kirmaier, C.; Nurco, D. J.; Medforth, C. J.; Smith, K. M.; Sazanovich, I. V.; Chirvony, V. S.; Fajer, J.; Holten, D. Photoinduced Axial Ligation and Deligation Dynamics of Nonplanar Nickel Dodecaarylporphyrins. *J. Am. Chem. Soc.* **2003**, *125*, 9787-9800.

89. Rodriguez, J.; Kirmaier, C.; Holten, D. Time-resolved and static optical properties of vibrationally excited porphyrins. *J. Chem. Phys.* **1991**, *94*, 6020.

90. Mack, J.; Kobayashi, N. Low symmetry phthalocyanines and their analogues. *Chem. Rev.* **2011**, *111*, 281-321.

91. Rio, Y.; Salome Rodriguez-Morgade, M.; Torres, T. Modulating the electronic properties of porphyrinoids: a voyage from the violet to the infrared regions of the electromagnetic spectrum. *Org. Biomol. Chem.* **2008**, *6*, 1877-1894.

92. Li, R.; Zhang, X.; Zhu, P.; Ng, D. K.; Kobayashi, N.; Jiang, J. Electron-donating or -withdrawing nature of substituents revealed by the electrochemistry of metal-free phthalocyanines. *Inorg. Chem.* **2006**, *45*, 2327-2334.

93. Shinohara, H.; Tsaryova, O.; Schnurpfeil, G.; Wöhrle, D. Differently substituted phthalocyanines: Comparison of calculated energy levels, singlet oxygen quantum yields, photo-oxidative stabilities, photocatalytic and catalytic activities. *J. Photochem. Photobiol., A Chem.* **2006**, *184*, 50-57.

94. Gouterman, M. Spectra of porphyrins. *J. Mol. Spectrosc.* **1961**, *6*, 138-163.

95. Gouterman, M.; Wagnière, G. H.; Snyder, L. C. Spectra of porphyrins: Part II. Four orbital model. *J. Mol. Spectrosc.* **1963**, *11*, 108-127.

96. Chidawanyika, W.; Mack, J.; Shimizu, S.; Kobayashi, N.; Nyokong, T. Effect of peripheral fused ring substitution on the optical spectroscopy and electronic structure of metal phthalocyanine complexes. *J. Porphyrins Phthalocyanines.* **2009**, *13*, 1053-1062.

97. Das, S. K.; Mahler, A.; Wilson, A. K.; D'Souza, F. High-potential perfluorinated phthalocyanine-fullerene dyads for generation of high-energy charge-separated states: formation and photoinduced electron-transfer studies. *ChemPhysChem.* **2014**, *15*, 2462-2472.

98. Lee, S. U. Influence of Exchange-Correlation Functional in the Calculations of Vertical Excitation Energies of Halogenated Copper Phthalocyanines using Time-Dependent Density Functional Theory (TD-DFT). *Bull. Korean Chem. Soc.* **2013**, *34*, 2276-2280.

99. Furche, F.; Rappoport, D. In *Computational Photochemistry*; Olivucci, M., Ed.; Elsevier: New York, **2005**; Vol. 16.

100. Fukuda, R.; Ehara, M. Excited states and electronic spectra of annulated dinuclear free-base phthalocyanines: a theoretical study on near-infrared-absorbing dyes. *J. Chem. Phys.* **2012**, *136*, 114304.

101. Zakavi, S.; Omidyan, R.; Talebzadeh, S. Porphine core saddling: Effects on the HOMO/LUMO gap and the macrocycle bond lengths and bond angles. *Polyhedron.* **2013**, *49*, 36-40.

102. Zhang, Y. H.; Zhao, W.; Jiang, P.; Zhang, L. J.; Zhang, T.; Wang, J. Structural parameters and vibrational spectra of a series of zinc meso-phenylporphyrins: a DFT and experimental study. *Spectrochim. Acta A Mol. Biomol. Spectrosc.* **2010**, *75*, 880-890.

103. Haddad, R. E.; Gazeau, S.; Pecaut, J.; Marchon, J. C.; Medforth, C. J.; Shelnutt, J. A. Origin of the red shifts in the optical absorption bands of nonplanar tetraalkylporphyrins. *J. Am. Chem. Soc.* **2003**, *125*, 1253-1268.

104. Ryeng, H.; Ghosh, A. Do Nonplanar Distortions of Porphyrins Bring about Strongly Red-Shifted Electronic Spectra? Controversy, Consensus, New Developments, and Relevance to Chelatases. *J. Am. Chem. Soc.* **2002**, *124*, 8099-8103.

105. Wertsching, A. K.; Koch, A. S.; DiMagno, S. G. On the Negligible Impact of Ruffling on the Electronic Spectra of Porphine, Tetramethylporphyrin, and Perfluoroalkylporphyrins. *J. Am. Chem. Soc.* **2001**, *123*, 3932-3939.

106. Parusel, A. B. J.; Wondimagegn, T.; Ghosh, A. Do Nonplanar Porphyrins Have Red-Shifted Electronic Spectra? A DFT/SCI Study and Reinvestigation of a Recent Proposal. *J. Am. Chem. Soc.* **2000**, *122*, 6371-6374.

107. DiMagno, S. G.; Wertsching, A. K.; Ross, C. R. Electronic Consequences of Nonplanar Core Conformations in Electron-Deficient Porphyrins: The Structure and Spectroscopic Properties of [5,10,15,20-Tetrakis(heptafluoropropyl)porphinato]cobalt(II). *J. Am. Chem. Soc.* **1995**, *117*, 8279-8280.

**Chapter 5.**

1. Seybold, P. G.; Gouterman, M. Porphyrins : XIII: Fluorescence spectra and quantum yields. *Journal of Molecular Spectroscopy.* **1969**, *31*, 1-13.

2. Hosomizu, K.; Oodoi, M.; Umeyama, T.; Matano, Y.; Yoshida, K.; Isoda, S.; Isosomppi, M.; Tkachenko, N. V.; Lemmetyinen, H.; Imahori, H. Substituent Effects of Porphyrins on Structures and Photophysical Properties of Amphiphilic Porphyrin Aggregates. *The Journal of Physical Chemistry B.* **2008**, *112*, 16517-16524.

3. Mathew, S.; Iijima, H.; Toude, Y.; Umeyama, T.; Matano, Y.; Ito, S.; Tkachenko, N. V.; Lemmetyinen, H.; Imahori, H. Optical, Electrochemical, and Photovoltaic Effects of an Electron-Withdrawing Tetrafluorophenylene Bridge in a Push–Pull Porphyrin Sensitizer Used for Dye-Sensitized Solar Cells. *The Journal of Physical Chemistry C.* **2011**, *115*, 14415-14424.

4. Grover, N.; Sankar, M.; Song, Y.; Kadish, K. M. Asymmetrically Crowded "Push-Pull" Octaphenylporphyrins with Modulated Frontier Orbitals: Syntheses, Photophysical, and Electrochemical Redox Properties. *Inorganic chemistry.* **2016**, *55*, 584-597.

5. Wang, L.; She, Y.; Zhong, R.; Ji, H.; Zhang, Y.; Song, X. A Green Process for Oxidation of p-Nitrotoluene Catalyzed by Metalloporphyrins under Mild Conditions. *Organic Process Research & Development.* **2006**, *10*, 757-761.

6. Schiavon, M. A.; Iamamoto, Y.; Nascimento, O. R.; Assis, M. d. D. Catalytic activity of nitro- and carboxy-substituted iron porphyrins in hydrocarbon oxidation. *Journal of Molecular Catalysis A: Chemical.* **2001**, *174*, 213-222.

7. Zakavi, S.; Heidarizadi, F.; Rayati, S. Comparative study of catalytic activity of some biomimetic models of cytochrome P450 in oxidation of olefins with tetra-n-butylammonium periodate: Electron-rich Mn-porphyrins versus the electron-deficient ones. *Inorganic Chemistry Communications.* **2011**, *14*, 1010-1013.

8. Gong, L.-C.; Dolphin, D. Nitrooctaethylporphyrins: synthesis, optical and redox properties. *Canadian Journal of Chemistry.* **1985**, *63*, 401-405.

9. Ozette, K.; Leduc, P.; Palacio, M.; Bartoli, J.-F.; Barkigia, K. M.; Fajer, J.; Battioni, P.; Mansuy, D. New Metalloporphyrins with Extremely Altered Redox Properties: Synthesis, Structure, and Facile Reduction to Air-Stable π-Anion Radicals of Zinc and Nickel β-Heptanitroporphyrins. *Journal of the American Chemical Society.* **1997**, *119*, 6442-6443.

10. Bartoli, J. F.; Battioni, P.; De Foor, W. R.; Mansuy, D. Synthesis and remarkable properties of iron β-polynitroporphyrins as catalysts for monooxygenation reactions. *Journal of the Chemical Society, Chemical Communications.* **1994**, 23-24.

11. Sun, B.; Ou, Z.; Yang, S.; Meng, D.; Lu, G.; Fang, Y.; Kadish, K. M. Synthesis and electrochemistry of beta-pyrrole nitro-substituted cobalt(II) porphyrins. The effect of the NO(2) group on redox potentials, the electron transfer mechanism and catalytic reduction of molecular oxygen in acidic media. *Dalton Transactions.* **2014**, *43*, 10809-10815.

12. Suslick, K. S.; Chen, C. T.; Meredith, G. R.; Cheng, L. T. Push-pull porphyrins as nonlinear optical materials. *Journal of the American Chemical Society.* **1992**, *114*, 6928-6930.

13. Sen, A.; Krishnan, V. Synthesis, spectral and electrochemical properties of donor/acceptor substituted fluoroarylporphyrins. *Tetrahedron Letters.* **1996**, *37*, 5421-5424.

14. Senge, M. O.; Ryppa, C.; Fazekas, M.; Zawadzka, M.; Dahms, K. 5,10-A2B2-type meso-substituted porphyrins-a unique class of porphyrins with a realigned dipole moment. *Chemistry.* **2011**, *17*, 13562-13573.

15. Chou, J.-h.; Kosal, M. E.; Nalwa, H. S.; Rakow, N. A.; Suslick, K. S. In *The Porphyrin Handbook*; Academic Press: New York, **2000**; Vol. 6, p 43-131.

16. Schiavon, M. A.; Iwamoto, L. S.; Ferreira, A. G.; Iamamoto, Y.; Zanoni, M. V. B.; Assis, M. d. D. Synthesis and characterization of a novel series of meso (nitrophenyl) and meso (carboxyphenyl) substituted porphyrins. *Journal of the Brazilian Chemical Society.* **2000**, *11*, 458-466.

17. Gros, C. P.; Desbois, N.; Michelin, C.; Demilly, E.; Tilkin-Mariamé, A.-F.; Mariamé, B.; Gallardo, F. Synthesis and Antiviral Activity Evaluation of Nitroporphyrins and Nitrocorroles as Potential Agents against HumanCytomegalovirusInfection. *ACS Infectious Diseases.* **2015**, *1*, 350-356.

18. Maiya, G. B.; Krishnan, V. Intramolecular electron transfer in donor-acceptor systems. Porphyrins bearing trinitroaryl acceptor group. *The Journal of Physical Chemistry.* **1985**, *89*, 5225-5235.

19. Kim, H.-S.; Kim, C.-H.; Ha, C.-S.; Lee, J.-K. Organic solar cell devices based on PVK/porphyrin system. *Synthetic Metals.* **2001**, *117*, 289-291.

20. Tingting, X.; He, H.; Wang, Q.; Dubey, M.; Xingzhong, Y.; Galipeau, D.; Ropp, M. In *Photovoltaic Specialists Conference, 33rd IEEE*; IEEE: San Diego, CA, 2008, p 1-3.

21. Kim, J. B.; Leonard, J. J.; Longo, F. R. Mechanistic study of the synthesis and spectral properties of meso-tetraarylporphyrins. *Journal of the American Chemical Society.* **1972**, *94*, 3986-3992.

22. Karki, L.; Vance, F. W.; Hupp, J. T.; LeCours, S. M.; Therien, M. J. Electronic Stark Effect Studies of a Porphyrin-Based Push−Pull Chromophore Displaying a Large First Hyperpolarizability: State-Specific Contributions to β. *Journal of the American Chemical Society.* **1998**, *120*, 2606-2611.

23. Karelson, M.; Pihlaja, K.; Tamm, T.; Uri, A.; Zerner, M. C. UV-visible spectra of some nitro-substituted porphyrins. *Journal of Photochemistry and Photobiology A: Chemistry.* **1995**, *85*, 119-126.

24. Crossley, M. J.; Harding, M. M.; Sternhell, S. Tautomerism in 2-substituted 5,10,15,20-tetraphenylporphyrins. *Journal of the American Chemical Society.* **1986**, *108*, 3608-3613.

25. Yang, S.; Sun, B.; Ou, Z.; Meng, D.; Lu, G.; Fang, Y.; Kadish, K. M. β-Nitro-substituted free-base, iron(III) and manganese(III) tetraarylporphyrins: synthesis, electrochemistry and effect of the NO2substituent on spectra and redox potentials in non-aqueous media. *Journal of Porphyrins and Phthalocyanines.* **2013**, *17*, 857-869.

26. Siri, O.; Jaquinod, L.; Smith, K. M. Coplanar conjugated β-nitroporphyrins and some aspects of nitration of porphyrins with N2O4. *Tetrahedron Letters.* **2000**, *41*, 3583-3587.

27. Vicente, M. G. H.; Neves, M. G. P. M. S.; Cavaleiro, J. S.; Hombrecher, H. K.; Koll, D. Electrochemical and spectroscopic properties of Cu(II) β-nitro meso-tetra(pentafluorophenyl)porphyrins. *Tetrahedron Letters.* **1996**, *37*, 261-262.

28. Hindin, E.; Kirmaier, C.; Diers, J. R.; Tomizaki, K.-y.; Taniguchi, M.; Lindsey, J. S.; Bocian, D. F.; Holten, D. Photophysical Properties of Phenylethyne-Linked Porphyrin and Oxochlorin Dyads. *The Journal of Physical Chemistry B.* **2004**, *108*, 8190-8200.

29. Barkigia, K. M.; Renner, M. W.; Senge, M. O.; Fajer, J. Interplay of Axial Ligation, Hydrogen Bonding, Self-Assembly, and Conformational Landscapes in High-Spin Ni(II) Porphyrins. *The Journal of Physical Chemistry B.* **2004**, *108*, 2173-2180.

30. Hsiao, J.-S.; Krueger, B. P.; Wagner, R. W.; Johnson, T. E.; Delaney, J. K.; Mauzerall, D. C.; Fleming, G. R.; Lindsey, J. S.; Bocian, D. F.; Donohoe, R. J. Soluble Synthetic Multiporphyrin Arrays. 2. Photodynamics of Energy-Transfer Processes. *Journal of the American Chemical Society.* **1996**, *118*, 11181-11193.

31. Pukhovskaya, S. G.; Ivanova, Y. B.; Nam, D. T.; Vashurin, A. S. Dependence of the basic properties of meso-nitro-substituted derivatives of β-octaethylporphyrin on the nature of substituents. *Russian Journal of Physical Chemistry A.* **2014**, *88*, 1670-1676.

32. Ivanova, Y. B.; Nam, D. T.; Chizhova, N. V.; Mamardashvili, N. Z. Spectrophotometric study of acid-base and complexing properties of 5,10,15-trinitro-2,3,7,8,12,13,17,18-

octaethylporphyrin in acetonitrile. *Russian Journal of General Chemistry.* **2014**, *84*, 1207-1211.

33. Ivanova, Y. B.; Chizhova, N. V.; Mamardashvili, N. Z. Spectrophotometric study of the complexing properties of 2,3,7,8,12,13,17,18-Octaethyl-5,10,15-trinitroporphyrin and its dianion toward Zn(OAc)2 in acetonitrile. *Russian Journal of General Chemistry.* **2014**, *84*, 1394-1398.
34. Dey, S.; Ikbal, S. A.; Rath, S. P. Self-assembly of cobalt(ii) and zinc(ii) tetranitrooctaethylporphyrin via bidentate axial ligands: synthesis, structure, surface morphology and effect of axial coordination. *New Journal of Chemistry.* **2014**, *38*, 1458-1470.
35. Kleij, A. W.; Kuil, M.; Tooke, D. M.; Spek, A. L.; Reek, J. N. Template-assisted ligand encapsulation; the impact of an unusual coordination geometry on a supramolecular pyridylphosphine-Zn(II)porphyrin assembly. *Inorganic chemistry.* **2005**, *44*, 7696-7698.
36. Weimin, S.; Qi, S.; Yucheng, W.; Lihong, L.; Jingchao, T. An alternative approach to amino porphyrins. *Journal of Heterocyclic Chemistry.* **2010**, *47*, 1221-1224.
37. Luguya, R.; Jaquinod, L.; Fronczek, F. R.; Vicente, M. G. H.; Smith, K. M. Synthesis and reactions of meso-(p-nitrophenyl)porphyrins. *Tetrahedron.* **2004**, *60*, 2757-2763.
38. Ormond, A. B.; Freeman, H. S. Effects of substituents on the photophysical properties of symmetrical porphyrins. *Dyes and Pigments.* **2013**, *96*, 440-448.
39. Rose, E.; Cardon-Pilotaz, A.; Quelquejeu, M.; Bernard, N.; Kossanyi, A.; Desmazieres, B. Efficient Preparation of the .alpha.,.alpha.,.beta.,.beta.-Atropoisomer of meso-Tetrakis(o-aminophenyl)porphyrin. *The Journal of Organic Chemistry.* **1995**, *60*, 3919-3920.
40. Serra, V. I. V.; Pires, S. M. G.; Alonso, C. M. A.; Neves, M. G. P. M. S.; Tomé, A. C.; Cavaleiro, J. A. S. Meso-Tetraarylporphyrins Bearing Nitro or Amino Groups: Synthetic Strategies and Reactivity Profiles. *Topics in Heterocyclic Chemistry.* **2014**, *33*, 35-78.
41. Karolczak, J.; Kowalska, D.; Lukaszewicz, A.; Maciejewski, A.; Steer, R. P. Photophysical Studies of Porphyrins and Metalloporphyrins: Accurate Measurements of Fluorescence Spectra and Fluorescence Quantum Yields for Soret Band Excitation of Zinc Tetraphenylporphyrin. *The Journal of Physical Chemistry A.* **2004**, *108*, 4570-4575.
42. Chirvony, V. S.; van Hoek, A.; Schaafsma, T. J.; Pershukevich, P. P.; Filatov, I. V.; Avilov, I. V.; Shishporenok, S. I.; Terekhov, S. N.; Malinovskii, V. L. On the Nature of the Fluorescent State in β-Nitrotetraarylporphyrins. *The Journal of Physical Chemistry B.* **1998**, *102*, 9714-9724.
43. Barnett, G. H.; Hudson, M. F.; Smith, K. M. Concerning meso-tetraphenylporphyrin purification. *Journal of the Chemical Society, Perkin Transactions 1.* **1975**, 1401-1403.
44. Senge, M. O.; Eigenbrot, C. W.; Brennan, T. D.; Shusta, J.; Scheidt, W. R.; Smith, K. M. Aggregation properties of nitroporphyrins: comparisons between solid-state and solution structures. *Inorganic chemistry.* **1993**, *32*, 3134-3142.
45. Ono, N.; Muratani, E.; Fumoto, Y.; Ogawa, T.; Tazima, K. Synthesis of 2,7,12,17-tetraaryl-3,8,13,18-tetranitroporphyrins; electronic effects on aggregation properties of porphyrins. *Journal of the Chemical Society, Perkin Transactions 1.* **1998**, 3819-3824.

46. Zhao, Z.; Nyokong, T.; Maree, M. D. Synthesis and photochemical characterization of a zinc phthalocyanine–zinc porphyrin heterotrimer and heterononamer. *Dalton Transactions.* **2005**, 3732-3737.

47. Drain, C. M.; Kirmaier, C.; Medforth, C. J.; Nurco, D. J.; Smith, K. M.; Holten, D. Dynamic Photophysical Properties of Conformationally Distorted Nickel Porphyrins. 1. Nickel(II) Dodecaphenylporphyrin. *The Journal of Physical Chemistry.* **1996**, *100*, 11984-11993.

48. Hwang, I. W.; Kamada, T.; Ahn, T. K.; Ko, D. M.; Nakamura, T.; Tsuda, A.; Osuka, A.; Kim, D. Porphyrin boxes constructed by homochiral self-sorting assembly: optical separation, exciton coupling, and efficient excitation energy migration. *J Am Chem Soc.* **2004**, *126*, 16187-16198.

49. Knyukshto, V.; Zenkevich, E.; Sagun, E.; Shulga, A.; Bachilo, S. Pathways for photoinduced electron transfer in meso-nitro-phenyl-octaethylporphyrins and their chemical dimers. *Chemical Physics Letters.* **1999**, *304*, 155-166.

50. Knyukshto, V. N.; Zen'kevich, É. I.; Sagun, E. I.; Shul'ga, A. M.; Bachilo, S. M. Photophysical properties of mesonitrophenyl-substituted porphyrins and their dimers at 295 K. *Journal of Applied Spectroscopy.* **1999**, *66*, 588-592.

51. Knyukshto, V. N.; Sagun, E. I.; Shul'ga, A. M.; Bachilo, S. M.; Zen'kevich, É. I. Photoinduced electron transfer in meso-nitrophenyl-substituted porphyrins and their chemical dimers. *Optics and Spectroscopy.* **2000**, *88*, 205-216.

52. Dahal, S.; Krishnan, V. Charge transfer excited states of zinc(II) derivatives of β-substituted dinitrotetraphenylporphyrin. *Journal of Photochemistry and Photobiology A: Chemistry.* **1995**, *89*, 105-112.

53. Dahal, S.; Krishnan, V. Excited singlet state intramolecular charge transfer in di and trinitrotetraphenylporphyrins. *Chemical Physics Letters.* **1997**, *274*, 390-395.

54. Gust, D.; Moore, T. A.; Luttrull, D. K.; Seely, G. R.; Bittersmann, E.; Bensasson, R. V.; Rougée, M.; Land, E. J.; Schryver, F. C. D.; Auweraer, M. V. d. Photophysical properties of 2-nitro-5,10,15,20-tetra-p-tolylporphyrins. *Photochemistry and Photobiology.* **1990**, *51*, 419-426.

55. Harriman, A.; Hosie, R. J. Luminescence of porphyrins and metalloporphyrins. Part 4.—Fluorescence of substituted tetraphenylporphyrins. *Journal of the Chemical Society, Faraday Transactions 2.* **1981**, *77*, 1695-1702.

56. Wickramasinghe, A.; Jaquinod, L.; Nurco, D. J.; Smith, K. M. Investigations on the directive effects of a single meso-substituent via nitration of 5,12,13,17,18-pentasubstituted porphyrins: syntheses of conjugated β-nitroporphyrins. *Tetrahedron.* **2001**, *57*, 4261-4269.

57. Lan, M.; Zhao, H.; Yuan, H.; Jiang, C.; Zuo, S.; Jiang, Y. Absorption and EPR spectra of some porphyrins and metalloporphyrins. *Dyes and Pigments.* **2007**, *74*, 357-362.

58. Wróbel, D.; Łukasiewicz, J.; Goc, J.; Waszkowiak, A.; Ion, R. Photocurrent generation in an electrochemical cell with substituted metalloporphyrins. *Journal of Molecular Structure.* **2000**, *555*, 407-417.

59. Vogel, G. C.; Stahlbush, J. R. Thermodynamic study of the adduct formation of zinc tetraphenylporphine with several neutral donors in cyclohexane. *Inorganic chemistry.* **1977**, *16*, 950-953.

60. Cole, S. J.; Curthoys, G. C.; Magnusson, E. A.; Phillips, J. N. Ligand binding by metalloporphyrins. III. Thermodynamic functions for the addition of substituted pyridines to nickel(II) and zinc(II) porphyrins. *Inorganic chemistry.* **1972**, *11*, 1024-1028.

61. Nappa, M.; Valentine, J. S. The influence of axial ligands on metalloporphyrin visible absorption spectra. Complexes of tetraphenylporphinatozinc. *Journal of the American Chemical Society.* **1978**, *100*, 5075-5080.

62. Kolling, O. W. Soret red shift for zinc tetraphenylporphine in the presence of uncharged Lewis bases. *Inorganic chemistry.* **1979**, *18*, 1175-1176.

63. Kolling, O. W. Comparison of donor-acceptor parameters in nonaqueous solvents. *Analytical Chemistry.* **1982**, *54*, 260-264.

64. Takahashi, K.; Hase, S.; Komura, T.; Imanaga, H.; Ohno, O. The Fluorescence Properties of (2-Nitro-5,10,15,20-tetraphenylporphyrinato)zinc. *Bulletin of the Chemical Society of Japan.* **1992**, *65*, 1475-1481.

65. Krishnan, V. Supramolecular assemblies for molecular scale information transport processes. *Journal of the Indian Institute of Science.* **1999**, *79*, 3-16.

66. Taylor, P. J.; van der Zwan, G.; Antonov, L. In *Tautomerism: Methods and Theories*; Antonov, L., Ed.; Wiley-VCH Verlag GmbH & Co. KGaA: Weinheim, Germany, **2014**.

67. Elsaesser, T.; Schmetzer, B.; Lipp, M.; Bäuerle, R. J. Excited-state proton transfer in 2-(2′-hydroxyphenyl)benzothiazole: Transient electronic absorption measured on the picosecond time scale. *Chemical Physics Letters.* **1988**, *148*, 112-118.

68. Laermer, F.; Elsaesser, T.; Kaiser, W. Femtosecond spectroscopy of excited-state proton transfer in 2-(2′-hydroxyphenyl)benzothiazole. *Chemical Physics Letters.* **1988**, *148*, 119-124.

69. Elsaesser, T.; Schmetzer, B. Excited-state proton transfer in 2-(2'-hydroxyphenyl)benzothiazole: formation of the anion in polar solvents. *Chemical Physics Letters.* **1987**, *140*, 293-299.

70. Gentemann, S.; Medforth, C. J.; Forsyth, T. P.; Nurco, D. J.; Smith, K. M.; Fajer, J.; Holten, D. Photophysical Properties of Conformationally Distorted Metal-Free Porphyrins. Investigation into the Deactivation Mechanisms of the Lowest Excited Singlet State. *Journal of the American Chemical Society.* **1994**, *116*, 7363-7368.

71. Roder, B.; Buchner, M.; Ruckmann, I.; Senge, M. O. Correlation of photophysical parameters with macrocycle distortion in porphyrins with graded degree of saddle distortion. *Photochemical & photobiological sciences : Official journal of the European Photochemistry Association and the European Society for Photobiology.* **2010**, *9*, 1152-1158.

72. Regev, A.; Galili, T.; Medforth, C. J.; Smith, K. M.; Barkigia, K. M.; Fajer, J.; Levanon, H. Triplet Dynamics of Conformationally Distorted Porphyrins: Time-Resolved Electron Paramagnetic Resonance. *The Journal of Physical Chemistry.* **1994**, *98*, 2520-2526.

73. Steiner, E. Density-difference maps in quantum chemistry. *Theoretica Chimica Acta.* **1982**, *60*, 561-572.

74. Sazanovich, I. V.; Galievsky, V. A.; van Hoek, A.; Schaafsma, T. J.; Malinovskii, V. L.; Holten, D.; Chirvony, V. S. Photophysical and Structural Properties of Saddle-Shaped Free Base Porphyrins: Evidence for an "Orthogonal" Dipole Moment. *The Journal of Physical Chemistry B.* **2001**, *105*, 7818-7829.

**Appendix A.**

1. Vollhardt, D.; Fainerman, V. B.; Liu, F. Thermodynamic and Structural Characterization of Amphiphilic Melamine-type Monolayers. *J. Phys. Chem. B.* **2005**, *109*, 11706.

2. Fainerman, V. B.; Vollhardt, D.; Aksenenko, E. V.; Liu, F. Molecular Recognition Kinetics of Nonsurface Active Pyrimidine Derivatives Dissolved in the Aqueous Subphase by an Amphiphilic Melamine Type Monolayer: A Theoretical Approach. *J. Phys. Chem. B.* **2005**, *109*, 14137.

3. Kimizuka, N.; Kawasaki, T.; Hirata, K.; Kunitake, T. Supramolecular Membranes. Spontaneous Assembly of Aqueous Bilayer Membrane via Formation of Hydrogen Bonded Pairs of Melamine and Cyanuric Acid Derivatives. *J. Am. Chem. Soc.* **1998**, *120*, 4094.

4. Baliani, A.; Bueno, G. J.; Stewart, M. L.; Yardley, V.; Brun, R.; Barrett, M. P.; Gilbert, I. H. Design and Synthesis of a Series of Melamine-based Nitroheterocycles with Activity against Trypanosomatid Parasites. *J. Med. Chem.* **2005**, *48*, 5570.

**Appendix C.**

1. Williams, A. Loopless Generation of Multiset Permutations using a Constant Number of Variables by Prefix Shifts. *Proceedings of the Twentieth Annual ACM-SIAM Symposium on Discrete Algorithms* **2009**, 987.

2. Golchoubian, H.; Hosseinpoor, F. Effective Oxidation of Sulfides to Sulfoxides with Hydrogen Peroxide under Transition-Metal-Free Conditions. *Molecules* **2007**, *12*, 304.

3. Chidawanyika, W.; Nyokong, T. The synthesis and photophysicochemical properties of low-symmetry zinc phthalocyanine analogues. *J. Photochem. Photobiol., A Chem.* **2009**, *206*, 169.

4. Garcia, A. M.; Alarcon, E.; Munoz, M.; Scaiano, J. C.; Edwards, A. M.; Lissi, E. Photophysical behaviour and photodynamic activity of zinc phthalocyanines associated to liposomes. *Photochem. Photobiol. Sci.* **2011**, *10*, 507.